Improving cargo delivery in cancer therapy with the help of cell-penetrating peptides

Inaugural-Dissertation

zur

Erlangung des Doktorgrades

der Mathematisch-Naturwissenschaftlichen Fakultät

der Universität zu Köln

vorgelegt von

Lucia Feni

aus Chiari

Köln

2019

Berichterstatter: Prof. Dr. Ines Neundorf

Prof. Dr. Norbert Sewald

Tag der mündlichen Prüfung: 29. März 2019

Die im Rahmen der vorliegenden Arbeit durchgeführten Experimente und Untersuchungen wurden im Zeitraum von September 2015 bis Dezember 2018 am Institut für Biochemie der Universität zu Köln unter der Anleitung von Frau Prof. Dr. Ines Neundorf durchgeführt.

Corpora non agunt nisi ligata

Abstract

A major obstacle of many active pharmaceutical compounds is their low ability to cross body barriers, especially cell membranes. Cell permeability of a drug is therefore considered as a key step for therapeutic efficacy. Over the last decades, different approaches to overcome this limitation have been studied intensively. Among these are so-called cell-penetrating peptides (CPPs). CPPs are able to autonomously internalize into cells without the need for auxiliary proteins. However, not only the cellular uptake is important but also cell selectivity has to be addressed. Over the past two decades, cancer research has dramatically evolved, particularly with the appearance of targeted molecular therapies and advances in antibody engineering that allowed the discovery and validation of innovative molecules, more effective and less harmful than conventional chemotherapy. Especially small molecule-drug conjugates, like peptide-drug conjugates, became of particular interest since they combine several advantages as deep tissue penetration, possibility of cell organelle targeting and relatively easy access by chemical synthesis.

This work focuses on the design and synthesis of an array of tumor-targeting peptide-drug conjugates combining known tumor-homing peptides with a well-described CPP and potent cytotoxic drugs. The development of these hybrids was followed by a validation of the model *via in vitro* studies where their selectivity towards different cell lines was evaluated. Two targeting ligands (GnRH-III and c[DKP*f3*RGD]) were employed for the conjugation to the CPP sC18 and a very straightforward synthesis could be developed in both cases. The conjugates maintained a remarkable binding affinity in low nanomolar range towards GnRH and $\alpha_v\beta_3$ integrin receptors, respectively, and for further *in vitro* experiments, the expression of the receptors in different cell lines was explored. For the investigation of the final compounds, a new *in vitro* model based on a short contact time with the cells was established in order to emphasize the role of the fast CPP-mediated internalization after reversible binding to the receptors. While for the GnRH-III-conjugates a selectivity was difficult to detect, the c[DKP*f3*RGD] was identified as very effective targeting moiety for the synthesis of an efficient drug delivery system. Different drugs were attached to the CPP and daunorubicin turned out to be the most advantageous in terms of simple synthesis and stability. Fluorescence analysis demonstrated that the internalization was mainly mediated by the CPP but that the ligand had an important role in targeting the surface of the cells overexpressing the receptor. The selectivity could also be proved by anti-proliferative assays providing another demonstration that with this approach it would be possible to overcome the drawbacks of CPP-mediated drug transport leading to higher target selectivity and better bioavailability.

In the second part of the thesis, cyclic CPPs with peculiar diketopiperazine scaffolds (*trans* DKP3 and *cis* DKP1) were synthesized starting from the sequence of a truncated variant of

sC18. An optimized cyclization strategy could be developed and the secondary structure of these peptides was analyzed and compared with the linear counterparts by different techniques. The biological activity of these compounds was also evaluated in cell systems where the ability to transport cytotoxic drugs inside the cells was explored by using both a non-covalent as well as covalent drug coupling approach. Notably, the cycle actually showed a higher ability to increase the activity of daunorubicin than the linear CPP, proving that cyclization *via* a diketopiperazine scaffold is a promising strategy to improve CPP-mediated drug delivery.

Zusammenfassung

Viele aktive pharmazeutische Verbindungen sind nicht in der Lage Barrieren, insbesondere Zellmembranen, ohne Hilfe zu überwinden, um ihren spezifischen Wirkort zu erreichen. Aus diesem Grund gilt diese Zellpermeabilität eines Arzneimittels als Schlüsselschritt für die therapeutische Wirksamkeit. Um diese Verbindungen zu transportieren, wurden bereits verschiedene Strategien etabliert, unter denen sich auch sogenannte zellpenetrierenden Peptide (CPP, *cell-penetrating peptides*) einreihen. CPPs sind in der Lage von einer Vielzahl von Zellen aufgenommen zu werden, ohne dabei auf Hilfe von Transportproteinen angewiesen zu sein. Aber nicht nur die zelluläre Aufnahme steht im Fokus der Forschung, insbesondere die Zellselektivität ist von großem Interesse. In den letzten zwei Jahrzehnten hat sich die Krebsforschung stark weiterentwickelt, vor allem durch gezielte molekulare Therapien und Fortschritte in der Antikörperentwicklung, die die Entdeckung und Validierung innovativer Moleküle ermöglichten, die dadurch sowohl wirksamer als auch weniger schädlich als konventionelle Chemotherapien sind. Besonders kleine Molekül-Wirkstoff Konjugate, wie zum Beispiel Peptid-Wirkstoff Konjugate, sind vielversprechend, da sie sich durch tiefe Gewebepenetration und mögliches Ansteuern verschiedenster Zellkompartimente auszeichnen. Desweitern sind diese Konjugate relativ einfach herzustellen und so einfach zugänglich.

Diese Arbeit konzentriert sich auf das Design und die Synthese von Krebs spezifischen Peptid-Wirkstoff-Konjugaten, bei der ein Peptidfragment, das in der Lage ist ein bestimmte Tumorart anzusteuern, mit einem bekannten CPP und einem Zytostatikum kombiniert wird. Nach der Herstellung dieser Hybride folgte eine Validierung ihrer Aktivität durch verschiedenste *in vitro* Studien. Zwei spezifische Ziel-Liganden (GnRH-III und c[DKP*f3*RGD]) wurden für die Konjugation an das CPP sC18 verwendet, und in beiden Fällen konnte eine optimierte Syntheseroute entwickelt werden. Die Konjugate zeigten eine bemerkenswerte Bindungsaffinität im niedrigen nanomolaren Bereich zu GnRH bzw. $\alpha_v\beta_3$ Integrin-Rezeptoren. Für weitere *in vitro* Experimente wurde außerdem die Expression der Rezeptoren in verschiedenen Zelllinien untersucht. Für die Analyse der Verbindungen wurde ein neues *in vitro* Modell etabliert, das auf einer kurzen Kontaktzeit mit den Zellen basiert, um die Rolle der schnellen Internalisierung durch das CPP nach der Bindung zu den Rezeptoren zu untersuchen. Während für die GnRH-III-Konjugate eine Selektivität schwer nachzuweisen war, wurde c[DKP*f3*RGD] als sehr wirksame Zielgruppe für die Synthese eines effizienten Transportsystems identifiziert. Verschiedene Toxine wurden an das CPP gebunden, wobei sich Daunorubicin im Hinblick auf die einfache Synthese und Stabilität als das vielversprechendste erwies. Aufnahmestudien zeigten, dass die Internalisierung hauptsächlich durch das CPP vermittelt wurde, der Ligand jedoch möglicherweise eine wichtige Rolle beim

Binden an die Oberfläche der Zellen hatte, die den Rezeptor überexprimieren. Die Selektivität konnte auch durch antiproliferative Versuche nachgewiesen werden. Somit liefert der hier vorgestellte Ansatz eine mögliche Lösung CPPs mit einer Zellselektivität auszustatten.

Im zweiten Teil dieser Doktorarbeit wurden verschiedene zyklische CPPs synthetisiert. Dafür wurden spezielle Bausteine, basierend auf Diketopiperazinen (*trans* DKP3 und *cis* DKP1), verwendet. Es konnte eine optimierte Zyklisierungsstrategie entwickelt werden und die Sekundärstruktur dieser neuen Peptide wurde durch verschiedene Techniken analysiert und mit den linearen Versionen verglichen. Die biologische Aktivität dieser Verbindungen wurde in Zellen getestet, dabei stand besonders im Vordergrund, zytotoxische Wirkstoffe in Zellen zu schleusen. Die Wirkstoffe wurden dabei sowohl nicht-kovalent als auch kovalent an das Peptid gekuppelt. Das zyklische Peptid war in der Lage die Aktivität von Daunorubicin deutlich zu verbessern im Vergleich zum linearen Peptid. Dieses Ergebnis unterstreicht, dass die Zyklisierung mittels eines Diketopiperazingerüstes zu neuen CPPs mit sehr vielversprechenden Aktivitäten führt.

Table of contents

1. Introduction

Over the last year, 18.1 million new cases of cancer have been reported worldwide. In other words, one in five men and one in six women is diagnosed with cancer and these numbers increase constantly. These data from the Globocan report have been published in the journal *CA: A Cancer Journal for Clinicians* and represent a "photograph" of the diagnoses of cancer registered globally. The statistics show an increase in cancer diagnosis, which may be due to several factors from the aging of the population to the precarious conditions of social and economic development that are recorded in different areas of the planet. This second aspect also affects cancer-caused mortality, which in 2018 should be almost about ten million, while over 43 million people are expected to live within the five-year prevalence. [1] In fact, research has led to increasingly effective therapies with fewer side effects, which in many cases are able to reduce mortality. The progresses made in the last century are highlighted in Figure 1. The main treatments of tumors are represented by surgical resection, [2] chemotherapy, [3-4] radiation therapy [5-6] but also by the more innovative hormone therapies, [7-9] targeted therapies, [10-11] immuno-oncology and gene therapy, used individually or in combination. [12-13]

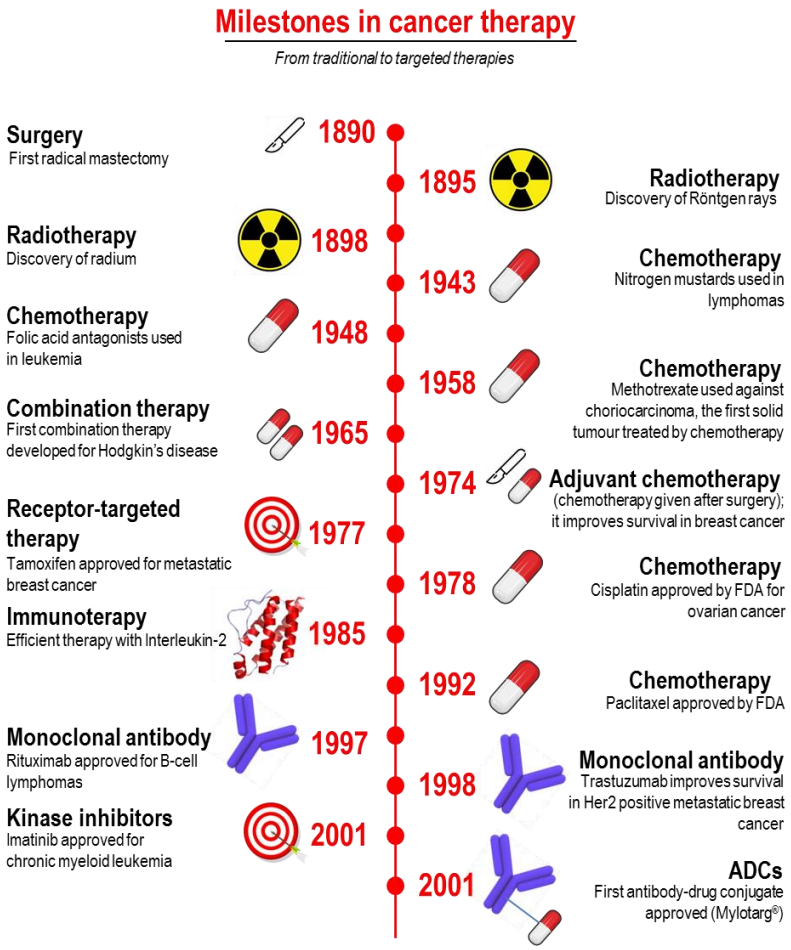

Figure 1. Timeline: milestones in cancer therapy. From traditional to targeted therapies. Adapted from DeVita *et al.* and Chabner *et al.* [14-15]

1.1. Traditional chemotherapy versus targeted chemotherapeutics

Conventional chemotherapy is still widely applied in cancer treatment. 5-fluorouracil/leucovorin and oxaliplatin, for example, are still the gold standard for colorectal cancer, [16] while a regimen of cisplatin or carboplatin combined with paclitaxel, gemcitabine or docetaxel is currently used for the treatment of non-small cell liver cancer at stage IV. [17] However, the compounds used as chemotherapeutic agents localize with low efficiency in solid tumors. This unfavorable biodistribution profile, exemplified in Figure 2, combined with a mechanism of non-selective action, causes serious side effects and prevents a dose increase at therapeutically active regimens. [18]

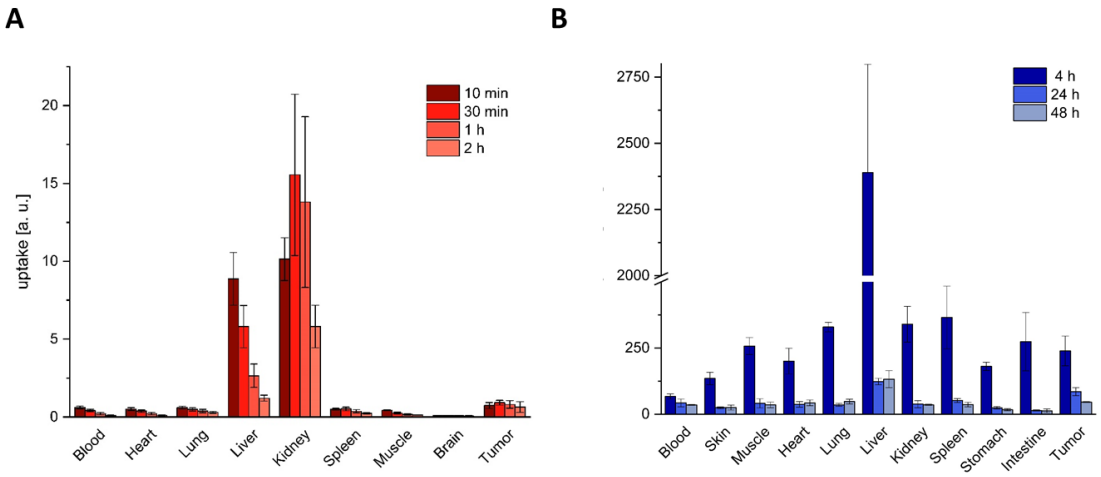

Figure 2. Unfavorable biodistribution profile of traditional chemotherapeutic drugs. A: Tissue distribution of 5-Fluorouracil (5-FU) in ascitic hepatoma bearing rats. **B**: Tissue distribution of ^{3}H-Paclitaxel in Balb/c nude mice bearing MDA-MB-435 tumors (melanoma). Adapted from Abe *et al.* and Cao *et al.* [19-20]

Two main approaches have been followed to reach the final goal of widening the therapeutic window: the combination of two or more cancer drugs without overlapping mechanism and/or toxicity [21] and the introduction of more potent drugs administrated at lower dosage. [22] Both strategies could lead to encouraging results in terms of efficacy, although an absolutely positive safety profile could not be achieved. Researchers understood that the unique key to completely avoid a systemic toxicity was the enhancement of selectivity. Targeted therapies, for instance, are interfering in a much more directed way with a molecule or a specific process of cell growth, not causing damage to healthy tissues, thus reducing side effects. [23-24] In fact, they selectively act on specific cell receptors, hence improving the tolerability of the treatment, to the benefit of the patient and his quality of life. [25]

Targeted therapies represent one of the most important tools of personalized medicine, since the treatment is no longer chosen only based on the development of the tumor, but also in relation to its molecular characteristics and expression of biomarkers, which can be different from patient to patient. [26-30] Many efforts have been made in this field and the results obtained

in the last few years are exciting. Even if novel targeted therapies are pioneering and reserved for particular types of cancer, they already display an important role in the fight against this disease. In fact, many data show that they have prolonged survival and improved the quality of life of many patients. [31-33] Over the years a number of directed agents have been used and these therapies are able to:

- manipulate the endocrine system through external administration of precise hormones or drugs that inhibit their production (**hormone therapy** for hormone-dependent tumors, e.g. anti-estrogens, [34-36] aromatase inhibitors, [37] GnRH agonists, [38-39] anti-androgens [40-41]);
- stimulate the immune system to identify and destroy cancer cells (**immuno-oncology**); [42-43]
- hinder angiogenesis, [44-45] inhibit tumor-related kinases [46] and other oncoproteins (**targeted therapy**);
- selectively release toxic substances that act on cancer cells through different ways, e.g promoting apoptosis or decreasing their uncontrolled ability to grow and divide (**targeted delivery**). [47-48]

The last example, in particular, has been proposed as an alternative method to overcome the limits of classic chemotherapy, carrying powerful cytotoxic compounds at the tumor site after conjugation to ligands that are specific towards tumor-associated targets. [24] The conjugation of these pharmacodelivery vehicles with a cytotoxic drug realizes the concept of "magic bullet" as it was conceived more than a century ago by Paul Ehrlich (1854-1915), who was awarded the Nobel Prize for Medicine in 1908. [49-50] In Figure 3 the peculiar and advantageous characteristic of these new compounds is illustrated with a schematic representation of their mode of action. The selectivity of these drug-delivery systems is driven by the high binding affinity towards particular tumor cell substrates resulting in a moderate occurrence of undesirable effects since the healthy cell lines should not be affected.

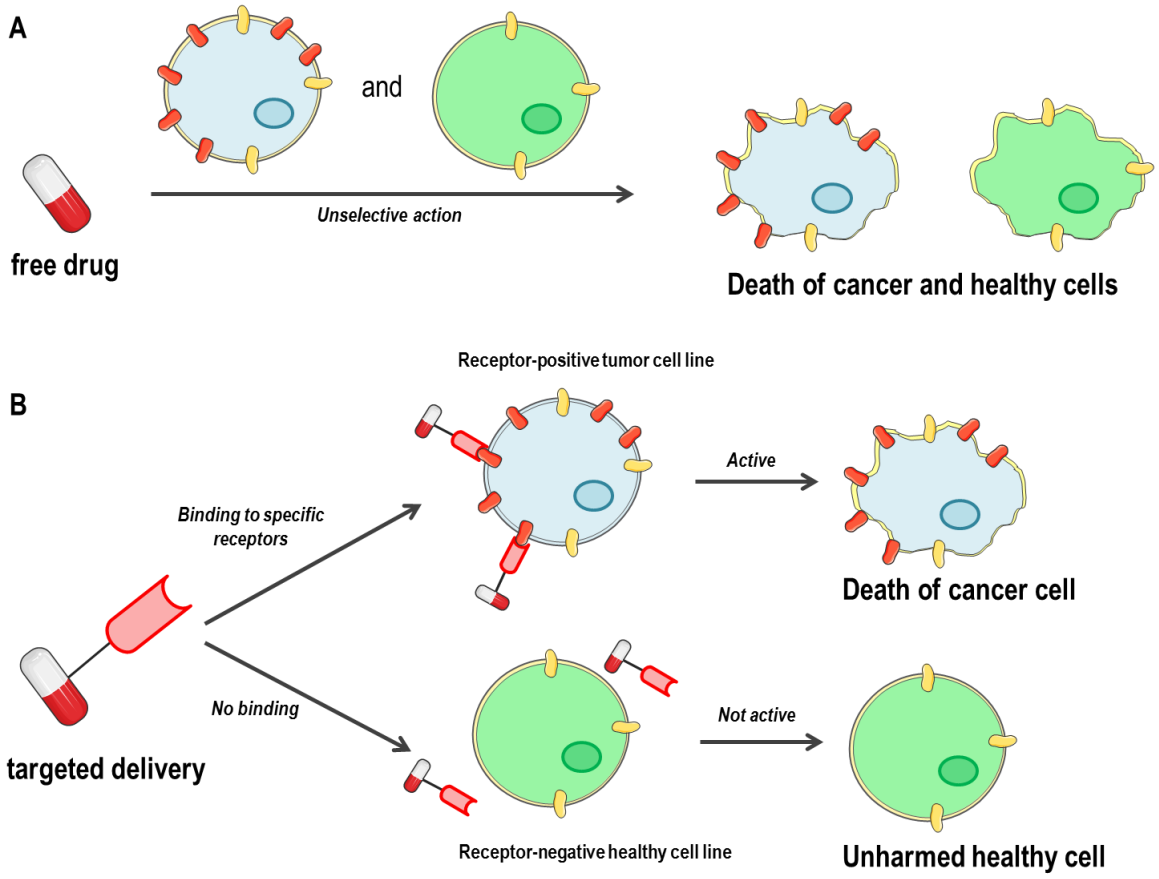

Figure 3. Traditional chemotherapy vs targeted delivery of chemotherapeutics. A: General strategy of traditional chemotherapy; **B:** The "magic bullet" concept.

Antibody-drug conjugates (ADCs) and small molecule-drug conjugates (SMDCs) represent two innovative classes of biopharmaceutical products, designed to selectively bring cytotoxic agents to the tumor tissue. They combine the best features of two therapeutic modalities. In particular, antibodies and small ligands that display target specificity but limited antitumor activity are conjugated to cytotoxic agents, very potent but with poor safety and pharmaceutical profiles. The following sections will first focus on three commonly used drugs, which were also employed in this work, and will further highlight two novel delivery strategies.

1.2. Cytotoxic payloads

1.2.1. Daunorubicin

Daunorubicin and doxorubicin are the parent compounds of the anthracycline antibiotics. Mostly isolated from natural sources (*Streptomyces peucetius*), [51] they are extensively used for the treatment of cancer alone or in combination and widely investigated as cytotoxic payloads in conjugation with tumor homing peptides [52-54] or antibodies. [55-56] In fact, they are very effective but also very toxic, as they do not discriminate between malignant and healthy cells, leading in particular to cardio-toxicity [57-58] and myelosuppression. From the structural point of view, anthracycline antibiotics are characterized by a planar tetracyclic portion, glycosidically linked to an aminosugar (daunosamine). The molecular structures of daunorubicin and doxorubicin differ only in one of the terminal substituents, as it is shown in Figure 4.

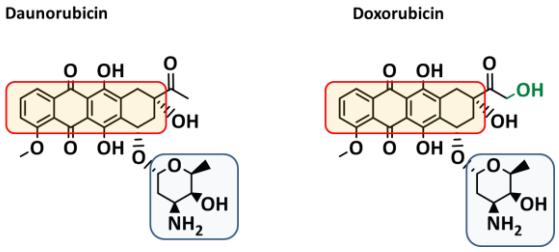

Figure 4. Structures of the two anthracycline parent compounds: daunorubicin and doxorubicin. Red box: planar tetracyclic portion; blue box: daunosamine; green: hydroxyl group substituent in doxorubicin that is missing in daunorubicin.

Although small, this structural difference has important consequences on the activity spectrum of the two cytotoxic antibiotics. Doxorubicin, in fact, has significant clinical applications especially in solid tumors, [59-62] while the main indication of daunorubicin is acute leukemia. [63] The current tendency is to consider the DNA intercalation as necessary but not sufficient for anti-tumor action. [64] In fact, numerous results have indicated topoisomerase II as the main anthracycline target. This nuclear enzyme relaxes the supercoiled DNA by the formation of a phosphodiester bond between the OH group of its active-site tyrosyl residue and the phosphoric group of DNA. This allows the free end of the nucleic acid to rotate, solving the supercoiling. At this point the OH group at the free end of the DNA can restore the continuity of the helix by attacking the activated phosphate. [65] At present, it is known that anthracyclines, after intercalating in the double helix, stabilize a ternary cleavage complex between the DNA, tied to the enzyme, and the drug. Therefore the action of the drug leads to irreversible cuts in DNA that open the way to the programmed cell death in cancer cells. [66] Two further mechanisms were identified as responsible for toxicity, notably the production of free oxygen radicals through an enzymatic reduction process [67] and induction of histone eviction from open chromatin. [68]

1.2.2. Chlorambucil

Chlorambucil is a chemotherapeutic agent belonging to the class of the so-called alkylating drugs, in particular deriving from nitrogen mustards.

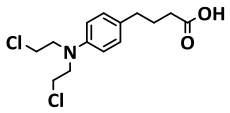

Figure 5. Structure of chlorambucil.

At physiological pH, chlorambucil forms a very reactive cyclic intermediate (aziridinium ion) which attacks the nitrogen in position 7 of a guanine, present in the DNA chain, building a covalent bond. The same process takes place on the other chain ($ClCH_2CH_2N$-) of the chlorambucil, which in turn will interact with a new guanine, present in the same or in the other DNA helix. Inter or intra helix bridges do not allow anymore DNA to perform its biological functions (duplication and transcription). [69-70] The alteration that the chlorambucil induces in the DNA prevents the cancer cell from dividing, forcing it to undergo apoptosis. [71] It is mainly used for the treatment of chronic lymphocytic leukemia, [72-73] normally in combination with other chemotherapeutic agents. As previously described in the case of daunorubicin, chlorambucil provokes the common side effects of the non-targeted therapies; hence, its conjugation to targeting moieties has been studied and researched intensively. [74-77]

1.2.3. Cryptophycin

Cryptophycins are 16-membered macrocycles with bacterial origin composed by four units, [78] having potent activity towards cancer cells and MDR (multi-drug resistant) cancer cells (IC_{50} in the pM range), as the human cervical carcinoma cell line KB-V1. [79-80] They are able to coordinate to β-tubulin interacting with the *vinca* domain. In particular, they inhibit tubulin polymerization, inflicting a conformational change on tubulin dimers and depolymerize microtubules *in vitro*, reducing microtubule dynamics. [81] This leads to mitotic arrest and apoptosis.

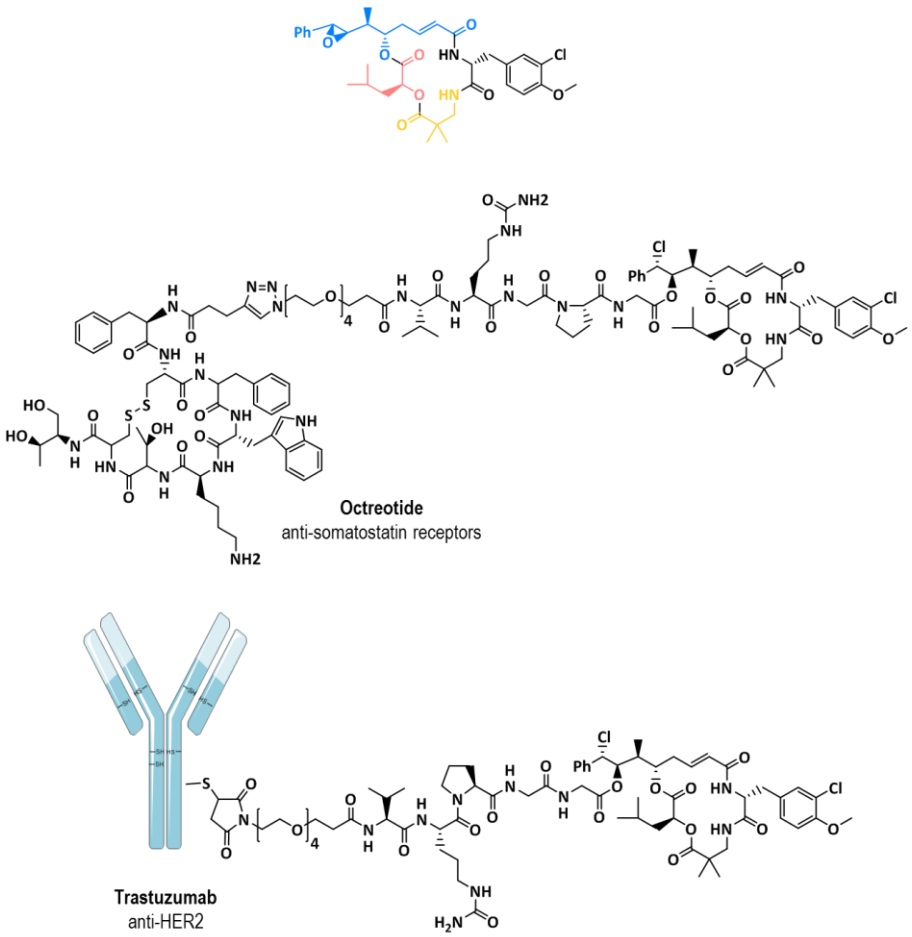

Figure 6. Structure of cryptophycin-52 and derivatives of cryptophycin-55 glycinate conjugated to a targeting peptide and a mAb. Blue: unit A; black: unit B; yellow: unit C; pink: unit D. Adapted from Weiss *et al.* [82]

Cryptophycin-52 is the lead compound within this class and was tested in clinical Phase II, where it unfortunately showed a lack of *in vivo* efficacy and high toxicity (in particular neurotoxicity since neurons are the main tubulin producers for the transport of neurotransmitters). Cryptophycin-55 (the chlorohydrin of Cry-52) and its glycinate correspondent derivative were described as highly active *in vivo* in preclinical models, displaying a better pharmacokinetic profile. [83-84] Under physiological conditions the chlorohydrins are converted to the original epoxides, hence they are considered as prodrugs of the epoxides. After esterification with the glycine, improvement in water solubility and stability was also reached and this most importantly allowed the conjugation to homing peptides, like octreotide, but also antibodies [82, 85] and other ligands, e.g. acetazolamide [86] (Figure 6).

1.3. Antibody-drug conjugates (ADCs)

An antibody-drug conjugate (ADC) is the unique combination of a monoclonal antibody, a linker and a potent cytotoxic agent. It is designed to provide therapeutic potency to the antibody and specificity to the anti-cancer agents, which can be directed to the tumor cell in a targeted way

to limit systemic exposure. [87] This idea dates back to the early eighties. However, the first products did not obtain the desired results due to a series of technological limits, inadequate knowledge of the receptor target, use of insufficiently potent drugs and instability of the linker in biological fluids. [88] Notable improvements in the conjugation technology associated with a greater understanding of the biology of the system led to the discovery of a second generation of ADCs. These new therapeutic agents have better stability in biological fluids and allow an appropriate release of the toxic agent to the target cell. [89] ADCs include some of the most promising molecules in the oncology pipeline of large pharmaceutical companies. The peculiarity of ADCs is their long half-life (over a week), no systemic toxicity in circulation and activity only upon binding to tumors. All these characteristics lead to a maximum efficiency in administering the cytotoxic substance to the tumor cells in a perfectly selective way. [90] To date, there are four ADCs approved by the FDA: Adcetris ® for the treatment of refractory Hodgkin's lymphoma [91] and anaplastic large cell lymphoma, [92-94] Kadcyla ® for the treatment of HER2-positive metastatic breast cancer, [95-96] Mylotarg ® for adulte acute myeloid leukemia [97-98] and Besponsa ® for adult acute lymphoblastic leukemia, [99-100] as represented in Figure 7. Auristatin (MMAE), maytansine (DM1) and *N*-acetyl-gamma-calicheamicin (CCM) are used as cytotoxic agents, respectively. On average, two to four toxins are conjugated to the mAb. In addition to the four commercial ADCs, nearly forty are under investigation in many different types of cancer. [101]

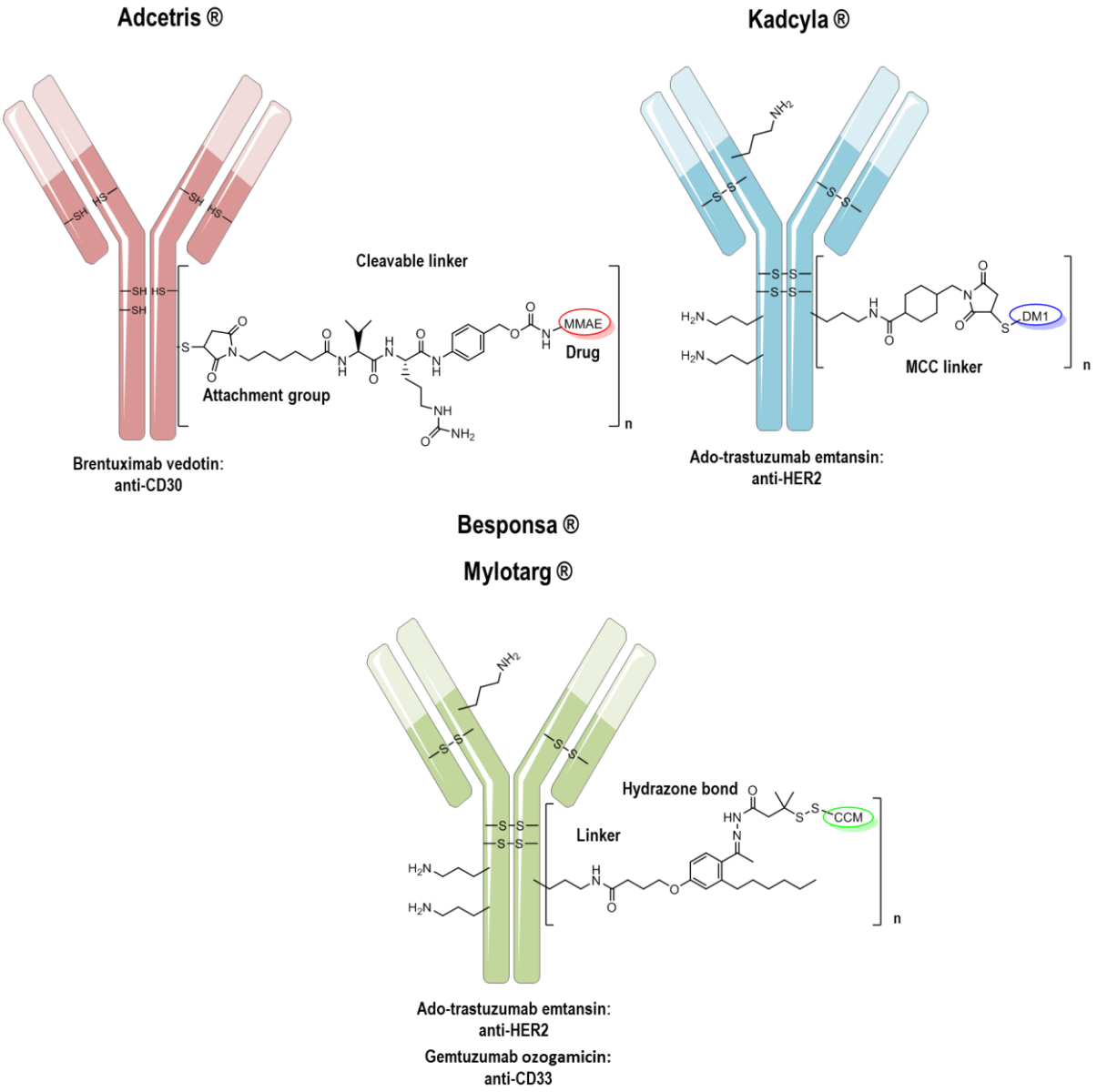

Figure 7. FDA approved ADCs. Drug-to-Antibody ratio is different, dependently from the conjugation strategy. *n*=4 (Adcetris ®), *n*=3.5 (Kadcyla ®), *n*=2.5 (Besponsa ® and Mylotarg ®).

Despite their growing success, the clinical advances of ADC products may be restricted by some limitations. Among these, heterogeneity is a crucial drawback leading to analytical and process challenges [102] and difficulties in administrating these compounds to patients. [103-104] The optimal design to obtain homogeneous compounds with the same average and distribution of payloads is a key point to achieve product safety and it is being addressed by researchers with new methods involving site-specific conjugation like engineering of the antibody sequence, [105] site-selective conjugation strategies [106] or modular approaches. [107] A high Drug-to-Antibody Ratio (DAR) is also affecting the propensity of the ADCs to aggregate, especially after being conjugated to very hydrophobic linker-drugs, so that the introduction of hydrophilic molecules could help to solve this major problem. [108] Besides that, increased stability against extracellular proteases needs to be reached to avoid dangerous off-site toxicity

after administration if the linker is not stable enough to prevent the premature release of the drug in the circulation before being introduced in the tumor cell. [109] Last but not least, the slow extravasation that characterizes immunoglobulins (IgG) is hindering their activity against solid tumors leading to the need of optimizing the format of the targeting moiety like for example by the introduction of small immune proteins (SIP) distinguished by a fast clearance, good extravasation and very good tumor/blood and tumor/organ ratio. [110]

1.4. Small-molecule drug conjugates (SMDC)

SMDC products, in particular peptide-drug conjugates, have been proposed to overcome some typical limits of antibodies. [111] In fact, small organic ligands can penetrate into depth of solid organs and tumors within a few minutes after administration, conveying the drug to the tumor with greater efficiency, and are typically characterized by rapid excretion from circulation. [112] In addition, they are easily developed, obtainable with inexpensive production and are easy to manipulate. However, they are often less selective than the correspondent antibodies. [47, 113] Some of the prerequisites for a peptide to become a receptor-mediated carrier are:

- overexpression of the receptors on the surface of tumor cells;

- knowledge of SAR to efficiently synthesize peptide analogues;

- high affinity for the target;

- efficient internalization (to provide the introduction of the drug).

Two examples of receptor targeting moieties are gonadotropin-releasing hormone (GnRH) agonists and integrin ligands, whose biological background is introduced in the following paragraphs.

1.4.1. GnRH receptors

GnRH and its analogs have been widely used in clinical medicine since they were identified and synthesized in 1971 by Schally's group. [114] The native GnRH-I, also called luteinizing hormone-releasing hormone (LHRH), is a decapeptide (pGlu-His-Trp-Ser-Tyr-Gly-Leu-Arg-Pro-Gly-NH_2), produced and released in a pulsatile manner by the hypothalamus. After binding to specific receptors (GnRH-I R) on the plasma membrane of the gonadotrophs (Figure 8), it stimulates them to secrete follicle-stimulating hormone (FSH) and luteinizing hormone (LH) with a consequent gonadal response. [115] A second form of GnRH (GnRH II) is ubiquitous and maintained in its structure throughout different species. Nevertheless, the GnRH-II receptor has not been identified yet in humans, even if there is strong evidence that this receptor exists. [116] GnRH receptors are highly expressed on various cancer cells and apart from pituitary cells and reproductive organs, they are present in a very limited number in healthy tissues. They are for this reason a good target for selective cancer chemotherapy. [117-118]

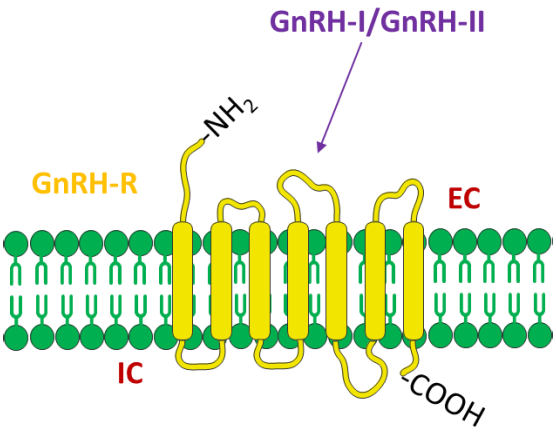

Figure 8. Binding of GnRH to its receptor. [119] IC: intracellular; EC: extracellular

In order to increase the power and duration of action of the GnRH-I, through modifications of the molecular structure of this decapeptide, many analogs have been synthesized, and are available for clinical use. The substitution with D-amino acids in position 6 (involved in the enzymatic cleavage) or 10 (important for the tridimensional structure) resulted in analogs with agonist activity with a greater potency and a longer half-life than the native GnRH-I. These produce an initial stimulation of the pituitary cells followed by the down-regulation and inhibition of the hypophysis-gonadal axis. GnRH-I analogs are powerful therapeutic agents, proved to be very useful in various clinical indications, including the therapy of some hormone-dependent tumors, like prostate or breast cancer. In this context, doxorubicin was conjugated by an ester bond to a GnRH-I agonist called zoptarelin. [120-121] The final conjugate AEZS-108 was tested till Phase III of clinical trials on endometrial cancer but failed to extend survival in the advanced disease. [122]

Taking advantage of these findings, some researchers are paying a special attention on the improvement of GnRH-based drug delivery systems, by starting from the sequence of a third form of GnRH (GnRH-III) discovered in sea lamprey, able to selectively bind to GnRH receptors but with a lower endocrine effect compared to GnRH-I agonists. [123-127] In the group of Prof. Mező (ELTE University, Budapest) the native sequence was modified in order to obtain a higher stability and allow drug-conjugation and many strategies have been pursued. [128-130] In particular Ser^4 was substituted with a butyrylated lysine, Lys(Bu), while Lys^8, functionalized with an aminooxyacetic acid linker, was conjugated to daunorubicin by an oxime linkage, in order to prevent the enzymatic cleavage of the ester bond by carboxylesterases (Figure 9). [131]

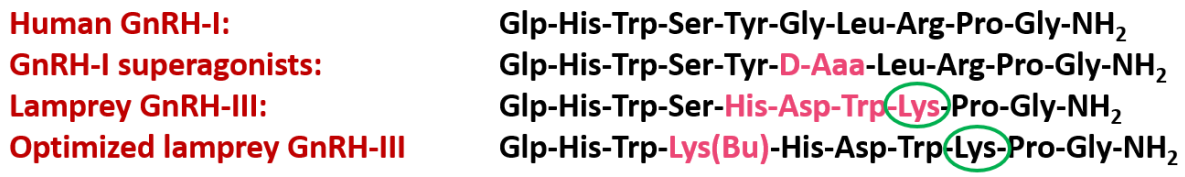

Figure 9. Optimization of the GnRH sequence. Pink: changes in the sequence; Green circle: conjugation point for the attachment of the drug. Bu: butyryl.

The conjugates are very stable in human serum from the chemical and enzymatic point of view but in presence of lysosomal homogenate they are degraded with subsequent release of different metabolites. H-Lys(Dau=Aoa)-OH was recognized as the smallest drug containing metabolite which is still able to bind to DNA *in vitro*. [132] The stability and selectivity of the conjugate have been favored at the expense of the cytotoxicity that is in fact lower than the free drug. The introduced peptide was chosen in this work for further studies.

1.4.2. Integrin receptors and integrin ligands

Adhesive contacts with neighboring cells and with the extracellular matrix (ECM) control cell behavior and development. These interactions are mediated by proteins of the cell surface, called cell adhesion receptors, divided in four groups: cadherins, selectins, immunoglobulin superfamily and integrins. [133]

Integrins form the largest and most versatile receptor family, being implied in both cell-ECM and cell-cell interactions. They are transmembrane heterodimeric glycoprotein receptors found in mammals in 24 combinations, constituted from 18 different α- and β-subunits. [134] The subunits are not covalently linked and consist of an ectodomain, a transmembrane region and a short unstructured cytoplasmic tail (Figure 10). [135] The *N*-terminal regions of all α subunits contain seven repeating sections, folded in the form of a seven-bladed β-propeller, supported by a *thigh* and two *calves*. The β-chains of α_v integrins present a domain I for the interaction with the matrix followed by a hybrid and a PSI (plexin-semaphorin-integrin) domain, four cysteine-rich EGF-like repeats and a β-tail. [136] A conserved region called MIDAS (metal ion-dependent adhesion site) in the β-I domain, is particularly important for the sequence recognition, because it binds divalent cations (e.g., Ca^{2+}, Mg^{2+}, Mn^{2+}) that can possibly coordinate a carboxylic acid residue of the ligand, e.g., aspartic acid residue of the RGD pattern. [137]

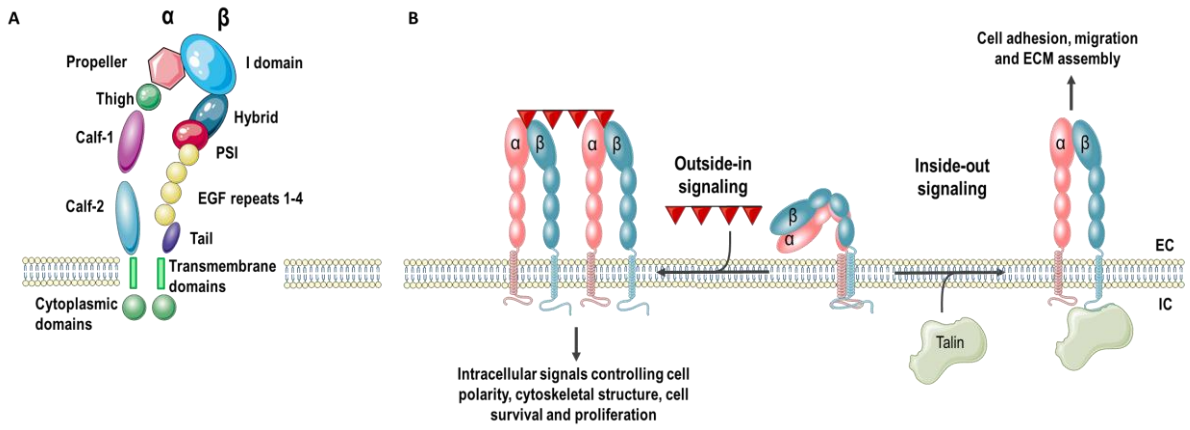

Figure 10. Integrin structure and activation. A: α and β subunits of an integrin receptor. **B**: Outside-in and inside-out signaling pathways. Adapted from Shattil *et al.* [138] EC: extracellular; IC: intracellular.

The connection between ECM and cytoskeleton provided by integrins is highly dynamic and involves a bidirectional transfer of information: while the cytoskeleton regulates the affinity of the integrin extracellular domain, the binding of ECM proteins or cell-surface ligands to integrins alter the arrangement of the cytoskeletal system. [139]

In the pathway of signal transduction from the cell interior to outside (inside-out signaling), the integrin ectodomain initially adopts a collapsed configuration stabilized by a salt bridge between the cytoplasmic domains of the two subunits. This arrangement is susceptible to unfold after the recruitment of certain cytosolic proteins, especially talin and kindlin that bind to the β-subunit, stimulating the integrin to assume an activated form. [135, 140] Subsequently, interaction sites with the extracellular matrix are revealed allowing the interaction with the appropriated ligand. At the same time, the interaction of integrins with their extracellular ligands changes the conformation of the integrin generating signals in the inside of the cell (outside-in signaling). The formation of integrin clusters stimulated by multimeric ligands causes an increased ligand-receptor interaction inducing the formation of focal adhesion complexes and causing a transfer of stronger signals. [135] The two processes are reciprocally influencing each other: while the integrin activation can promote ligand binding, concurrently interaction with the ligand can generate intracellular signals. [138] The activation of these receptors can control the change of the cell shape, migration and tissue organization playing a crucial role in many physiological but also pathological processes like cancer development because of their role on the one hand in tumor cells (development of metastases) and, on the other hand, in endothelial cells (neo-angiogenesis). For this reason, the pharmacological targeting of these receptors for these indications has been the subject of numerous studies. [141]

In this work, the integrin $\alpha_v\beta_3$, will serve as a target in the development of tumor therapeutics, therefore this class of integrins will be characterized here in more detail. The $\alpha_v\beta_3$ integrin is

overexpressed on tumor cells rather than on healthy tissues, e.g. melanoma, breast cancer and glioblastoma cells, which is why it is also used as an indicator of the invasive phase of tumors. [141] Ligand oriented design was the starting point for the synthesis of new selective compounds: each integrin is able to recognize well-defined ligands at the level of extracellular matrix and the integrin $\alpha_v\beta_3$ recognizes the motive Arg-Gly-Asp (RGD) on fibronectin and some other proteins. Pierschbacher and Ruoslathi found the tripeptide sequence RGD in fibronectin in 1984. [142] This was identified as the minimal fragment for stimulating cell adhesion and called 'universal' cell recognition motif, as it is present in about half of the matrix proteins and it is recognized by eight members of the 24 membered integrin family. [143] Starting from this natural binding sequence, a variety of peptidic and non-peptidic integrin ligands were developed, resulting in different receptor affinity, selectivity and bioavailability, partly superior to the natural ligand. [144] Conformational restriction is a way to achieve superactivity and selectivity of sub-type recognition; in peptides, cyclization and peptidomimetic constraints help to pin-down the active conformation. [145] It could be shown for example that flanking amino acids of the recognition sequence and their conformation are essential for the integrin-ligand interaction, the ligand affinity and selectivity. In the research group of Prof. Kessler, the incorporation of D-amino acids [146] and *N*-methylation [147-148] resulted in the first synthetic, metabolically stable $\alpha_v\beta_3$-selective ligand c[RGDf(*N*-Me)V], called cilengitide. [149] Unfortunately, it failed in Phase III of clinical trial because it did not meet its primary endpoint of significantly increasing overall survival when added to the current standard chemoradiotherapy regimen. [150] NMR spectroscopic studies combined with molecular dynamics simulations revealed that this particular conformational restriction was crucial to achieve maximal binding affinity and this was finally confirmed by the crystal structure of the $\alpha_v\beta_3$ integrin in complex with cilengitide, reported by Arnaout and coworkers. [151] As schematically illustrated in Figure 11 and 13, the side chains of arginine and aspartic acid come thereby in an optimal orientation for interaction with the $\alpha_v\beta_3$ integrin receptor (with Asp^{218}/Asp^{150} and with the metal ion in the MIDAS region, respectively) and have been identified as essential groups. The aromatic residue, adjacent to the carboxylic group, increases binding affinity by π-interaction with the receptor (Tyr^{122}). The role of the glycine imposing steric restrictions in the relatively flat binding pocket is also fundamental, thus analogous RAD peptides possess a much lower affinity and can be used as controls. On the contrary, the valine residue does not interact with the receptor, which is why it can be replaced through different amino acids without loss of integrin affinity and selectivity.

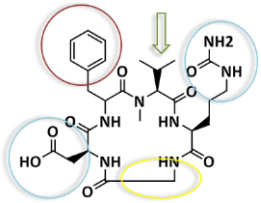

Figure 11. Interactions of cilengitide with the RGD binding pocket. Red circle: π-interaction; blue circle: ionic interactions; yellow circle: steric restriction; green arrow: no interaction. Adapted from Mas-Moruno *et al.* [149]

After the structure of the complex between receptors and ligands has been analyzed in detail, further optimization could be done via rational structure oriented design. This is what they tried to study and efficiently succeeded in the research groups of Prof. Gennari and Prof. Piarulli. In this case, important peptidomimetic variations, helping to optimize biological activity and selectivity between subtypes, were introduced in the new developed constrained peptides containing the RGD motif. They understood that to prepare effective compounds they had to work on the conformation; for this reason, various ligands were screened, which differed from each other because of the peculiar DKP (diketopiperazine) scaffold used to close the ring, each functionalized with a carboxylic acid and a Boc-protected amino group as showed in Figure 12 and obtained with good overall yields. [152-154]

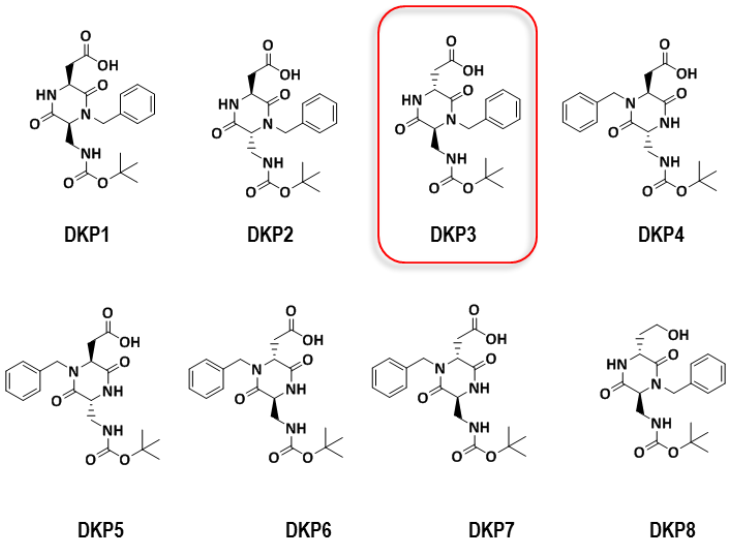

Figure 12. DKP library developed in the research groups of Prof. Gennari and Prof. Piarulli. Red box: elected DKP scaffold for the synthesis of a DKP-RGD ligand with high affinity and selectivity towards the receptor sub-type $\alpha_v\beta_3$.

Binding affinity studies on the purified $\alpha_v\beta_3$ and $\alpha_v\beta_5$ integrin receptors showed very promising results: the affinity rate was in general in nM range a part from the DKP1-containing ligand, characterized by a non-extended arrangement. DKP3RGD was chosen for further studies, since it showed a high affinity in low nanomolar range, comparable to cilengitide but contrarily to the latter, a much higher selectivity for $\alpha_v\beta_3$ (for the binding to $\alpha_v\beta_5$ IC_{50} values in micromolar

range were measured). These results were confirmed also by the investigation of ligand-integrin interactions. The best pose of the ligand into the crystal structure of $\alpha_v\beta_3$ binding site was overlaid on cilengitide during docking studies and showed that all the important interactions of the X-ray complex were conserved, in particular the distance between Arg and Asp was maintained (Figure 13). [153]

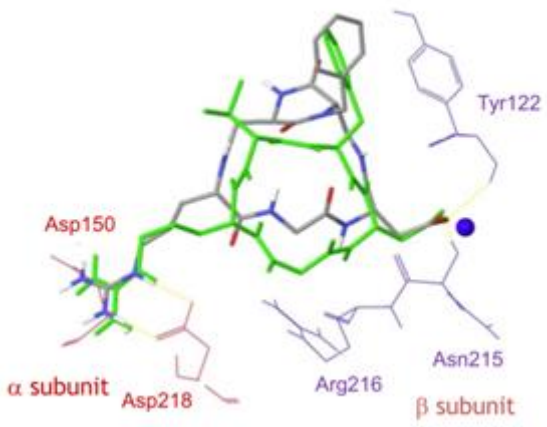

Figure 13. Docking into $\alpha_v\beta_3$ binding site. All the important interactions are conserved. The metal ion in the MIDAS region is represented by a blue sphere. Green: cilengitide. Grey: c[DKP*3*RGD]. [155]

Since 2012 a functionalized version of the integrin ligand c[DKP3RGD] was employed as tumor-homing device for site-directed delivery of paclitaxel, [156-157] SMAC (second mitochondrial-derived activator of caspases) mimetic proapoptotic compounds [158] and antiangiogenic helical peptides targeting VEGF receptors. [159] In *in vivo* tumor-targeting experiments the paclitaxel conjugate exhibited a superior activity than the free drug despite the lower molar dosage used. [156] These results could demonstrate that the position of the functionalization was ideal not to interfere with the binding to the integrins and that very likely integrin-mediated endocytosis occurred.

1.5. Receptor-mediated uptake

Receptor-mediated uptake is a type of endocytosis where specific ligands are combined with receptor proteins of the cell membrane and subsequently internalized. These receptors are localized and concentrated in particular areas of the membrane called coated pits or migrate in these zones after binding to the molecule, which should be transported. The coated pits are characterized by the presence of a layer of peripheral membrane proteins known as clathrins. Once the receptors are bound to specific molecules, the dimple folds back into the cell and forms a vesicle covered by the clathrin layer and containing the substance of interest. Subsequently the vesicle loses the clathrin becoming an endosome, which then forms two vesicles: one containing the receptors and the other containing the ligand. The receptors are

recycled and return to the plasma membrane while the ligand-containing vesicle merges with the lysosome to form a secondary lysosome whose content, once digested, is released into the cell (Figure 14). [160]

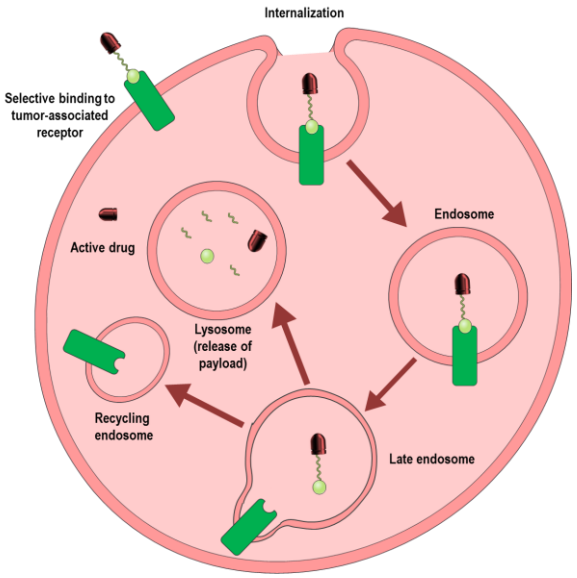

Figure 14. Receptor mediated uptake of SMDCs. After internalization, the linker is cleaved in the lysosome, the free drug is released from the ligand and it can express the activity on the particular target (tubulin, DNA, neighbouring cells). Adapted from Khalil *et al.* [160]

An integrin heterodimer can follow more than one internalization route. Both proteins caveolin and clathrin are able to interact with the tails of $\alpha_v\beta_3$ integrin and trigger the vesicles formation. [161-163] In this context, Coll and coworkers investigated the integrin mediated-internalization pathway of a multimeric cRGD ligand showing that this was able to bind to two integrins at the same time favoring clustering and subsequent internalization *via* clathrin coated vesicles. [164] However, issues concerning the respective contributions made by integrin dependent vs independent endocytosis remain largely unresolved. [165-166]

For the GnRH receptors, it has been demonstrated that ligand binding induces receptor dimerization and the formation of small receptor groups, which are internalized. Following the internalization, the hormone-receptor complex undergoes degradation in the lysosomes and a fraction of the receptors is recovered on the plasma membrane, thus participating in a recycling process strongly related to the up-regulation of receptors after GnRH stimulation. The agonists are internalized very fast: after 15 minutes, the complexes are already transferred to the lysosomes and after 30 minutes the shift is completed. [167]

1.6. CPPs as carrier molecules and their role in cancer therapy

The bioavailability and efficiency of many biological therapeutic molecules is frequently restricted by their chemical features, in particular their large size and hydrophilicity, which

contrast with the ability to passively diffuse through the membrane and internalize in the cell reaching their site of action. This issue consequently leads to a diminished therapeutic effect or even complete loss of activity. The conception of an efficient drug delivery in living cells is therefore an essential challenge in the development of new drugs. [168] To overcome this problem, during the last years, many research groups have been working on new transport vectors called cell-penetrating peptides (CPP). These are short peptides, up to 30 amino acids, with low cytotoxicity and exceptional translocation properties being able to pass cell membranes without destroying membrane integrity. [169-170]

Since the discovery of TAT in 1988, originated from a transactivating regulatory protein in HIV, [171-172] and penetratin a few years later, derived from the *Drosophila antennapedia* homeodomain, [173-174] the development of innovative CPPs has rapidly expanded. [175] Other members included in the class of natural CPPs were identified later, as for example VP22 from virus Herpes simplex [176] and pVEC, [177] a peptide of 18 amino acids derived from the cadherin of murine vascular endothelium. Based on these discoveries and on SAR studies showing that the amino acid arginine plays a fundamental role in the uptake, various synthetic CPPs have been also developed and comparable results in cell internalization were obtained. The most known representatives of this group are the synthetic oligopeptides R8/9 consisting in poly-arginine sequences displaying maximum translocation efficiency. [178-179] In our research group the CPP sC18 was developed. [180] It derives from the *C*-terminal domain of the cationic antimicrobial protein CAP18, consists of 16 amino acids and belongs to the group of amphipathic CPPs. Its internalization is time- and concentration- dependent and mainly occurs through endosomal pathways, when cargoes are attached. [180-182] Furthermore, the *C*-terminal truncated fragment sC18*, lacking the last four amino acids, also shows a cell-penetrating ability, although weaker than sC18, probably due to the two missing positive charged lysine residues. [183-184] These two CPP variants have been used in this work. In Table 1, important members of the CPP family are listed with their correspondent amino acid sequences and origin.

Table 1. Name, sequence and source of some important CPPs.

Name	Sequence	Origin	Reference
TAT	GRKKRRQRRRPPQ	HIV-1	[171-172]
polyarginine	R_n	Synthetic	[178, 185]
pVEC	LLIILRRRIRKQAHAHSK	VE-cadherin	[177, 186]
Penetratin	RQIKIWFQNRRMKWKK	*Drosophila antennapedia*	[173-174]
VP22	NAATATRGRSAASRPTQR	VHS	[176]
sC18	GLRKRLRKFRNKIKEK	CAP18	[180-181, 187]
sC18*	GLRKRLRKFRNK		[183]

Notably, even if the sequence and secondary structure of these peptides are divergent, the mechanism of transfer within the cells seems to be quite similar. Thanks to the favorable attributes of these peptides, they can transport inside the cell covalently or electrostatically bound cargoes, from small therapeutic molecules to plasmid or nanoparticles that otherwise could not pass through the cell membrane. [188-189] In order to ensure an efficient drug delivery into the target cell, it is fundamental to understand the uptake mechanism. So far, the exact process has not been definitively disclosed yet and contrasting data are described even if it is believed that the internalization always starts by interacting with the components on the surface of the plasma membrane (proteoglycan, phospholipids). The main uptake route for CPPs occurs *via* energy-dependent endocytosis, although direct translocation also exists under certain conditions and it cannot be excluded that the different internalization mechanisms are concomitantly used (Figure 15). In particular, the type of internalization depends on a variety of factors such as the type of CPP, the peptide concentration, the type of cargo molecule, the cell type, and the lipid composition. [190]

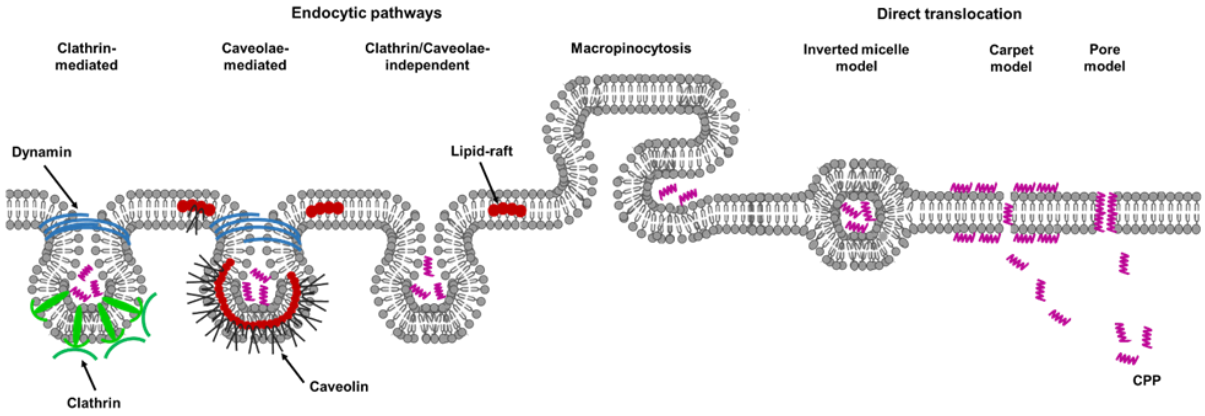

Figure 15. Cellular uptake mechanisms of CPPs. Adapted from Mickan *et al.* [191]

The internalization of CPPs *via* endocytosis is divided into different subclasses, including clathrin, caveolae, lipid-raft mediated endocytosis and macropinocytosis. [192-193] Differently, the uptake *via* direct translocation involves several models, primarily based on the interaction of the negatively charged membrane and the positively charged CPP sequence. The *inverted micelle* model, originally proposed for penetratin, describes the uptake of CPPs caused by the strong attractive potential between positive residues, in particular arginine, and the anionic phospholipids. After merging with the membrane, a subsequent interaction of the hydrophobic amino acids with the hydrophobic tails of the phospholipids occurs, resulting in the reorganization of the bilayer and formation of inverse micelles that release the CPPs into the intracellular space. The *pore formation* model describes the generation of transient pores resulting from the bundles originated from the amphipathic α-helical structure of CPPs, where the hydrophobic residues interact with the lipid tails of the phospholipids while the hydrophilic side chains are directed towards the lumen of the pore. Differently, in the *carpet model*, the

entry into the cell is facilitated by the parallel alignment of the CPP sequence on the membrane surface in a carpet-like manner until a maximal concentration is reached. This provokes the rotation of the peptide with the subsequent interaction with the hydrophobic core of the membrane leading to its destabilization and the subsequent penetration of the CPP. [194-198]

The indisputable efficiency of this drug delivery system in cancer therapy is hindered by the lack of selectivity so that many researchers had to deal with some new strategies in order to overcome this disadvantage, which could lead to unwanted toxicity and side effects on healthy cell lines. [197] One approach is to combine CPPs with homing peptides targeting particular receptors overexpressed on the surface of cancer cells. This strategy is depicted in Figure 16 where some examples of active targeted CPPs are exemplified.

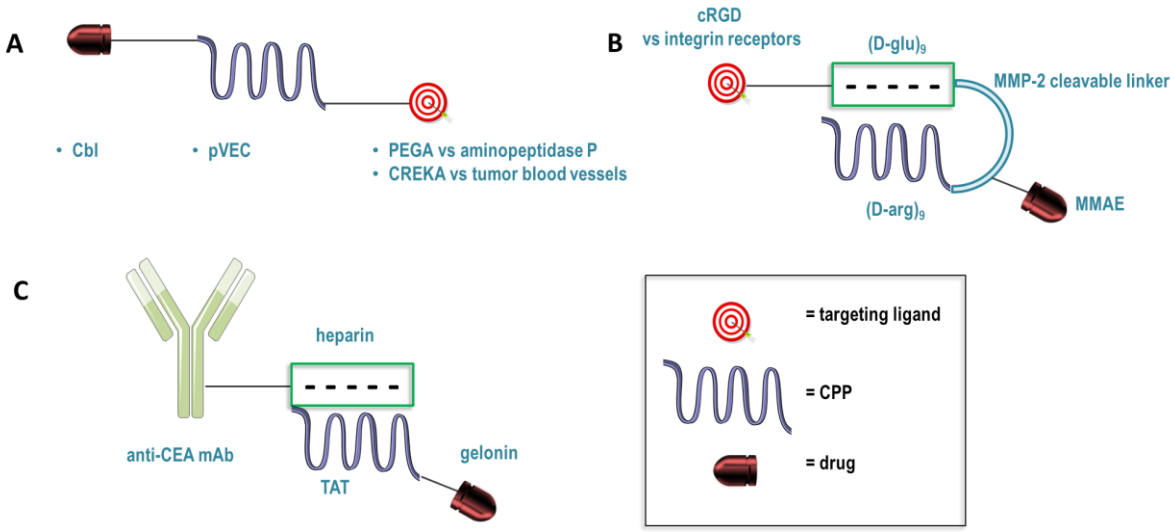

Figure 16. Different approaches to develop selective CPPs. A: Conjugation of a homing peptide to the CPP sequence; **B**: The CPP is masked by a negatively charged sequence and the construct is selectively directed towards tumor cells by the homing peptide. In the tumor environment, the linker will be cleaved by MMP-2 and the CPP will restore its penetration ability. **C**: The targeting moiety is represented by a mAb, conjugated to a molecule of heparin, which is electrostatically interacting with the CPP. Adapted from Martin *et al.* and Kurrikoff *et al.* [199-200]

For example, Langel and coworkers conjugated the two homing peptides PEGA and CREKA to the CPP pVEC to carry the cytotoxic payload chlorambucil in breast tumor cells. In both cases the system improved the cytotoxicity of the drug and the selectivity of the first compound could be even demonstrated *in vivo*. [74, 201] CPP-drug conjugates with monomethylauristatin E have been designed by Crisp *et al.* to selectively target tumor cells overexpressing integrin receptors, by adding the ligand cRGD. [202] This strategy involved the preparation of an activatable CPP attached to a negatively charged sequence that should prevent the anticipated internalization of the construct on healthy cell lines. These two elements are in fact combined *via* a MMP-2 cleavable linker that would be selectively cleaved in the tumor environment where

these enzymes are overexpressed. Also in this case, *in vivo* studies could demonstrate an improved tumor targeting. However, not only homing peptides could be used as targeting moieties. An example is the employment of a mAb conjugated to heparin and further complexed with a TAT-gelonin construct as described by Shin *et al.*, which was also validated in several *in vivo* models. [203]

A part from selectivity, blood stability is also a very important attribute that a drug should possess in order to reach the target without being degraded by blood proteases before arriving to the tissue. [204] This obstacle can be circumvented applying different shielding strategies in order to protect the structure of the CPPs till reaching the desired tissue and utilizing for instance more stable D-amino acid configurations or [205] backbone cyclization. [183, 206-207] Further development of CPPs through cyclization strategies will be highlighted in the following section.

1.7. Rational for cyclic peptides

Cyclic peptides are an unusual class of compounds, first discovered in microorganisms, [208] and subsequently object of great interest from the scientific community due to their attractive biological activities. [209] Among them are antibiotics, such as bacitracin [210] and polymyxin B, [211] immunosuppressive agents as cyclosporine A, [212] or also toxins such as α-amanitin, the poison of the mushroom *Amanita phalloides*. [213] All of these compounds have been very actively investigated as potential sources for new drugs and antibiotics. The three-dimensional conformation of these peptides is more rigid than that of their linear analogues, which could partly explain the observed increase in receptor selectivity and biological activity. [214] Moreover, one of their most interesting features is the enhanced resistance to proteolytic enzymes in comparison to correspondent linear peptide chains, reaching a higher stability in the human body.[215-219] In addition, such cyclic peptides often include unusual amino acids, further enhancing their resistance against proteolytic degradation and improving their bioavailability. [220-222]

The concept of cyclization has been found wide acceptance with respect to modulate the biological activity of peptides including peptide carriers, such as CPPs. Their cyclization has been demonstrated to be an effective strategy for enhancing their proteolytic stability, cellular uptake rates and promoting endosomal escape, thus cytoplasmic distribution. [223-224] Indeed, endosomal escape is a decisive concern, since for many CPPs the main entry pathways proceed *via* endocytic mechanisms. In fact, the CPP construct must be internalized by cells, but more importantly, cargoes have to be released and reach their extra-endosomal targets in the cytosol or in the nucleus.

1.7.1. Previous work

Recently, triazole-bridged cyclic peptides were synthesized and characterized in our research group. [206] In more detail, a fragment of the cell penetrating peptide sC18 (GLRKRLRKFRNK, namely sC18*) was cyclized *via* chemoselective copper-catalyzed azide-alkyne cycloaddition (CuAAC) in three different ways, yielding three different ring sizes.

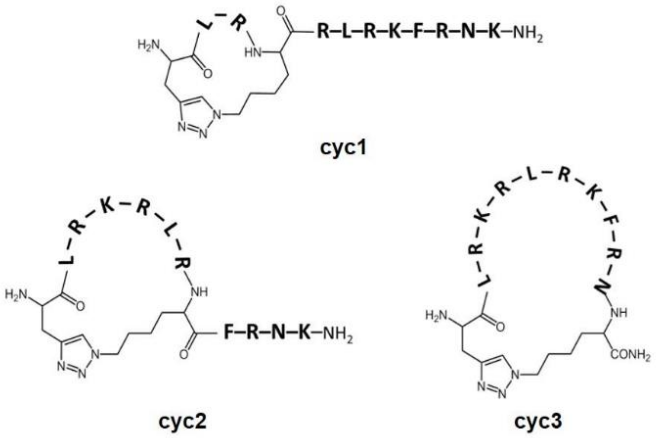

Figure 17.Structures of the sC18*-derived cyclic peptides synthesized in our group. [184]

These cyclic CPPs were evaluated regarding cellular uptake, toxicity and interaction with lipid systems. It has been observed that the internalization rate was strongly associated with the number of arginine residues included in the cycle. The peptides contain respectively one, three or five arginine residues and show an improved cell internalization in this order. The rigid presentation of guanidinium groups leading to the enhancement of the internalization efficiency has been already described by Lättig-Tünnemann *et al.* in 2011: when guanidinium groups were forced into maximally distant positions by peptide cyclization higher uptake rates have been registered. [225] Also in this case, the improved interaction with negatively charged constituents of the membrane played an important role in cell entry. A certain cancer selectivity was demonstrated too, since the internalization pattern in MCF-7 breast cancer cells was mainly cytosolic and nuclear, speaking for a direct penetration and good membrane permeability, differently from the endosomal distribution observed in HEK-293 (human embryonic kidney) healthy cells. Our results let conclude that particularly **cyc-3** benefited from cyclization, since it demonstrated improved lipid-peptide interaction and thus, cellular uptake properties.

1.7.2. DKP scaffolds

Peptide cyclization can be achieved in different ways, commonly divided into two groups: head-to-tail (*C*-terminus to *N*-terminus) and side chain-to-side chain cyclization, the latter involving various strategies, like thioether and disulfide bond formation, lactone/lactame formation, ring closing metathesis and the previously mentioned CuAAC. [226-227] Encouraged by the previously

described results, we planned to replace the triazole bridge with a more spatially oriented and rigid scaffold such as the bifunctional diketopiperazine scaffold (DKP).

From the DKP library developed in the group of Prof. Piarulli and Gennari, the cis (DKP1) and trans (DKP3) diketopiperazine rigid scaffolds, previously depicted in Figure 12, were chosen for the synthesis of cyclic compounds. These two DKP scaffolds showed completely different characteristics in the conformation of small cyclic peptide sequences evaluated in previous studies. While DKP1 acted as a reverse turn inducer, DKP3 promoted the formation of an extended structure. [152-153] Therefore, the comparison of cyclic peptides containing different DKP scaffolds would be of great interest.

2. Aims of the thesis

2.1. Receptor-targeted CPPs for selective delivery of anticancer therapeutics

Insufficient cellular uptake of new therapeutic drug candidates often limits their clinical use. A promising strategy to solve this permeability obstacle is represented by CPPs, conveniently used as appropriate vectors for these applications. They appear to be very advantageous and versatile tools to deliver anticancer molecules which otherwise would not be able to cross the plasma membrane barrier by their own and the safety of these devices was demonstrated in many works, allowing their extensive use for *in vitro* or *in vivo* studies. However, their entry mechanisms appear to vary with experimental conditions, cargo, types and the details of the various uptake ways are poorly understood. Furthermore, none of the studied internalization pathways indicated certain selectivity towards cancer cells and this is in total contrast with the outstanding development in the course of the last years of selective strategies to limit side effects. Trying to fill this gap in the research, the first part of this work will be dedicated to the synthesis of novel drug delivery systems constituted by a CPP (sC18) bearing a cytotoxic warhead and attached to a targeting ligand (GnRH-R or integrin ligand) by a PEG spacer. By this way, we wanted to overcome the selectivity issue in CPP delivery, trying to study which entry mechanism would prevail when this construct came in contact with different cell lines expressing the receptor of interest at a different level. For this purpose, we wanted to find an optimal strategy for the successful synthesis of these conjugates and subsequently biologically test them in different cell systems. In particular, we wanted to analyze which role would play the receptor-mediated uptake compared to the traditional entry mechanisms previously described for CPPs, including endocytosis and direct penetration through the membrane. We tried to evaluate this tendency by choosing ideal cell models, which would permit the comparison of the different uptake behaviors in presence or absence of the receptors of interest.

2.2. Cyclic CPPs for cargo delivery

A part from the difficulties encountered in designing selective molecules, the use of CPPs is often severely restricted because of their low proteolytic stability in biological fluids and rapid degradation in the organism after administration. By cyclization of the peptide backbone, the linear truncated version of sC18 has recently displayed an increased internalization rate and stability. In the second part of this work, the focus was on the synthesis and characterization of analogues of the cyclized sC18* derivatives recently synthesized by Florian Reichart during his PhD thesis. Therefore, the triazole bridge obtained by CuAAC reaction should be substituted with a DKP scaffold and different conditions should be attempted to obtain a final optimization of the cyclization reaction. Afterwards, the secondary structure of the obtained

molecules should be investigated in details by CD and NMR spectroscopy and compared to the linear peptides. Furthermore, their potential for drug delivery should be determined by generating non-covalent and covalent complexes with cytotoxic drugs. To measure the efficacy of the drug transport through the membrane and of the effect on cell viability, cytotoxicity assays and cellular uptake studies should be performed and the results compared to those of the linear counterparts.

3. Novel CPP-drug conjugates bearing a targeting moiety

3.1. GnRH-III as targeting moiety and daunorubicin as cytotoxic payload

Since GnRH receptors are expressed in different types of tumors but not in healthy cells, they could represent an interesting target in the context of tumor selectivity. For this reason, many GnRH-drug conjugates have been synthesized and investigated. In this work, the GnRH-III derivative developed by Mező and co-workers, where Lys^4 was butyrylated, has been used as targeting moiety in our drug delivery system, while daunorubicin (Dau) served as cytotoxic payload. [131] To simplify the nomenclature of the synthesized conjugates, from now on the sequence <EHWK(Bu)HDWKPG-NH_2 will be indicated with the name GnRH-III. Any further conjugation to the GnRH-III sequence always occurred at Lys^8, since it was often confirmed to be a good conjugation site, not invalidating the selectivity and activity of the conjugate (Figure 9). [228-229]

Considering that small variations at the sugar moiety of daunorubicin caused a drastical decrease in activity, it could be deduced that the daunosamine is involved in the interaction with DNA; [126, 230] for this reason, to easily conjugate the drug to the peptide, the amide bond formation with the amino group of the sugar was not possible without the contemporary drastic loss of activity. Due to its structural properties, daunorubicin cannot be conjugated to the targeting moiety by ester bond like doxorubicin but the ketone group allows the formation of oxime bonds originating conjugates with high stability under physiological conditions. In some works an enzymatic cleavable linker, the commonly used tetrapeptide GFLG, was added to allow the release of the drug after cleavage by cathepsin B, which is known to be overexpressed in tumor cells. [231-232] It has been demonstrated that the release of the free drug is not necessary for the antitumor activity of the conjugate since the amino acid-Dau metabolite is also able to intercalate with the DNA with sufficient efficiency. [132] Through this approach, it was possible to obtain selectivity with a small decrease in activity compared to the free drug. [131]

To further investigate the intracellular drug release and the effect on multi-drug resistant cancer cells, we decided to add another important portion to the construct resulting in a new hybrid conjugate composed by a targeting moiety (GnRH-III), a carrier moiety (CPP) and the drug. Two different variants, with and without cleavable linker were designed and synthesized. The synthetic strategy will be discussed and most importantly, the binding affinity of these conjugates will be analyzed in detail comparing two overexpressing cell lines (healthy pituitary gland and prostate cancer cells). Moreover, cytotoxicity of the novel conjugates on receptor positive and negative cell lines will be shown.

3.1.1. Synthetic strategy

The peptide sC18 served as starting point for the conjugation of daunorubicin. As illustrated in Figure 18, one first modification was introduced at the side chain of lysine at position 8 within the peptide sequence, whereby coupling of daunorubicin was performed *via* oxime ligation by insertion of an aminooxyacetic acid spacer yielding the two CPP-drug conjugates **sC18(Dau)** and **sC18(GFLG-Dau)**, the latter containing the enzymatic cleavage site GFLG. These two conjugates were used as control peptides for further investigation of the selectivity in comparison with the targeting constructs. Drug conjugation by oxime bond was successfully performed but particular care had to be taken to increase the yields and facilitate the purification of the final product. Notably, as already described by Mező *et al*., [233] 10 eq. of Boc-aminooxyacetic acid were added to the cleavage cocktail and in general use of acetone and plastic consumables was limited in order to prevent the formation of the acetone and formaldehyde adducts with delta mass +40 and +12. [228, 234] In addition, the temperature for every reaction step was maintained under 40 °C to avoid the release of the sugar moiety and the subsequent decrease of the cytotoxicity. For the conjugation of the two elements, the glycine at the *N*-terminus of the CPP sequence was replaced by propargylglycine, while, in collaboration with the PhD student Sabine Schuster (ELTE University, group of Prof. Mező, Budapest), the GnRH-III ligand was synthesized and the side chain of Lys^8 within the GnRH-III sequence was functionalized by incorporation of 2-azidoacetic acid. This allowed the “click” reaction (CuAAC) within the two moieties.

Nevertheless, the conjugation to the functionalized GnRH-III was the yield-limiting factor. The reaction was carried out as described by Raposo Moreira Dias *et al.* [235] and the azido-functionalized ligand was used in excess (1.3 eq.). The reaction worked very well and no limiting reactant was detectable after completion but some difficulties occurred with the purification of the crude product, leading to very low yields (20-30%). Furthermore, the recovered mixed fractions could not be separated even by changing the gradient or using columns with different polarity. This problem could be solved by modifying the reaction conditions. This time an excess of the more hydrophilic alkyne-functionalized sC18 (1.3 eq.) was added, by means of which the starting GnRH-III was completely converted in the product and the CPP could be easily separated from the final conjugate due to their different retention time, reaching 91% yield (see Table 20 in the attachment).

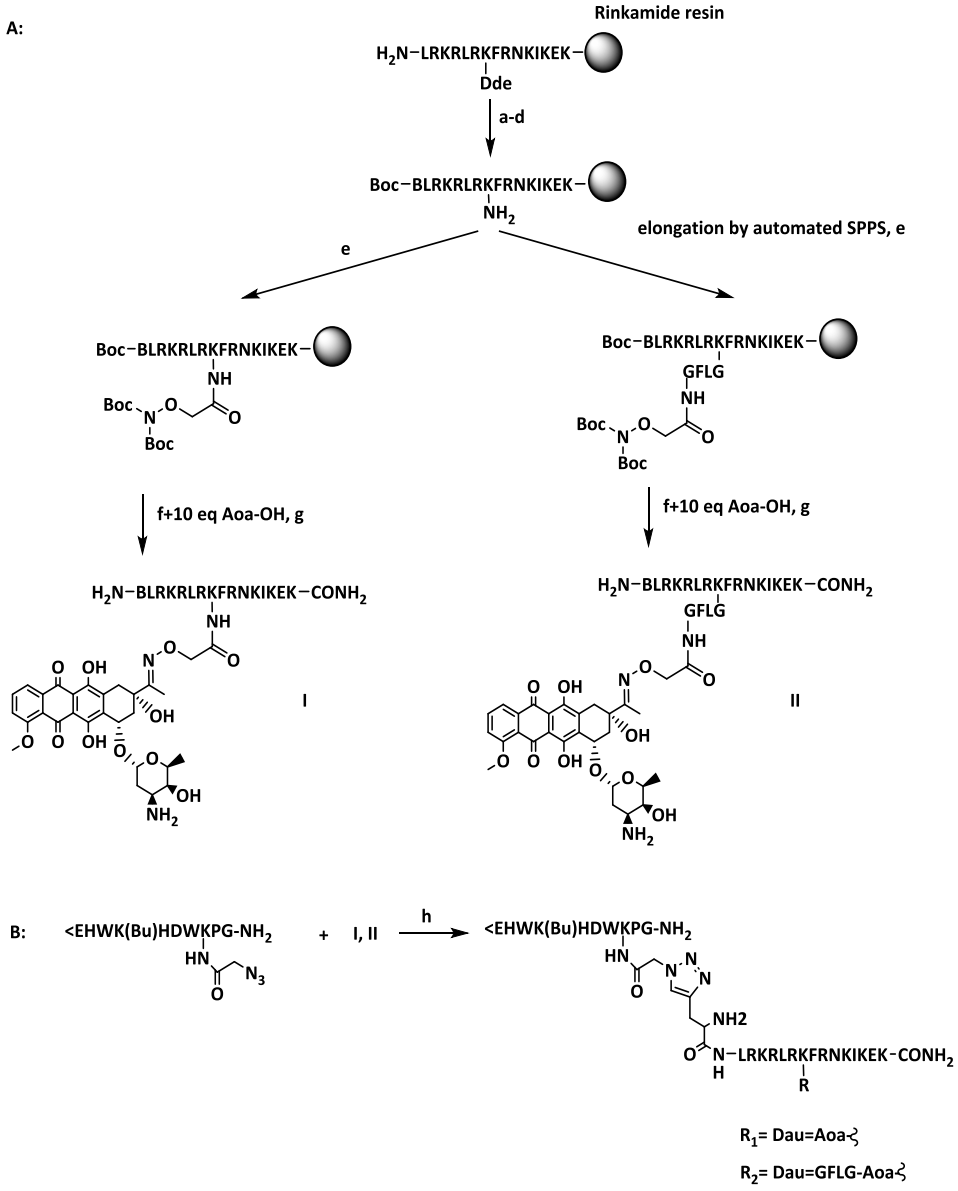

Figure 18. Synthetic strategy of the full conjugates GnRH-III-sC18(Dau) and GnRH-III-sC18(GFLG-Dau). A: Synthesis of the peptide sequence by SPPS, followed by conjugation of daunorubicin. **B**: "Click" reaction between the azido group of GnRH-III and the alkyne group at the *N*-terminus of the CPP. Reagents and conditions: **a**: 5 eq. Fmoc-L-Pra-OH (B), 5 eq. Oxyma, 5 eq. DIC in DMF, overnight; **b**: 30% piperidine in DMF (20 min x 2); **c**: 10 eq. Boc_2O, 1 eq. DIPEA in DCM for 2 h (2x); **d**: 2% hydrazine in DMF (10x); **e**: 5 eq. Bis-Boc aminooxyacetic acid, 5 eq. Oxyma, 5 eq. DIC in DMF, overnight; **f**: TFA/TIS/H_2O (95:2,5:2,5), 3 h; **g**: 30% excess daunorubicin, 0.2 M NH_4OAc, pH 5, 10 mg/ml; **h**: 1 eq. GnRH-III(N_3), 1.5 eq. **I** or **II**, 0.5 eq. $CuSO_4 \cdot 5H_2O$, 0.6 eq. Na ascorbate, H_2O:DMF 1:1, 10 mM, 40 °C, N_2, 24 h

Three different conjugates were synthesized (see Table 2). **GnRH-III-sC18**, not bearing the drug, served as a control conjugate in order to investigate the selectivity in presence of the large and hydrophilic CPP. The additional GFLG linker in **GnRH-III-sC18(GFLG-Dau)** was introduced between the drug and the CPP to evaluate if the activity could be enhanced in respect to **GnRH-III-sC18(Dau)**.

Table 2. List of the synthesized GnRH-III conjugates and controls with their names, structures and molecular weights (calculated and experimental).

Conjugate	Structure	MW [g/mol]	MW_{exp} [g/mol]
GnRH-III-sC18	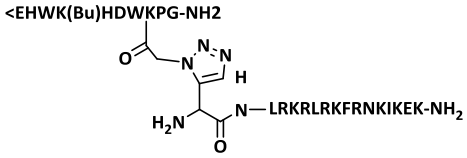	3561.2	3560.7
GnRH-III-sC18(Dau)	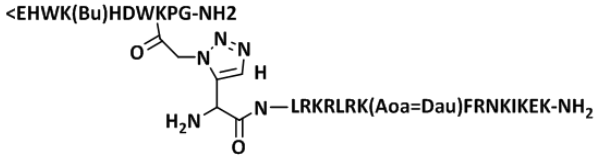	4144.3	4145.2
GnRH-III-sC18(GFLG-Dau)	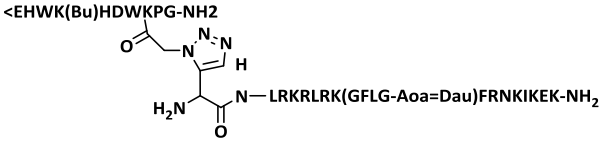	4518.7	4519.7
sC18(Dau)	GLRKRLRK(Aoa=Dau)FRNKIKEK-NH_2	2652.2	2653.2
sC18(GFLG-Dau)	GLRKRLRK(GFLG-Aoa=Dau)FRNKIKEK-NH_2	3027.0	3027.9

3.1.2. Triptorelin binding assay

The affinity of the novel GnRH-III conjugates to GnRH-Rs was investigated by means of a radioligand binding study, performed at the Department of Biopharmacy (Faculty of Pharmacy) at the University of Debrecen, as previously described. [131] Radioiodinated triptorelin was used for this purpose, since it provides a high binding affinity to GnRH-I receptors. In the present study, the *in vitro* competition assay was executed on human pituitary and human prostate cancer cells, both overexpressing the receptors, and the displacement of the radiolabeled triptorelin was evaluated to characterize the binding affinity of the novel conjugates. It has been confirmed by many studies that the receptors in cancer cells are exactly the same as the pituitary receptors [236] but, at the same time, it has been also speculated about the presence of distinct receptor conformations in different tissues leading to selective binding to specific ligands and various intracellular signaling pathways (antagonist or agonist action). [237-238] Furthermore, high affinity/low capacity and low-affinity/high capacity receptors have been found from the investigation of different research groups. [239] To prove that our conjugates could bind with high affinity also on cancer cells, both tissues were analyzed.

Table 3. IC_{50} values corresponding to the ability of the GnRH-III conjugates to replace [^{125}I]-triptorelin. K2 was also analyzed and served as reference.

Conjugate	IC_{50} (nM) Human pituitary gland	IC_{50} (nM) Human prostate cancer
GnRH-III-sC18	14.7 ± 2.3	17.8 ± 2.2
GnRH-III-sC18(Dau)	24.5 ± 0.8	20.9 ± 2.7
GnRH-III-sC18(GFLG-Dau)	27.1 ± 1.4	29.6 ± 1.4
K2 (GnRH-III-Dau)	3.9 ± 0.7	3.0 ± 1.1

The novel conjugates were compared to the lead compound **K2** (<EHWK(Bu)HDWK(Aoa=Dau)PG-NH_2, synthesized by Sabine Schuster) that was recently reported to have a high affinity in low nM range towards GnRH-I receptors. [54] The results illustrated in Table 3 are very promising: even if control K2 displays better results, the binding affinity of the hybrid-conjugates is slightly reduced, but still in low nM range, underlining that the attachment of the CPP does not substantially alter the overall receptor binding. In fact, one could think that the CPP would be too large to preserve the selectivity of the GnRH peptide but, as already demonstrated in many studies, the Lys^8 of GnRH-III, is a very good attachment point in order to maintain the structure of the targeting moiety and subsequently the high affinity. Another important remark that can be made after analyzing the data is connected with the size of the whole conjugate: the larger the dimension, the lower is the affinity to the receptor leading to almost a 10-fold decrease for **GnRH-III-sC18(GFLG-Dau)** in prostate cancer tissue compared to **K2**. Furthermore, as expected, no significant selectivity between pituitary gland and cancer cells could be detected and this is valid also for **K2**. The **GnRH-III-Dau** conjugate cannot easily cross the blood-brain barrier (BBB); therefore, it has only moderate toxic side effects at the level of the hypophysis. The remaining question is how the CPP would influence the crossing of the BBB. A recent study demonstrated that this ability is not directly connected with the cell-penetrating property of the CPP, but that arginine rich cationic amphipathic CPPs show a better internalization. [240] This circumstance was evaluated for sC18 in more detail and a recent *in vivo* study shows that sC18 is not accumulating in the brain but only in the ventricles, which would circumvent the possible generation of side effects in pituitary gland. [241]

3.1.3. Cell viability assays

Since the results from the receptor binding studies were very encouraging, we decided to investigate the cytotoxicity of the compounds on GnRH-IR positive and negative cell lines. The expression of the receptor on the surface of different cell lines was evaluated by Sabine Schuster by western blot analysis. The western blot was performed on whole cell lysates using an anti-GnRH-receptor antibody (Proteintech) and various cell lines were analyzed. As

depicted in Figure 19, PANC-1 showed a very low signal together with Ovcar-3 and MRC-5 cells while good positive controls were represented by A549 and U87 cells.

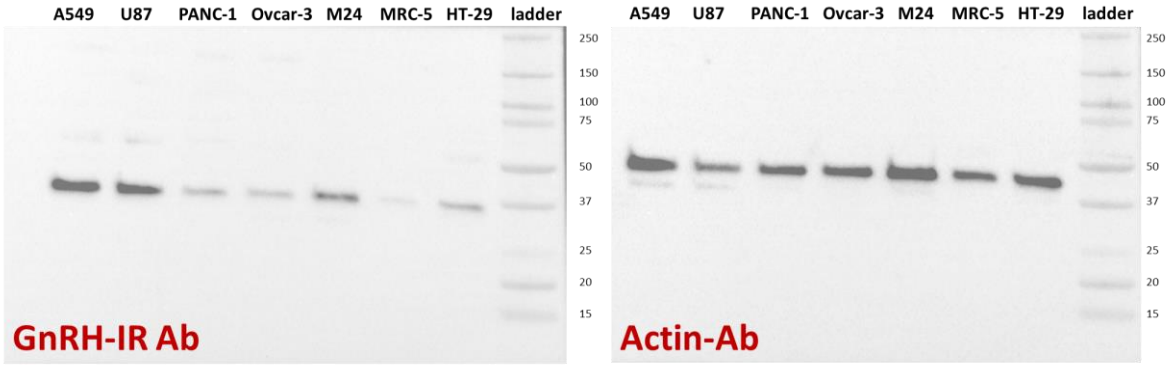

Figure 19. Western blot studies on cell lysates of A549, U87, PANC-1, Ovcar-3, M24, MRC-5 and HT-29 cells. Actin expression was evaluated as loading control.

The cytotoxicity of **K2** was already evaluated by Sabine Schuster on all these cell lines after 24 h incubation (data not shown). While in U87 and A549 cells the drug conjugate showed almost the same median effective concentration EC_{50} (around 10 µM), a remarkable difference was detected in the case of the other cell lines. In particular, the results obtained from MRC-5 and Ovcar-3 cells showed a 4- to 5-fold higher value of EC_{50} and this value was doubled in the case of PANC-1 (>100 µM). This was a further confirmation of the results of the western blot. For this reason, PANC-1 and U87 cells were chosen as negative and positive control cell lines, respectively.

In the case of our novel constructs, we decided to adopt the strategy of a short treatment time to ideally simulate the *in vivo* situation, where the drug, after administration of the therapeutic molecule, should easily and selectively penetrate cancer cells as soon as it is in their proximity. In order to choose the right contact time of the novel conjugates, the uptake of CF-labelled sC18 in U87 cells was analyzed *via* flow cytometry at different incubation times (Figure 20). The cellular uptake of CF-sC18 was evaluated after 5, 15 and 30 minutes, as we reasoned that these intervals could highlight the importance of the CPP for a quick and efficient penetration and at the same time emphasize the relevance of the ligand targeting ability for a selective approach. A 15 minutes incubation time was chosen as optimal compromise between 5 minutes (too much stress to the cells and poor reproducibility of results) and 30 minutes (too long, since the cell-penetrating activity could be too high and cause a negative influence on the selectivity of the system and the conjugates could interact with the receptors on the surface of the negative control cell lines, even if expressed at lower level).

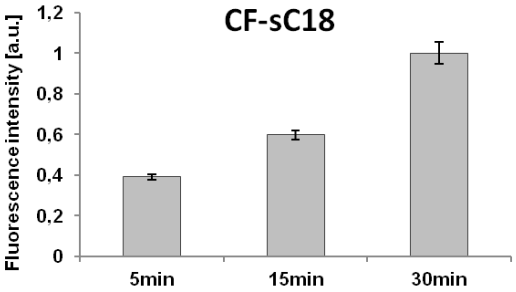

Figure 20. Quantification of the cellular uptake of the CF-labeled sC18 after 5, 15 and 30 min incubation with U87 cells. U87 cells were incubated for 5, 15 and 30 minutes with 10 µM peptide solution. The value corresponding to the untreated cells was used as negative control and subtracted from the other values. The experiment was performed in triplicate with *n=1.*

Before analyzing the activity of the drug conjugates, **GnRH-III-sC18** needed to be tested to prove that the targeted CPP could be considered as a good drug delivery system without showing any conspicuous toxicity. The CPP and the targeting moiety alone were also analyzed as controls.

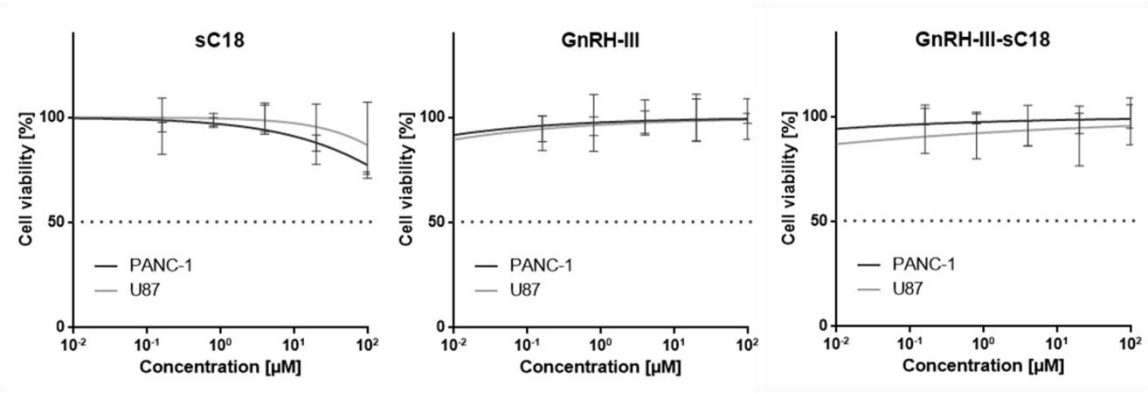

Figure 21. MTT-based antiproliferative activity of the targeted conjugate GnRH-III-sC18 and the controls sC18 and GnRH-III. The assay was performed incubating U87 and PANC-1 cells for 72 h with washout of the peptide solution after 15 min. Values from the positive control (DMSO/EtOH; 1:1) were substracted from all data and the untreated cells were set to 100%. The experiment was performed in triplicate with n=2.

As depicted in Figure 21, only **sC18** showed a slight toxicity but just at the highest concentration of 100 µM, which is in line with previous studies. [186] In general we can affirm that the targeted CPP could be used as safe and selective carrier, showing a high binding affinity to the receptor and no antiproliferative activity on both cell lines tested.

Afterwards, the drug conjugates **GnRH-III-sC18(Dau)** and **GnRH-III-sC18(GFLG-Dau)** were analyzed under the same conditions (Figure 22 and Table 4). In particular, we were interested to observe if the selectivity of the ligand detected by Sabine Schuster could still be preserved and how the toxicity changed in comparison to the free drug and the control peptides containing

exclusively the targeting sequence, **GnRH-III-Dau**, or the CPP, **sC18(Dau)** and **sC18(GFLG-Dau)**.

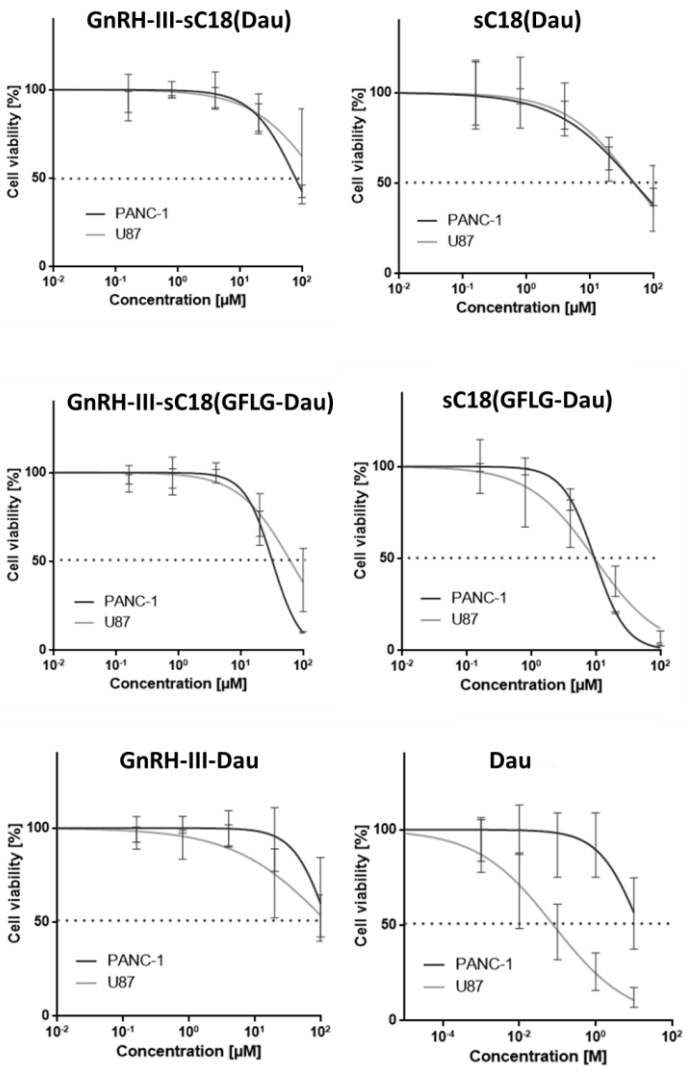

Figure 22. MTT-based antiproliferative activity of the targeted conjugates GnRH-III-sC18(Dau) and GnRH-III-sC18(GFLG-Dau), the controls sC18(Dau) and sC18(GFLG-Dau), the reference K2 (GnRH-III-Dau) and the free drug. The assay was performed incubating U87 and PANC-1 cells for 72 h incubation with washout of the peptide solution after 15 min. Values from the positive control (DMSO/EtOH; 1:1) were substracted from all data and the untreated cells were set to 100%. The experiment was performed in triplicate with n=2.

Table 4. EC_{50} values from the antiproliferative assay depicted in Figure 22 (washout after 15 minutes and further incubation for 72h).

EC_{50} (µM)						
	GnRH-III-sC18(Dau)	**sC18(Dau)**	**GnRH-III-sC18(GFLG-Dau)**	**sC18(GFLG-Dau)**	**GnRH-III-Dau (K2)**	**Dau**
U87	>100	42.2 ± 19.2	62.9 ± 20.3	9.6 ± 3.2	>100	0.078 ± 0.008
PANC-1	78.8 ± 23.1	79.9 ± 56.4	32.13 ± 5.8	9.4 ±0.9	>140	>10

Considering the results of the free daunorubicin, we directly notice an outstanding difference between the two cell lines, whereby the EC_{50} in PANC-1 cells is around 50 times higher than in U87 cells which is not correlated with the receptor expression since the free drug directly penetrates through the cell membrane. This result could be explained by literature data indicating PANC-1 as a MDR cell line expressing the Multidrug Resistance associated Protein1 (MRP1). [242] Daunorubicin typically enters cells *via* passive diffusion and is thus an easy target for the drug efflux pumps on the inner side of the plasma membrane. Thus, we can also correlate in a very rational way the results obtained by Sabine Schuster, in particular the much lower toxicity of **GnRH-III-Dau (K2)** shown in PANC-1 cells after 24h incubation in comparison to other negative control cell lines and the more than 10-fold lower EC_{50} compared to U87 cells (data not shown). A different pattern was observed when **K2** was tested under the short contact time conditions: in this case, the discrepancy between the two cell lines was not as evident as for the free drug. If we consider that the difference is not significant, we could conclude that 15 minutes are probably not enough time for the ligand to bind to the receptor and subsequently internalize at high efficiency. In contrast to this hypothesis, in previous works GnRH-gold conjugates were detected in the lysosomes of gonadotrophs already after 30 minutes [243] and the time-dependent uptake of **K2** was described with CLSM pictures by Schuster *et al*., displaying a colocalization with endosomes and lysosomes after 5 minutes incubation in MCF-7 cells. [54] Probably, after 15 minutes there could be a moderate but not sufficient uptake and the selectivity towards positive cell lines would be detected only after a longer incubation time. This highly interesting aspect was explored by Sedgley *et al*., who indicated that the absence of a cytosolic C-tail in GnRH receptors could penalize the plasma membrane localization. GnRH-R was found to be primarily an intracellular protein that traffics to the membrane surface from the endoplasmic reticulum and from cryptic receptor pools in the cytosol. [244] Extracellular signaling would recruit these intracellular receptors but this is a slow process pointing out that maybe the 15 minutes incubation are not enough. Additionally, the reason for the lower cytotoxicity of **K2** in U87 cells compared to the free drug, a part from the different uptake mechanism followed (receptor-mediated endocytosis and passive diffusion, respectively), was presumably attributed to the already described inability of releasing the free daunorubicin due to the high stability of the oxime bond and this is also true for all the other conjugates. The cleavage sites after incubation with rat liver lysosomal homogenate have been identified by Sabine Schuster [54] and H-Lys(Dau=Aoa)-OH was recognized as the smallest metabolite. Referring to the new synthesized compounds we could suppose that the release of the drug would occur after proteolysis at the level of the amino acid lysine, in the case of **GnRH-III-sC18(Dau)** and **sC18(Dau)**, and glycine in the compounds containing the cathepsin B cleavage site, **GnRH-III-sC18(GFLG-Dau)** and **sC18(GFLG-Dau)**. These metabolites

(Figure 23) are still able to intercalate to DNA but with a weaker activity leading to lower EC_{50} values than the free toxin.

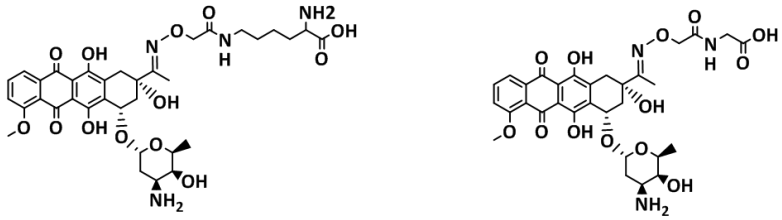

H-Lys(Dau=Aoa)-OH

Dau=Aoa-Gly-OH

Figure 23. Structure of the smallest Dau-containing metabolites obtained after lysosomal degradation of the peptide sequence.

If we analyze the conjugates containing the CPP sequence, we were very pleased to observe that the resistance in PANC-1 cells seemed to be overcome with the use of the CPP. The EC_{50} measured for **sC18(GFLG-Dau)** in PANC-1 cells was surprisingly lower than the value of the free drug and comparable to the EC_{50} measured for U87 cells. The ability of the drug to directly internalize in the cell is decreased but at the same time the intracellular accumulation of the drug was enhanced reducing the drug efflux, as already described by Zheng *et al*. [245] This emphasizes once more the potential of CPP for drug delivery. In this context, Lelle *et al.* in 2017 published a work about this aspect: utilizing a CPP carrier they could successfully bypass the activity of membrane proteins such as P-glycoprotein, effectively increase the intracellular concentration and enhance efficacy of the drug in anthracycline resistant cells. [246] Observing the EC_{50} values of the CPP controls, we can notice that their activity is stronger than for **K2** in both cell lines, presupposing an efficient internalization mechanism guided by direct translocation or endocytosis with subsequent lysosomal cleavage. This demonstrates that sC18 can be used as very proficient carrier. In general, the compounds containing the GFLG cleavage site displayed a stronger activity and **sC18(GFLG-Dau)** could be identified as the most powerful compound of these series. The higher toxicity can be explained with the overexpression of cathepsin B inside the cells, which is able to cleave the peptide sequence at the level of the GFLG cleavable linker. We could think that the smaller metabolite Dau=Aoa-Gly-OH would favor the intercalation of the DNA but Orban *et al*. already demonstrated that the two metabolites (including glycine and lysine) show the same DNA binding characteristics. [132] On the contrary, the GFLG spacer is probably cleaved faster than the CPP sequence in the lysosomes. This would mean that Dau=Aoa-Gly-OH would be more rapidly released than H-Lys(Dau=Aoa)-OH. Since the drug is released in a much faster and more efficient way, this could also favor a further internalization of the peptide in the cytosol. Furthermore, the increase of hydrophobicity of the peptide sequence by addition of the linker could promote the penetration of the CPP leading to a subsequent higher toxicity. The comparison of the retention

time of compounds **sC18(Dau)** and **sC18(GFLG-Dau)** is illustrated in Figure 88 in the attachment. Other considerations should be done by comparing the conjugates containing the GnRH-III ligand, **GnRH-III-sC18(Dau)** and **GnRH-III-sC18(GFLG-Dau)**. The EC_{50} of the full conjugates are always higher if correlated to the CPPs and this could be explained by the addition of the targeting sequence, which is probably influencing the uptake ability of the CPP. We could in fact imagine that if the CPP alone could be taken up by direct translocation and endocytosis, the CPP bound to the ligand presumably internalize in a less efficient way. This hypothesis could be verified by secondary structure analysis of the conjugate (e.g. CD spectroscopy) to detect if the tendency of the CPP to form an α-helix would be hindered. Anyway, already by simple observation of the structure, we could imagine that such a branched system would not be inserted so easily inside the cell membrane. Unfortunately, the reduced cell-penetrating ability did not even favor selectivity: the conjugates containing the targeting moiety **GnRH-III-sC18(Dau)** and **GnRH-III-sC18(GFLG-Dau)** show a better activity in PANC-1 cells differently from U87 cells. This was unexpected, since the affinity shown by the triptorelin binding assay was pretty high but again this could be explained with the short incubation time as already described for **K2**.

In general, we could improve an efficient synthetic strategy to develop conjugates that involve a GnRH targeting unit and a CPP showing a very high binding affinity to receptors and demonstrating that the presence of CPP does not invalidate the ability to bind the receptor and the cytotoxicity of the drug. Unfortunately *in vitro* studies were not so decisive to show selectivity but these results could be justified by the unlucky choice of many factors, in particular the model used and the conditions of the experiment. First of all PANC-1 cells were chosen as negative control, since they express the receptor at a low level but during the experiments we could recognize that they were also resistant to the drug. This of course did not facilitate the evaluation of the data because it is a further factor to take into consideration. The other unfortunate condition was the choice of the incubation time. Even **K2** did not show a strong selectivity towards U87 cells after 15 min and this of course negatively influenced also the results for the CPP conjugates. It is possible that these selectivity issues could be overcome *in vivo* and this could be proven also by choosing other *in vitro* cell models and more ideal conditions. For example the choice of the short contact time was a very astute idea but maybe 30 minutes or one hour incubation could be also tested and would maybe lead to more consistent outcomes. A part from that, a positive result could be reached in the context of drug resistance and for this reason these conjugates, particularly **sC18(GFLG-Dau)**, are worth for a further investigation in this direction.

3.2. DKP*3*RGD as targeting moiety

Since the GnRH system did not show the expected results in terms of selectivity, we concentrated on another model using as targeting unit the previously introduced c[DKP*3*RGD]

synthesized in the research group of Prof. Gennari and Prof. Piarulli, which shows a high binding affinity towards $\alpha_v\beta_3$ integrin receptors. [153, 156] Various works where this ligand was conjugated to anticancer drugs have been already published showing a favorable targeting index when monomeric or multimeric RGD-paclitaxel conjugates were tested on different cell lines expressing the integrin receptors at different extent. [157, 235] However, contrasting results have been described in recent publications related to the possible interaction of this ligand with different integrins and subsequent loss of selectivity. [166, 247] Until now, no study has been done with the insertion of CPPs, thus we wanted to investigate how the activity and selectivity of these conjugates could be influenced by the presence of this carrier peptide.

3.2.1. Synthesis and biological evaluation of the drug delivery system

The functionalized integrin targeting ligand *c*[DKP*f3*RGD] was prepared as previously described [156] by the PhD students Silvia Panzeri and Sara Parente (research group of Prof. Piarulli). This was then functionalized with a commercially available bifunctional azido carboxylic PEG_4-spacer by a pH-sensitive reaction in ACN/phosphate buffer. The maintenance of a specific pH at 7.3-7.5 was necessary to allow the binding between the nucleophilic benzylic amine of the ligand and the carboxylic group of the spacer. The conditions were the same as described in Zanella *et al.* [159] and 88% yield was obtained. Afterwards, sC18 was connected to the ligand by CuAAC *via* its *N*-terminal propargylglycine leading to compound **1**. To study the cellular uptake, an additional modification was introduced at the side chain of lysine at position 8 within the sC18 sequence: labeling with 5(6)-carboxyfluorescein (CF) resulted in compound **1a**. The synthetic strategy, depicted in Figure 24, worked straightforward and, after optimizing the conditions, good yields could be obtained (see Table 20 in the attachment). At the beginning, the reaction was performed in *t*-BuOH:H_2O but the best results were achieved with DMF and H_2O, following the procedure described in Raposo Moreira Dias *et al*. [235]. Contrary to the GnRH-III-conjugates, the use of an excess of the azido compound led to better yields since the retention time of the CPP and the final conjugate would be otherwise too similar and problems during the purification would occur. The unlabeled and labeled CPPs (**2** and **2a**) were also synthesized as control to allow a direct comparison with the novel targeted drug delivery system. The synthesized compounds are listed in Table 5.

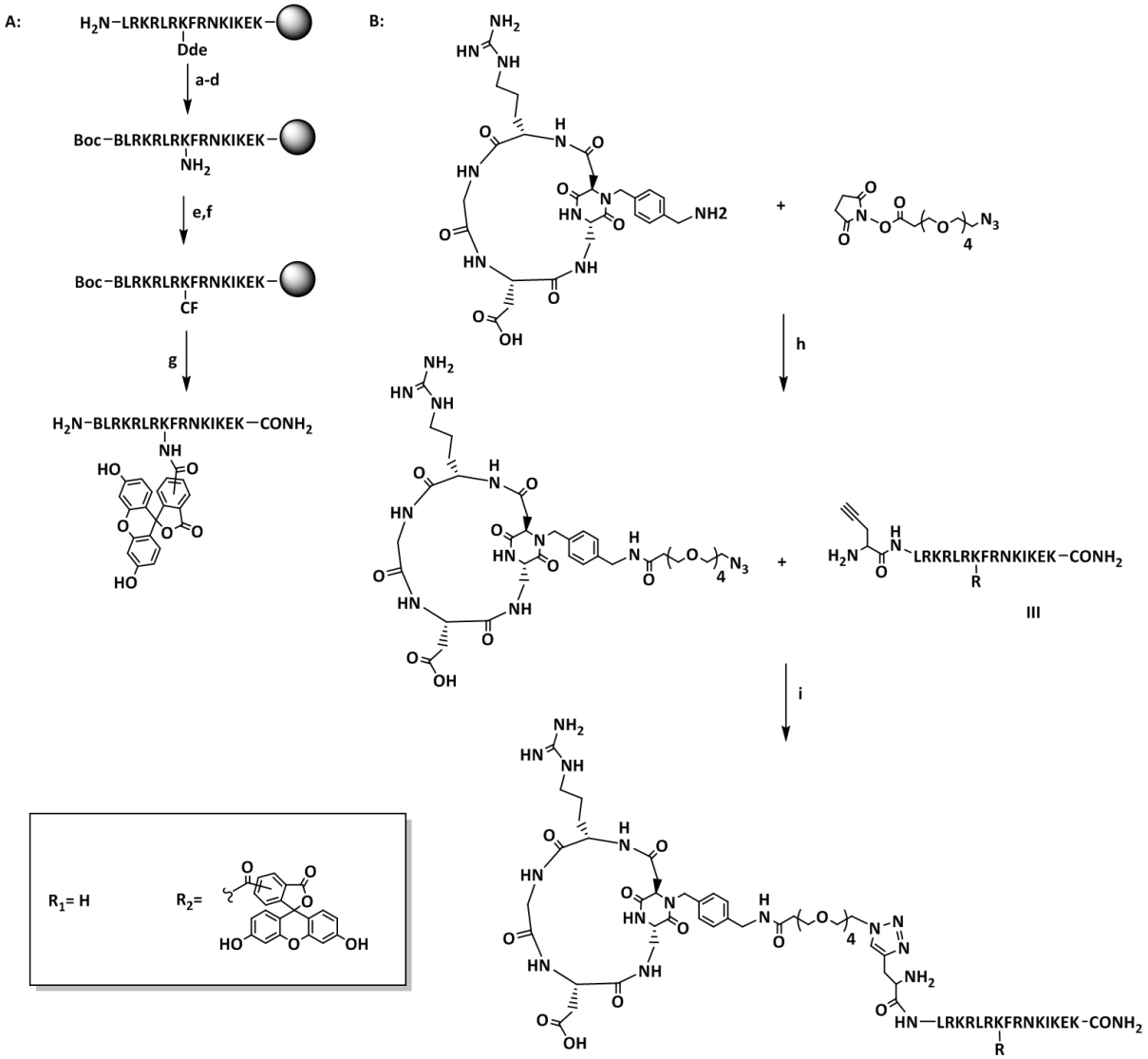

Figure 24. Synthetic strategy of the full conjugates 1 and 1a. A: Synthesis of the CF-labeled sequence by SPPS. **B**: pH-sensitive reaction for the attachment of the PEG_4-linker to the functionalized ligand and "click" reaction between the azido group of the linker and the alkyne group at the *N*-terminus of the CPP. Reagents and conditions: **a**: 5 eq. Fmoc-L-Pra-OH (B), 5 eq. Oxyma, 5 eq. DIC in DMF, overnight; **b**: 30% piperidine in DMF (20 min x 2); **c**: 10 eq. Boc_2O, 1 eq. DIPEA in DCM for 2 h (2x); **d**: 2% hydrazine in DMF (10x); **e**: 2 eq. CF, 2 eq. HATU, 2 eq. DIPEA in DMF for 2 h, then 5 eq. CF, 5 eq. Oxyma, 5 eq. DIC in DMF overnight; **f**: 20% piperidine in DMF, 45 min; **g**: TFA/TIS/H_2O (95:2,5:2,5), 3 h, rt; **h**: 1 eq. c[DKP*f3*RGD]-NH_2, 2 eq. HOOC-PEG_4-N_3, PBS/MeCN, pH 7.3-7.5, overnight; **i**: 1 eq. **III**, 1.3 eq. c[DKP*f3*RGD]-PEG_4-N_3, 0.5 eq. $CuSO_4$ $5H_2O$, 0.6 eq. Na ascorbate, H_2O: DMF 1:1, 10 mM, 40 °C, N_2, 24 h

Table 5. List of the synthesized compounds with their codes, names and MW (calculated and experimental).

Code	Conjugate	MW (g/mol)	MW_{exp} (g/mol)
1	c[DKP*f3*RGD]-sC18	2998.2	2998.3
1a	c[DKP*f3*RGD]-sC18(Lys^8-CF)	3355.9	3356.6
2	sC18	2069.6	2069.9
2a	sC18(Lys^8-CF)	2427.9	2428.9

Next, we measured the binding affinity of the new conjugates towards the isolated integrin receptors $\alpha_v\beta_3$ and $\alpha_v\beta_5$, which are both tumor-associated integrins (Table 6). The assay was performed by Dr. Daniela Arosio (Istituto di Scienze e Tecnologie Molecolari in Milan). Compounds **1** and **1a** were both able to inhibit biotinylated vitronectin binding to $\alpha_v\beta_3$ with low nanomolar affinity, indicating that the presence of the CPP as well as the fluorophore did not interfere with the receptor binding. The free functionalized ligand c[DKP*f3*RGD] is added in the table as reference and it was already reported to be up to 200-fold more selective to $\alpha_v\beta_3$. [156, 159] Interestingly, the selectivity was even more pronounced for the conjugate **1** (up to 1.500-fold) within this assay. If we compare these results with the binding values obtained for the dual-action ligand VEGFR-integrin targeting conjugate synthesized in the group of Prof. Gennari, we can observe a significant difference. [159] Overall, our results indicated a stronger affinity and selectivity even if the size and characteristics of the molecules attached to the RGD ligand are comparable (both α-helical peptides, 15 and 16 amino acids for VEGFR ligand and sC18, respectively). One explanation for this effect might be the choice of the PEG spacer. For the dual action ligand a PEG_8 linker was employed in order to create enough distance between the two ligands in accordance with a previous work of Papo *et al*. [248]. Contrarily, we based our approach on a work of Penco and co-workers, which pointed out the crucial role of the spacer between the targeting device and the drug in small molecule drug conjugates. [249] The spacer, in fact, should be able to adequately separate the two moieties in order to prevent a negative impact on the receptor binding but also maintain the individual features of each component. Short-length PEG spacers were selected to enhance solubility and minimize the formation of bulky loops that can interfere with the binding. As a demonstration, to connect the *c*[DKP*f3*RGD] ligands to a multimeric scaffold, tetraethylene glycol spacers were employed by Raposo Moreira Dias *et al.* in order to render the conjugates more water-soluble and flexible, reaching a very high selectivity. [235]

Table 6. Inhibition of biotinylated vitronectin binding to $\alpha_v\beta_3$ and $\alpha_v\beta_5$ receptors. IC_{50} values were calculated as the concentration of compound required for 50% inhibition of biotinylated vitronectin binding as estimated by GraphPad Prism software; all values are the arithmetic mean SD of triplicate determinations. The values corresponding to the free functionalized ligand were previously described and are added here as reference. [156]

Code	IC_{50}[nM] $\alpha_v\beta_3$	IC_{50}[μM] $\alpha_v\beta_5$
1	16.7 ± 0.6	24.9 ± 2.7
1a	15.3 ± 5.2	2.5 ± 0.2
c[DKP*f3*RGD]-NH_2	26.4 ± 3.7	>5

For further *in vitro* cell studies, we first investigated which cell lines could be used as positive and negative control. From literature data, U87 cells have been reported to display an enhanced expression of $\alpha_v\beta_3$ integrins; on the contrary, HT-29 cells are documented to express $\alpha_v\beta_5$ but not $\alpha_v\beta_3$ receptors, while MCF-7 cells showed controversial results. [250-252] We verified the integrin receptor expression for these cell lines by flow cytometry using for this purpose a FITC-labeled anti-integrin $\alpha_v\beta_3$ monoclonal antibody. The assay was run following a protocol developed by the PhD student Ivan Randelovic, in the research group of Dr. József Tóvári at the National Institute of Oncology in Budapest. After fixation, the cells were incubated with a BSA solution to occupy all the unspecific binding sites on the surface and then incubated with the antibody for 1 h. Afterwards, the fluorescence intensity was measured by flow cytometry and the value obtained from the measurement of the untreated cells was subtracted. All cell lines were tested in the same day to better compare the flow cytometry results.

From our assay (Figure 25), U87 cells confirmed the literature data expressing $\alpha_v\beta_3$ integrins at higher level compared to HT-29 and MCF-7 cells (7.5 and 5 times higher value, respectively), which were therefore used as negative controls. Since *in vitro* experiments were performed in two different laboratories (OOI in Budapest and University of Cologne) using the correspondent cell lines (same type but different stocks), the integrin expression was evaluated in both cases and showed comparable results (data not shown). This was an essential demonstration to assure that the results from different labs could be correlated.

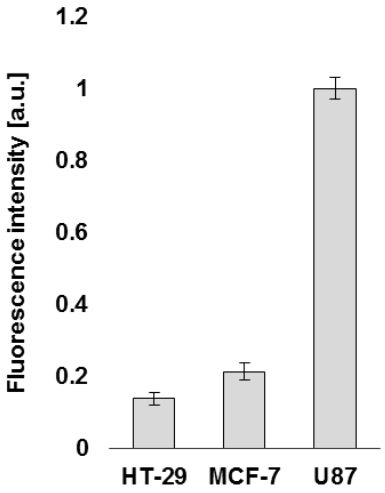

Figure 25. $\alpha_v\beta_3$ integrin expression level measured by flow cytometry analysis using FITC-conjugated anti-integrin antibody clone LM609. This is an allosteric inhibitor of integrin **$\alpha_v\beta_3$**, which binds to a conformational epitope resulting from the post-translational association of the **α_v** and **β_3** subunits. The experiment was performed in duplicate with *n=2.*

In a next step, we investigated the cytotoxic profiles of the drug-free peptides, **1** and **2**. Thus, U87 cells as positive control and HT-29 and MCF-7 cells as negative controls, were incubated for 72h with different concentrations of the conjugates (Figure 26).

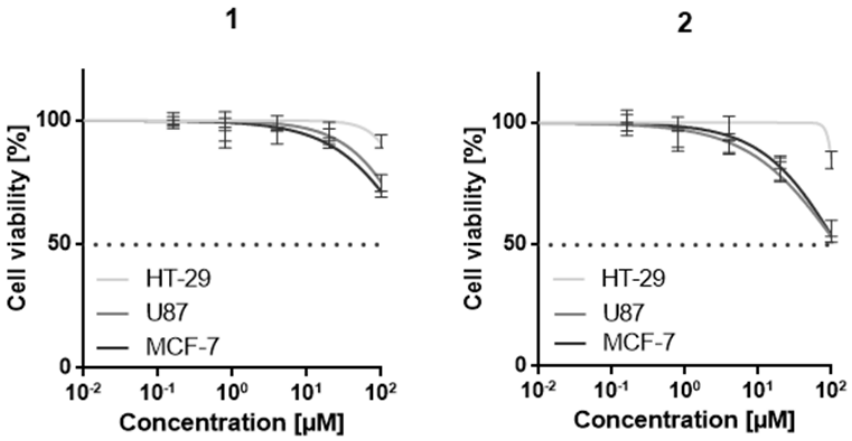

Figure 26. MTT-based antiproliferative study with compounds 1 and 2 on U87, HT-29 cells and MCF-7 cells. The peptides were incubated for 72 h without washout. Values from the positive control (DMSO/EtOH; 1:1) were substracted from all data and the untreated cells were set to 100%. The experiment was performed in triplicate with *n=2.*

In U87 and MCF-7 cells, at the highest concentration of 100 µM, compound **1** showed minor toxicity whereas the free peptide sC18 (**2**) significantly harmed the cells. Differently, both compounds showed nearly no influence on cell viability when applied to HT-29 cells, even if a slightly higher activity of peptide **2** could be recognized also in this case. The lower cytotoxicity in HT-29 cells probably directly reflects the reduced sensitivity of this cell line. The high toxicity of **2** has not been verified by previous results, but this is maybe related to the fact that the cytotoxicity profile has never been tested for 72h. In fact, when the toxicity was tested after 24h, no effect could be detected even at the highest concentration, showing a very similar profile between the different cells (figure 89 in attachment).

In a 72h experiment, too many factors are playing with each other and the binding affinity features of the conjugates could be definitely annulled after such a long incubation time by the internalization ability of the CPP and the presence, even if at lower level, of $\alpha_v\beta_3$ integrin receptors also in the control cell lines. For this reason, the distinctive activities of the two compounds in the different cell lines should be related to the peculiar biological characteristics of each cell type and no theory about selectivity could be drawn. A much more interesting investigation to corroborate our hypothesis would be to examine the uptake profiles of compounds **1a** and **2a**, taking into consideration not only different incubation times but also the internalization behavior in presence of binding competitors or inhibitors of peculiar transport pathways. This was considered as decisive to let us understand the underlying mechanisms that influence the cell penetration of the construct, in particular evaluating the dependence on receptor-binding.

First, the time-dependence of peptide uptake was quantified in U87, HT-29 and MCF-7 cells (Figure 27A). The three cell lines were incubated with the fluorescently labeled conjugates **1a**

and **2a** for 30 and 60 min and the fluorescence intensity was quantitatively measured by flow cytometry. All the results were normalized within the different cell lines to better compare the outcomes, not only between the peptides but also between the different systems.

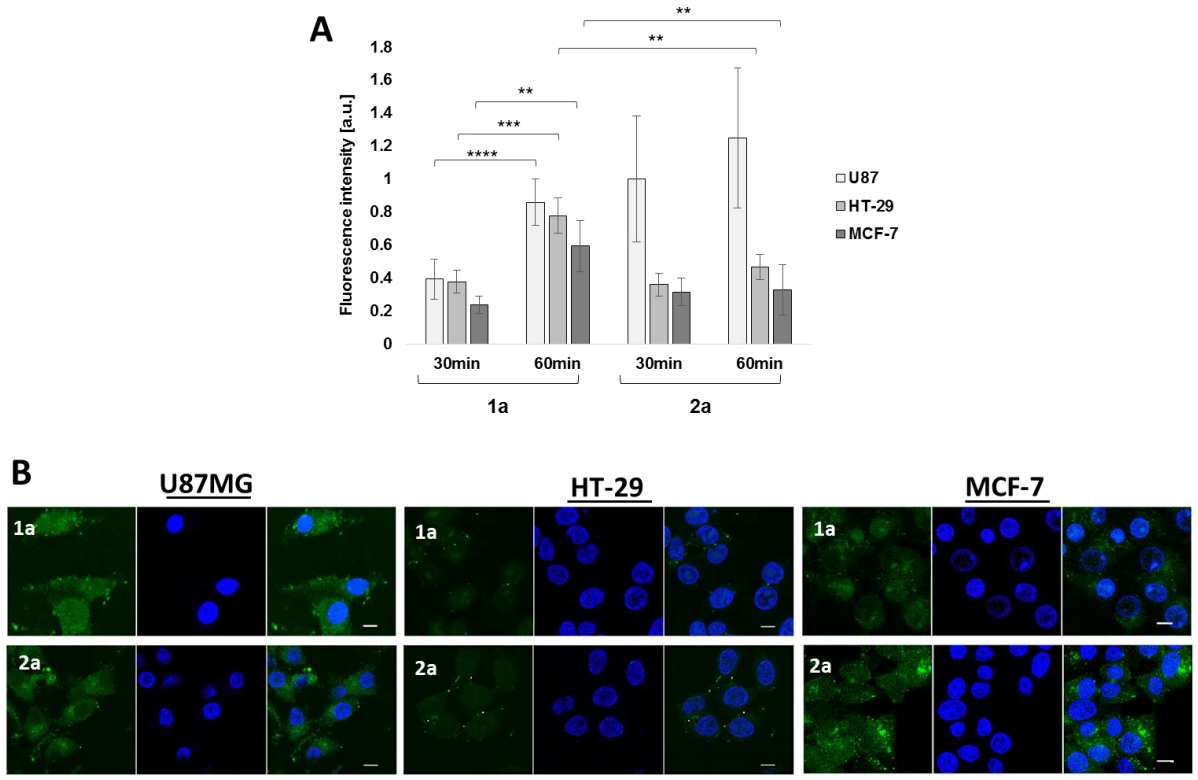

Figure 27. Cellular uptake of 1a and 2a in U87, HT-29 and MCF-7 cells. A: Cellular uptake was quantified by flow cytometry. Cells were incubated with 10 µM peptide solution for 30 or 60 min at 37°C. The results are normalized to the value of sC18 in U87 cells that is set to 1. The experiment was performed in triplicate with *n=2.* (**: p ≤ 0.01; ***: p ≤ 0.001; ****: p ≤ 0.0001). **B**: Cellular uptake was analyzed by CLSM. Cells were incubated for 30 min with 10 µM of CF-labeled peptide solution at 37°C. External fluorescence was quenched by treatment with 150 µM trypan blue for 15 sec. Green: CF-labeled peptide; blue: Hoechst 33342 nuclear stain; scale bar is 10 µm.

Interestingly, in all the cell lines the uptake of **1a** was time-dependent, differently from **2a** where such a tendency could not be recognized. A general remark about these results is that, as already stated for the cytotoxicity, differences in the uptake are sometimes merely influenced by the biological characteristics that distinguish a particular cell line from the others. Nevertheless, if we compare the two compounds we can notice different behaviors that are worth to be described in details for every cell line. What we can observe is that, differently from the negative control cell lines, in U87 the internalization of **2a** after 30 minutes was stronger than **1a**. This reduced uptake can be explained with the different uptake modalities distinguishing these two peptides. We already showed that the conjugate **1a** displays a high affinity towards integrin $\alpha_v\beta_3$. For this reason, we can imagine that, when in contact with the cell surface, the compound would tend to bind to the receptor and afterwards internalize by receptor- or by CPP-mediated uptake. This important interaction would definitely shorten the

time available for internalization leading to an overall reduced penetration. Indeed, since within this experiment we washed out the solution and trypsinized the cells, the conjugate, still bound to the receptor or interacting at the level of the outer membrane, would detach from the cell evolving in a lower cellular uptake. In addition, **1a** would be probably taken up at lower extent because of the different structure. It has been already demonstrated that the insertion of a PEG spacer would enhance the hydrophilicity of the molecule leading to a lower internalization rate, since the direct translocation through the lipid phase of the membrane would be limited. [253] After 60 min incubation more peptide was able to internalize and for this reason the fluorescence intensity measured for **1a** and **2a** are leveled. Other considerations should be made in case of MCF-7 and HT-29 cells since in this case the receptors are present at a lower level and should not exert any role in the internalization. In these cell lines, after 30 min the uptake levels of the two compounds are comparable while after 60 min incubation, the situation is completely overturned in relation to U87 cells, which is a good sign because it means that this behavior is dependent on the different integrin expression. What we can presume is that **1a** is probably more stable than **2a**, therefore it would not be rapidly degraded so that, after 60 minutes, **1a** would internalize at higher extent. Another hypothesis could be connected with a possible receptor-mediated uptake, which could play an important role after longer incubation time. As I already illustrated, our control cell lines do not completely lack of integrin receptors and their presence should be taken into consideration in the evaluation of the experimental results. To clearly understand this phenomenon and concretely imagine what could happen on the surface of the cell, the structure of the conjugate **1a** was calculated using the Phenix software and illustrated with Pymol (Figure 28).

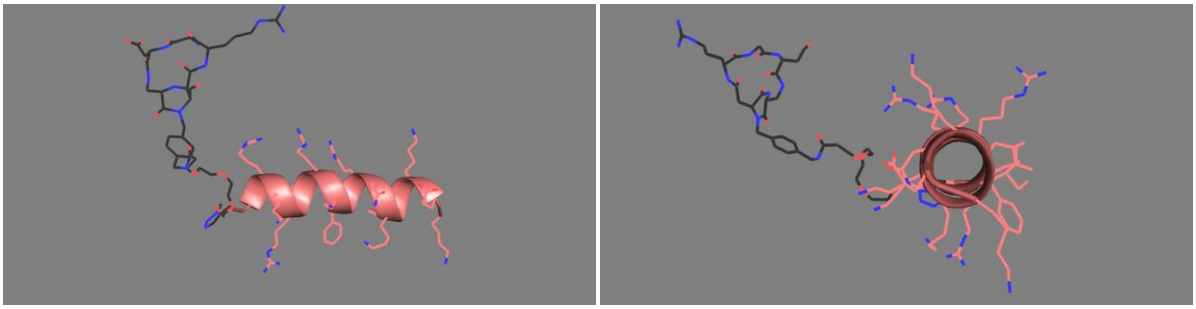

Figure 28. Structure calculation of conjugate 1a illustrated with Pymol. Calculation was performed by the PhD student Dirk Lindenblatt (research group of Prof. Niefind, University of Cologne).

This picture is quite significant for our study since we can directly observe how the helix generated by the CPP forms a 90° angle with the targeting moiety and this could allow an efficient insertion through the two receptor subunits and effective binding, as already demonstrated by the binding studies.

The cellular uptake was also qualitatively examined by CLSM (Figure 27B): the cells were incubated for 30 minutes with the peptide solutions, nuclei were stained with Hoechst 44432

and the external fluorescence was quenched with trypan blue. While MCF-7 and HT-29 cells were pretty easy to handle, many problems have been met with U87 cells. This cell line is very sensitive to every treatment, in particular when many steps are performed in a short time interval as it happens for microscopy measurements (treatment, quenching, washout). Indeed, the cells rapidly detach from the well surface, become round and cannot be visualized so well. For this reason, the outcomes are also difficult to compare within different cell lines. Nevertheless, all the cell lines have been tested and from the pictures, we notice a quite similar internalization pattern between **1a** and **2a**. The quantitative difference in uptake shown in the FACS results for U87 cells between the two compounds is not clearly visible here but **2a** displays a high standard deviation, what would explain this result. In the case of MCF-7 and HT-29 cells, the FACS results are here validated since the uptake of the two compounds is comparable. As already described in the introduction, different entry pathways can be followed by CPPs and these could be influenced, a part from the size of the cargo and the concentration of the peptide, also by the different cell lines tested. [254] In fact, regard to the uptake pattern, we can detect a distinctive vesicular distribution in HT-29 cells, opposed to a more diffuse dispersion in the cytosol of U87 and MCF-7 cells, indicating a possible explanation for the higher toxicity of **2** in these cell lines observed in the previous antiproliferative assay (Figure 26). Since the microscope investigation did not offer us more relevant information than the quantitative assay by flow cytometry, it would be interesting to perform the same experiment after 60 minutes incubation to observe if some variations in the internalization pattern could be detected in particular for **1a**.

To better understand this important mechanism of internalization into U87 cells we decided to perform more experiments using flow cytometry starting with a competition assay (Figure 29). To do so, the competitor used was the free unfunctionalized ligand c[DKP*3*RGD] synthesized by the PhD student Clémence Robert, in the group of Prof. Piarulli. The assay was based on the addition of this molecule to the **1a** peptide solution followed by incubation with U87 cells for 30 or 60 min for a better comparison with the previous results obtained from the cellular uptake studies.

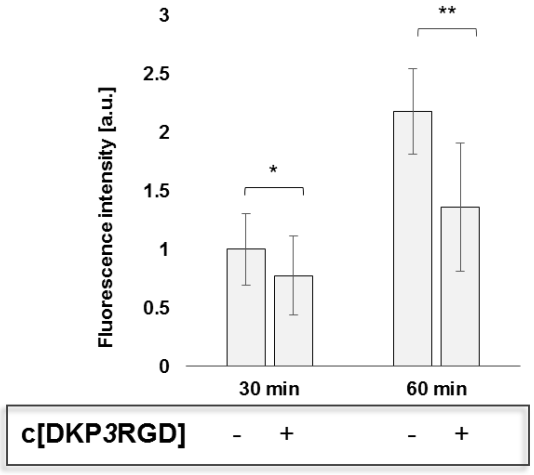

Figure 29. Competition experiment. Co-incubation of the peptide **1a** (10 µM) with a 10-fold excess of the free ligand c[DKP*3*RGD] for 30 and 60 min. The cellular uptake was quantified by flow cytometry. (*: $p \leq 0.05$; **: $p \leq 0.01$). The experiment was performed in triplicate with *n=2.*

A maximal 10-fold excess of the ligand (100 µM) was used because as soon as we increased its concentration, we encountered many problems by handling the cells. This was a further demonstration that U87 cells overexpress integrin receptors and that these receptors are very important for the adhesion on the surface of the plate. In fact, when RGD was added in excess, the cells started to detach even if high care was taken while treating them as already described by Russo *et al*. [255] In the presence of a 100-fold excess of the ligand, in fact, after 30 min incubation the cells were completely detached so that a significant number of cells could not be counted. Starting from the 30 min incubation, we can see a slight inhibition in the uptake of conjugate **1a**. After 60 min the effect is higher, corroborating that, after longer incubation, the integrin-mediated internalization could have a stronger effect. Since the influence is not substantial, we could state that integrin-receptor mediated uptake may have a slight relevance on the internalization of **1a** but assumedly not as meaningful as the CPP-mediated uptake. An additional theory could be that the conjugate recognizes the receptor but does not bind to it following a “kiss and run model” being then quickly taken up by CPP-mediated uptake. This hypothesis was already described by Reina and coworkers, who proved that the internalization of a cRGD ligand was not integrin-dependent but that, after binding the receptors, it would follow a fluid-phase endocytosis pathway to lysosomes. [165]

This assumption could be exemplified by the model depicted in Figure 30 where two mechanisms are present at the same time: a receptor-mediated uptake and a CPP-mediated uptake. Probably in our case the CPP-mediated uptake is stronger but the recognition of the receptor is very important and allows the conjugates to target the cell.

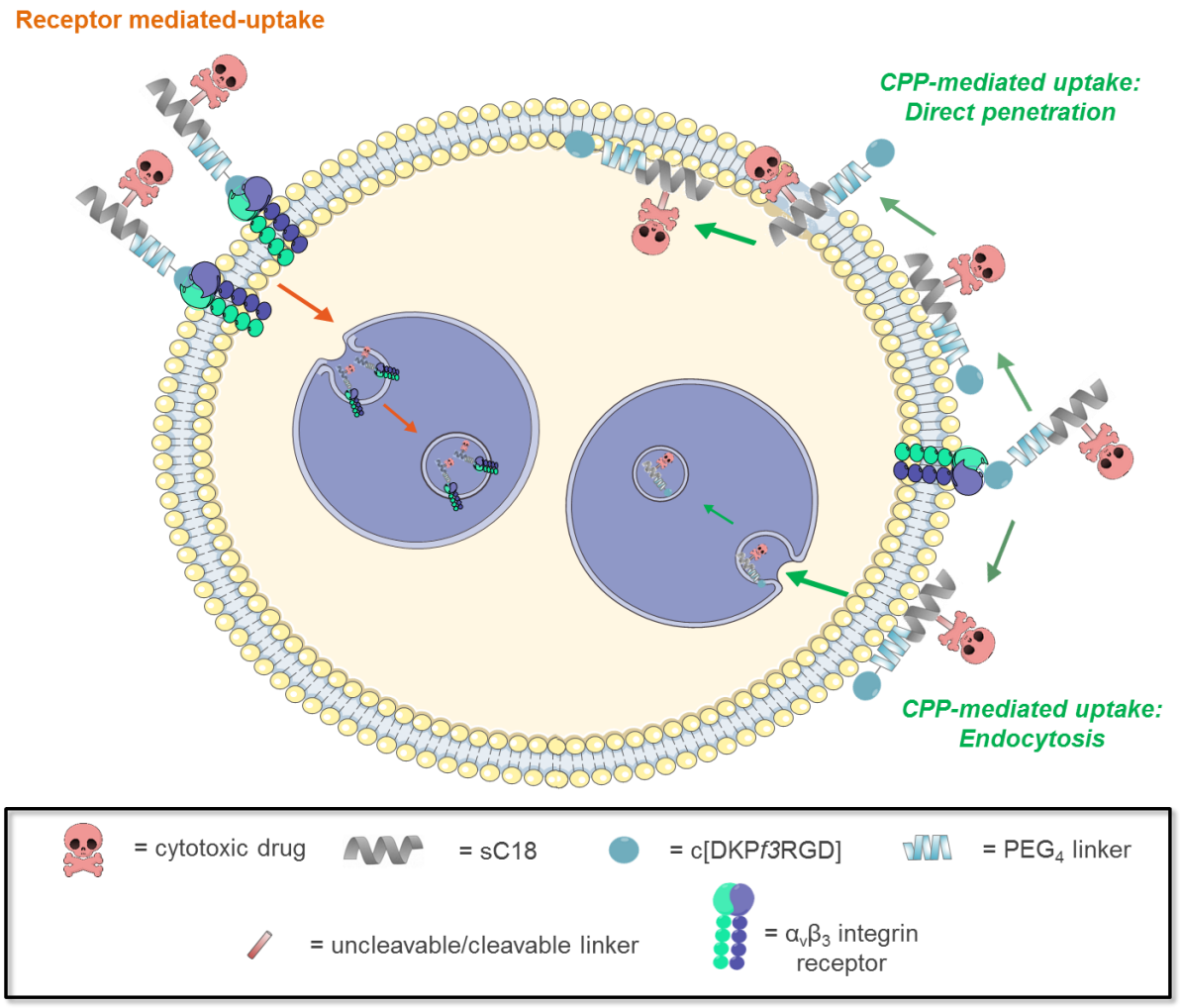

Figure 30. Graphic model describing the hypothetical internalization mechanism of the new drug delivery system. The selective targeting to receptor-overexpressing cells is allowed by the integrin ligand and the good permeability of the CPP improves drug cellular uptake. The CPP-mediated uptake plays a big role: the peptide-drug conjugate is first recognized by the receptor and then internalized by CPP-mediated mechanisms (endocytosis or direct penetration). Next to this, the peptide drug-conjugate could also internalize inside the cell by receptor-mediated endocytosis. In the endosomes the conjugates are degraded and the drug released.

Since we could not demonstrate that only integrin-dependent uptake plays a role in the internalization of the constructs, we performed a blocking experiment that would be useful to understand the whole mechanism (Figure 31). In this case, the cells were pretreated for 30 minutes with the correspondent inhibitors, afterwards the blocking solution was removed and the cells were incubated for further 30 min with **1a**. Additionally to the free ligand c[DKP*3*RGD], other reagents have been used to block some entry pathways typical of CPP internalization. Poly-L-lysine (PLL) was used to inhibit the direct membrane translocation of the peptide: this inhibitor is meant to interact with the negative charges of the cell membrane and inhibit the interaction of the positively charged CPP helix blocking its penetration. The other reagent used was methyl-β-cyclodextrin (mβ-cd), responsible for depleting the membrane from cholesterol and blocking any cholesterol-dependent endocytic uptake.

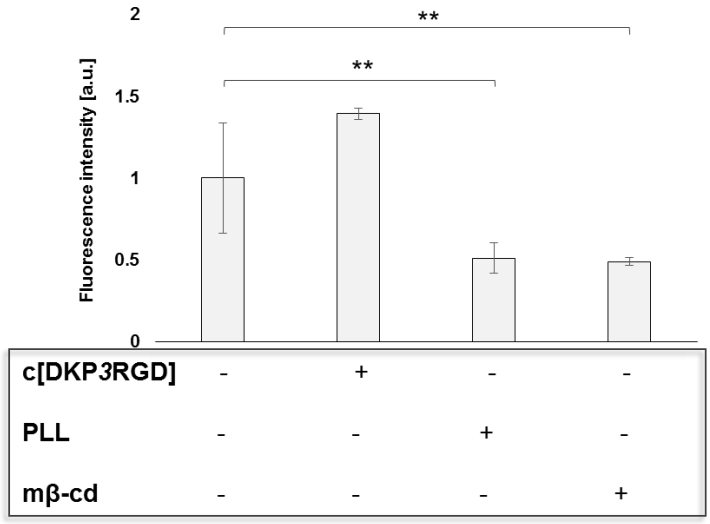

Figure 31. Blocking experiment. 30 min pre-incubation with c[DKP*3*RGD] (10 µM), PLL or mβ-cd (1 mM) followed by 30 min incubation with 10 µM **1a** solution. The experiment was performed in triplicate with *n=1.*

It seems from these results that the integrin receptor-mediated uptake has practically no influence in the internalization of the conjugate **1a** while the CPP-mediated uptake plays a crucial role. In fact after treatment with PLL and mβ-cd, the uptake is reduced to the half, respect to the control. This does not happen for the free ligand, where we can surprisingly see an increase of the uptake probably due to the increment of other ways of penetration mediated by the CPP.

In general, the results achieved so far proved that the ligand chosen to increase the selectivity of the CPP could actually lead to crucial differences in the uptake of the conjugate **1** compared to the CPP **2** but that the internalization is probably influenced by the CPP while the ligand could play an important role in targeting the conjugates towards the cells overexpressing the receptors. Since our final goal is connected with the improvement of the traditional chemotherapy, especially concerning the reduction of side effects by increasing selectivity, new research directions have been undertaken, starting with the development of synthetic strategies to accomplish the conjugation to various cytotoxic payloads.

3.2.2. Development of cryptophycin conjugates

The first drug to be conjugated with the drug delivery system was cryptophycin-55. The molecule was synthesized by the PhD student Eduard Figueras Agustì (research group of Prof. Norbert Sewald, University of Bielefeld) and functionalized as glycinate ester of the hydroxyl group of the chlorohydrin (Cry-55 glycinate) in order to allow the attachment of a linker. The synthetic strategy followed for the preparation of the conjugates, listed in Table 7, is depicted in Figure 32.

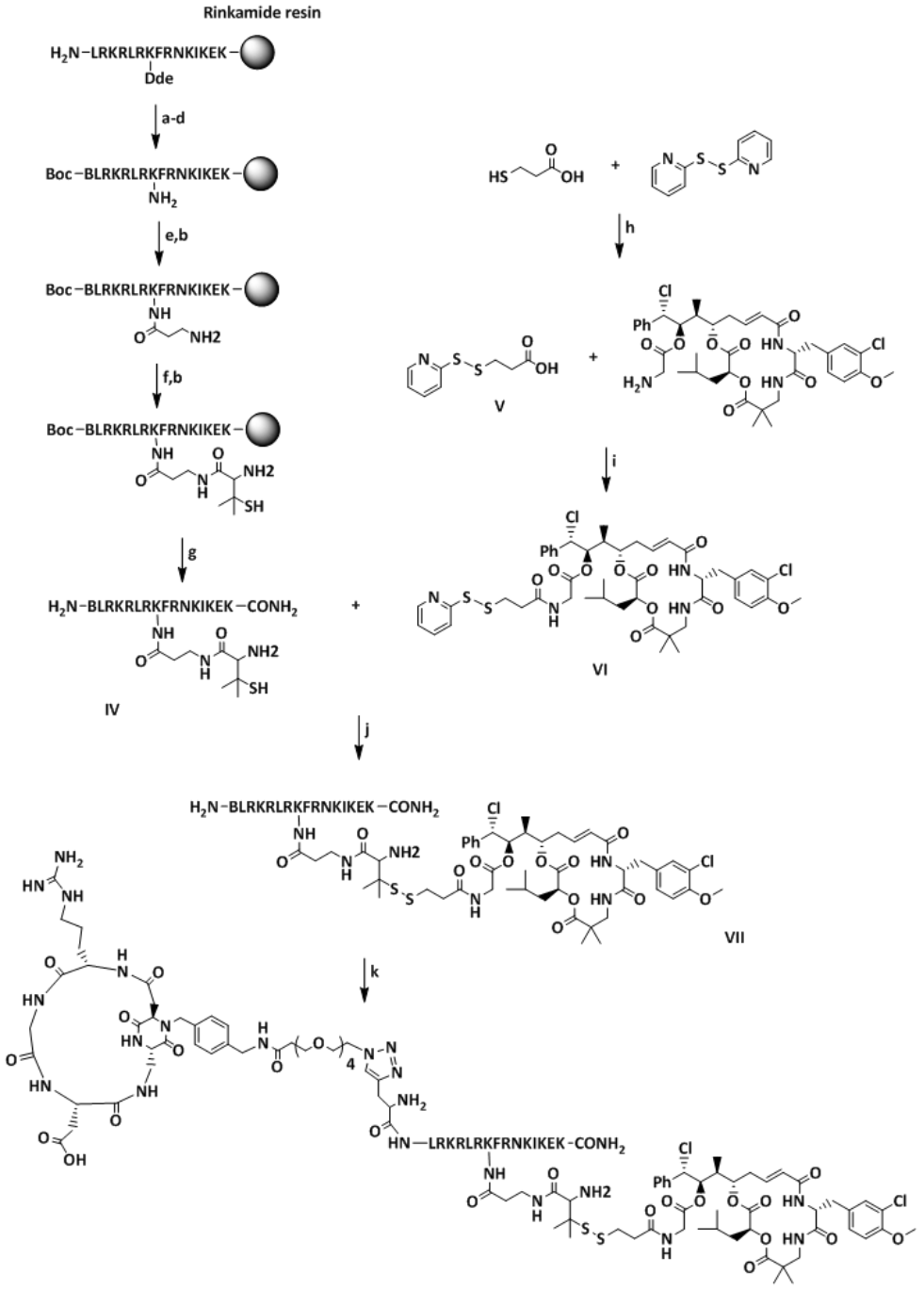

Figure 32. Synthetic strategy for the synthesis of c[DKP*f3*RGD]-sC18-S-S-Cry. Reagents and conditions: **a**: 5 eq. Fmoc-L-Pra-OH (B), 5 eq. Oxyma, 5 eq. DIC in DMF, overnight; **b**: 30% piperidine in DMF (20minx2); **c**: 10 eq. Boc_2O, 1 eq. DIPEA in DCM for 2 h (2x) **d**: 2% hydrazine in DMF (10x); **e**: 5 eq. Fmoc-β-Alanine-OH, 5 eq. Oxyma, 5 eq. DIC in DMF, overnight; **f**: 5 eq. Fmoc-Pen(Trt)-OH, 5 eq. Oxyma, 5 eq. DIC in DMF, overnight; **g**: TFA/thioanisole/EDT (90:7:3), 3 h; **h**: 1 eq. 3-mercaptopropionic acid, 2.3 eq. dithiopiridine, MeOH, 3 h, rt; **i**: 1 eq. Cry-55-gly, 4 eq. **V**, 4 eq. PyBOP, 4.5 eq. HOBt, 5 eq. DIPEA in dry DMF, N_2, 5 h, rt; **j**: 1 eq. **VI**, 1 eq. **IV**, dry DMF; **k**: 1 eq. **VII**, 1.3 eq. c[DKP*f3*RGD]-PEG_4-N_3, 0.5 eq. $CuSO_4$ $5H_2O$, 0.6 eq. Na ascorbate, H_2O: DMF 1:1, 10 mM, 40 °C, N_2, 24 h.

The synthesis of the CPP moiety **IV** was performed as already described but at the side chain of Lys^8 a β-alanine was attached functioning as spacer and a penicillamine residue was bound to it. The penicillamine was chosen because of the branched side chain that could protect the

disulfide bridge from the cleavage in biological fluids, thus improving the stability of the conjugate and hindering the premature release of the drug causing an off-target effect. [256] For the preparation of the drug-linker molecule **VI**, dithiopyridine was reacted with a thiol acid [257] to allow the formation of a peptide bond with the amino group of the glycine residue attached to the drug. Particular care had to be taken during all these steps because of the sensitivity of the drug. In fact, the maximum temperature that could be used was 40 °C in order to prevent the hydrolysis of the chlorine atom. The synthetic strategy until the formation of the CPP-drug conjugate **VII**, easily obtained in DMF solution, [258] worked successfully in optimal yields. The critical step during the synthesis turned out to be the "click" reaction. The previously described conditions were used but we directly understood that the linker would not be stable in presence of the reductive agent sodium ascorbate. The reaction was followed by LC-MS and samples were taken at regular intervals. Already after 10 minutes, the peak corresponding to the final product was detectable almost at the same retention time of the educt. After 1.5 h the situation did not change and there was still the same educt/product ratio. The reaction was left overnight and the next day new peaks were detectable corresponding to the oxidized CPP and the oxidized CPP conjugated to the ligand (Figure 33).

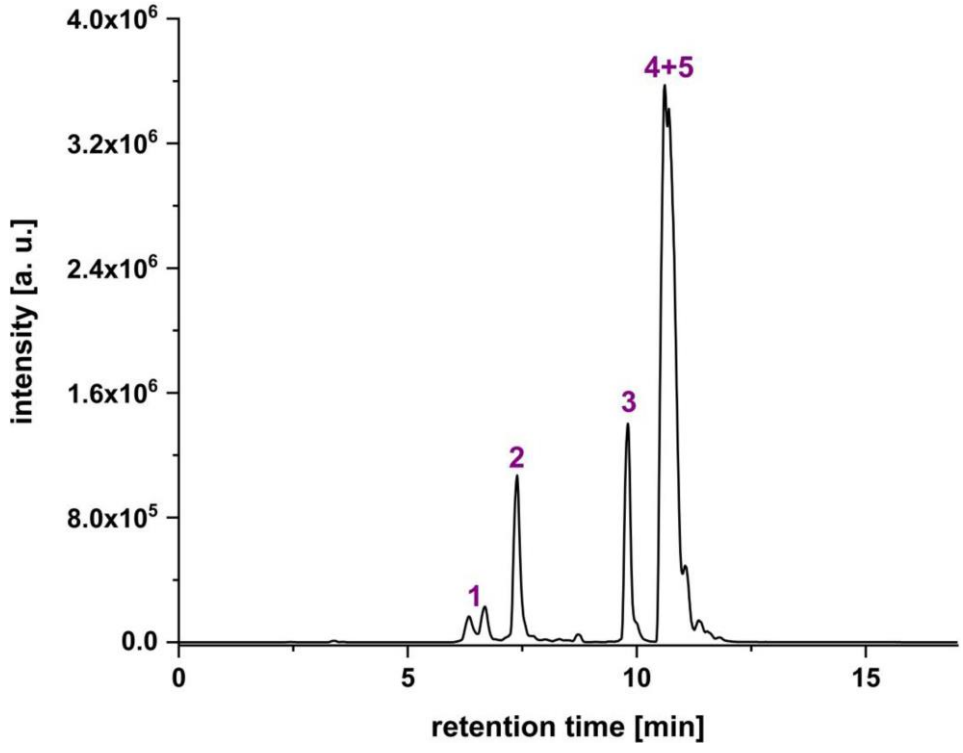

Figure 33. ESI-MS mass spectrum of the "click" reaction between VII and c[DKP*f3*RGD]-PEG$_4$-N$_3$ after 24 h at rt. 1: oxidized **IV**; **2**: oxidized c[DKP*f3*RGD]-IV conjugate (without Cry-linker); **3**: c[DKP*f3*RGD]-PEG$_4$-N3; **4+5**: **VII** and **c[DKP*f3*RGD]-sC18-S-S-Cry**

The product could be obtained in only very low amounts, the yield was very low and the starting material could not be recovered (Table 20 in the attachment). Alternative conditions have been considered in order to avoid the presence of reductive agents. In this sense, a publication from

Prof. Sewald showed the optimal alternative, where copper powder was used and the yields were quite satisfactory. [259] Unfortunately, because of the few amounts available of the c[DKP*f3*RGD] ligand and the cryptophycin variant, it was not possible to optimize the reaction with the right solvents and right equivalents and some work still has to be done in this direction. Since the compound obtained until now was not sufficient to start biological studies, we considered changing the cytotoxic payload but taking into consideration that the synthesis of these constructs should be further investigated because of the very promising activity of the highly active cryptophycin.

Table 7. List of Cry-55-glycinate conjugates with their names, structures and MW (calculated and experimental)

Name	Structure	MW (g/mol)	MW_{exp} (g/mol)
c[DKP*f3*RGD]-sC18-S-S-Cry	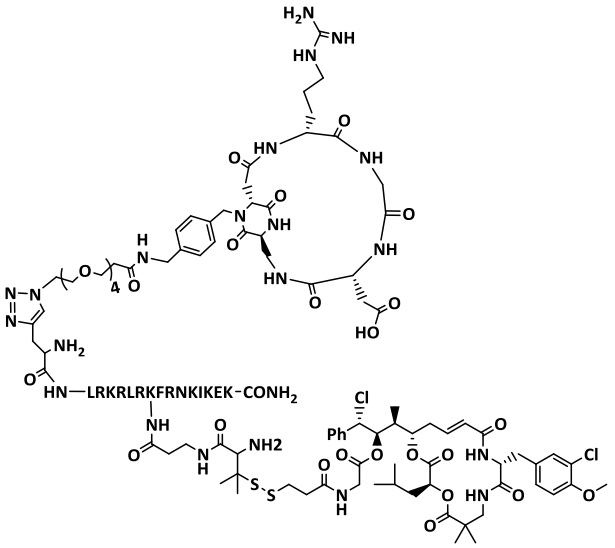	4050.7	4049.7
sC18-S-S-Cry	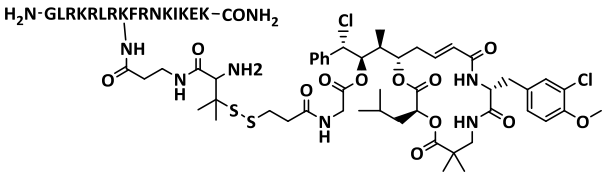	3121.7	3121.4

3.2.3. Development of chlorambucil conjugates and their biological evaluation

Because of the easier way of conjugation, chlorambucil was considered as new cytotoxic payload. This project was in collaboration with the PhD student Clémence Robert, who synthesized these novel conjugates during her secondment at the University of Cologne. The synthetic strategy is not shown but followed the same steps as for the other conjugates. In this case, the drug was coupled following the traditional SPPS strategy. The synthesis seemed to be easy and straightforward but as soon as the peptide was cleaved from the resin, lyophilized and purified, a lot of problems were encountered connected with the high tendency of

chlorambucil to hydrolyze when in contact with water, in particular at acidic pH. This hydrolysis had been previously described and it could be limited by shortening the time between one synthesis step and the other. [260] For this reason, after purification, the dissolved peptide was put on ice or directly frozen for freeze-drying and the peptides were preserved at -20 °C or -80 °C. Stock solutions were prepared in DMSO. Despite these problems, the CPP-conjugates could be successfully synthesized and analyzed by LC-MS (Table 8).

Table 8. List of Chlorambucil conjugates with their names, structures and MW (calculated and experimental).

Name	Structure	MW (g/mol)	MW_{exp} (g/mol)
c[DKP*f3*RGD]-sC18(Cbl)	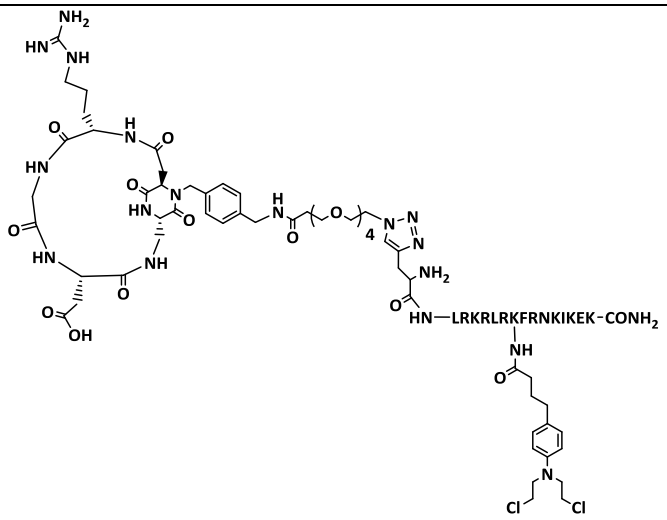	3297.8	3298.4
Cbl-sC18	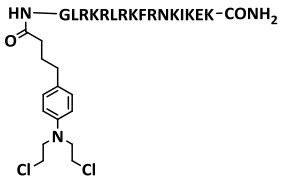	2356.8	2356.4

The cytotoxicity of the conjugates could be finally evaluated by MTT-based assay and short incubation times were used, for the same reasons as for the GnRH conjugates (Figure 34). As we can see, the free cytostatic agent was not active in both cell lines. This outcome is in strong relation with the weak internalization of the drug; the CPP in this case would improve a lot its efficacy. In fact, if we analyze the graph of **Cbl-sC18** we can see that the measured EC_{50} value is much lower in particular for U87 cells and we could improve the cytotoxicity of the drug. In the context of selectivity, the results, were not as expected. The conjugate **c[DKP*f3*RGD]-sC18(Cbl)** was slightly more toxic in U87 than in HT-29 cells but the activity compared to the free drug was pretty the same if not worse and anyway much less active than **Cbl-sC18** (almost 4-fold higher EC_{50} for U87 cells). We tried to figure out which could be the reason for that and, we realized that this could be connected with the problem of hydrolysis in the cell culture

medium. Also in this case we could think about the internalization pathway of the conjugate. As already hypothesized before, the conjugate **1** was not internalized so well as **2** because of the presence of PEG that could disturb the direct translocation of the peptide. Additionally, in U87 cells the targeted conjugate could bind to the receptors hindering a fast CPP-mediated penetration. In fact, the same theories shown before could be validated also in this case. Therefore, in HT-29 cells the conjugate is simply washed out after 15 min while for U87 cells the conjugate is still binding outside on the surface of the cell but, before and after being internalized, hydrolysis would occur hampering the alkylating activity when the conjugate finally reaches the site of action inside the nucleus.

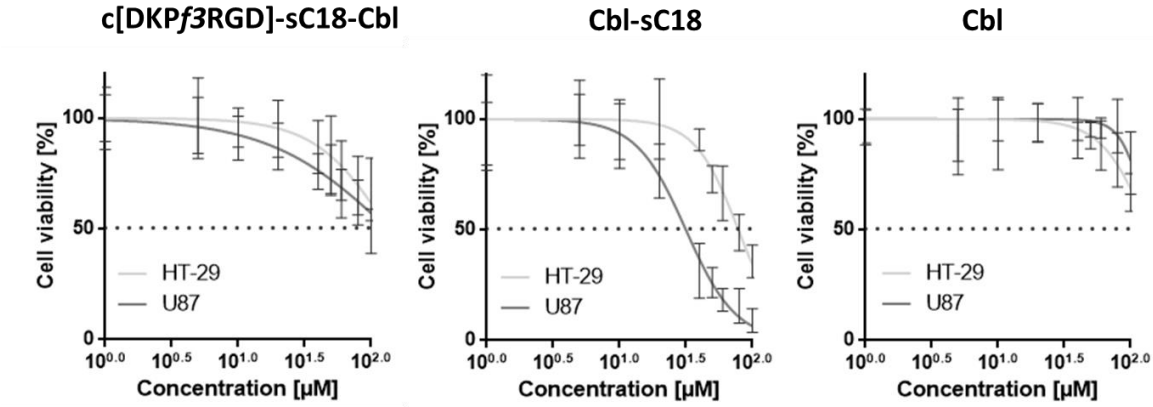

Figure 34. MTT-based antiproliferative study with compounds c[DKP*f3*RGD]-sC18(Cbl), Cbl-sC18 and Cbl on U87 and HT-29 cells. After 15 min incubation, the peptide solution was removed and the cells were incubated for additional 72 h with fresh medium. Values from the positive control (DMSO/EtOH; 1:1) were substracted from all data and the untreated cells were set to 100%. The experiment was performed in triplicate with *n=2.*

Table 9. EC_{50} values of the compounds c[DKP*f3*RGD]-sC18(Cbl), Cbl-sC18 and Cbl referred to figure 34.

EC_{50} (µM)		
	U87	**HT-29**
c[DKP*f3*RGD]-sC18(Cbl)	>110	>170
Cbl-sC18	31.6 ± 3.3	78.6 ± 7.1
Cbl	>140	>140

Since the hydrolysis of the compounds would add a further factor to take into consideration in this already complex system, we reasoned that chlorambucil was not the ideal drug to be used to investigate the selectivity of these conjugates.

3.2.4. Development of daunorubicin conjugates and their biological evaluation

Since the conjugation to the previous drugs caused some problems, due to the difficult synthesis or the instability of the molecules, we decided to use the same strategy described for the GnRH-III-conjugates: daunorubicin was used again for the conjugation to the CPP *via* oxime bond. In the case of GnRH-III conjugates, the main problem was the resistance in

PANC-1 cells and the lack of efficacy of the GnRH receptor binding after the short incubation time, but the drug showed a relatively good activity and an efficient conjugation strategy. Furthermore, the CPP clearly improved the internalization of the homing peptide playing a very important role in the delivery of the drug. The CPPs **I** and **II** were synthesized as already described for the GnRH-III conjugates (Figure 18). The "click" reaction with the ligand worked pretty well reaching yields from 75% to 90% (Table 20 in the attachment). In this case, in addition to the controls including only the CPP sequence (**2b** and **2c**, previously named **sC18(Dau)** and **sC18(GFLG-Dau)**), two other determinant controls (Figure 35B) were synthesized by the PhD student Sara Parente from the research group of Prof. Piarulli. The first one **3b**, containing the c[DKP*f3*RGD] moiety separated from the drug by a PEG_4 chain, the second one **3c**, where the two elements were outdistanced by a GFLG cleavable linker. For the last compound, the PEG_4 linker was not inserted in order to keep more or less the same distance between the targeting moiety and the drug, so that the binding would not be influenced. These two controls were synthesized in order to strictly analyze the contribution of the RGD moiety to the activity of the drug and compare this to the other conjugates containing the CPP as carrier moiety or both the CPP and the c[DKP*f3*RGD]. The general synthetic strategy for the full conjugates is depicted in Figure 35A and all the synthesized compounds are listed in Table 10.

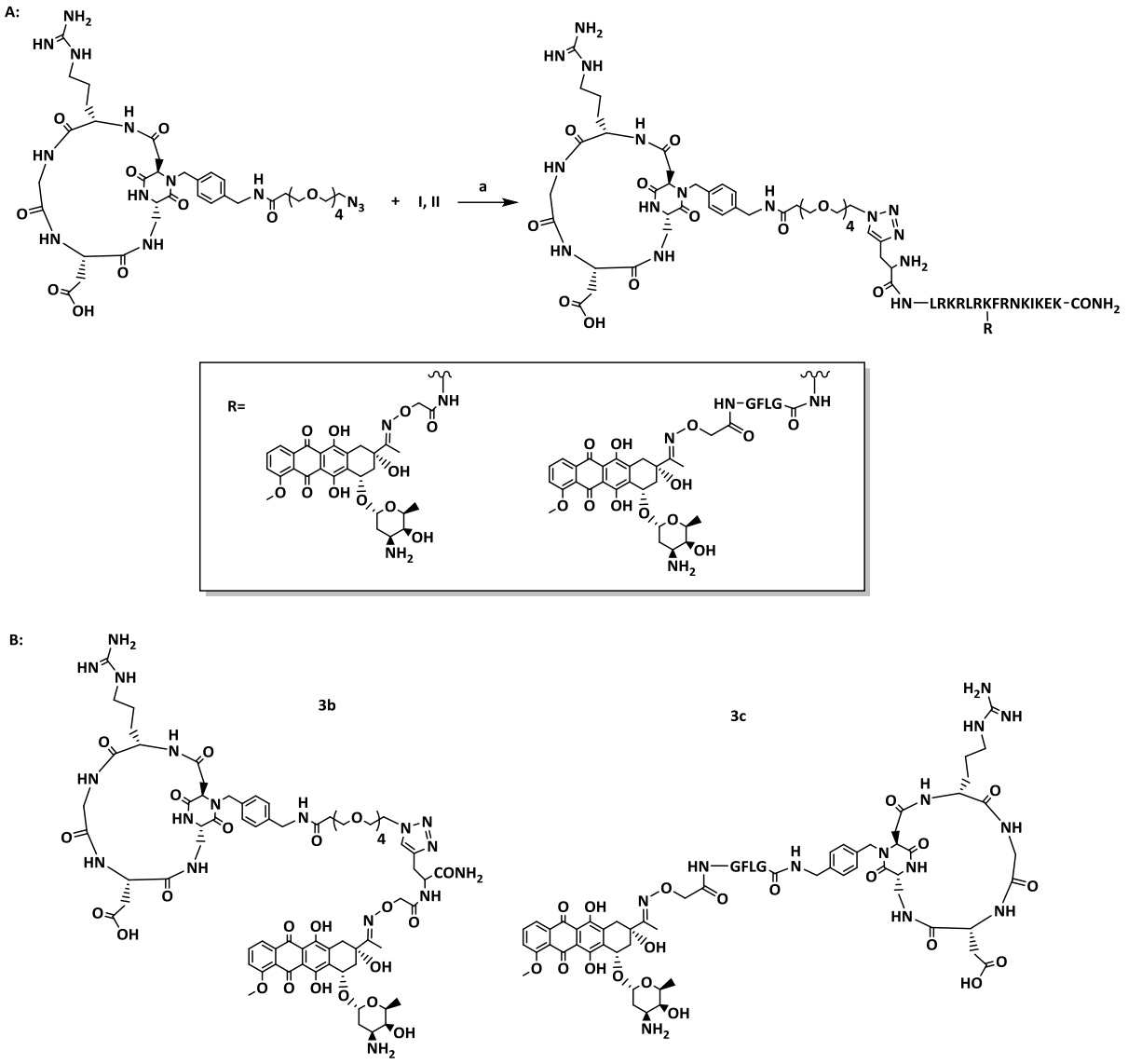

Figure 35. Synthetic strategy for the synthesis of 1b, 1c (A) and structure of the controls 3b and 3c (B). See figure 18 for the synthesis of **I** and **II**. Reagents and conditions: **a**: 1 eq. **I** or **II**, 1.3 eq. c[DKP*f3*RGD]-PEG$_4$-N$_3$, 0.5 eq. CuSO$_4$ 5H$_2$O, 0.6 eq. Na ascorbate, H$_2$O: DMF 1:1, 10 mM, 40 °C, N$_2$, 24 h.

Table 10. List of synthesized c[DKP*f3*RGD] conjugates and controls with their codes, names and MW (calculated and experimental).

Code	Name	MW (g/mol)	MW_{exp} (g/mol)
1b	c[DKP*f3*RGD]-sC18(Dau=Aoa-Lys^8)	3580.1	3581.1
2b	sC18(Dau=Aoa-Lys^8)	2652.2	2653.2
3b	c[DKP*f3*RGD]-PEG$_4$-Aoa=Dau	1584.2	1585.0
1c	c[DKP*f3*RGD]-sC18(Dau=Aoa-GFLG-Lys^8)	3954.6	3955.6
2c	sC18(Dau=Aoa-GFLG-Lys^8)	3027.0	3027.9
3c	Dau=Aoa-GFLG-c[DKP*f3*RGD]	1587.4	1587.9

The same binding assay as for the drug-free conjugates was performed by Dr. Arosio with the drug conjugates and the results were quite promising and similar to the previous ones (Table 11).

Table 11. Inhibition of biotinylated vitronectin binding to $\alpha_v\beta_3$ and $\alpha_v\beta_5$ receptors. IC50 values were calculated as the concentration of compound required for 50% inhibition of biotinylated vitronectin binding as estimated by GraphPad Prism software; all values are the arithmetic mean SD of triplicate determinations. The values corresponding to the free ligand were previously described and are added here as reference. [156]

Code	IC_{50}[nM] $\alpha_v\beta_3$	IC_{50}[μM] $\alpha_v\beta_5$
1b	31.7 ± 4.2	>10
1c	9.7 ± 4.0	>10
3b	14.0 ± 1.6	6.3 ± 0.4
3c	5.8 ± 0.6	2.1 ± 0.1
c[DKP*f3*RGD]-NH_2	26.4 ± 3.7	>5

The presence of daunorubicin did not influence the binding to the receptors, contrarily the affinity, compared to the free functionalized ligand c[DKP*f3*RGD], was in some cases even improved (**1c, 3b, 3c**). Furthermore, the selectivity towards the two integrin types was maintained. Especially, we can recognize a difference between **1b** and **1c** but also **3b** and **3c**. It seems that a better binding is connected with the presence of the hydrophobic cleavable linker GFLG. An explanation for this result could be only demonstrated by docking studies where we could effectively see how the construct is positioned inside the receptor and which interactions are feasible to stabilize the complex.

After these encouraging results, we were interested to see how the secondary structure of the CPP-bearing conjugates would change with the addition of the drug and/or the ligand. The amphipathic helix is a common motif encountered in various proteins and peptides. Amphipathicity induces the partition of hydrophobic and polar residues between the two opposite faces of the α-helix, favoring membrane binding and penetration. [261] Previous works already demonstrated that sC18 assumes an amphipathic α-helical conformation when in contact with artificial lipid membranes, [183] therefore the tendency of the novel conjugates to form an α-helix was analyzed by CD spectroscopy.

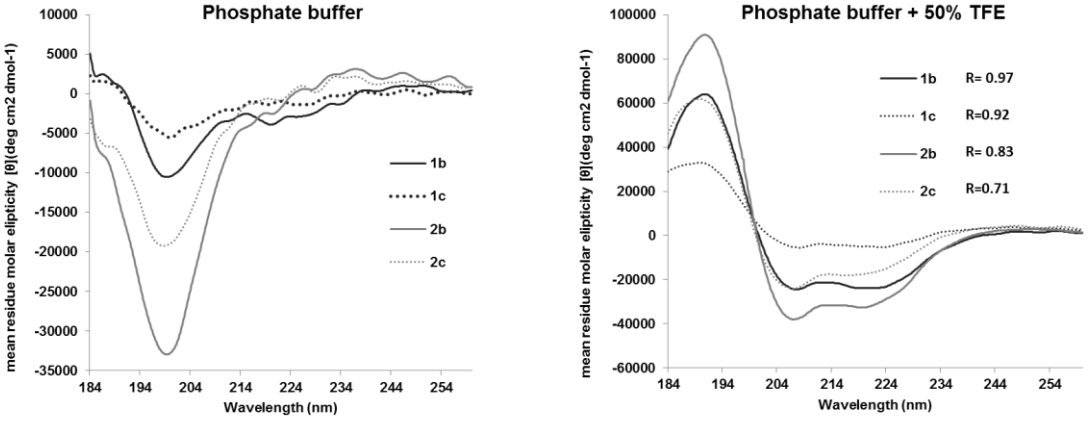

Figure 36. CD spectra of 1b, 1c, 2b and 2c in 10 mM phosphate buffer (left) and 10 mM phosphate buffer/TFE 1:1 (right). Peptide concentration was 20 µM.

The conjugates were dissolved in phosphate buffer but also in a 1:1 mixture of phosphate buffer and the secondary structure inducer TFE. The α-helical content can be quantitatively expressed through the R-value determined by the ratio between the ellipticity values at 220 nm and 208 nm, [262] where R=1 corresponds to an ideal α-helix. [263] While in phosphate buffer only a random-coil structure could be recognized, in the presence of TFE all the conjugates displayed the typical curve of an α helix (Figure 36). The first important observation that can be evidenced is the higher tendency of the c[DKP*f3*RGD] conjugates **1b** and **1c** to form a helix. This can be explained by the presence of the cyclic rigid construct at the *N*-terminus of the complex that could stabilize and elongate the whole structure. On the other hand it is possible that the c[DKP*f3*RGD]-linker is well inserted in the amphipathic sequence reinforcing the helix. This last theory would not be consistent with the calculated structure of the conjugate represented in Figure 28. In fact, in that case, the illustrated construct does not seem so homogeneous and it looks like the ligand is not embedded so well in the helical arrangement. Conversely, this structure was only calculated and the behavior in presence of a membrane could change the resulting organization. The corresponding GFLG variants **1c** and **2c** always display lower R values indicating that the helix is somehow hindered by the presence of this linker located in the middle of the sequence. Surprisingly, these results are exactly the opposite as for the binding studies: it seems that the presence of a better helix could somehow disturb the binding to the receptor. To demonstrate this, we should prove that during the cell-free binding assay in the presence of the receptors, an α-helix is also built.

Like for the GnRH-III conjugates, the coupling to daunorubicin proved to be very effective and the compounds could be obtained in a sufficient amount to perform further studies. In particular, the binding studies demonstrated that the coupling to daunorubicin did not affect the affinity to the receptor, indicating that Lys^8 in the sequence of the CPP was an ideal conjugation site. Furthermore, the secondary structure of the CPP was not disturbed by the presence of the drug in the central part of the sequence, since the R-value for **2b** is comparable to the one

of **2**, as already illustrated in previous works. [186] As a further improvement, the ligand even seemed to favor the formation of the helix and subsequently also a possibly interaction with the cell membrane. Based on these results, we thought that it was worth to continue investigating these conjugates starting with the examination of their cytotoxic effect on the already introduced cell lines U87, HT-29 and MCF-7.

First, the cytotoxic activity of the full-conjugates (**1b** and **1c**) and controls (**2b**, **3b** and **2c**, **3c**) was tested after 72h incubation in presence of the three cell lines. In Figure 37, the EC_{50} curves of every compound are depicted. For a more schematic summary, Table 12 shows the EC_{50} values for every cell line. The outstanding difference between the cytotoxic activity of the synthesized compounds (low micromolar range) and the EC_{50} of Dau (low nanomolar range) after 72h incubation had been already observed for the GnRH-III conjugates and, as previously outlined, it depends from the release of a metabolite that intercalates DNA with lower efficiency than the free drug (see Figure 23). Anyway, the lower activity of daunorubicin was not considered as a big problem as long as selectivity would be reached and a directed transport towards a specific cell line would be achieved. The different activity of the free drug observed in the three cell lines is purely depending on the different cellular uptake and not from a targeted transport as we want to achieve for our conjugates. These differences can be seen also in the case of the CPP controls and are purely connected to the different characteristics of every cell line. As already foreseen for the GnRH-III conjugates, after this long incubation time, we could not demonstrate any selectivity towards the integrin-overexpressing cell line U87. This is not valid for the controls **3b** and **3c**, where the lowest EC_{50} value is always exhibited by U87 cells, followed by HT-29 and MCF-7 cells. In this case, in fact, the CPP portion is missing and the internalization should be totally dependent on the presence of the receptor. Anyway, as already described by Bodero et al., within the 72h incubation a different uptake could be preferred mediated for example by other integrin receptors and this would explain why the EC_{50} values are not so divergent. [247] The best control to demonstrate this, would be to use isogenic knocked-out cells where the α_v subunit is not present to definitely confirm that the uptake is completely integrin-dependent.

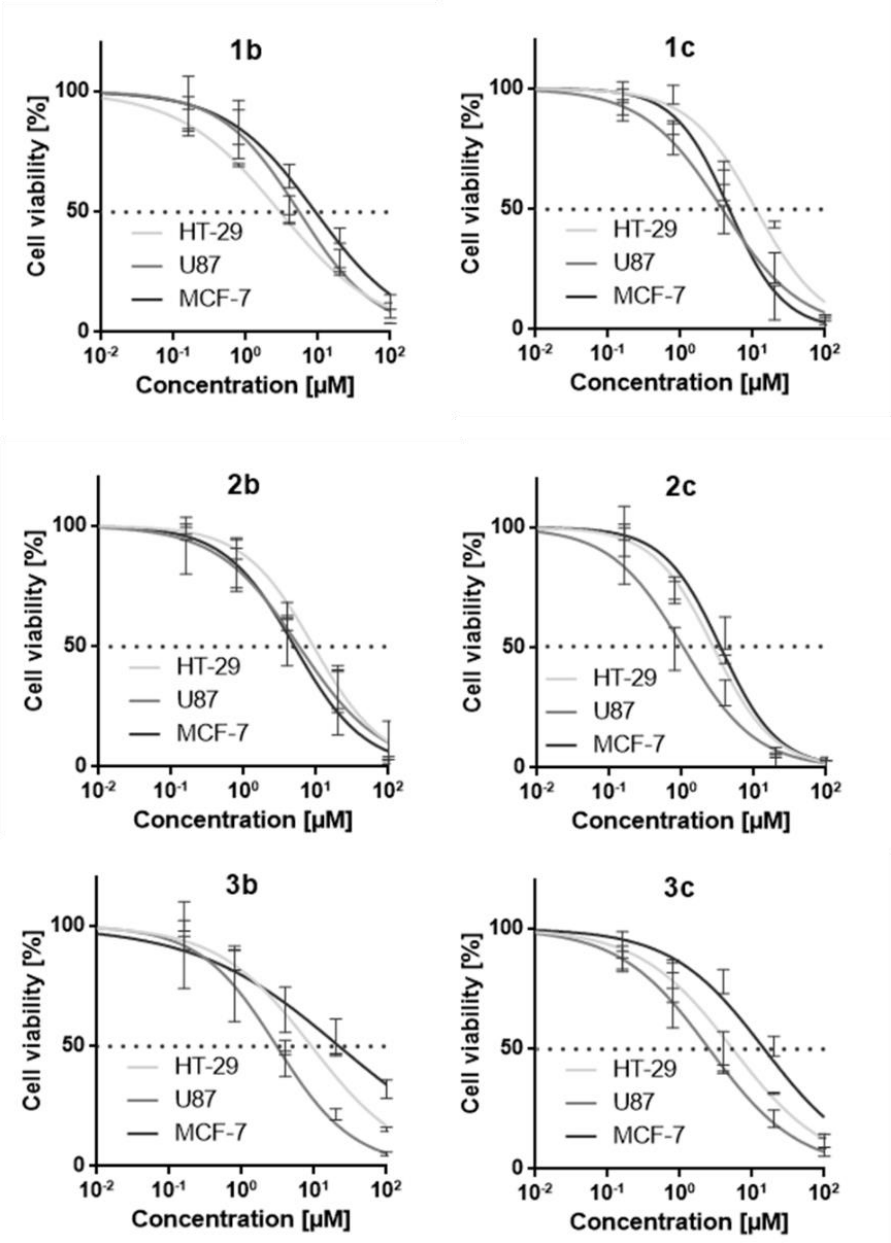

Figure 37. Antiproliferative assay with compounds 1b, 2b, 3b, 1c, 2c, 3c on U87, HT-29 and MCF-7 cells (72 h incubation). The peptides were incubated for 72 h without washout. Values from the positive control (DMSO/EtOH; 1:1) were subtracted from all data and the untreated cells were set to 100%. The experiment was performed in triplicate with *n=2.*

Table 12. EC_{50} values referred to the antiproliferative assays showed in Figure 37.

	EC_{50} [µM]						EC_{50} [nM]
	1b	**2b**	**3b**	**1c**	**2c**	**3c**	**Dau**
U87	5.6 ± 1.1	5.8 ± 1.5	3.0 ± 0.7	3.9 ± 3.9	1.1 ± 0.2	2.5 ± 0.7	7.8 ± 2.4
HT-29	2.9 ± 0.2	9.2 ± 0.1	9.2 ± 0.9	11.0 ± 1.1	2.8 ± 0.2	5.4 ± 1.3	37.9 ± 7.7
MCF-7	9.1 ± 2.11	5.0 ± 1.1	21.7 ± 8.3	2.7 ± 0.8	3.5 ± 0.4	14.7 ± 6.5	65.1 ± 18.3

We imagined that, since conjugates **1b** and **1c** showed a noteworthy binding affinity to $\alpha_v\beta_3$, they would selectively bind to the surface of U87 cells. In the case of MCF-7 and HT-29 cells this would also occur since they also express integrins but in a limited grade. If the incubation time is too long, the role of the ligand for the selective targeting would be surely annulled and the CPP internalization would not bring so many advantages in the activity of the drug. As we can see, after 72 h, the EC_{50} values of **3b** and **3c** are comparable to the outcomes of **1b**, **2b** and **1c**, **2c** at least for U87 and HT-29 cells. In general, as we already introduced for the GnRH-III conjugates, we thought that the incubation time should be shortened if we wanted to achieve the best results in terms of targeting since otherwise the different activities of each single conjugate would be leveled to the others after such a long interval. Our suggestion was in fact to demonstrate the consistent contribution of the CPP in the internalization of the CPP-bearing molecules meanwhile restricting the relevance of the ligand in the uptake process. Nevertheless, the binding should be efficient even in this short incubation and allow the conjugates to target the surface of the cell and subsequently improve the CPP-mediated uptake in the cell line displaying the integrin receptors, following the previously described "kiss and run" process. In fact we wanted to establish a model where we could visualize the *in vivo* condition where, after the therapeutics are administrated, they are only shortly in contact with the tissue and should exert their action very fast. By this strategy, we wanted to show that our novel compounds, in such a short time would be able to get in contact to the receptors, bind to them, but then be internalized through CPP-mediated uptake as we could infer from the results of the flow cytometry. With the intention to find better conditions to explore the biological activity of this drug-delivery system, we decided to perform the next experiments using shorter incubation times. The same strategy as for the GnRH-III conjugates was used, but before studying their cytotoxic effect, a deeper inspection in the internalization of the conjugates was carried out. The impact of the ligand and the CPP on the cellular uptake of all the conjugates and controls was analyzed by flow cytometry after 15 min incubation (Figure 38) and by CLSM after 30 min incubation (Figure 39) with the three cell lines. The choice of the different incubation time was due to the peculiar experimental conditions of the two assays. For CLSM, 15 minutes would be in fact too short to easily handle the cells and this would perturbate their condition complicating the entire experiment.

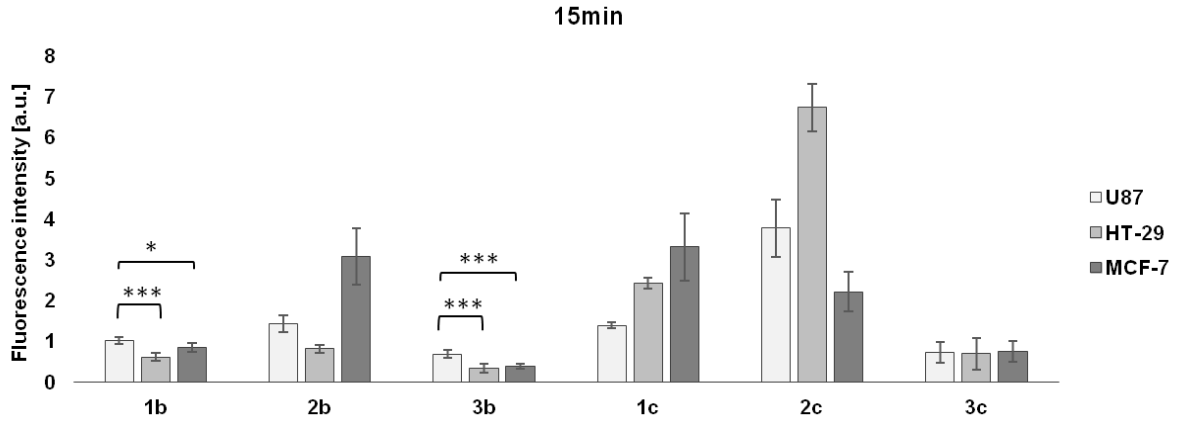

Figure 38. Cellular uptake of 1b, 2b, 3b and 1c, 2c, 3c in U87, MCF-7 and HT-29 cells quantified by flow cytometry. Cells were incubated with 10 µM peptide solution for 15 min at 37 °C. (*: $p \leq 0.05$; ***: $p \leq 0.001$). The results were normalized to the value of **1b** in U87 cells that is set to 1. The experiment was performed in triplicate with *n=2.*

A first general glance at the results starting from the conjugates without cleavable linker (**1b-3b**) shows us that the uptake of the compounds containing the ligand (**1b**, **3b**) is reduced if compared to the CPP (**2b**). **3b** shows a lower uptake compared to the CPP-containing counterpart since in this case the ligand is directly connected to the drug without the interposition of the CPP molecule. The internalization, being just receptor dependent, would be therefore reduced and slowed down. As for the other conjugate **1b**, in case of U87 cells it follows the same internalization tendency like for the CF-labeled compounds **1a** and **2a** (Figure 27, uptake after 30 min incubation) suggesting that the c[DKP*f3*RGD] containing conjugate would bind to the receptors and for this reason the uptake would be decreased, at least at the beginning. Since the incubation time in this case is even lower (15 min) this supposition would be even more justified. In the case of HT-29 and MCF-7 cells, this tendency could be explained by the worse internalization of these conjugates because of the presence of the ligand and the PEG linker, which somehow hinder the transport inside the cell as we previously discussed. This observation does not fit with the results obtained with the CF-labeled compounds where for HT-29 and MCF-7 cells no significant difference between **1a** and **2a** after 30 minutes could be recognized. It is important to notice that in this case the incubation time was different (15 minutes instead of 30 minutes) and that the uptake of **1a**, differently from **2a**, was previously recognized to be time-dependent. Therefore, it is possible that after 15 minutes **1b** is still taken up at a lower level. Furthermore, the labeling with a different molecule could also lead to discrepancies in uptake. In fact if we compare the uptake of **2b** in the three cell lines we also notice an outstanding contrast with the CF-compounds where U87 was the favored cell line. In this case the behavior is dissimilar and highly probably it is also connected with the different physicochemical properties of the two attached groups. In Figure 87 in the attachment the retention time of **1a** and **2a** is compared.

If we correlate the higher inclination of **1b** to generate a helix, we would expect that the full conjugate **1b** would be taken up at higher extent in every cell line, or at least in the negative controls since there, the uptake is not dependent on the receptor. On the contrary, the uptake of **1b** is always lower than **2b**. We could explain this contradictory result, changing the prospective from CD measurement to a real interaction with the cell membrane. At the beginning, the unfolded peptide is laying in parallel with the membrane interacting with the phospholipid heads. Afterwards, the peptide spontaneously moves to the core of the membrane interacting with the hydrophobic tails (hydrophobic effect) and the sequences rearrange to form a helix that reduces the exposition of the peptide bonds. In the case of **1b** we demonstrated that the helix could be also formed but the initial transfer and insertion inside the membrane could be limited by the presence of the highly hydrophilic ligand-linker construct. For this reason, these two characteristics (α-helix formation and better cellular uptake) cannot be directly correlated without considering other important factors.

Anyway, most importantly, if we compare the three cell lines we can observe a significant selectivity for the conjugates **1b** and **3b** towards U87 cells that is not present for **2b** (lacking the targeting moiety). This is a very good result because we can see that at the extent of better cellular uptake, a targeting could be favored. The internalization of **3b** in U87, being just receptor dependent, is reduced compared to the CPP but anyway consistent because of the over-expression of the receptors on the surface of these cells, in contrast to the control cell lines. In this context, contrasting observations were done in the group of Prof. Gennari where RGD-camptothecin conjugates labeled with a naphtalimide fluorophore were tested on U87 cells and the β_3-KO isogenic cells. In this case, after 3 h incubation, no correlation between the integrin expression and the cellular uptake could be determined because an observed reduction of fluorescence intensity between 7 and 12% could be measured while in our case the uptake in the control cell lines HT-29 and MCF-7 was reduced to around 50%. An explanation of this behavior was explained by Pina et al. with a possible role of other integrins in the uptake of the conjugates in this longer incubation time as we already described for the previous cytotoxicity assays. [166] In our case the minimal uptake observed in HT-29 and MCF-7 cells could be explained by the choice of the control cell lines, which seems to be a crucial problem in many works. In fact it would be highly desirable to have α_v-KO cells for this purpose. In the case of **1b** we can say that we could succeed in synthesizing a compound that is taken up better than the homing peptide alone and more selectively than the CPP where in fact the selectivity is completely lost. We could demonstrate here that the ligand is slightly hindering the ability of the CPP to translocate through the membrane but it is also favoring a good targeting. The 15 minutes incubation has been a very important model in this case because it could mimic the *in vivo* situation where the compounds come in contact with the cells for a very

short time interval and the binding to the receptor could ideally direct the system to interact with the surface.

The microscope images underline the same tendencies observed for the first three conjugates by flow cytometry analysis (Figure 39). Nevertheless, in this case, a direct comparison between the three cell lines is not so simple since, as already mentioned before, in this kind of experiment the strong influence of the biological characteristics of each cellular system has to be taken into account, starting from the tendency of U87 cells to form clusters that easily detach as soon as the medium is removed and a new solution is added. Indeed, the shape of U87 cells cannot be defined so well as for the other cell lines and this is a sign that these cells do not perfectly adhere to the well surface. Anyway, we can state that for all the conjugates a consistent uptake inside the nuclei could be determined proving that a daunorubicin-containing metabolite is always generated and can reach its site of action. All in all, a lysosomal degradation assay would be very interesting to see how each conjugate is processed after being internalized in the cells and which metabolite would be able to translocate through the nuclear membrane to reach its target. In this case we could even justify the different relocation of every conjugate inside the cell, observed in the CLSM pictures.

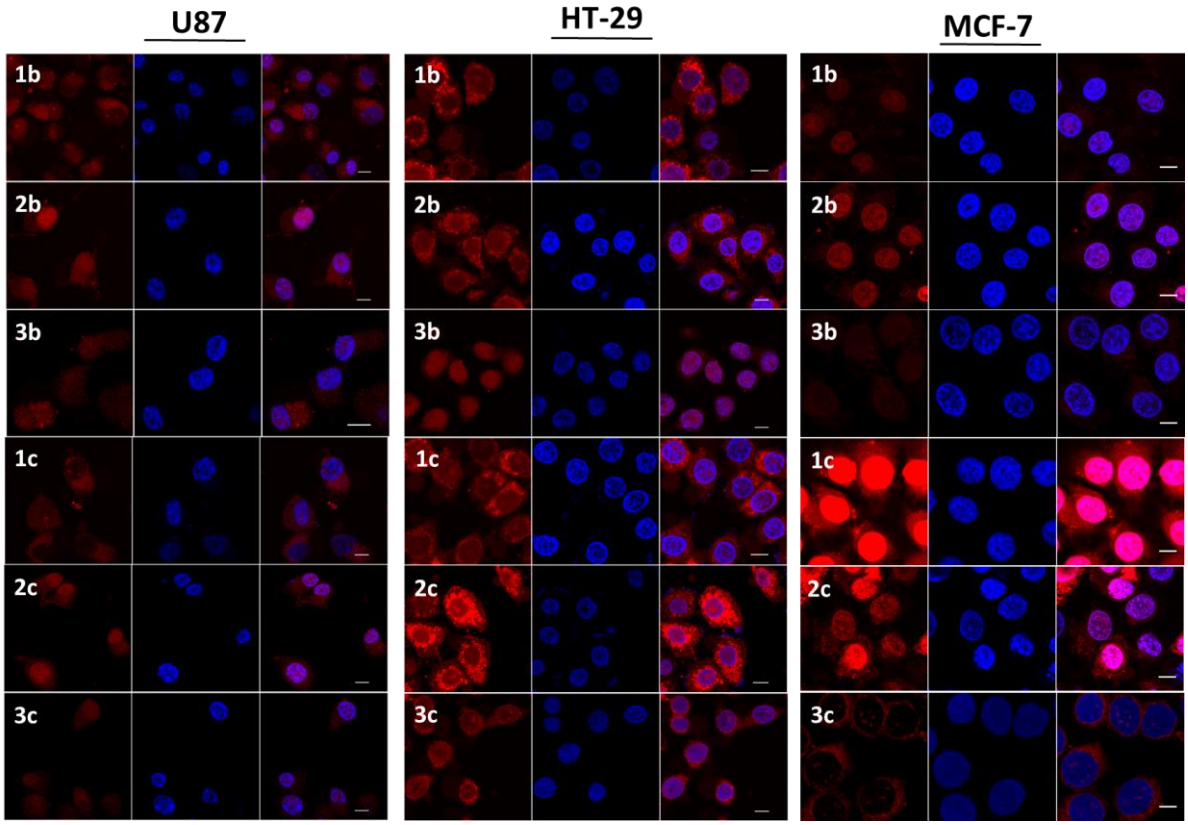

Figure 39. Cellular uptake of compounds 1b, 2b, 3b and 1c, 2c, 3c analyzed by CLSM in U87, HT-29 and MCF-7 cells. Cells were incubated for 30 min with 10 µM of the Dau-conjugate solution at 37°C. External fluorescence was quenched by treatment with 150 µM trypan blue for 15 sec. Red: Dau-conjugate; blue: Hoechst 33342 nuclear stain; scale bar is 10 µm.

Unfortunately, the previously observed selectivity was completely lost in the case of the conjugates containing the cleavable linker between the CPP and the drug molecule (**1c-3c**). In general, the GFLG linker increases the unselective uptake compared to the previously described conjugates. In this regard, we have to take into consideration that cathepsin B could play a big role by promoting the cleavage of the drug and presumably favor the further penetration of the conjugates and at this point, the investigation on the expression level of cathepsin B in the different cell lines would be crucial. In general, the GFLG conjugates are taken up at higher extent in every cell line but have a great influence in particular in HT-29 and MCF-7 cells. This is an outstanding improvement regarding the penetration ability of the CPP but it is of course a disadvantage in terms of selectivity. Furthermore, we should take into consideration also different factors connected with the physicochemical characteristics of these compounds. In fact, in the case of **1c** and **2c** the uptake improvement is maybe explained by the increase of the hydrophobicity introduced by the cleavage site that facilitates the internalization compared to **1b** and **2b** (see Figure 88 in the attachment for the comparison of the retention time of **2b** and **2c**). The higher uptake is verified also in the case of **3c** in comparison to **3b**, but still at a lower extent respect to the CPP-containing conjugates. Since in this case only the ligand should be responsible for the internalization, a hypothesis for the higher uptake in every cell line, leading to comparable fluorescence intensities, could be connected with the higher binding affinity shown by the binding assay. Furthermore, overexpression of cathepsin B in HT-29 and MCF-7 cells could lead to a faster degradation of the compound in the endosomes, a more rapid receptor recycling and promoted uptake. The microscopy pictures (Figure 39) are in line with the FACS studies. In particular, the higher uptake of **1c** and **2c** in HT-29 and MCF-7 cells is remarkable and a cytotoxic effect can be evidenced as a sign of a higher internalization.

The results of this last experiment could finally support a significant selectivity for **1b** and **3b**. In contrast to this observation, the GFLG bearing conjugate **1c** showed an enhanced uptake with a contemporary loss of selectivity while **3c** showed comparable results in the different cells. These data were qualitatively and quantitatively confirmed by flow cytometry and CLSM data, which are in good correlation. As a further demonstration of our finding, another very important experiment was performed testing the cytotoxicity of all these compounds after 15 min incubation. In order to assure the activity of the drug, the medium was removed but fresh medium was added for further 72 h. Notably, since we wanted to avoid a premature cell detachment, no washing step was performed. Especially, we wanted to correlate the results of the cellular uptake with the outcomes of this assay.

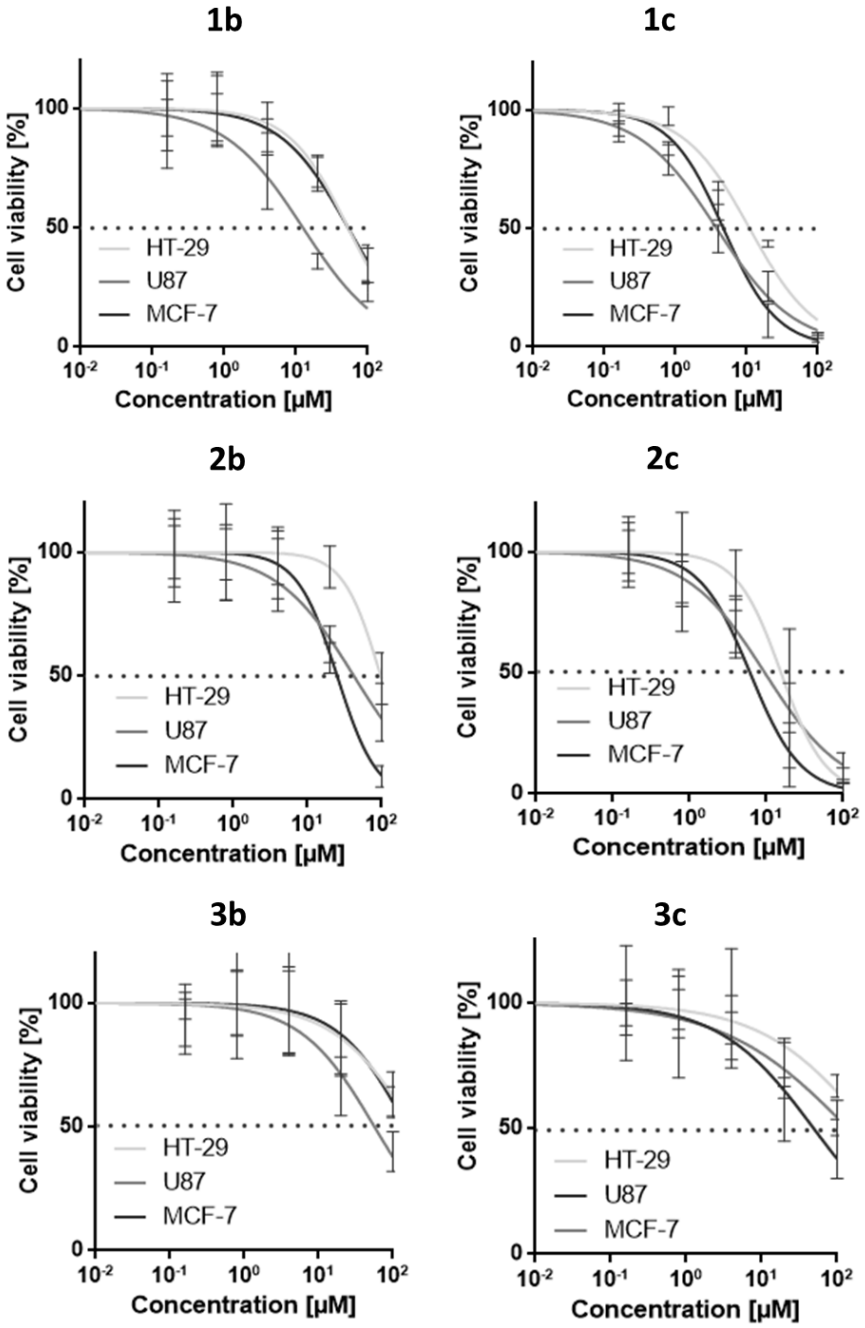

Figure 40. Antiproliferative assay with compounds 1b, 2b, 3b and 1c, 2c, 3c on U87, HT-29 and MCF-7 cells (15 min incubation). The peptides were incubated for 15 min and, after removing the medium, the cells were incubated for further 72 h. Values from the positive control (DMSO/EtOH; 1:1) were substracted from all data and the untreated cells were set to 100%. The experiment was performed in triplicate with *n=2.*

Table 13. EC_{50} values referred to the antiproliferative assays showed in Figure 40.

	EC_{50} [µM]						EC_{50} [nM]
	1b	**2b**	**3b**	**1c**	**2c**	**3c**	**Dau**
U87	12.5 ± 3	42.2 ± 12.3	56.9 ± 26.3	23.8 ± 4.4	9.6 ± 3.2	49.37 ± 16.0	78 ± 8
HT-29	50.5 ± 14.0	>80	>180	>80	22.0 ± 7.5	>250	215 ± 105
MCF-7	53.4 ± 15.6	25.1 ± 4.5	>140	7.8 ± 1.5	6.1 ± 1.2	>140	220 ± 89

The EC_{50} curves are depicted in figure 40 and the EC_{50} values are summarized in table 13. Essentially, we can repeat the same observations made for the FACS studies. The selectivity towards **1b** and **3b** is here clearly detectable; in particular for both compounds the curves of HT-29 and MCF-7 cells are overlaying leading to very similar EC_{50} (differences are connected with the standard deviations obtained for each measurement point) while U87 cells presents a 4-fold lower EC_{50} compared to the control cell lines. Also in the case of **2b** the cytotoxic profile in each cell line fits very well to the FACS data: the higher the internalization, the stronger the toxicity in the order MCF-7 > U87 > HT-29. For **1c,** as we previously mentioned, the selectivity is lost but the EC_{50} does not exactly correlate with the previous data, as also in the case of **2c**. In this assay, in fact, cathepsin B enzymes could have a more relevant role in the activity of the conjugates since, after internalization, they could exert their enzymatic activity within the 72 hours. Surprisingly, the selectivity is also maintained for **3c**. An explanation for this could be related with the high binding affinity of **3c** to the receptors, which would allow the conjugate to bind to the cell surface and be internalized even after removing the medium with the peptide solution, since no intermediate washing step was performed. This is a good point, which would also explain the higher selectivity obtained in this assay for **1b** and **3b** compared to the FACS data.

Finally, we proved that **1b** could be a very efficient peptide-drug conjugate with selectivity to $\alpha_v\beta_3$ expressing cells. Every element of this hybrid conjugate is essential for the distinctive behavior of this compound, for instance the presence of the c[DKP*f3*RGD] ligand is necessary for the targeting ability (**1b** is selective in comparison to **2b**), the CPP is enhancing the internalization of the construct, leading to greater toxicity even in a short treatment (**1b** is taken up at higher extent in comparison to **3b**) and the PEG is fundamental to separate the two moieties and allow the maintenance of the distinguishing features of every component.

4. Head-to-tail cyclization of a cell-penetrating peptide through DKP scaffolds

4.1. Novel cyclic peptides bearing a DKP scaffold

The project presented in this part of the thesis has been developed during my secondment in Como, in the group of Prof. Piarulli at Università dell'Insubria. Thanks to the expertize in synthesizing DKP scaffolds, I was taught how to proceed with the preparation of DKP3, which I could successfully synthesize but, most importantly, I started a very strong collaboration with the PhD student Sara Parente, who provided me many times with various batches of DKP1 and DKP3. Aside from this, we also worked in deep contact, trying to optimize the cyclization conditions.

4.1.1. Synthetic strategy

First, the scaffolds DKP1 and DKP3 were synthesized as already reported [153]. The linear peptide sC18* was synthesized by automated Fmoc/tBu-based SPPS. Chlorotrityl resin was used as solid support because of the very mild conditions required cleaving the protected peptide fragment from the resin prior to cyclization. We observed that loading of the chlorotrityl resin with Fmoc-Lys(Boc)-OH was not very effective, so we decided to use a preloaded resin. Afterwards, the DKP scaffold was manually coupled to the *N*-terminal sC18* peptide chain, still immobilized on the solid support, followed by reduction of the azido group with dithiotreitol occurring in almost quantitative yields (Figure 41). [264]

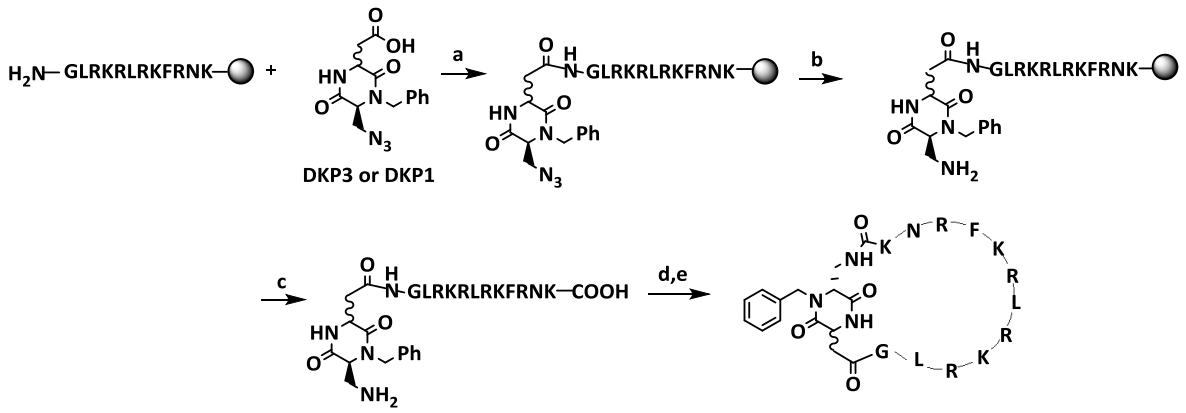

Figure 41. Synthetic strategy for the synthesis of the DKP scaffold-bearing cyclic peptides cyc-DKP1 and cyc-DKP3. Reagents and conditions: **a**: 3 eq. Oxyma, 3 eq. DIC, overnight; **b**: DTT (2M), DIPEA (1M), DCM, 3 h; **c**: acetic acid/ TFE/ DCM 1:1:8, 2h; **d**: BOP (6 eq.), HOBt (6 eq.), DIPEA (12 eq.), DMF (0,2 mM), rt, overnight; **e**: full cleavage with TFA/phenol/H_2O/thioanisol/EDT 82.5:5:5:5:2.5, 3h.

Trying to obtain the best performance, using the most favorable conditions, Sara Parente planned to exploit the tendency of the *cis*-DKP1 scaffold to keep the two branched ends in the same direction like forming a β-hairpin. [265-267] In this case the disconnection was inserted in the middle of the sequence and the cyclization would not directly involve the DKP scaffold as

in the previous cases. Unfortunately, no improvement of the cyclization yield was obtained (data not shown). Comparable results were achieved by using a reverse sequence of the peptide: the strategy behind this was to insert the glycine residue at the *C*-terminus, avoiding racemization and allowing the cyclization with a less steric hindered amino acid instead of lysine (data not shown). Other expedients have been successfully investigated and actually led to a meaningful advancement. After cleavage of the protected linear peptide from the resin, the acidic solution was removed by reduced pressure and the remaining acetic acid was evaporated in many cycles by adding hexane, acting as azeotrope. A fundamental point in this process has been determined by the washing and digestion of the obtained white powder with a 5% $NaHCO_3$ solution, filtration and further washing with H_2O to remove the salts that could disturb the next steps (e.g. by acetylation of the *N*-terminus). Subsequently, solution-phase cyclization could be carried out on the crude lyophilized peptide. Use of dry DMF was not considered as necessary since the yields with normal DMF were comparable, but a high dilution was crucial to favor the intramolecular reaction at the expense of dimer formation; for this reason, the concentration was lowered from 0.65 mM to 0.2 mM. [268] Another decisive adjustment was a second addition of BOP after 6-8 hours from the beginning of the reaction, since this coupling reagent is degraded after 8-10 hours, contrarily from HOBt, which is regenerated. Thanks to these numerous arrangements, yield of cyclization, after cleavage of the protecting groups and purification of the final compound, ranged from 22% for **cyc-DKP1** to 36% for **cyc-DKP3**. Generally, we assumed that the DKP3 scaffold allows a more efficient cyclization by favoring a pre-organized conformation. However, in both cases the cyclization remained the major yield-limiting step. The linear versions including the two DKP scaffolds at the *N*-terminus, **lin-DKP3, lin-DKP1**, were also synthesized (Table 14) and were important to better investigate, not only the role of the cyclization regarding both the spatial and the biological activity, but also the influence of a non-natural building block inside the peptide structure and how this heterocycle could interfere with the features of the CPP.

Table 14. List of DKP-bearing synthesized compounds with their names, sequences and molecular weights (MW calculated and experimental). ____: amino acids involved in cyclization

Name	Sequence	MW [g/mol]	MW_{exp} [g/mol]
cyc-DKP3	DKP3-GLRKRLRKFRNK	1827.3	1827.7
lin-DKP3	H_2N-DKP3-GLRKRLRKFRNK-OH	1845.3	1845.7
cyc-DKP1	DKP1-GLRKRLRKFRNK	1827.3	1827.7
lin-DKP1	H_2N-DKP1-GLRKRLRKFRNK-OH	1845.3	1845.7

4.1.2. Circular dichroism

In order to generate an overall picture of the peptide structure, circular dichroism spectra of the synthesized compounds were measured in phosphate buffer alone or in presence of the α-helix inducer TFE (figure 42). In agreement with known literature data [183, 269], the linear compounds showed a disordered random coil structure in aqueous phosphate-buffered solution, while after addition of TFE preferably formed an α-helix. For **lin-DKP1** we obtained R=0.7, while for **lin-DKP3** a lower value of 0.62 was calculated. This means that this small DKP scaffold at the *N*-terminus of the sequence seems to have an influence on the tendency to develop a helix stabilizing the structure in a different manner depending on the *cis* or t*rans* conformation. Probably the DKP1 follows the right arrangement to continue the helix framework, while the DKP3 generates a certain disorder, counterposed to the helical arrangement. Regarding the cyclic peptides, **cyc-DKP1** appeared to be pretty flexible switching from random coil to helical arrangement, in particular in the presence of TFE. As shortly presented in the introduction, the DKP1 was often used as β-hairpin inducer to stabilize the formation of β-sheets: this is not the case within the cyclic organization but this is also not favoring the generation of a helix. In contrast, **cyc-DKP3** appeared more structured displaying the typical spectra of slightly helical peptides even in phosphate buffer. These observations were made after looking at the general pattern and comparing it to the traditional schemes; since the minima and maxima are slightly shifted, we cannot refer to these curves as the typical spectra of helical peptides and the R-values were not calculated. Therefore, we considered that the linear and cyclic compounds should be further investigated by NMR analysis to prove what we could observe through these preliminary assays.

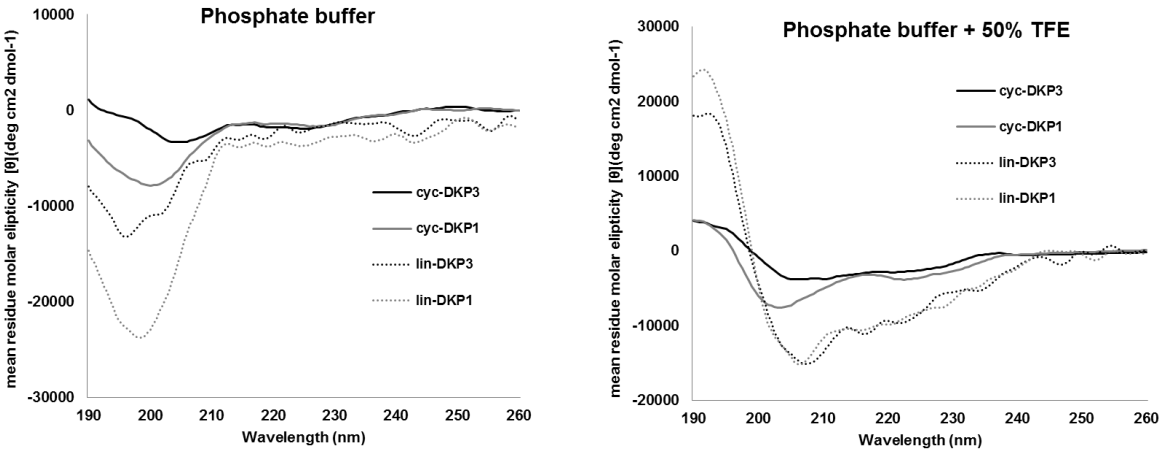

Figure 42. Secondary structure investigation of the linear and cyclic compounds by circular dichroism. CD spectra of the cyclic (**cyc-DKP3** and **cyc-DKP1**) and linear (**lin-DKP3** and **lin-DKP1**) peptides in 10 mM phosphate buffer (left) and 10 mM phosphate buffer/TFE 1:1 (right). Peptide concentration was 20 µM.

4.1.3. NMR-based structure elucidation

The three dimensional structures of both linear and cyclic derivatives have been investigated by NMR spectroscopy by Dr. Díaz and the PhD student Linda Jütten (Department of Chemistry, University Cologne). Although peptides were not isotopically labeled (i.e., 13C and/or 15N) and the availability of sample was limited, their size (12 amino acids and DKP linker, MW ca. 2 kDa) was fortunately appropriate to carry out a full structural analysis based exclusively on mono- and bidimensional homonuclear proton NMR spectra. [270]

Overall, the 2D TOCSY and 2D NOESY spectra of the linear peptides **lin-DKP1** and **lin-DKP3** in aqueous buffer solution suggested a lack of secondary structure. The NMR data acquired at 298 K indicated a random coil structure also for the cyclic peptides. Contrarily, the 2D NOESY spectra of **cyc-DKP3** and **cyc-DKP1** acquired at lower temperatures (i.e., the lowest temperature allowed for aqueous NMR samples is 283 K) seemed to address specific conformational preferences for these peptides pointing out that the stereochemistry of the DKP unit is determinant for the conformational arrangement of cyclic peptides, as already described by Potenza and coworkers. [271] A closer inspection of all the structures suggested that not only one but several structural families may coexist in solution, what has been already demonstrated for other DKP-cyclic peptides (Figure 43).

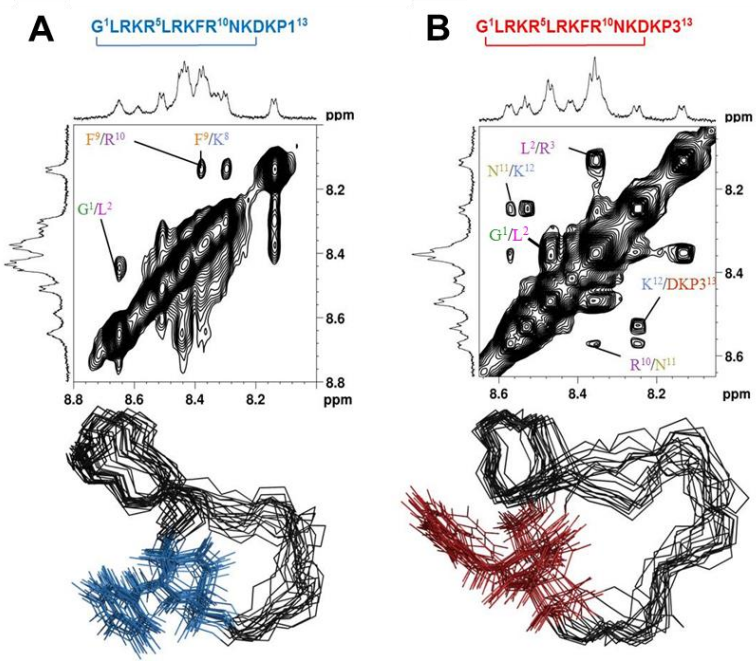

Figure 43. 2D NOESY spectra of cyc-DKP3 and cyc-DKP1 acquired at 283 K and correspondent structural families. (top) Amide-amide region of the 2D $^{1}H,^{1}H$- NOESY spectra of cyclic peptides (**A**) cyc-DKP1 and (**B**) cyc-DKP3 in solution (50 mM phosphate buffer, pH 6.08, water:D_2O 9:1, 283 K, mixing time 200ms, 600MHz). (bottom) Overlay of the ensemble of 20 final energy-minimized CYANA structures of the peptides in solution. The main chains are shown in black and DKP unit at the N-terminus with color ((**A**) DKP1, blue; (**B**) DKP3, red).

Most importantly, according to these structure calculations, the mostly preferred conformation within the structural families described at 283K for **cyc-DKP3** seems to exhibit hydrogen bond interactions including Lys^{8}(C=O)-(HN)Asn^{11}, Lys^{8}(C=O)-(HN)Lys^{12} and Arg^{5}(C=O)-(HN)Arg^{7} residues (Figure 44).

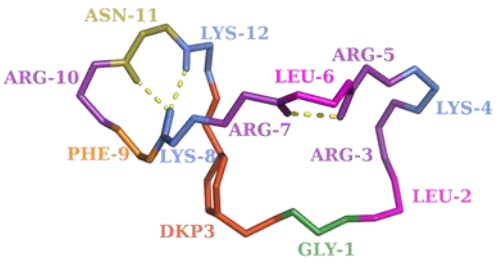

Figure 44. Line plot of the solution structure of cyc-DKP3, calculated from NMR derived data collected at 283 K. Hydrogen bond interactions are shown as yellow dashes.

To shed light onto a possible interaction of the peptides with cell membranes, NMR experiments were conducted not only in aqueous medium but also in SDS micellar medium as it is considered, among others, a suitable membrane mimetic agent. In Figure 45 the 1D ^{1}H NMR spectra of the linear DKP-peptides in the presence of SDS micelles are displayed. Generally, an evident broadening of the signals was observed, what is normally taken as indication of an effective interaction of the peptide with the micelles. The signals in the amide region were also comparatively more dispersed than the equivalent ones in aqueous medium, what pointed out that peptide conformational changes have been induced by the presence of the micelles.

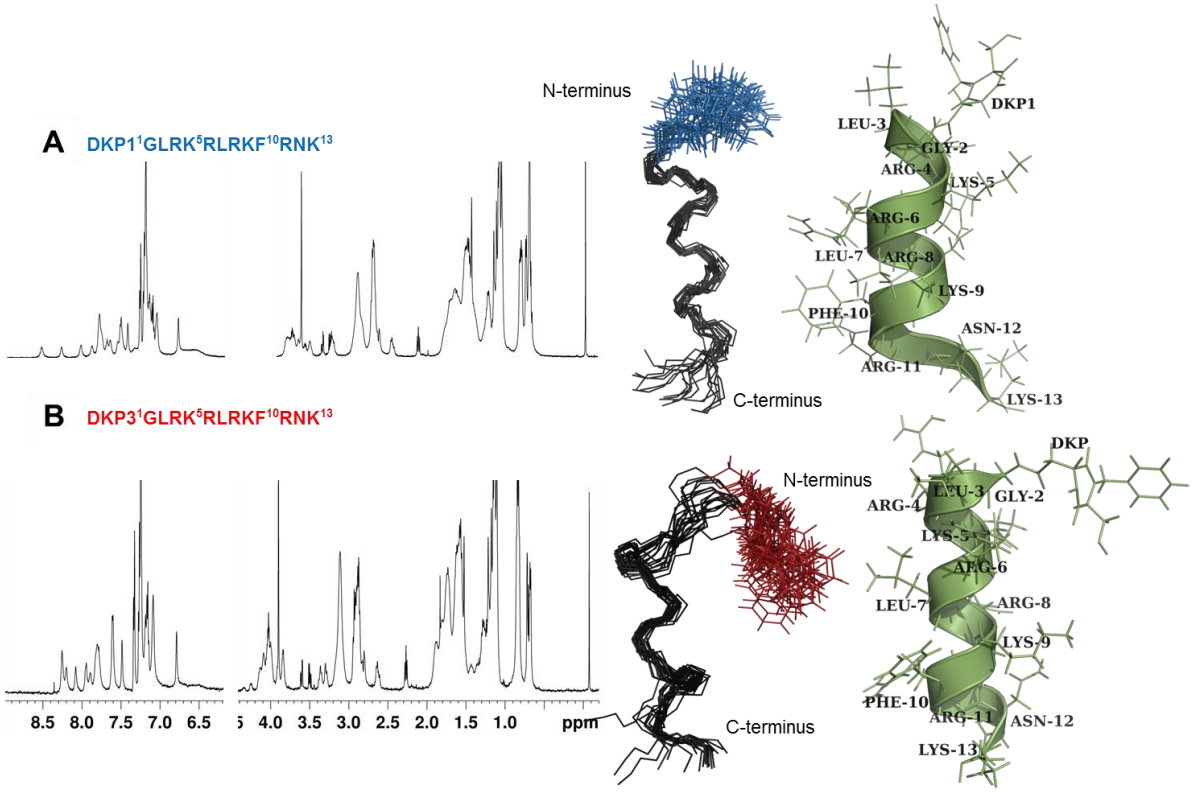

Figure 45. Structure evaluation of the linear peptides in presence of SDS micelles. (left) 1D ^{1}H NMR spectra of linear peptides (**A**) **lin-DKP1** and (**B**) **lin-DKP3** in the presence of SDS micelles (peptide concentration ca. 1.3 mM, peptide:SDS 1:80, 50 mM phosphate buffer, pH 6.08, water:D_2O 9:1, 298 K, 600MHz). (right) Overlay of the ensemble of 20 final energy-minimized CYANA structures of the peptides in the presence of SDS micelles. The main chains are shown in black and the DKP unit at the N-terminus with color ((**A**) DKP1, blue; (**B**) DKP3, red). Also the ribbon diagrams of the lowest energy structures are shown in a stick model.

This result correlates very well with the outcomes from the circular dichroism in presence of TFE even if in this case, the insertion of a DKP residue in the sequence does not seem to play an important role since no interaction between DKP and any other residue of the peptide sequence was observed.

The preparation of the NMR samples containing the cyclic peptides and SDS micelles has been until now quite complicated. The spectra of cyclic peptides in the presence of SDS micelles exhibit an extraordinary broadening of the signals that could indicate a more efficient interaction between cyclic derivatives and micelles than the one occurring between linear peptides and micelles (Figure 46A). Because of the poor resolution of the spectra, the standard methods for assignment and structural elucidation failed systematically. As a proof of peptide-micelle interaction, however, the diffusion coefficient values of **cyc-DKP3**, both in solution and in the presence of micelles, were measured and the results were then compared and analyzed (Figure 46B). Although perdeuterated SDS micelles were employed (i.e., d_{25}-SDS), remaining protonated signals of the micelles were visible and could be easily identified. The experiment

provided information about the diffusion coefficients of peptide and micelles as well as about any other species present in the solution mixture including impurities or the chemical shift reference system (i.e., TSP).

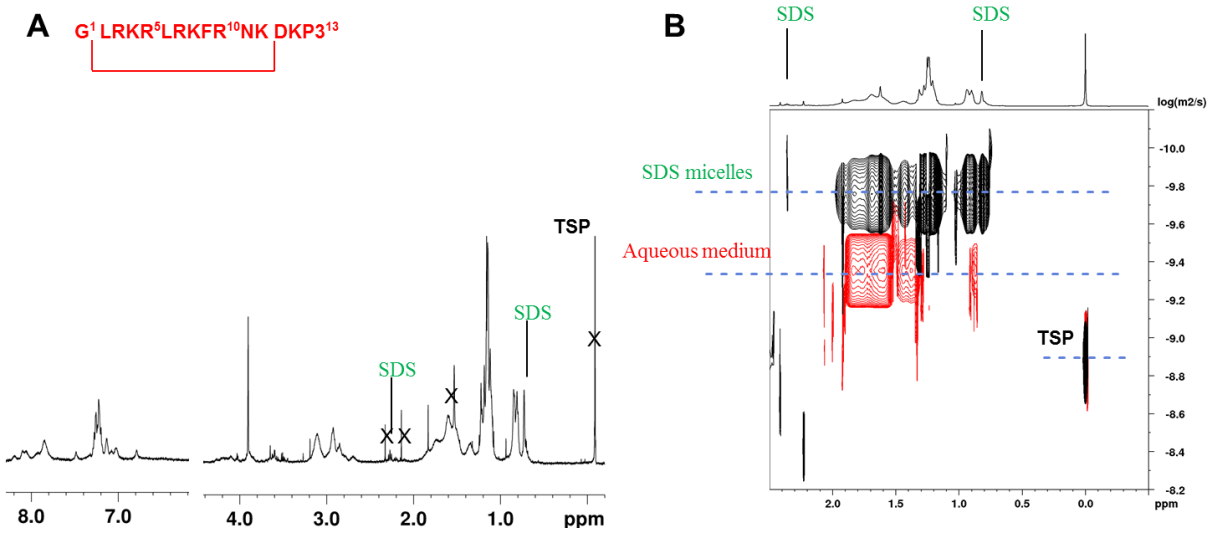

Figure 46. Structure evaluation of cyc-DKP3 in presence of SDS micelles. A: 1D ^{1}H NMR spectra of **cyc-DKP3** in the presence of SDS micelles. **B**: Overlapped DOSY NMR spectra of the peptide free (red) and in the presence of SDS micelles (black) (peptide:SDS 1:80, 50 mM phosphate buffer, pH 6.08, water:D_2O 9:1, 298 K, 600MHz).

As it can be deduced from the DOSY spectra, the diffusion coefficient values of peptide and micelles are coincident although the molecular weight of both the micelle (theoretically ca. 60x SDS) and peptide are very much uneven and substantial different diffusion properties were expected. Since TSP does not seem to interact with the micelle, its diffusion coefficient was taken as diffusion reference and, from this result, one can clearly assert that **cyc-DKP3** is effectively interacting with the micelle since its diffusion coefficient changes drastically in the presence of SDS micelles and has the same value as the micelle itself.

4.1.4. Biological evaluation

Taking advantage of the interesting results obtained from the investigation of the secondary structure, further examinations of the cyclic peptides in cellular systems were performed. First, the influence of cyclization on cell viability was determined. To this purpose, the cytotoxicity of all peptides on the tumor cell line HeLa was tested (figure 47). After 24 h incubation, the peptide solution was washed-out and the cells were further incubated for additional 48 hours. As first evidence, the cyclic peptides show a more significant toxicity compared to the correspondent linear versions. As we could already infer from the calculation of the diffusion coefficient of **cyc-DKP3** in micellar medium, the cyclic peptides are presumably interacting with the lipid environment at higher extent than their linear counterpart. As a consequence, even distinct entry pathways could be imagined leading to a different cellular uptake level, and finally, cytotoxicity. However, this is not the only consideration that can be drawn from the analysis of

these results. In fact, a very meaningful difference can be observed in association with the use of *cis* or *trans* DKP scaffolds. Since preliminary studies in presence of SDS micelles were performed only for **cyc-DKP3** we cannot directly explain this result by a concrete demonstration even if a strong influence of the DKP scaffold was already remarked from the analysis of the NOE cross peaks at lower temperature (Figure 43). Furthermore, **cyc-DKP3** also showed a higher tendency to form H-bond within the residues which could lead to a more rigid structure. Nonetheless, the highest toxicity corresponding to around 60% viability was only observed at peptide concentrations of 100 µM. Since at lower concentrations, the toxicity was still around 80% after 72h, we concluded that the cyclic compounds could be safely used for further experiments.

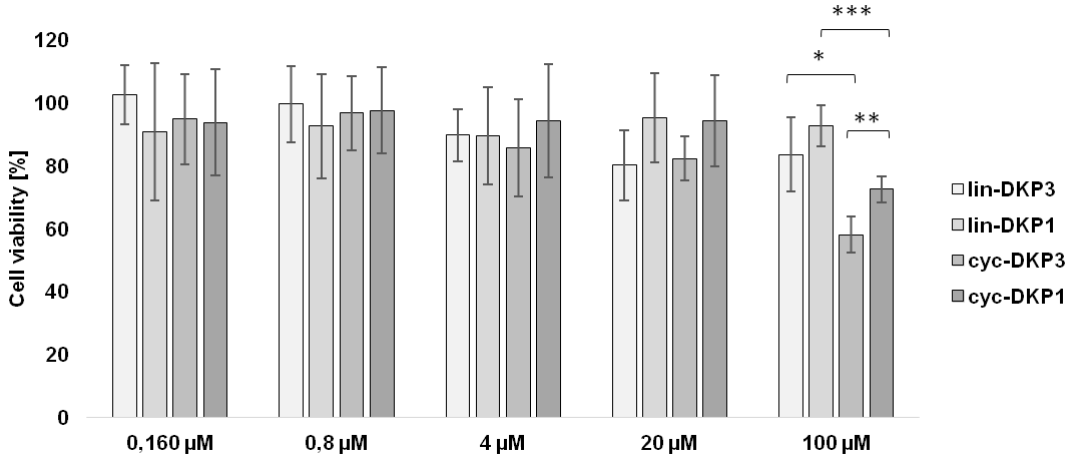

Figure 47. Effect of the linear (lin-DKP3 and lin-DKP1) and cyclic (cyc-DKP3 and cyc-DKP1) peptides on the viability of HeLa cells measured by resazurin-based assay. Evaluation of the resorufin fluorescence generated from resazurin by viable cells after 24h incubation with the peptide solutions, washout and further incubation for 48h. Untreated cells were used as negative control and set to 100%; positive control was represented by cells treated for 10 minutes with 70% EtOH and it was subtracted from the other values. (*: p≤ 0.05; p**: p ≤ 0.01; ***: p ≤ 0.001). The experiment was performed in triplicate with *n=2.*

4.2. Drug delivery with cyclic peptides

The peculiar interplay between the cyclic peptides and the cell membrane could promote the cellular uptake of other molecules, such as cytostatics. To demonstrate this hypothesis, we investigated if the peptides were able to support and enhance the intracellular uptake of daunorubicin. The anticancer activity of the drug was evaluated, with and without the presence of the peptide. Co-incubation was performed using 10 µM of **cyc-DKP3** solution and 80 nM of daunorubicin (concentration at which almost 40% of cells were still viable). From Figure 48, it can be clearly seen that the co-treatment with the peptide and the drug revealed an increased toxic activity in comparison with the drug alone. This was already a hint about a possible mechanism showing the peptide as useful promoter of penetration.

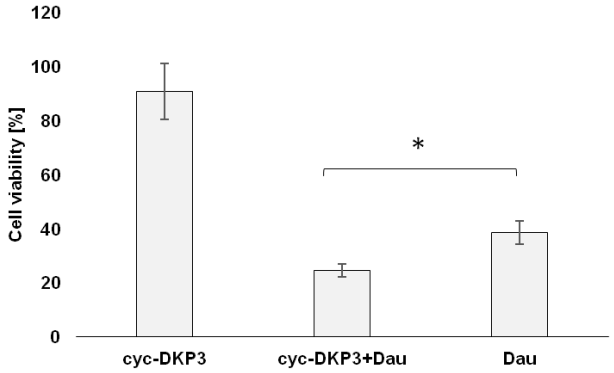

Figure 48. Influence of daunorubicin on the viability of HeLa cells with or without the cyclic peptide cyc-DKP3 measured by resazurin-based assay. Evaluation of the resorufin fluorescence generated from resazurin by viable cells after 24h incubation with the peptide solutions, washout and further incubation for 48h. The assay was performed adding 10 µM of peptide solution together with 80 nM daunorubicin solution or only the free drug without peptide. The peptide alone was evaluated as a reference to prove the absence of toxicity at the tested concentration. (*: p≤ 0.05). The experiment was performed in triplicate with *n=2.*

The same feature was evaluated also by CLSM (Figure 49). Co-incubation was performed using 10 µM of **cyc-DKP3** solution and 1 µM of daunorubicin. We were interested in observing if, in the presence of the peptide, the uptake of the drug molecule would be stronger, thus corroborating the outcomes of the cytotoxicity assay. We were pleased to observe that the cyclic peptide could really act as efficient carrier transporting daunorubicin at much higher extent inside the cells if compared with the drug alone. It is known from the literature that daunorubicin enters the cell via direct transportation through the membrane, being a small molecule, able to interact with the negatively charged outer surface of the cell membrane and capable to insert within the lipid phase of the membrane. [272] We can imagine that the cyclic CPP could mediate the formation of pores through which the drug could easily enter the cells in a faster way than passive diffusion. The distribution is uniform but with the presence of a punctuate pattern that shows a coexistence of endocytic pathway and direct penetration, so we could also imagine that being the CPP also internalized by endocytic pathway, the drug could also interact with the negatively charged phospholipids and be inserted in the endosomes together with the peptide.

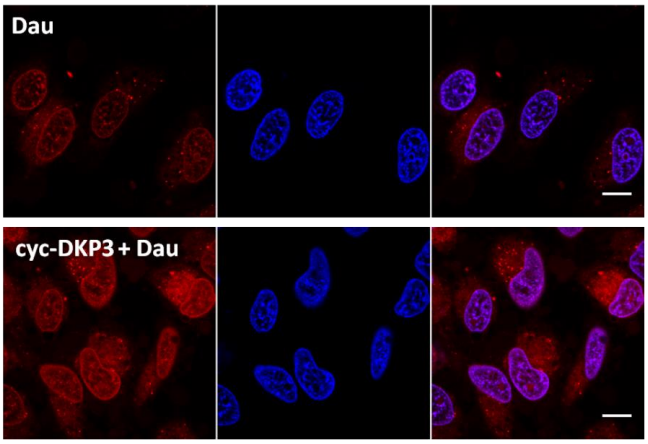

Figure 49. Cellular uptake after co-incubation of daunorubicin and the cyclic peptide cyc-DKP3 investigated by CLSM on HeLa cells. 1 µM daunorubicin alone (top) or together with 10 µM peptide solution (bottom) was added to HeLa cells and the uptake was evaluated after 30 minutes incubation. External fluorescence was quenched by treatment with 150 µM trypan blue for 15 sec. Red: daunorubicin; blue: nuclear stain with Hoechst 33342. Scale: 10 µm.

After these promising results with the compound **cyc-DKP3**, we decided to investigate a covalent delivery approach, too. For this purpose, a molecule of daunorubicin was covalently coupled to the cycle according to the synthetic strategy depicted in Figure 50. In brief, the peptide chain was again synthesized via SPPS, but the Lys^4 of sC18* was modified with a protected aminooxy group. After cleavage from the resin and cyclization, which occurred as already described above, deprotection of the aminooxyacetic acid and coupling with daunorubicin by oxime bond formation was performed. This reaction has been very problematic since the aminooxyacetic acid, after completion of deprotection, directly reacted with some ketones present in the atmosphere of the laboratory or in the plastic instruments, so that, after purification of the deprotection reaction, the only product collected was in fact the protected starting peptide. This side reaction could not be avoided even if the glassware used was not cleaned with acetone and no plastic tubes were used. This reaction had to be repeated many times until I decided to add instantaneously an excess of daunorubicin to the deprotected product before its purification and in the tube of the collected pure fraction. By this way, I could obtain 1.2 mg of the final product even if the yield of the steps of deprotection and daunorubicin conjugation reaction was reduced from 80% (observed in general for other conjugates) to 20% because of the repetitive purification steps.

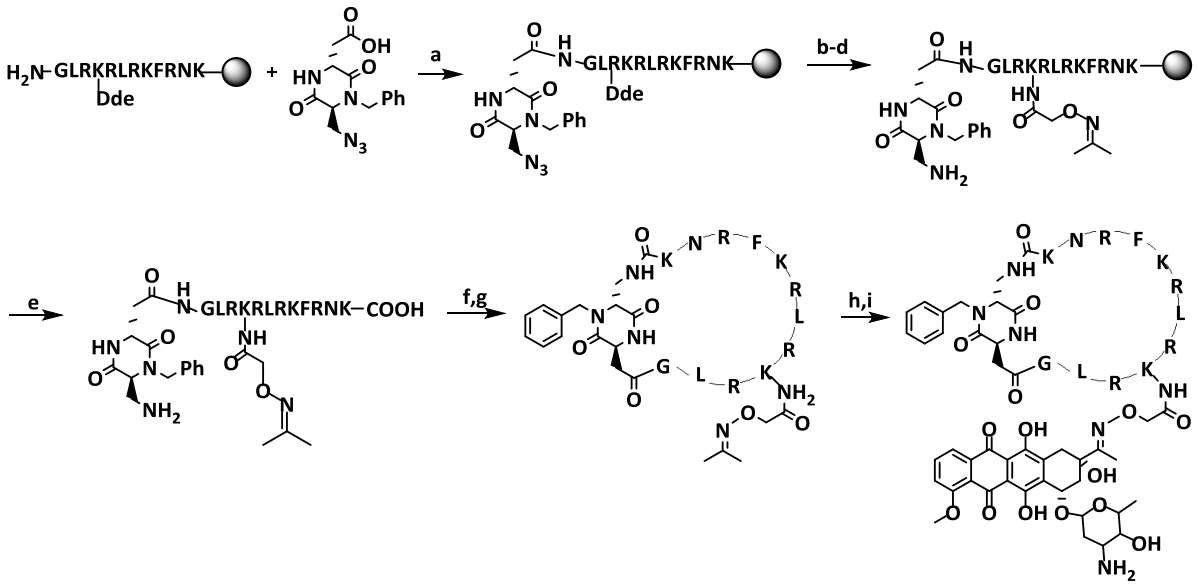

Figure 50. Synthetic strategy for the synthesis of the cyclic drug conjugate cyc-DKP3(Dau). Reagents and conditions: **a**: 3 eq. oxyma, 3 eq. DIC, overnight; **b**: 2% hydrazine in DMF (10x); **c**: 5 eq. >=Aoa, 5 eq. oxyma, 5 eq. DIC, overnight; **d**: DTT (2M), DIPEA (1M), DCM, 3 h; **e**: acetic acid/TFE/DCM 1:1:8, 2h; **f**: BOP (6 eq.), HOBt (6 eq.), DIPEA (12 eq.), DMF (0,2 mM), rt, overnight; **g**: full cleavage with TFA/phenol/H_2O/thioanisol/EDT 82.5:5:5:5:2.5, 3h; **h**: Methoxylamine 1M, NH_4OAc 0.2 M, pH 5; **i**: 30% excess daunorubicin, 0.2 M NH_4OAc, pH 5, 10 mg/ml.

The product was purified using reversed-phase HPLC and identified via LC-MS. As control we used the Dau-modified sC18* version, namely **sC18*(Dau)**, whose synthesis followed the same protocol observed for the conjugates described in the previous chapter. (Table 15).

Table 15. List of the synthesized drug conjugates with the correspondent names, sequences and molecular weight (calculated and experimental).

Name	Sequence	MW [g/mol]	Mw_{exp} [g/mol]
cyc-DKP3(Dau)	DKP3-GLRK(Aoa=Dau)RLRKFRNK	2409.8	2410.5
sC18*(Dau)	H_2N-GLRK(Aoa=Dau)RLRKFRNK-OH	2154.5	2155.2

The anticancer activity of the novel drug conjugates in HeLa cells was measured by resazurin-based toxicity assay. Notably, the cyclic conjugate showed a better activity compared to the linear one, which would support our first hypothesis of a better cellular uptake of the cyclic peptide (Figure 51 and Table 16). Furthermore, since the target of the drug is the DNA located in the nucleus, these results could indicate a more efficient endosomal escape of the cyclic peptide.

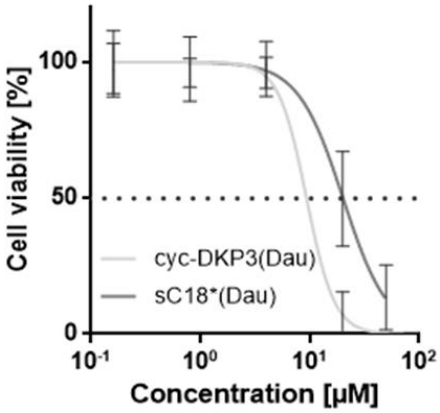

Figure 51. Effect of the drug conjugates cyc-DKP3(Dau) and lin-DKP3(Dau) on the viability of HeLa cells measured by resazurin-based assay. Evaluation of the resorufin fluorescence generated from resazurin by viable cells after 24h incubation with the peptide solutions, washout and further incubation for 48h. Untreated cells were used as negative control and set to 100%; positive control was represented by cells treated for 10 minutes with 70% EtOH and it was subtracted from the other values. The experiment was performed in triplicate with *n=2.*

Table 16. EC_{50} values referred to the cytotoxicity assay showed in Figure 51.

Name	EC_{50} [µM]
cyc-DKP3(Dau)	9.3 ± 1.7
sC18*(Dau)	20.1 ± 3.3

One could think that the lower activity of **sC18*(Dau)** compared to the cycle would be merely connected to the presence of a negative charge at the *C*-terminus of the sequence, since the peptide synthesis was performed on chlorotrytil resin, as previously described. To argue this hypothesis, the cellular uptake of the cyclic peptide **cyc-DKP3(Dau)** and the two linear peptides **sC18*(Dau)** and **2b** was evaluated. Since previously published results illustrated that the truncated sC18* shows a weaker uptake efficiency than sC18, maybe due to the missing positive charged lysine residues at the *C*-terminus of the sequence, [184] we were interested in a direct correlation between the cycle and the two linear versions. Notably, a significant increased uptake of the cyclic peptide in comparison to both linear variants was observed (Figure 52), confirming that the better efficacy of the cyclic peptide could undoubtedly be correlated with the cyclization. All in all, these data indicate that the **cyc-DKP3(Dau)** appears to be a very efficient alternative to the original CPP **2b** and correspond very well to all the results obtained until now. In fact, also in the cytotoxicity studies of the drug delivery system (drug-free peptides), the toxicity of the cyclic peptides was higher than the linear, possibly depending on the different interaction with the membrane clearly leading to a different cellular uptake.

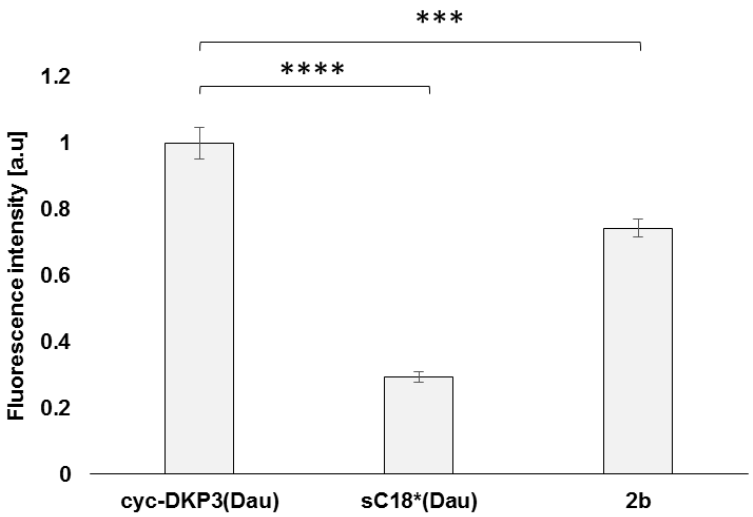

Figure 52. Cellular uptake evaluation of the cyclic and linear drug conjugates cyc-DKP3(Dau), sC18*(Dau) and sC18(Dau) by flow cytometry. HeLa cells were incubated for 30 minutes with 10 µM peptide solution. The value corresponding to the untreated cells was used as negative control and subtracted from the other values. . (***: p ≤ 0.001; (***: p ≤ 0.0001). The experiment was performed in triplicate with *n=2.*

For a further confirmation, we evaluated the cellular uptake by CLSM. From this analysis, it was pretty clear that both peptides were taken up to high extent after 30 minutes incubation, while distributing throughout the cytosol as well as the nuclei; in particular, the nuclear envelope is well delineated, revealing localization on the nuclear membrane in both cases (Figure 53). Also in this case **cyc-DKP3** showed an enhanced uptake compared to **sC18*(Dau)** corroborating the flow cytometry data.

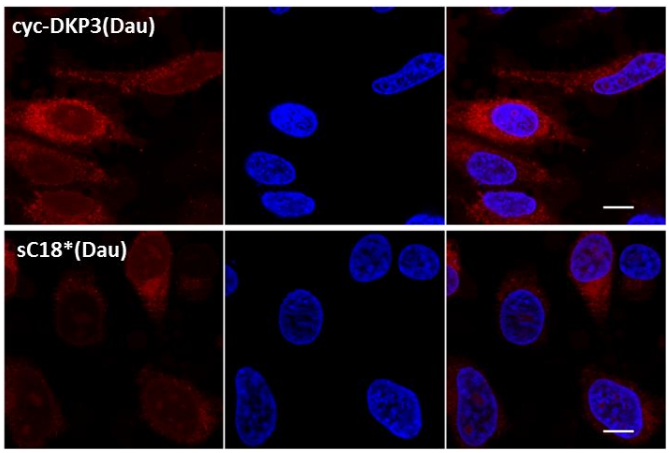

Figure 53. Cellular uptake evaluation of the drug conjugates cyc-DKP3(Dau) and sC18*-Dau by CLSM. HeLa cells were incubated for 30 minutes with 10 µM peptide solutions, Red: Dau-conjugates; blue: nuclear stain with Hoechst 33342. Scale: 10 µm

We tried to explain this behavior with the higher rigidity of the structure, translated into higher and more stable interaction with the membrane. As we could already infer from the NMR studies, since the side chains of the polar amino acids are directed towards the outside of the

cycle, we could imagine that there is a strong and fast interaction with the hydrophilic heads of the phospholipids bilayer generating a curvature that could lead to membrane destabilization and subsequent peptide penetration (Figure 54).

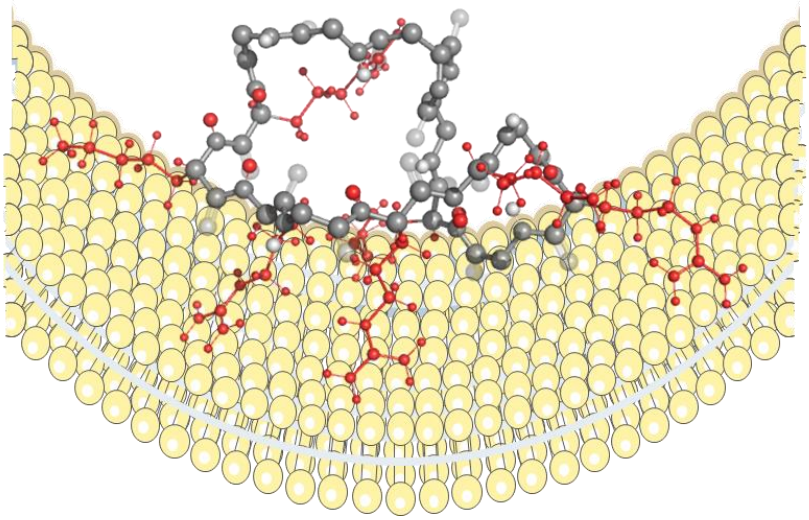

Figure 54. Schematic representation of the possible interaction between cyc-DKP3 and the cell membrane. The ball-and-stick representation of the solution structure of cyc-DKP3 was calculated from NMR derived data collected at 283 K. Side chains of charged amino acids, i.e. Lys and Arg are shown in red.

This behavior is maybe not so immediate and direct for the more flexible linear peptides providing a logical explanation for the enhanced activity of the cyclic peptides.

5. Conclusion and Outlook

5.1. Receptor-targeted CPPs for selective delivery of anticancer therapeutics

In recent years, research on new antineoplastic drugs has raised great hopes and expectations for more specific and less toxic treatments in the field of oncology. New targeted therapies have been developed using selective drugs that act on different targets (growth factors, receptors, enzymes) responsible for the growth and uncontrolled spread of cancer cells, for their resistance to traditional therapies and for the production of new blood vessels, resulting in less toxicity. [10-11] Peptide-drug conjugates represent novel chemical entities with a targeted delivery approach, where highly cytotoxic drugs are combined with peptides that are able to recognize tumor cells. [111]

At the same time, cell-penetrating peptides gained special interest because they can facilitate cellular transfer of various molecular therapeutics, from small chemical molecules to big nanoparticles and large DNA fragments. [198] Because of this feature, CPPs hold great potential as *in vitro* and *in vivo* delivery vehicles, but at the same time they also lack selectivity, restoring the previously described issue. [197]

The aim of the first part of my work was to combine these two important elements and obtain a drug delivery system, which would be able to efficiently deliver drugs to the cytosol (*via* the CPP) but at the same time be selective on tumor cells without damaging the healthy cells (*via* the targeting ligand). GnRH and integrin receptors have been indicated as ideal pharmacological targets based on their overexpression on the surface of many cancer cell types in comparison to healthy cells.

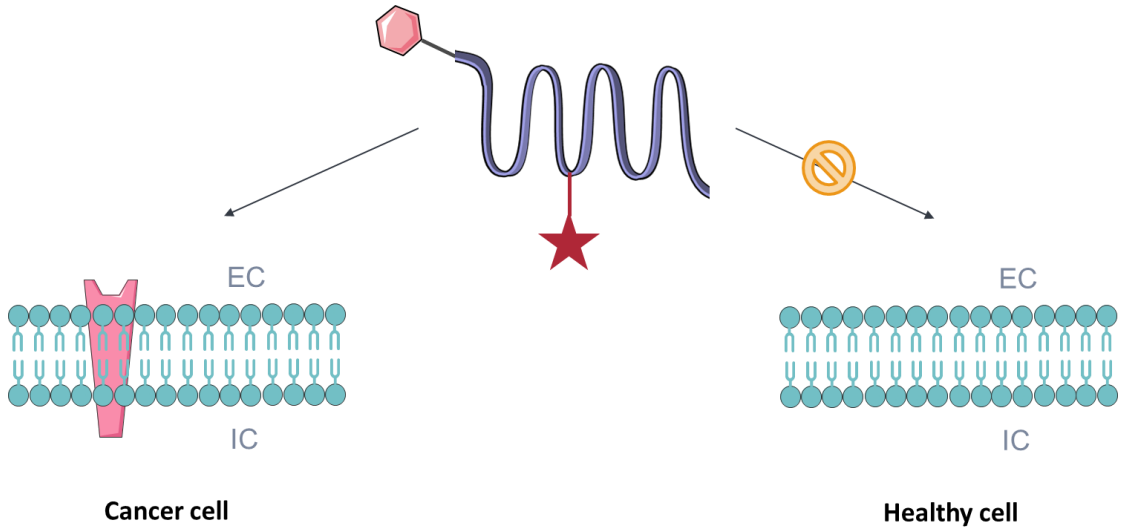

Figure 55. General concept of the targeting delivery.

As targeting ligand towards GnRH receptors a variant of the GnRH-III peptide, developed by the group of Prof. Mező, [131] was employed and conjugated to the CPP sC18 by "click" chemistry. The designed synthetic strategy worked well, and after optimization, the drug delivery system could be obtained in high yields. Drug conjugates have been also prepared where a molecule of daunorubicin was conjugated to the CPP sequence via an uncleavable (aminooxy) or cleavable (GFLG) linker. The GnRH-III conjugates showed a low nanomolar binding affinity towards GnRH receptors expressed on pituitary and prostate cancer cells and the CPP did not display a dramatic influence on the binding validating the choice of the conjugation site. The toxic effects of the compounds on cell types with varying expression levels of GnRH receptors were evaluated. For this purpose, a short treatment was estimated to be the optimal condition in order to underline the targeting ability of the ligand and contemporarily highlight the fast CPP-mediated penetration. Nevertheless, a lack of selectivity was observed for the control (**GnRH-III-Dau**) as well as for the full conjugates **GnRH-III-sC18(Dau)** and **GnRH-III-sC18(GFLG-Dau)** and was attributed to the poor expression of the receptor at the cell surface and their slow recruitment mechanism. [244] After these considerations, a very interesting experiment would be to examine longer incubation times and the correspondent internalization mechanisms. In this sense, cellular uptake studies would be crucial to determine which pathways are followed and to demonstrate which role the receptor-mediated uptake plays in this context. Nevertheless, the CPP conjugates displayed a very efficient activity in this short incubation time indicating the importance of the CPP for the penetration of the construct. In addition, a remarkable activity of daunorubicin in the resistant cell line PANC-1 has been recognized, in particular after treatment with **sC18(GFLG-Dau)** and should be further investigated even with other drugs to corroborate previous observations that MDR can be overcome by the use of CPPs. [245, 258, 273-274]

In the framework of integrin receptors, a recently developed cyclic peptidomimetic consisting of a DKP scaffold and a RGD peptide called c[DKP*f3*RGD] [153] was employed as tumor homing device after conjugation to the CPP by “click” reaction *via* intersection of a PEG_4 linker. After proving that the binding affinity of the compound to the receptors was not seriously altered by the CPP, cells were treated with the fluorescently labeled conjugate **1a** and the uptake was measured after co-incubation of the drug delivery system with the free ligand. A significant but not dramatic reduction of the uptake was measured in particular after 60 minutes incubation compared to 30 minutes and this observation led us to conclude that the binding to the receptor is essential for the targeting but that mainly the CPP is involved in the internalization of the construct. A blocking experiment with the free ligand led us to draw the same conclusions and to imagine a so called “kiss and run” process for our compound, where the ligand recognizes the receptor but the strong membrane interaction of the CPP and its mobility on the membrane surface lead to the dissociation of the ligand from its binding pocket and the subsequent internalization. Since the construct showed remarkable toxicity only at the highest tested concentration after 72 h, it could be demonstrated that the compound could be safely used as drug delivery system. In a first attempt, the potent drug cryptophycin was attached to the CPP by a disulfide bridge but since the “click” reaction for the conjugation to the ligand involved the use of the reducing reagent sodium ascorbate, the disulfide bridge was partially broken, and oxidized side products were recovered. To optimize this step new strategies should be investigated, among those the use of copper powder [259] but also copper-free modalities should be attempted. Problems connected with the stability of chlorambucil led us to favor the same strategy as for the GnRH-III conjugates by coupling daunorubicin to the CPP *via* uncleavable and cleavable (GFLG) linkers. In this case the synthesis was again successfully achieved and the selectivity between cells with different receptor expression was demonstrated by cytotoxicity assays and cellular uptake studies proving that the short contact time between the cells and the drug delivery system worked well in this case. The most promising conjugate **1b** is depicted in figure 56.

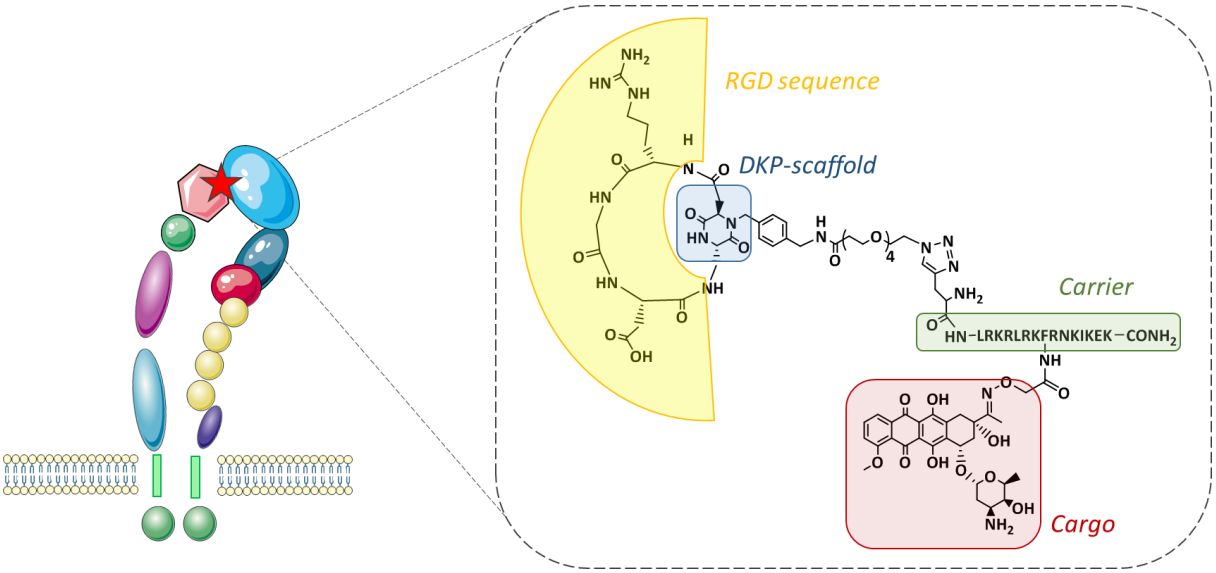

Figure 56. Binding of the lead compound 1b to the integrin receptor. Every element of this hybrid conjugate is here highlighted.

In conclusion, the combination of a ligand with a CPP proved to be a very promising strategy that is worth to be further investigated in the future. Anyhow, there is still a long way to go and a lot of room for improvement.

In general, for both targeting strategies presented, to get a deeper understanding of all the steps occurring from the binding to the internalization, the intracellular organelles could be stained to perform co-localization studies with the labeled compounds and interpret their fate in the cytosol. Additionally, the receptors could be labeled via SNAP tag technology followed by CLSM in living cells in order to monitor them and study their internalization process after binding to the ligand. [275] This could really provide us with an important hint to discern the receptor and the CPP-mediated uptake. In this context, a very interesting experiment described by Sancey *et al.* involved the biotinylation of the integrin receptors on the cell surface, incubation with different concentrations of the peptide followed by lysis of the cells and subsequent quantification of the receptors internalized by endocytosis. This would be a definitive indication of the internalization mechanism followed. [164] Furthermore, the use of inhibitors like amantadine, which blocks the clathrin mediated uptake, would be also useful for our understanding.

Regarding the binding to the receptor, a cell-free based competitive binding study was performed and showed low nanomolar binding affinity between the conjugates and the receptors but to increase the knowledge about this binding, docking studies with the crystallized receptor could be performed and in the best case a co-crystallization of the two elements would determine the whole structure. Another interesting experiment could be to measure the Kd value of our conjugates by fluorescence correlation spectroscopy in order to

measure an equilibrium constant that could be correlated with the binding affinity obtained by the competition assay with vitronectin. [164]

To increase the selectivity, a very astute strategy published by Crisp *et al.*, already described in the introduction, involved the conjugation of the CPP to a negatively charged sequence via a MMP-2 cleavable linker. By this approach, the penetrating capability of the CPP could be masked until the construct reaches the tumor environment and would be then cleaved by the MMP-2 enzymes overexpressed in the tumor stroma. [202] Another way to improve the targeting ability could be to substitute the positive charged residues in the sequence of the CPP with His residues, known to be negative at neutral pH but positive at the acidic pH of the tumor environment. [276] [277]

To demonstrate the ability of this construct to carry even bigger and more hydrophilic molecules inside the cells other cargos could be also employed. In this work small therapeutics were conjugated to the CPP but it is known that CPPs are characterized by a great efficiency in carrying much bigger and complex systems. [198] For instance, the intercellular transposition of protein- and nucleic acid-based drugs, otherwise restricted by their size and hydrophilicity, could be increased and subsequently even their potency could be enhanced.

It would be recommended before going *in vivo*, to test these conjugates on co-culture models. Some trials have been already performed using U87 cells overexpressing the receptor and the control cell line HT-29. Unfortunately, the results were difficult to interpret also because the cells were hardly distinguishable. A solution to this problem could be to use GFP-labeled U87 cells, which would help to distinguish one cell line from the other but also the employment of inserts to separate the two cell lines in the same well. In the latter case, anyway, the co-culture would not exactly mimic the *in vivo* situation where the different cells are in close contact to each other. In general, for these further studies, it would be advisable to use α_v-knock out cell lines to have an ideal negative control.

Another important point to be examined is the stability of the conjugates and this should be done at different levels starting from the extracellular environment (plasma and blood stability) to the lysosomal vesicles (stability in lysosomal homogenate). This is important to see how the drug is released and if determinant differences can be shown between the conjugates with and without cleavable linker. Since the stability of the sC18 in plasma membrane has been determined (Figure 90 in attachment) and the peptide seemed to be highly unstable, for future *in vivo* studies the substitution of all amino acids with D-amino acids should be taken into consideration. [241] For the same purpose, the use of PEG shells, liposomes or nanoparticles would be highly favorable, leading to the generation of interesting multimodal drug delivery systems. These constructs could be used to enhance the stability, since the charged CPP sequence would be shielded until it reaches its site of action and thanks to the EPR effect, the

extravasation and accumulation at the tumor site would be favored, followed by a slow release of the drug. Furthermore, the ADME features of the drug-CPP system would be improved, since these molecules would be otherwise degraded very quickly. Trying to overcome the stability issue, some developments have been already done in this direction and cyclic variants of sC18* were synthesized as described in the second part of this work.

5.2. Cyclic CPPs for cargo delivery

By cyclization of known linear cell-penetrating peptides increased proteolytic stability, enhancement of cell penetration and high potential for drug delivery should be achieved. Based on previous studies, [183] the CAP18 (106-117) fragment of the cationic antimicrobial peptide sC18 was used as starting peptide and cyclized by means of a DKP scaffold, namely DKP3 and DKP1, *trans* and *cis*, respectively. After the synthesis by SPPS of the linear sequence, the head-to-tail cyclization was performed in solution and the conditions were optimized to suppress the formation of undesired dimers and oligomers achieving the two cyclic peptides in satisfying yields. The two cyclic versions with their correspondent linear counterparts, were evaluated about their tendency to form a secondary structure. In fact, when in contact with cell membranes, secondary amphipathic CPPs as sC18 adopt an α-helical structure that allows the interaction with the phospholipidic bilayer and favors the internalization. CD spectra of the novel molecules have been measured and the formation of an α-helix after addition of TFE was corroborated in the case of the linear peptides. As for the cyclic compounds, this analysis showed particularly interesting results since **cyc-DKP3** tended to develop a secondary structure even in phosphate buffer, while for **cyc-DKP1** this was observed only after addition of TFE. Based on this preliminary information we were very curious to investigate more about this aspect and NMR was elected as ideal technique to do this. The NMR data in combination with the CD data suggest that the cyclic peptides display a higher preference to form a structure in aqueous buffer solution in comparison to the linear variants and that **cyc-DKP3** tends to generate a slightly more rigid conformation in comparison with **cyc-DKP1**.

A very important experiment to better understand the impact of a membrane in the arrangement evolution of secondary structure would be to directly test the peptides in the presence of artificial membranes to observe changes in their structural organization or also their effect on membrane destabilization. In general, interaction with artificial membrane systems like neutral or negatively charged large unilamellar vesicles, mimicking the specific composition of particular cell types, would be a possible strategy to examine the influence of individual membrane components on the internalization mechanisms of these cyclic peptides. This would be interesting even to prove a selectivity towards cancer cell lines, characterized by a higher negative charged distribution on their cell surface. An investigation in this direction has been already started since the secondary structure of the linear peptides have been evaluated by NMR in the presence of SDS micelles showing the formation of an α-helix as we

expected. The same analysis has been also performed for **cyc-DKP3** and the still preliminary results already suggest that the cyclic peptide is deeply embedded in the micelle. Further examination is ongoing and will surely give us very important elements to understand these different interactions.

Up to now, the cyclic and linear peptides were tested in HeLa cells where a significant cytotoxic effect of the cyclic peptides was shown at the highest concentration (100 µM) after 24 h treatment followed by washout and further 48 h incubation. This effect was not so remarkable in the case of the linear peptides and this could be explained with the different cellular uptake mechanisms involved and the possibly higher internalization rates of the cyclic peptides compared to the linear ones, as later demonstrated by the cellular uptake evaluation of the labeled compounds. If we look at the three-dimensional structure obtained with the NMR measurements, we could imagine that the side chains of the basic residues, in particular arginine residues, could effectively stick to the surface of the membrane interacting with the negatively charged phospholipids or proteoglycans leading to re-structuring of the double layer and subsequent pore formation. To validate this theory, the studies with SDS micelles would be in this case very useful. Since the toxic activity was observed only at the highest concentration, the cyclic peptides should be promising candidates for the cellular transport of cytotoxic payloads. Since from CD and NMR measurements, **cyc-DKP3** seemed to bear ideal features to improve drug transport inside the cell, further biological experiments were performed with this variant. To prove that, the evaluation of a non-covalent daunorubicin-CPP complex was planned: in fact, a non-covalent drug delivery could be very desirable since the drug does not have to be cleaved from the peptide before reaching its site of action. **Cyc-DKP3** was co-incubated with daunorubicin and could improve the internalization of the drug, probably promoting the permeability to a higher number of drug molecules after pore formation, as previously hypothesized. A covalent link would also have an advantageous impact and for this reason a synthetic strategy for the conjugation of the peptide to daunorubicin was proposed and realized. It could be immediately noticed that the cyclization positively influenced the internalization. The final conjugate was directly compared to the linear version and the cellular uptake was quantitatively and qualitatively analyzed. As already introduced for the other conjugates, also in this case a lysosomal staining would be particularly relevant to describe the destiny of the peptides after internalization and different incubation times could be tested to outline a time-dependent uptake. Since we already described that the daunorubicin is not released as free drug, the metabolite formation after degradation in lysosomal homogenate could be analyzed.

All in all, enhancement of cell penetration, absence of cytotoxicity and high potential for drug delivery could be actually gained. On the contrary, an improvement in the proteolytic stability have not been analyzed yet but it would be relevant to examine the influence of the *cis* and

trans DKP scaffold on the peptide stability against trypsin and in blood plasma and this would represent a very important point to be tested in the near future.

6. Material and Methods

6.1. Materials

6.1.1. Chemicals and consumables

Unless otherwise stated, all reagents, solvents and consumables used were purchased from the companies Alfa Aesar (Karlsruhe, Germany), Greiner Bio-One (Kremsmünster, Austria), IRIS Biotech GmbH (Marktredwitz, Germany), LP Italiana SPA (Milano, Italy), Merck (Darmstadt, Germany), Roth (Karlsruhe, Germany), Ratiolab GmBH (Dreieich, Germany), Sigma-Aldrich (Taufkirchen, Germany), Sarstedt (Nümbrecht, Germany) and VWR BDH Prolabo (Darmstadt, Germany), and their purity fulfilled at least the specifications for synthesis quality.

6.1.2. Media and solutions for cell culture

Table 17. An overview about cell culture media and solutions used during the thesis and the correspondent producers. If not specified, the producer is referred to the medium/solution used at University of Cologne.

Media and solutions	Producer
Medium for U87 cells	*University of Cologne* Dulbecco's Modified Eagle's Medium (DMEM) complemented 4500 mg/l glucose, Sigma Aldrich *OOI* Dulbecco's Modified Eagle's Medium (DMEM) complemented with 4500 mg/l glucose, Lonza (Basel, Switzerland)
Medium for HT-29, MCF-7, HeLa and PANC-1 cells	*University of Cologne* RPMI 1640 Medium, Sigma Aldrich *OOI* RPMI 1640 Medium, Lonza
Medium for FACS	RPMI 1145 Medium
DMSO	*University of Cologne and OOI* Sigma Aldrich
Dulbecco's Phosphate Buffered Saline (DPBS) 1X	*University of Cologne* Sigma *OOI* Lonza
EtOH	*University of Cologne* VWR *OOI* Molar Chemicals Kft. (Halásztelek, Hungary)
FBS	*University of Cologne*

	Fetal Bovine Serum, sterile filtered, Sigma Aldrich *OOI* Biosera (Nuaillé, France)
L-glutamine	L-glutamine solution 7513, Sigma Aldrich
Penicilline/Streptomycin	*OOI* Lonza
Trypsin-EDTA	*University of Cologne* Trypsin-EDTA solution 3924, Sigma Aldrich *OOI* Trypsin 10X and EDTA: Lonza
Trypsin-EDTA for FACS	*University of Cologne* Trypsin-EDTA 1X in PBS, Biowest (Nuaillé, France)

6.1.3. Equipment

Table 18. An overview about the equipment used during the thesis and the correspondent producers. If not specified, the producer is referred to the instrument used at University of Cologne.

Instrument	**Producer**
Balance	Analytical balance: FA-210-4, Faust (Klettgau, Germany)
CD spectrometer	Jasco J-715 spectropolarimeter
Cell culture clean bench	*University of Cologne* Herasafe HS12, Thermo scientific (Waltham, Massachusetts, USA) *OOI* Holten Lamin Air HB2436
Centrifuges	*University of Cologne* Cell culture lab: Centrifuge 5417R, Eppendorf (Hamburg, Germany) Chemistry lab: Heraeus Multifuge X1R, Thermo Scientific *OOI* Heraeus Instruments Function Line Labofuge 400R, Thermo Scientific
CO_2-incubator	*University of Cologne* CB Series, Binder (Tuttlingen, Germany) *OOI* MCO-17AIC, Sanyo (Osaka, Japan)
Evaporator/ Concentrator	XcelVap, Horizon Technology (Salem, New Hampshire, USA)
Flow cytometer	Guava® easyCyte, Merck

Haemocytometer	Neubauer improved, superior Marienfeld (Lauda-Königshofen, Germany)
Heating block	Thermomixer compact, Eppendorf
HPLC (analytical)	Hewlett Packard Series 1100, Agilent (Waldbronn, Germany) Column: EC125/4.6 NUCLEODUR 100-5 C18ec, Macherey-Nagel (Düren, Germany) (solvents incl. 0.1% trifluoroacetic acid)
HPLC (preparative)	*University of Cologne* Elite Lachrom, Hitachi (Chiyoda, Japan): Pump L-2130; Autosampler L-2200; Diode Array Detector L-2455 and Fraction Collector Foxy R1, Teledyne ISCO (Lincoln, Nebraska, USA) column: - VP250/16 NUCLEODUR 100-5 C18ec, Macherey-Nagel (preparative) - VP250/8 NUCLEODUR 100-5 C18ec, Macherey-Nagel (semi-preparative) *ELTE University* KNAUER 2501 HPLC system (H.Knauer, Bad Homburg, Germany) column: Jupiter® 10 µm C18 300 Å, 250 x 10 mm, Phenomenex (Torrance, California, USA)
LC-MS	*University of Cologne* LC: 1100 Series and 1200 Series, Agilent (Santa Clara, California, USA) MS: LTQ-XL, Thermo Scientific column: - Chromolith®Performance RP-18e, 100–4.6 mm, Merck - Eclipse Plus C18, 3,5 µm, 4.6 x 100 mm, Agilent - EC 125/4.6 NUCLEODUR 100-5 C18ec, Macherey Nagel (solvents incl. 0.1% formic acid) *ELTE University* LC: Agilent 1100 MS: Esquire 3000+ ion trap, Bruker Daltonics (Bremen, Germany) column: Supelco C18 (150 mm x 2.1 mm, 3µm) (Hesperia, California, USA) (solvents incl. 0.1% formic acid)

Lyophilizer	Alpha 2-4 LDplus, Christ (Osterode am Harz, Germany)
Magnetic stirrer	VMS-C7, VWR Advanced
Microscope	*University of Cologne* Inverted microscope: AE31, Motic (Wetzlar, Germany) Confocal laser scanning system: D-Eclipse C1, Nikon (Tokyo, Japan) and SP8, Leica (Wetzlar, Germany), equipped with a 60V oil-immersion objective. *OOI* Inverted microscope: CK2, Olympus (Shinjuku, Japan)
Pipettes	*University of Cologne* Eppendorf (Hamburg, Germany) *ELTE University* Finnpipette F2, Thermo Fisher Scientific (Waltham, Massachusetts, USA)
Plate reader	*University of Cologne* Infinite M200, Tecan (Männedorf, Switzerland) *OOI* Bio-Rad microplate reader model 550
Robot for automated SPPS	SyroI, MultiSynTech (Bochum, Germany)
Rotary evaporator	Labo Rota S300, Resona Technics
Rotary shaker	KL-2, Edmund Bühler GmbH (Bodelshausen, Germany)
Speed-Vac	Speedvac Concentrator Savant SC210A and RVT5105 Refrigerated Vapor Trap VLP80 Vacuum Pump, Thermo Scientific
Vacuum pump	VWR
Vortex	Vortex Genie 2, Scientific industries (Bohemia, USA)
Water bath	SW22, Julabo (Seelbach, Germany)

6.2. Methods

6.2.1. Automated Solid Phase Peptide Synthesis

The peptide synthesis was usually carried out on a polymeric, swellable but insoluble support material (resin) of divinylbenzene cross-linked polystyrene, modified with Fmoc-Rink amide aminomethyl for the anchoring of the first amino acid (Fmoc-Rink amide AM resin, 100-200 mesh, 75-150 µm, loading 0.48 mmol/g). For the synthesis of the cyclic peptides a preloaded 2-chlorotrytil chloride resin (H-L-Lys(Boc)-2CT, loading 0.74mmol/g) was used. In both cases,

the resin (15 µmol) was loaded in 2 ml propylene syringes, equipped with matching teflon frits. The automated synthesis was carried out using a multiple synthesizer robot according to the Fmoc/tBu strategy. All used amino acids (aa) were N-terminally Fmoc-protected, while the side chains of trifunctional aa were protected with orthogonal, acid labile groups. The following side chain protecting groups were used: 2,2,4,6,7-pentamethyldihydrobenzofuran-5-sulfonyl (Pbf)for Arg; Trityl (Trt) for Asn, His, Gln and Pen; tert-Butyl (tBu) for Asp and Glu and tert-butyloxycarbonyl (Boc) for Lys. For the selective deprotection of side chains also Fmoc-Lys(Dde)-OH was used. During the automated synthesis, the resin was first pre-swollen for 10 min in 800 µl of DMF, the solvent was then filtered off and afterwards the Fmoc protecting group on the resin was cleaved with 40% piperidine in DMF (400 µl, 3 min) and 20% piperidine in DMF (400 µl, 10 min), followed by 4 washing steps with 600 µl DMF each. The aa were dissolved to 0.4 M in DMF (Fmoc-Phe-OH: 0.4 M in NMP) and 300 µl (0.12 mmol) of the aa solution together with 50 µl (0.12 mmol) Oxyma (2.4 M in DMF) were pipetted to the resin and pre-incubated for 3 minutes. After addition of 50 µl (0.12 mmol) of DIC (2.4 M in DMF) the resin was left 40 min at rt, shaking occasionally. To improve the coupling yield, after a washing step with 800 µl DMF, the reaction was repeated once again (double coupling strategy) and finally washed twice with 800 µl of DMF. Consequently, the N-terminal Fmoc protecting group was cleaved as already described. All other aa were coupled analogously, with each cycle including a double coupling followed by Fmoc-cleavage. Finally, the resin was washed manually with DMF, DCM, MeOH and Et_2O five times respectively and dried under reduced pressure in a vacuum concentrator for 10 min.

6.2.2. Fmoc-cleavage

The resin (15 µmol) was initially pre-swollen for at least 10 minutes in 1 ml of DMF. After removing the solvent, 500 µl of 30% piperidine in DMF were added and left 20 min shaking at rt; the procedure was repeated twice. The resin was then washed with DMF, DCM, MeOH and Et_2O five times each and dried under reduced pressure in a vacuum concentrator.

6.2.3. Manual coupling

The resin (15 µmol) was initially pre-swollen for at least 10 minutes in 1 ml of DMF. Afterwards, the solvent was filtered off and the Fmoc-protected aa (45 µmol or 75 µmol) and Oxyma (45 µmol or 75 µmol) were dissolved in 300 µl DMF. DIC (45 µmol or 75 µmol) was added to the mixture that was then loaded to the resin and left shaking at rt, overnight. Alternatively, the coupling was carried out with HATU (45 µmol) and DIPEA (45 µmol) for 2 h at rt. The resin was then washed with DMF, DCM, MeOH and Et_2O five times each and dried under reduced pressure. To check the completeness of the coupling a Kaiser test was performed. Manual coupling was performed for particularly expensive aa and difficult couplings like for Fmoc-Lys(Dde)-OH, Fmoc-Propargylglycine-OH, Fmoc-Penicillamine(Trt)-OH,

Bis-Boc-aminooxyacetic acid, fluorophores like 5(6)-carboxyfluorescein (CF) and acid functionalized azido DKP scaffolds.

6.2.4. Coupling of 5(6)-carboxyfluorescein (CF) and polymer cleavage

The manual coupling was performed as already described. Particular care had to be taken to avoid the exposure to direct light and the reaction vessels were therefore precautionary covered with aluminium foil. After having verified by Kaiser test that the reaction was completed, a polymer cleavage was performed. The resin was swollen in 1 ml DMF for at least 10 min, the solvent was filtered off and 1 ml of 20% piperidine in DMF was added to the resin and left shaking 45 min at rt. The resin was then washed as usual and dried.

6.2.5. Kaiser test

With the Kaiser test, any primary and secondary amine can be detected through a colorimetric reaction with ninhydrin, thus the completion of a coupling or deprotection reaction can be demonstrated. Some dry resin beads were transferred in a closable 1.5 ml tube and one drop of each of the following solutions was added in this order:

- solution I: 1 g of ninhydrin in 20 ml of ethanol (absolute);

- solution II: 80 g of phenol in 20 ml of ethanol (absolute);

- solution III: 0.4 ml of 1 mM aqueous KCN solution in 20 ml of pyridine.

The reaction mixture was incubated for 5 min at 95 °C in a thermomixer. A blue color of the solution or the resin beads suggested the presence of amines, indicating the incompleteness of the coupling reaction (positive test). On the contrary, a yellow color implied the absence of free amino groups (negative test). Positive control was ethanolamine, as negative control only the solutions were added to the vial.

6.2.6. Boc protection

The resin (15 µmol) was first pre-swollen for at least 10 minutes in 1 ml DCM. After that, the solvent was filtered off and Boc_2O (150 µmol) and DIPEA (15 µmol) were dissolved in 500 µl DCM, added to the resin and shaken for at least 2 h at rt. Particular attention had to be paid handling the Boc_2O, since this substance is very dangerous. Scaling was performed under the hood to avoid inhalation of poisoning fumes. Subsequently, the resin was washed five times with DCM, MeOH and Et_2O and then dried under reduced pressure. To check the completeness of the protection, a Kaiser test was carried out.

6.2.7. Dde-cleavage

The resin (15 µmol) was initially pre-swollen for at least 10 minutes in 1 ml of DMF. The solvent was removed and 1 ml of a hydrazine solution (2% in DMF) was added to the resin and shaken

for 10 min at rt. The solution was then filtered off while collecting the flow-through, the resin was washed twice with 1 ml of DMF and the reaction repeated at least ten times. The absorption at 301 nm of the collected solutions after the first and last cleavage were measured photometrically. The Dde cleavage was considered complete when the absorption of the first solution >1 and of the last solution was <0.1. If the cleavage after 10 repetitions was not complete, the hydrazine content was increased to 3% and the reaction repeated till completion. Subsequently, the resin was washed five times with DCM, MeOH and Et_2O and then dried under reduced pressure.

6.2.8. Sample cleavage

To monitor the synthesis, in particular after critical steps, the peptide was cleaved from a small amount of resin with the simultaneous removal of all acid-labile protective groups. A small amount of dry resin beads were transferred into a 1.5 ml closable reaction tube; first scavengers (2.5 µl water, 2.5 µl TIS) and then 95 µl TFA were added. For peptides containing Pen, 7 µl thioanisole and 3 µl EDT were used instead and filled up with 90 µl TFA. The reaction was left 3h shaking at rt and then 1 ml of ice-cold, dried Et_2O was added. For very short peptidic sequences a mixture of Et_2O/n-hexane (3:1) was used. To complete the precipitation of the peptide, the reaction vessel was stored at -20 °C for at least 30 min. Afterwards, it was centrifuged (4 °C, 10000 g, 5 min), the supernatant was discarded and the pellet of the peptide washed at least five times with ice-cold Et_2O. The pellet was dried under reduced pressure and the peptide was dissolved in 100 µl of H_2O or H_2O/t-BuOH (3:1) and centrifuged to allow the precipitation of the resin beads. For the LC-MS analysis 10 µl of the supernatant were diluted with 10 µl of the starting gradient ACN/H_2O/0.1% FA.

6.2.9. Full cleavage

To cleave the peptide from the resin with simultaneous removal of all acid labile protecting groups, first scavenger (25 µl water, 25 µl TIS) and then 950 µl of TFA were added to the dry resin directly in the reactor. In presence of thiol groups (Pen residue), a mixture of thioanisole/EDT/TFA (7:3:90) has been used instead, in order to avoid undesired oxidation. The solution was shaken for 3 h at rt and afterwards the reaction solution was filtered through the teflon frit from the syringe into a 15 ml centrifuge tube containing 10 ml of ice-cold, dry Et_2O. Residual resin was washed with 200 µl of TFA and the solution was added to the Et_2O too. For very short peptides instead of Et_2O, a mixture of Et_2O/n-hexane (3:1) was used. For complete precipitation of the peptide, the tube was stored at -20 °C for at least 30 min. Then, the solution was centrifuged off (4 °C, 5000 g, 5 min), the supernatant discarded and the peptide pellet washed at least five times with ice-cold Et_2O by iterative resuspension and centrifugation. The pellet was dried under reduced pressure and then dissolved in 2-3 ml of H_2O or H_2O/t-BuOH (3:1). For LC-MS analysis, 5 µl of the solution were mixed with 15 µl

ACN/H_2O/0.1% FA at different ratios according to the HPLC gradient used. As last step, the peptide was freeze-dried.

6.2.10. Coupling of daunorubicin

For the conjugation of daunorubicin to the peptide by oxime binding, a molecule of Bis-Boc aminooxyacetic acid was coupled to the side chain of a Lys (3 eq. with oxyma and DIC overnight). The success of the coupling was checked by Kaiser test. The cleavage from the resin occurred with the standard scavenger but, as already described by Mezö et al.[44], 10 eq. of Boc-aminooxyacetic acid were added in the cleavage cocktail in order to avoid the formation of acetone adducts with a delta mass of +40. To circumvent the generation of formaldehyde adducts, glas tubes were preferably used to collect the pure fractions and for the washing steps. After precipitation, washing and purification, the peptide was freeze-dried and then dissolved in ammonium acetate buffer 0.2 M at pH 5 reaching a concentration of around 10 mg peptide/ml or less. Daunorubicin was added in excess of about 30% and the reaction was stirred overnight. In order to remove unreacted daunorubicin, the reaction solution was directly injected into the HPLC on a semipreparative RP18 column. ACN/H_2O with 0.1% TFA were used as eluents changing gradient as needed. The collected fractions were evaporated to remove the ACN, analyzed with LC-MS and lyophilized to obtain the purified peptides with purities >95%.

6.2.11. Copper(I)-catalyzed azide alkyne cycloaddition (CuAAC)

The c[DKP*f3*RGD]-PEG_4-N_3 or the azido functionalized GnRH-III were conjugated to the CPP by a copper (I) catalyzed azide-alkyne cycloaddition (“click” reaction) occurring between the azido group of the ligand and the alkyne group of the propargylglycine at the *N*-terminus of the CPP. In the case of the c[DKP*f3*RGD] conjugates,1.3 eq. of the azido compound were dissolved with 1 eq. of the alkyne-containing peptide in a 1:1 mixture of dry DMF and degassed H_2O in a Schlenk tube under N_2 atmosphere reaching a concentration of 10mM. The same conditions were used also for the GnRH-III conjugates even if here the reaction was performed with an excess (1.3 eq.) of the alkyne-including compound. Stock solutions of $CuSO_4$ and Na ascorbate in degassed H_2O were prepared and 0.5 eq. and 0.6 eq. respectively were added to the reaction. The solution was stirred overnight under N_2 atmosphere at 40 °C. The reaction was controlled by LC-MS till completion and then directly injected into the HPLC on a semipreparative RP18 column for purification obtaining final conjugates with purities >95%.

6.2.12. Synthesis of compound V

3-mercaptopropanoic acid (20.8 mg, 17 µl, 0.196 µmol, 1 eq.) and dithiopyridine (100 mg, 0.45 µmol, 2.3 eq.) were dissolved in MeOH (1.2 ml, 0.2 mM) and the solution was stirred for 3 h at rt. After completion of the reaction, followed by HPLC, the solvent was removed by reduced pressure and the crude was purified by preparative RP-HPLC. The collected fractions were

analyzed by LC-MS and those corresponding to the pure product were freeze-dried. A transparent oil (26 mg, 0.14 µmol) was obtained with 62% yield and analyzed by LC-MS and NMR.

6.2.13. Synthesis of compound VI

Cry-55-gly (10.4 mg, 13.6 µmol, 1 eq.), compound **V** (11.7 mg, 54.5 µmol, 4 eq.), PyBOP (28 mg, 54.5 µmol, 4 eq.) and HOBt•H_2O (8.3 mg, 61.2 µmol, 4.5 eq.) were combined under inert atmosphere and dissolved in dry DMF (0.5 ml, 27 mM). As soon as all the reagents were dissolved, DIPEA was added (8.8 mg, 11.85 µl, 68 µmol, 5 eq.). The solution was stirred at rt and followed by HPLC; after 5 h the reaction was completed and directly purified by RP-HPLC. After freeze-drying, a white solid (9.2 mg, 9.6 µmol) was obtained with 70% yield.

6.2.14. Synthesis of compound VII

For the conjugation to the drug, the peptide (16.13 mg, 4.68 µmol, 1.5 eq.) was dissolved in dry DMF together with compound **VI** (3 mg, 3.12 µmol, 1 eq.). After overnight reaction under N_2 atmosphere stirring at rt, the reaction was directly injected in the HPLC and purified. The peptide was freeze-dried from water obtaining a white solid (8.8 mg, 1.99 µmol, 64% yield).

6.2.15. Azide reduction

For the reduction of the azido group, the resin (15 µmol) was pre-swollen for at least 10 minutes in DCM and then treated with DTT (2M) in 500µL of DCM. Then, DIPEA (1 M, 87 µL) was added and the reaction was left shaking at rt for 2h. Afterwards, the solvent was removed and the resin was washed and dried. The success of the reaction was verified by Kaiser test or sample cleavage.

6.2.16. Cyclization

The synthesis followed the same steps as for the linear peptides. Since during the cyclization reaction the aa side chains have to be protected, the cleavage from the resin occurred in milder conditions. The resin was treated with a solution of DCM/TFE/AcOH (8:1:1) for 2 h at rt. The solution was then filtered and transferred to a flask and the resin was washed two more times with the same cleavage solution. The solvent was evaporated under reduced pressure and hexane was added to remove acetic acid as azeotrope. The crude was washed and digested with 5% $NaHCO_3$, filtered and washed with ddH_2O to remove all salts. After freeze-drying, the white solid product obtained was subjected to the next step of cyclization. 1 eq. of the fully protected linear peptide was dissolved in DMF (0.2 mM) and DIPEA was added till the solution reached pH 8 (around 12 eq.). Under these conditions, BOP (6 eq.) and HOBt (6 eq.) were added and the reaction was left under stirring at rt. After 6 hours, BOP was added again, the pH was adjusted with DIPEA (if necessary) and the reaction was left stirring overnight. For the treatment of the cyclization reaction, the mixture was diluted with EtOAc and extracted with

brine and saturated $NaHCO_3$. The organic phase was then dried at reduced pressure, freeze-dried and subjected to full cleavage. The crude was reacted with 1 ml of the cleavage cocktail K TFA/phenol/H_2O/thioanisole/EDT (82.5:5:5:5:2.5) and treated as described before. After washing, the crude was freeze-dried, dissolved in ACN/H_2O (10:90) with 0.1% TFA and purified on semipreparative RP-HPLC. The peptide was freeze-dried from water obtaining a white solid (22 to 36% yield).

6.2.17. Synthesis of the cyclic peptide conjugated to daunorubicin

Instead of the Bis-Boc aminooxyacetic acid as for the linear version, an isopropylidene protected aminooxyacetic acid was prepared by stirring for 30 minutes carboxymethoxylamine hemihydrochloride in acetone obtaining the protected product with quantitative yields. This was coupled manually to the peptide using 3 eq. of the reagent, 3 eq. Oxyma and 3 eq. DIC overnight. After the cyclization, deprotection of the aminooxyacetic acid was performed with a solution of 1 M methoxylamine containing NH_4OAc-buffer (0.2 M, pH 5). To avoid undesired side reactions with carbonylic groups (acetone or formaldehyde), an excess of daunorubicin was added directly after completion of the deprotection and the purification was performed directly. A sample for the LC-MS analysis was taken and the fractions were immediately frozen. The conjugation to the drug occurred after freeze-drying as previously described.

6.3. Peptide analysis

All solvents and eluents used for the HPLC fulfilled the required purity with the specification “HPLC Gradient quality” or “LC-MS Quality”.

6.3.1. Analytical HPLC-MS

The characterization of the peptides during and at the end of the synthesis was carried out by means of reverse phase high-performance liquid chromatography electrospray ionization mass spectrometry (HPLC-ESI-MS). Samples were diluted with the starting gradient; the dilutions have been previously described for every synthetic step. The linear gradient used was typically 10-60% B in A in 15 min with a flow rate of 0.6 ml / min (A: 0.1% FA in water, B: 0.1% FA in ACN). After chromatographic separation of the analytes from the column, the eluent was splitted into two parts (1:20). The main part was conducted to the UV detector for the measurement of UV absorbance at 220 or 195 nm; simultaneously the remaining part was ionized in the mass spectrometer and the *m/z* values of the pseudo-molecular ions were detected. Control of HPLC and ESI-MS systems as well as the evaluation of UV chromatograms and mass spectra were performed with the Software Xcalibur (Version 2.2, Thermo Scientific). Images of mass spectra were processed with Origin. The purity of the final compounds was determined by calculating the ratio of the product AUC to the total AUC in the UV-chromatogram.

6.3.2. Preparative HPLC

The purification of the lyophilized peptides was carried out by preparative reverse phase HPLC. The lyophilized peptide (maximum 30 mg for the preparative column and 5 mg for the semipreparative) was dissolved in 960µl of starting gradient solution, typically H_2O/ACN/TFA (90:10:0.1) but depending on the hydrophobicity of the peptide, vortexed and centrifuged. The supernatant was then transferred in a glass HPLC vial and 940 µl were automatically injected on the column. The elution was performed with a linear gradient, in general 10-60% B in A (A: 0.1% TFA in water, B: 0.08% TFA in ACN) in 45 min at a flow rate of 6 ml / min (preparative) or 1.5 ml/min (semipreparative). The UV absorbance was detected at 220 and 250 nm and the peptide containing fractions were collected in plastic tubes. Afterwards, the solution was concentrated using XcelVap or Speedvac for more sensitive products and then lyophilized. For LC-MS analysis, 2 µl of the solution were mixed with 18 µl ACN/H_2O/0.1% FA at different ratio according to the HPLC gradient used.

6.3.3. Circular dichroism spectroscopy

CD spectra were recorded from 260 nm to 184 nm at 20°C using a Jasco J-715 spectropolarimeter purged with N_2 gas. For measuring CD spectra the peptides were dissolved to a final concentration of 20 µM. Peptide samples were diluted in 10 mM sodium phosphate buffer (pH 7) containing 0 or 50% (v/v) TFE. Each measurement was repeated 4 times using a sample cell with a path length of 0.1 cm. Instrument parameters were: response time 2 s, scan speed 50 nm/min, sensitivity 100 mdeg, step resolution 0.5 nm and bandwidth 1.0 nm. The background was removed by subtraction of the CD spectrum of the solvent.

6.4. Biological methods

6.4.1. Cell lines and cell culture conditions

All the cell experiments were carried out under a laminar flow hood in sterile conditions. Pipettes and all consumable transferred under the hood were first autoclaved and then disinfected with 70% EtOH. Every working step was performed wearing a lab coat and disinfected gloves. Sterile Pasteur pipettes were directly connected to a vacuum pump in order to remove media during washing steps or by performing experiments. The temperature (37 °C) of the chemicals used was adjusted by a heating bath. The culturing of cells was carried out at 5% CO_2 at 37 °C, using 100x20 mm Petri plates. The cell lines included in this work are listed in Table 19.

Table 19: Cell lines used during the thesis.

Name	Cell type
HeLa	human cervix carcinoma
HT-29	human colon adenocarcinoma
MCF-7	human breast adenocarcinoma
PANC-1	human pancreas ductal adenocarcinoma
U87	human glioma cells

All the media for culturing the cells were supplemented with 10% FBS and adjusted with different contents of L-glutamine depending on the cell line (2mM for HT-29 and PANC-1 or 4mM for U87, HeLa and MCF-7 cells). For the detachment of confluent cells culture medium was first removed and the cells were washed twice with DPBS. Afterwards, the cells were treated with 1 ml trypsin-EDTA solution for a few minutes depending on the cell line, at 37 °C. For U87 cells the treatment with trypsin was not necessary as this cell line was easily detached just by resuspending with medium. 9 ml of the appropriate culture medium with FBS were finally added and the cells were resuspended and completely detached. 10 µl of the cell suspension were taken, inserted into a counting chamber and the total number of cells was calculated. The desired amount of cells was subsequently diluted with fresh medium and transferred in new Petri plates or in 8-, 24- or 96-well plates where they could grow till reaching the desired confluence.

6.4.2. Freezing and thawing cells

To freeze the cells, after detaching them with 1 ml trypsin-EDTA solution and resuspending them in 9 ml of appropriate cell culture medium, they were transferred in 15 ml tubes and centrifuged at 1000 x g for 5 min at 4 °C. Subsequently, the cell pellet was resuspended in 1.5 ml of freezing medium (appropriate full medium supplemented with 10% DMSO). The cell suspension was placed in a freezing vial and frozen in a mild, stepwise manner. The vial was stored inside a freezing container for 15 min at 4 °C and then for 2 h at -20 °C. The freezing vial was then stored overnight at -80 °C, before relocation in liquid nitrogen for long-term storage.

Thawing of cells stored in liquid nitrogen was carried out by defreezing the vial at 37 °C and rapidly transferring it into a 15 ml tube containing 8.5 ml of the appropriate medium. After centrifugation, the supernatant was removed and the pellet resuspended in fresh medium. In this way, the DMSO could be almost completely discarded from the cell suspension and its toxicity could be circumvented. After 24 h at the latest the medium was exchanged to eliminate dead cells and the remaining DMSO.

6.4.3. Cell viability assays

6.4.3.1. Resazurin-based cytotoxicity assay

In order to test the influence of the peptides on cell viability, a resazurin-based cytotoxicity assay was performed. For the assay 96-well plates were used. First, a cell suspension with a defined concentration (HeLa: 4500 cells per well) was pipetted into the wells and filled up with full medium reaching a final volume of 200 µl. The next day, the culture medium was replaced by 100 µl of culture medium (without FBS) with a defined peptide concentration. Cells were incubated for 24 h with the peptide solution. After removing the solvent, 200 µl of fresh medium were added and the cell s were incubated for further 48h. Subsequently, the medium was removed, the cells washed with DPBS and then incubated with 10 µl resazurin in 90 µl medium (without FBS) for 1 h. As negative and positive controls untreated cells and cells treated 10 min with 70% EtOH in H_2O were used. The fluorometrical measurement was performed with a microplate reader at 596 nm with excitation at 550 nm.

6.4.3.2. MTT-based cytotoxicity assay

To investigate the antiproliferative activity of the conjugates on the human tumor cell lines U87, HT-29, MCF-7 and PANC-1, a MTT assay was performed. Cells were seeded in a 96-well plate (U87, HT-29 and MCF-7: 6000 cells per well, PANC-1: 8000 cells per well), grown for 24 h and incubated with various concentrations of the conjugate in appropriate serum-containing medium for 72 h or for 15 minutes, followed by medium removal and incubation with fresh medium for additional 72 h under standard growth conditions. The MTT assay was performed by adding 20 µL of MTT solution (5 mg/ml in DPBS) to each well and after 3 h of incubation at 37°C, the supernatant was removed. The formazan crystals were dissolved in 100 µL of a 1:1 solution of DMSO and EtOH and the absorbance was determined at 570 nm with a microplate reader. Background value (absorbance of DMSO:EtOH) was subtracted from the measured values and the percentage decrease in cell proliferation was determined relatively to untreated cells.

6.4.4. Internalization studies

6.4.4.1. Flow cytometry

For uptake studies by flow cytometry, cells were seeded in a 24-well plate (Hela: 100000 cells per well, HT-29 and MCF-7: 120000 cells per well, U87: 150000 cells per well) and grown to 70–80% confluency. After incubation at 37°C for 15, 30 or 60 min with the labeled peptides (CF or daunorubicin) in serum-free medium, the cells were washed twice with DPBS, detached with indicator-free trypsin and resuspended in indicator-free serum containing-RPMI medium. The cell suspension was transferred into a 96-well FACS plate and the fluorescence was then measured by a flow cytometer where 10000 viable cells were counted. Cellular autofluorescence was subtracted and the experiments were performed twice in triplicates. For

competition experiments the unfunctionalized c[DKP*3*RGD] ligand was added to the cells in 10-fold excess together with the peptide. After 30 or 60 min incubation time the medium was removed and the cells were treated as described above. For blocking experiments the cells were pre-incubated with c[DKP*3*RGD] (10 µM), Poly-L-lysine or methyl-β-cyclodextrin (1mM) for 30 min followed by peptide incubation for 30 min.

6.4.4.2. Confocal laser scanning microscopy

For confocal microscopy uptake studies, cells were seeded in an eight-well (Ibidi) plate (U87: 70000 cells per well; HT-29 and MCF-7: 50000 cells per well, HeLa:30000 cells per well) and grown to 70–80% confluency. The next day the cells were incubated with CF- or daunorubicin-labeled peptides in serum-free medium for 30 min at 37 °C. The nuclei were stained for 10 min with Hoechst33342 nuclear dye (bisbenzimide H33342, 1 mg/mL in H_2O, sterile filtered) prior to the end of peptide incubation. Finally, the solution was removed and cells were treated with 200 µL trypan blue solution (150 mM in 0.1 M acetate buffer, pH 4.15) for 15 s. After washing once with serum-free medium and adding fresh, appropriate serum-containing medium, images were taken by using a Nikon Eclipse Ti or a Leica SP8 confocal laser scanning microscope. Images were recorded with Nikon EZ-C1 3.91 and Leica Mycrosystems software and adjusted with ImageJ 1.43 m and Fiji software.

6.4.5. Integrin expression on cell surface

Three million cells were counted for every cell line, then centrifuged in 15 ml tubes at 1000 rpm for 5 min at 4 °C; afterwards the supernatant was removed. To fix the cells 300 µl of 4% PFA were added to the pellet, which was then resuspended and left 10 minutes at rt. Afterwards, 2 ml of DPBS were added, the 15 ml tubes vortexed and centrifuged at 1000 rpm, 5 min at 4 °C. The supernatant was discarded and 3 ml DPBS were added to the 15 ml tubes. The solution was again resuspended and divided into 3 FACS tubes (one as control and two for the treatment with antibody). The antibody used was an anti-integrin $\alpha_v\beta_3$ Ab clone LM609 purchased from Merck Millipore. After addition of 2 ml of PBS to each tube, centrifugation followed with the same conditions as before and supernatant was removed. 50 µl of 3% BSA in PBS were added to each tube to block non-specific binding sites. The solution was left 10 min at rt and moved from time to time. After this blocking step, 50 µl of antibody mixture (dilution 1:25; 2µl antibody, 23µl DPBS and 25µl 3% BSA) were added to each FACS tube, incubated for 60 minutes at 37 °C and moved from time to time. After this incubation time, cells were washed by adding 2ml of DPBS. Centrifugation was performed, the supernatant removed and the pellet was then dissolved in FACS medium to proceed with the quantification of the fluorescence intensity.

6.4.6. Solid-phase integrin binding assay

Human integrin receptors $\alpha_v\beta_3$ (R&D Systems, Minneapolis, MN, USA) and $\alpha_v\beta_5$ (EMD Millipore Corporation, Inc., Temecula, CA, USA) were diluted to 0.5 µg/mL in coating buffer containing 20 mM Tris-HCl (pH 7.4), 150 mM NaCl, 1 mM $MnCl_2$, 2 mM $CaCl_2$, and 1 mM $MgCl_2$. An aliquot of diluted receptor (100 µL/well) was added to 96-well plates (Nunc MaxiSorp, Termo Fisher Scientific, Roskilde, DK) and incubated overnight at 4 °C. The plates were incubated with blocking solution (coating buffer plus 1% BSA) for additional 2 h at rt to block nonspecific binding. After washing 2 times with blocking solution, plates were incubated shaking in the dark for 3 h at rt, with various concentrations (10^{-5}–10^{-12} M) of test compounds in the presence of 1 µg/mL vitronectin (Molecular Innovations, Novi, MI, USA) biotinylated using an EZ-Link Sulfo-NHS-Biotinylation kit (Pierce, Rockford, IL, USA). After washing 3 times, the plates were incubated shaking for 1 h in the dark, at rt, with streptavidin-biotinylated peroxidase complex (Amersham Biosciences, Uppsala, Sweden). After washing 3 times with blocking solution, plates were incubated with 100 µL/well of Substrate Reagent Solution (R&D Systems, Minneapolis, MN, USA) for 30 min shaking in the dark, before stopping the reaction with the addition of 50 µL/well 2N H_2SO_4. Absorbance at 415 nm was read in a SynergyTM HT Multi-Detection Microplate Reader (BioTek Instruments, Inc.). Each data point represents the average of triplicate wells; data analysis was carried out by nonlinear regression analysis with GraphPad Prism software. Each experiment was repeated in duplicate.

7. References

[1] F. Bray, J. Ferlay, I. Soerjomataram, R. L. Siegel, L. A. Torre, A. Jemal, **2018**, *68*, 394-424.
[2] L. Wyld, R. A. Audisio, G. J. Poston, *Nat Rev Clin Oncol* **2015**, *12*, 115-124.
[3] V. T. DeVita, Jr., E. Chu, *Cancer Res* **2008**, *68*, 8643-8653.
[4] R. J. Papac, *Yale J Biol Med* **2001**, *74*, 391-398.
[5] R. Baskar, K. A. Lee, R. Yeo, K. W. Yeoh, *Int J Med Sci* **2012**, *9*, 193-199.
[6] M. Baumann, M. Krause, J. Overgaard, J. Debus, S. M. Bentzen, J. Daartz, C. Richter, D. Zips, T. Bortfeld, *Nat Rev Cancer* **2016**, *16*, 234-249.
[7] I. H. Abdulkareem, I. B. Zurmi, *Niger J Clin Pract* **2012**, *15*, 9-14.
[8] S. Puhalla, S. Bhattacharya, N. E. Davidson, *Mol Oncol* **2012**, *6*, 222-236.
[9] M. Colleoni, A. Giobbie-Hurder, *Ann Oncol* **2010**, *21 Suppl 7*, vii107-111.
[10] V. V. Padma, *Biomedicine (Taipei)* **2015**, *5*, 19.
[11] Z. R. Lu, P. Qiao, *Mol Pharm* **2018**, *15*, 3603-3616.
[12] A. Urruticoechea, R. Alemany, J. Balart, A. Villanueva, F. Vinals, G. Capella, *Curr Pharm Des* **2010**, *16*, 3-10.
[13] M. Arruebo, N. Vilaboa, B. Saez-Gutierrez, J. Lambea, A. Tres, M. Valladares, A. Gonzalez-Fernandez, *Cancers (Basel)* **2011**, *3*, 3279-3330.
[14] V. T. DeVita, Jr., S. A. Rosenberg, *The New England journal of medicine* **2012**, *366*, 2207-2214.
[15] B. A. Chabner, T. G. Roberts, Jr., *Nat Rev Cancer* **2005**, *5*, 65-72.
[16] R. Akhtar, S. Chandel, P. Sarotra, B. Medhi, *World journal of gastrointestinal oncology* **2014**, *6*, 177-183.
[17] G. A. Masters, S. Temin, C. G. Azzoli, G. Giaccone, S. Baker, Jr., J. R. Brahmer, P. M. Ellis, A. Gajra, N. Rackear, J. H. Schiller, T. J. Smith, J. R. Strawn, D. Trent, D. H. Johnson, *Journal of clinical oncology : official journal of the American Society of Clinical Oncology* **2015**, *33*, 3488-3515.
[18] N. Krall, J. Scheuermann, D. Neri, *Angew Chem Int Ed Engl* **2013**, *52*, 1384-1402.
[19] Y. Abe, H. Fukuda, K. Ishiwata, S. Yoshioka, K. Yamada, S. Endo, K. Kubota, T. Sato, T. Matsuzawa, T. Takahashi, T. Ido, *European journal of nuclear medicine* **1983**, *8*, 258-261.
[20] Q. Cao, Z. B. Li, K. Chen, Z. Wu, L. He, N. Neamati, X. Chen, *European journal of nuclear medicine and molecular imaging* **2008**, *35*, 1489-1498.
[21] R. Bayat Mokhtari, T. S. Homayouni, N. Baluch, E. Morgatskaya, S. Kumar, B. Das, H. Yeger, *Oncotarget* **2017**, *8*, 38022-38043.
[22] X. Xie, Y. Wu, S. Luo, H. Yang, L. Li, S. Zhou, R. Shen, H. Lin, *Asian Pacific journal of cancer prevention : APJCP* **2017**, *18*, 479-484.
[23] N. L. Syn, W. P. Yong, B. C. Goh, S. C. Lee, *Expert Opin Drug Metab Toxicol* **2016**, *12*, 911-922.
[24] S. Cazzamalli, A. D. Corso, D. Neri, *Chimia* **2017**, *71*, 712-715.
[25] M. Richter, H. Zhang, *DNA Cell Biol* **2005**, *24*, 271-282.
[26] M. Huang, A. Shen, J. Ding, M. Geng, *Trends Pharmacol Sci* **2014**, *35*, 41-50.
[27] R. Fleck, D. Bach, *J Pers Med* **2012**, *2*, 15-34.
[28] S. M. Tu, M. A. Bilen, N. M. Tannir, *J R Soc Med* **2016**, *109*, 98-105.
[29] M. Verma, *J Pers Med* **2012**, *2*, 1-14.
[30] L. De Mattos-Arruda, J. Rodon, *Oncologist* **2013**, *18*, 1180-1188.
[31] L. Krolicki, F. Bruchertseifer, J. Kunikowska, H. Koziara, B. Krolicki, M. Jakucinski, D. Pawlak, C. Apostolidis, S. Mirzadeh, R. Rola, A. Merlo, A. Morgenstern, *European journal of nuclear medicine and molecular imaging* **2018**, *45*, 1636-1644.
[32] R. S. Herbst, P. Baas, D. W. Kim, E. Felip, J. L. Perez-Gracia, J. Y. Han, J. Molina, J. H. Kim, C. D. Arvis, M. J. Ahn, M. Majem, M. J. Fidler, G. de Castro, Jr., M. Garrido, G. M. Lubiniecki, Y. Shentu, E. Im, M. Dolled-Filhart, E. B. Garon, *Lancet* **2016**, *387*, 1540-1550.
[33] A. P. Kater, J. F. Seymour, P. Hillmen, B. Eichhorst, A. W. Langerak, C. Owen, M. Verdugo, J. Wu, E. A. Punnoose, Y. Jiang, J. Wang, M. Boyer, K. Humphrey, M. Mobasher, T. J. Kipps, *Journal of clinical oncology : official journal of the American Society of Clinical Oncology* **2018**, JCO1801580.
[34] V. C. Jordan, *Current problems in cancer* **1992**, *16*, 129-176.
[35] C. L. Vogel, M. A. Johnston, C. Capers, D. Braccia, *Clinical breast cancer* **2014**, *14*, 1-9.
[36] K. Boer, *Therapeutic advances in medical oncology* **2017**, *9*, 465-479.
[37] M. D. C. Barros-Oliveira, D. R. Costa-Silva, D. B. Andrade, U. S. Borges, C. B. Tavares, R. S. Borges, J. M. Silva, B. B. D. Silva, *Rev Assoc Med Bras (1992)* **2017**, *63*, 371-378.
[38] R. Persad, *International journal of clinical practice* **2002**, *56*, 389-396.

[39] A. Hackshaw, M. Baum, T. Fornander, B. Nordenskjold, A. Nicolucci, K. Monson, S. Forsyth, K. Reczko, U. Johansson, H. Fohlin, M. Valentini, R. Sainsbury, *Journal of the National Cancer Institute* **2009**, *101*, 341-349.
[40] Y. Fradet, *Expert review of anticancer therapy* **2004**, *4*, 37-48.
[41] W. Kassouf, S. Tanguay, A. G. Aprikian, *The Journal of urology* **2003**, *169*, 1742-1744.
[42] O. J. Finn, *Ann Oncol* **2012**, *23 Suppl 8*, viii6-9.
[43] A. Hoos, *Nature reviews. Drug discovery* **2016**, *15*, 235-247.
[44] H. Hurwitz, L. Fehrenbacher, W. Novotny, T. Cartwright, J. Hainsworth, W. Heim, J. Berlin, A. Baron, S. Griffing, E. Holmgren, N. Ferrara, G. Fyfe, B. Rogers, R. Ross, F. Kabbinavar, *The New England journal of medicine* **2004**, *350*, 2335-2342.
[45] N. H. Fernando, H. I. Hurwitz, *Oncologist* **2004**, *9 Suppl 1*, 11-18.
[46] J. Zhang, P. L. Yang, N. S. Gray, *Nat Rev Cancer* **2009**, *9*, 28-39.
[47] G. Casi, D. Neri, *Journal of medicinal chemistry* **2015**, *58*, 8751-8761.
[48] P. Laakkonen, K. Vuorinen, *Integrative biology : quantitative biosciences from nano to macro* **2010**, *2*, 326-337.
[49] F. Winau, O. Westphal, R. Winau, *Microbes and infection* **2004**, *6*, 786-789.
[50] F. Bosch, L. Rosich, *Pharmacology* **2008**, *82*, 171-179.
[51] G. Cassinelli, *Tumori* **2016**, *2016*, 226-235.
[52] E. I. Vrettos, G. Mezo, A. G. Tzakos, *Beilstein journal of organic chemistry* **2018**, *14*, 930-954.
[53] K. N. Enyedi, S. Toth, G. Szakacs, G. Mezo, *PloS one* **2017**, *12*, e0178632.
[54] S. Schuster, B. Biri-Kovacs, B. Szeder, L. Buday, J. Gardi, Z. Szabo, G. Halmos, G. Mezo, *Pharmaceutics* **2018**, *10*.
[55] P. Sapra, R. Stein, J. Pickett, Z. Qu, S. V. Govindan, T. M. Cardillo, H. J. Hansen, I. D. Horak, G. L. Griffiths, D. M. Goldenberg, *Clinical cancer research : an official journal of the American Association for Cancer Research* **2005**, *11*, 5257-5264.
[56] A. W. Tolcher, S. Sugarman, K. A. Gelmon, R. Cohen, M. Saleh, C. Isaacs, L. Young, D. Healey, N. Onetto, W. Slichenmyer, *Journal of clinical oncology : official journal of the American Society of Clinical Oncology* **1999**, *17*, 478-484.
[57] J. V. McGowan, R. Chung, A. Maulik, I. Piotrowska, J. M. Walker, D. M. Yellon, *Cardiovascular drugs and therapy* **2017**, *31*, 63-75.
[58] M. Volkova, R. Russell, 3rd, *Current cardiology reviews* **2011**, *7*, 214-220.
[59] A. E. Green, P. G. Rose, *International journal of nanomedicine* **2006**, *1*, 229-239.
[60] A. Matuszczyk, S. Petersenn, A. Bockisch, R. Gorges, S. Y. Sheu, P. Veit, K. Mann, *Hormone and metabolic research = Hormon- und Stoffwechselforschung = Hormones et metabolisme* **2008**, *40*, 210-213.
[61] A. Lopez-Gonzalez, P. Diz, L. Gutierrez, E. Almagro, A. Garcia Palomo, M. Provencio, *Annals of translational medicine* **2013**, *1*, 5.
[62] H. C. Tran, A. Marachelian, R. Venkatramani, R. F. Jubran, L. Mascarenhas, *Pediatric hematology and oncology* **2015**, *32*, 26-31.
[63] T. Murphy, K. W. L. Yee, *Expert opinion on pharmacotherapy* **2017**, *18*, 1765-1780.
[64] D. A. Gewirtz, *Biochemical pharmacology* **1999**, *57*, 727-741.
[65] D. A. Burden, N. Osheroff, *Biochimica et biophysica acta* **1998**, *1400*, 139-154.
[66] J. Marinello, M. Delcuratolo, G. Capranico, *International journal of molecular sciences* **2018**, *19*.
[67] J. H. Doroshow, *Cancer Res* **1983**, *43*, 460-472.
[68] B. Pang, X. Qiao, L. Janssen, A. Velds, T. Groothuis, R. Kerkhoven, M. Nieuwland, H. Ovaa, S. Rottenberg, O. van Tellingen, J. Janssen, P. Huijgens, W. Zwart, J. Neefjes, *Nature communications* **2013**, *4*, 1908.
[69] J. A. Hartley, N. W. Gibson, K. W. Kohn, W. B. Mattes, *Cancer Res* **1986**, *46*, 1943-1947.
[70] W. B. Mattes, J. A. Hartley, K. W. Kohn, *Nucleic acids research* **1986**, *14*, 2971-2987.
[71] G. C. Kundu, J. R. Schullek, I. B. Wilson, *Pharmacology, biochemistry, and behavior* **1994**, *49*, 621-624.
[72] L. Vidal, R. Gurion, R. Ram, P. Raanani, O. Bairey, T. Robak, A. Gafter-Gvili, O. Shpilberg, *Leukemia & lymphoma* **2016**, *57*, 2047-2057.
[73] A. Begleiter, M. Mowat, L. G. Israels, J. B. Johnston, *Leukemia & lymphoma* **1996**, *23*, 187-201.
[74] H. Myrberg, L. Zhang, M. Mae, U. Langel, *Bioconjugate chemistry* **2008**, *19*, 70-75.
[75] A. Guaragna, A. Chiaviello, C. Paolella, D. D'Alonzo, G. Palumbo, *Bioconjugate chemistry* **2012**, *23*, 84-96.
[76] M. J. Smyth, G. A. Pietersz, B. J. Classon, I. F. McKenzie, *Journal of the National Cancer Institute* **1986**, *76*, 503-510.
[77] M. El Hilali, B. Reux, E. Debiton, F. Leal, M. J. Galmier, M. Vivier, J. M. Chezal, E. Miot-Noirault, P. Coudert, V. Weber, *Bioorganic & medicinal chemistry* **2017**, *25*, 5692-5708.
[78] C. Weiss, B. Sammet, N. Sewald, *Natural product reports* **2013**, *30*, 924-940.

[79] C. D. Smith, X. Zhang, S. L. Mooberry, G. M. Patterson, R. E. Moore, *Cancer Res* **1994**, *54*, 3779-3784.
[80] M. M. Wagner, D. C. Paul, C. Shih, M. A. Jordan, L. Wilson, D. C. Williams, *Cancer chemotherapy and pharmacology* **1999**, *43*, 115-125.
[81] R. Bai, R. E. Schwartz, J. A. Kepler, G. R. Pettit, E. Hamel, *Cancer Res* **1996**, *56*, 4398-4406.
[82] C. Weiss, E. Figueras, A. N. Borbely, N. Sewald, *Journal of peptide science : an official publication of the European Peptide Society* **2017**, *23*, 514-531.
[83] R. R. Boinpally, L. Polin, S. L. Zhou, B. R. Jasti, R. A. Wiegand, K. White, J. Kushner, J. P. Horwitz, T. H. Corbett, R. E. Parchment, *Cancer chemotherapy and pharmacology* **2003**, *52*, 25-33.
[84] J. Liang, R. E. Moore, E. D. Moher, J. E. Munroe, R. S. Al-awar, D. A. Hay, D. L. Varie, T. Y. Zhang, J. A. Aikins, M. J. Martinelli, C. Shih, J. E. Ray, L. L. Gibson, V. Vasudevan, L. Polin, K. White, J. Kushner, C. Simpson, S. Pugh, T. H. Corbett, *Invest New Drugs* **2005**, *23*, 213-224.
[85] C. Steinkuhler, P. Gallinari, B. Osswald, N. Sewald, M. Ritzefeld, M. Frese*, Vol. WO 2016/146638 Al*, **2015**.
[86] S. Cazzamalli, E. Figueras, L. Petho, A. Borbely, C. Steinkuhler, D. Neri, N. Sewald, *ACS omega* **2018**, *3*, 14726-14731.
[87] N. Diamantis, U. Banerji, *British journal of cancer* **2016**, *114*, 362-367.
[88] R. V. Chari, M. L. Miller, W. C. Widdison, *Angew Chem Int Ed Engl* **2014**, *53*, 3796-3827.
[89] C. Garcia-Echeverria, *Journal of medicinal chemistry* **2014**, *57*, 7888-7889.
[90] A. Beck, L. Goetsch, C. Dumontet, N. Corvaia, *Nature reviews. Drug discovery* **2017**, *16*, 315-337.
[91] P. L. Zinzani, S. Sasse, J. Radford, A. Gautam, V. Bonthapally, *Critical reviews in oncology/hematology* **2016**, *104*, 65-70.
[92] B. Pro, R. Advani, P. Brice, N. L. Bartlett, J. D. Rosenblatt, T. Illidge, J. Matous, R. Ramchandren, M. Fanale, J. M. Connors, K. Fenton, D. Huebner, J. M. Pinelli, D. A. Kennedy, A. Shustov, *Blood* **2017**, *130*, 2709-2717.
[93] E. M. Donato, M. Fernandez-Zarzoso, J. A. Hueso, J. de la Rubia, *OncoTargets and therapy* **2018**, *11*, 4583-4590.
[94] S. M. Ansell, *Blood* **2014**, *124*, 3197-3200.
[95] F. Montemurro, *The Lancet. Oncology* **2017**, *18*, 696-697.
[96] F. Ricci, C. Le Tourneau, *Chinese clinical oncology* **2018**, *7*, 3.
[97] F. R. Appelbaum, I. D. Bernstein, *Blood* **2017**, *130*, 2373-2376.
[98] J. Baron, E. S. Wang, *Expert review of clinical pharmacology* **2018**, *11*, 549-559.
[99] N. Uy, M. Nadeau, M. Stahl, A. M. Zeidan, *Journal of blood medicine* **2018**, *9*, 67-74.
[100] L. Bertamini, J. Nanni, G. Marconi, M. Abbenante, V. Robustelli, F. Bacci, A. Matti, S. Paolini, C. Sartor, S. L. Monaco, M. C. Fontana, S. De Polo, M. Cavo, A. Curti, G. Martinelli, C. Papayannidis, *BMC cancer* **2018**, *18*, 1117.
[101] https://clinicaltrials.gov
[102] J. P. Stephan, K. R. Kozak, W. L. Wong, *Bioanalysis* **2011**, *3*, 677-700.
[103] N. Jain, S. W. Smith, S. Ghone, B. Tomczuk, *Pharm Res* **2015**, *32*, 3526-3540.
[104] K. J. Hamblett, P. D. Senter, D. F. Chace, M. M. Sun, J. Lenox, C. G. Cerveny, K. M. Kissler, S. X. Bernhardt, A. K. Kopcha, R. F. Zabinski, D. L. Meyer, J. A. Francisco, *Clinical cancer research : an official journal of the American Association for Cancer Research* **2004**, *10*, 7063-7070.
[105] J. R. Junutula, H. Raab, S. Clark, S. Bhakta, D. D. Leipold, S. Weir, Y. Chen, M. Simpson, S. P. Tsai, M. S. Dennis, Y. Lu, Y. G. Meng, C. Ng, J. Yang, C. C. Lee, E. Duenas, J. Gorrell, V. Katta, A. Kim, K. McDorman, K. Flagella, R. Venook, S. Ross, S. D. Spencer, W. Lee Wong, H. B. Lowman, R. Vandlen, M. X. Sliwkowski, R. H. Scheller, P. Polakis, W. Mallet, *Nat Biotechnol* **2008**, *26*, 925-932.
[106] F. F. Schumacher, J. P. Nunes, A. Maruani, V. Chudasama, M. E. Smith, K. A. Chester, J. R. Baker, S. Caddick, *Organic & biomolecular chemistry* **2014**, *12*, 7261-7269.
[107] N. Joubert, M. C. Viaud-Massuard, R. Respaud, **2013**.
[108] W. Li, P. Prabakaran, W. Z. Chen, Z. Y. Zhu, Y. Feng, D. S. Dimitrov, *Antibodies* **2016**, *5*.
[109] P. M. Drake, D. Rabuka, *BioDrugs* **2017**, *31*, 521-531.
[110] M. P. Deonarain, *Drug Discov Today Technol* **2018**, *30*, 47-53.
[111] Y. Gilad, M. Firer, G. Gellerman, *Biomedicines* **2016**, *4*.
[112] L. Ma, C. Wang, Z. He, B. Cheng, L. Zheng, K. Huang, *Current medicinal chemistry* **2017**, *24*, 3373-3396.
[113] S. Cazzamalli, A. Dal Corso, F. Widmayer, D. Neri, *Journal of the American Chemical Society* **2018**, *140*, 1617-1621.
[114] A. V. Schally, A. Arimura, A. J. Kastin, H. Matsuo, Y. Baba, T. W. Redding, R. M. Nair, L. Debeljuk, W. F. White, *Science* **1971**, *173*, 1036-1038.
[115] A. M. Padula, *Animal reproduction science* **2005**, *88*, 115-126.

[116] J. D. Neill, L. C. Musgrove, L. W. Duck, *Trends in endocrinology and metabolism: TEM* **2004**, *15*, 383-392.
[117] R. P. Millar, *Animal reproduction science* **2005**, *88*, 5-28.
[118] G. Mezo, M. Manea, *Expert opinion on drug delivery* **2010**, *7*, 79-96.
[119] A. Ulloa-Aguirre, J. A. Janovick, A. Leanos-Miranda, P. M. Conn, *Human reproduction update* **2004**, *10*, 177-192.
[120] A. Nagy, A. V. Schally, P. Armatis, K. Szepeshazi, G. Halmos, M. Kovacs, M. Zarandi, K. Groot, M. Miyazaki, A. Jungwirth, J. Horvath, *Proceedings of the National Academy of Sciences of the United States of America* **1996**, *93*, 7269-7273.
[121] A. Nagy, A. V. Schally, *Biology of reproduction* **2005**, *73*, 851-859.
[122] Aeterna Zentaris Halts Zoptrex Development after Phase III Failure, **2017**, https://www.genengnews.com/topics/translational-medicine/aeterna-zentaris-halts-zoptrex-development-after-phase-iii-failure/
[123] I. Mezo, S. Lovas, I. Palyi, B. Vincze, A. Kalnay, G. Turi, Z. Vadasz, J. Seprodi, M. Idei, G. Toth, E. Gulyas, F. Otvos, M. Mak, J. E. Horvath, I. Teplan, R. F. Murphy, *Journal of medicinal chemistry* **1997**, *40*, 3353-3358.
[124] S. Lovas, I. Palyi, B. Vincze, J. Horvath, M. Kovacs, I. Mezo, G. Toth, I. Teplan, R. F. Murphy, *The journal of peptide research : official journal of the American Peptide Society* **1998**, *52*, 384-389.
[125] M. Kovacs, J. Seprodi, M. Koppan, J. E. Horvath, B. Vincze, I. Teplan, B. Flerko, *Journal of neuroendocrinology* **2002**, *14*, 647-655.
[126] G. Mezo, M. Manea, I. Szabi, B. Vincze, M. Kovacs, *Current medicinal chemistry* **2008**, *15*, 2366-2379.
[127] M. Manea, G. Mezo, *Protein and peptide letters* **2013**, *20*, 439-449.
[128] P. Schlage, G. Mezo, E. Orban, S. Bosze, M. Manea, *Journal of controlled release : official journal of the Controlled Release Society* **2011**, *156*, 170-178.
[129] M. Montagnani Marelli, M. Manea, R. M. Moretti, M. Marzagalli, P. Limonta, *International journal of oncology* **2015**, *46*, 243-253.
[130] M. Manea, U. Leurs, E. Orban, Z. Baranyai, P. Ohlschlager, A. Marquardt, A. Schulcz, M. Tejeda, B. Kapuvari, J. Tovari, G. Mezo, *Bioconjugate chemistry* **2011**, *22*, 1320-1329.
[131] R. Hegedus, M. Manea, E. Orban, I. Szabo, E. Kiss, E. Sipos, G. Halmos, G. Mezo, *European journal of medicinal chemistry* **2012**, *56*, 155-165.
[132] E. Orban, G. Mezo, P. Schlage, G. Csik, Z. Kulic, P. Ansorge, E. Fellinger, H. M. Moller, M. Manea, *Amino acids* **2011**, *41*, 469-483.
[133] R. L. Juliano, *Annual review of pharmacology and toxicology* **2002**, *42*, 283-323.
[134] Y. Takada, X. Ye, S. Simon, *Genome biology* **2007**, *8*, 215.
[135] I. D. Campbell, M. J. Humphries, *Cold Spring Harbor perspectives in biology* **2011**, *3*.
[136] J. A. Askari, P. A. Buckley, A. P. Mould, M. J. Humphries, *Journal of cell science* **2009**, *122*, 165-170.
[137] M. Barczyk, S. Carracedo, D. Gullberg, *Cell and tissue research* **2010**, *339*, 269-280.
[138] S. J. Shattil, C. Kim, M. H. Ginsberg, *Nature reviews. Molecular cell biology* **2010**, *11*, 288-300.
[139] M. A. Arnaout, S. L. Goodman, J. P. Xiong, *Current opinion in cell biology* **2007**, *19*, 495-507.
[140] M. A. Muller, L. Brunie, A. S. Bacher, H. Kessler, K. E. Gottschalk, U. Reuning, *Cell Signal* **2014**, *26*, 2493-2503.
[141] J. S. Desgrosellier, D. A. Cheresh, *Nat Rev Cancer* **2010**, *10*, 9-22.
[142] M. D. Pierschbacher, E. Ruoslahti, *Nature* **1984**, *309*, 30-33.
[143] C. Mas-Moruno, R. Fraioli, F. Rechenmacher, S. Neubauer, T. G. Kapp, H. Kessler, *Angew Chem Int Ed Engl* **2016**, *55*, 7048-7067.
[144] T. G. Kapp, F. Rechenmacher, S. Neubauer, O. V. Maltsev, E. A. Cavalcanti-Adam, R. Zarka, U. Reuning, J. Notni, H. J. Wester, C. Mas-Moruno, J. Spatz, B. Geiger, H. Kessler, *Sci Rep* **2017**, *7*, 39805.
[145] H. Kessler, *Angew Chem Int Edit* **1982**, *21*, 512-523.
[146] H. Kessler, R. Gratias, G. Hessler, M. Gurrath, G. Muller, *Pure Appl Chem* **1996**, *68*, 1201-1205.
[147] J. Chatterjee, F. Rechenmacher, H. Kessler, *Angew Chem Int Ed Engl* **2013**, *52*, 254-269.
[148] M. A. Dechantsreiter, E. Planker, B. Matha, E. Lohof, G. Holzemann, A. Jonczyk, S. L. Goodman, H. Kessler, *Journal of medicinal chemistry* **1999**, *42*, 3033-3040.
[149] C. Mas-Moruno, F. Rechenmacher, H. Kessler, *Anticancer Agents Med Chem* **2010**, *10*, 753-768.
[150] R. Stupp, M. E. Hegi, T. Gorlia, S. C. Erridge, J. Perry, Y. K. Hong, K. D. Aldape, B. Lhermitte, T. Pietsch, D. Grujicic, J. P. Steinbach, W. Wick, R. Tarnawski, D. H. Nam, P. Hau, A. Weyerbrock, M. J. Taphoorn, C. C. Shen, N. Rao, L. Thurzo, U. Herrlinger, T. Gupta, R. D. Kortmann, K. Adamska, C. McBain, A. A. Brandes, J. C. Tonn, O. Schnell, T. Wiegel, C. Y. Kim, L. B. Nabors, D. A. Reardon, M. J. van den Bent, C. Hicking, A. Markivskyy, M. Picard, M. Weller, R. European

Organisation for, C. Treatment of, C. Canadian Brain Tumor, C. s. team, *The Lancet. Oncology* **2014**, *15*, 1100-1108.
[151] J. P. Xiong, T. Stehle, B. Diefenbach, R. Zhang, R. Dunker, D. L. Scott, A. Joachimiak, S. L. Goodman, M. A. Arnaout, *Science* **2001**, *294*, 339-345.
[152] A. S. da Ressurreicao, A. Vidu, M. Civera, L. Belvisi, D. Potenza, L. Manzoni, S. Ongeri, C. Gennari, U. Piarulli, *Chemistry* **2009**, *15*, 12184-12188.
[153] M. Marchini, M. Mingozzi, R. Colombo, I. Guzzetti, L. Belvisi, F. Vasile, D. Potenza, U. Piarulli, D. Arosio, C. Gennari, *Chemistry* **2012**, *18*, 6195-6207.
[154] M. Mingozzi, A. Dal Corso, M. Marchini, I. Guzzetti, M. Civera, U. Piarulli, D. Arosio, L. Belvisi, D. Potenza, L. Pignataro, C. Gennari, *Chemistry* **2013**, *19*, 3563-3567.
[155] I. Guzzetti, Università degli Studi di Milano **2014**.
[156] R. Colombo, M. Mingozzi, L. Belvisi, D. Arosio, U. Piarulli, N. Carenini, P. Perego, N. Zaffaroni, M. De Cesare, V. Castiglioni, E. Scanziani, C. Gennari, *Journal of medicinal chemistry* **2012**, *55*, 10460-10474.
[157] A. Dal Corso, M. Caruso, L. Belvisi, D. Arosio, U. Piarulli, C. Albanese, F. Gasparri, A. Marsiglio, F. Sola, S. Troiani, B. Valsasina, L. Pignataro, D. Donati, C. Gennari, *Chemistry* **2015**, *21*, 6921-6929.
[158] M. Mingozzi, L. Manzoni, D. Arosio, A. Dal Corso, M. Manzotti, F. Innamorati, L. Pignataro, D. Lecis, D. Delia, P. Seneci, C. Gennari, *Organic & biomolecular chemistry* **2014**, *12*, 3288-3302.
[159] S. Zanella, M. Mingozzi, A. Dal Corso, R. Fanelli, D. Arosio, M. Cosentino, L. Schembri, F. Marino, M. De Zotti, F. Formaggio, L. Pignataro, L. Belvisi, U. Piarulli, C. Gennari, *Chemistryopen* **2015**, *4*, 633-641.
[160] I. A. Khalil, K. Kogure, H. Akita, H. Harashima, *Pharmacological reviews* **2006**, *58*, 32-45.
[161] P. Caswell, J. Norman, *Trends in cell biology* **2008**, *18*, 257-263.
[162] P. T. Caswell, S. Vadrevu, J. C. Norman, *Nature reviews. Molecular cell biology* **2009**, *10*, 843-853.
[163] A. G. Ramsay, J. F. Marshall, I. R. Hart, *Cancer metastasis reviews* **2007**, *26*, 567-578.
[164] L. Sancey, E. Garanger, S. Foillard, G. Schoehn, A. Hurbin, C. Albiges-Rizo, D. Boturyn, C. Souchier, A. Grichine, P. Dumy, J. L. Coll, *Molecular therapy : the journal of the American Society of Gene Therapy* **2009**, *17*, 837-843.
[165] S. Castel, R. Pagan, F. Mitjans, J. Piulats, S. Goodman, A. Jonczyk, F. Huber, S. Vilaro, M. Reina, *Laboratory investigation; a journal of technical methods and pathology* **2001**, *81*, 1615-1626.
[166] A. Pina, A. Dal Corso, M. Caruso, L. Belvisi, D. Arosio, S. Zanella, F. Gasparri, C. Albanese, U. Cucchi, I. Fraietta, A. Marsiglio, L. Pignataro, D. Donati, C. Gennari, *Chemistryselect* **2017**, *2*, 4759-4766.
[167] C. A. Suarez-Quian, P. C. Wynn, K. J. Catt, *Journal of steroid biochemistry* **1986**, *24*, 183-192.
[168] L. Feni, I. Neundorf, *Adv Exp Med Biol* **2017**, *1030*, 279-295.
[169] M. Kristensen, D. Birch, H. Morck Nielsen, *International journal of molecular sciences* **2016**, *17*.
[170] A. Bolhassani, B. S. Jafarzade, G. Mardani, *Peptides* **2017**, *87*, 50-63.
[171] A. D. Frankel, C. O. Pabo, *Cell* **1988**, *55*, 1189-1193.
[172] M. Green, P. M. Loewenstein, *Cell* **1988**, *55*, 1179-1188.
[173] D. Derossi, A. H. Joliot, G. Chassaing, A. Prochiantz, *The Journal of biological chemistry* **1994**, *269*, 10444-10450.
[174] A. Prochiantz, *Current opinion in neurobiology* **1996**, *6*, 629-634.
[175] D. J. Craik, D. P. Fairlie, S. Liras, D. Price, *Chemical biology & drug design* **2013**, *81*, 136-147.
[176] G. Elliott, P. O'Hare, *Cell* **1997**, *88*, 223-233.
[177] A. Elmquist, M. Lindgren, T. Bartfai, U. Langel, *Experimental cell research* **2001**, *269*, 237-244.
[178] D. J. Mitchell, D. T. Kim, L. Steinman, C. G. Fathman, J. B. Rothbard, *The journal of peptide research : official journal of the American Peptide Society* **2000**, *56*, 318-325.
[179] J. B. Rothbard, S. Garlington, Q. Lin, T. Kirschberg, E. Kreider, P. L. McGrane, P. A. Wender, P. A. Khavari, *Nature medicine* **2000**, *6*, 1253-1257.
[180] I. Neundorf, R. Rennert, J. Hoyer, F. Schramm, K. Lobner, I. Kitanovic, S. Wolfl, *Pharmaceuticals (Basel)* **2009**, *2*, 49-65.
[181] K. Splith, W. Hu, U. Schatzschneider, R. Gust, I. Ott, L. A. Onambele, A. Prokop, I. Neundorf, *Bioconjugate chemistry* **2010**, *21*, 1288-1296.
[182] K. Splith, R. Bergmann, J. Pietzsch, I. Neundorf, *ChemMedChem* **2012**, *7*, 57-61.
[183] M. Horn, F. Reichart, S. Natividad-Tietz, D. Diaz, I. Neundorf, *Chem Commun (Camb)* **2016**, *52*, 2261-2264.
[184] M. Horn, Universität zu Köln **2017**.
[185] S. Futaki, T. Suzuki, W. Ohashi, T. Yagami, S. Tanaka, K. Ueda, Y. Sugiura, *The Journal of biological chemistry* **2001**, *276*, 5836-5840.
[186] A. Gronewold, Universität zu Köln **2017**.

[187] S. Richter, V. Bouvet, M. Wuest, R. Bergmann, J. Steinbach, J. Pietzsch, I. Neundorf, F. Wuest, *Nucl Med Biol* **2012**, *39*, 1202-1212.
[188] T. Tashima, *Bioorganic & medicinal chemistry letters* **2017**, *27*, 121-130.
[189] A. Borrelli, A. L. Tornesello, M. L. Tornesello, F. M. Buonaguro, *Molecules* **2018**, *23*.
[190] J. D. Ramsey, N. H. Flynn, *Pharmacology & therapeutics* **2015**, *154*, 78-86.
[191] A. Mickan, D. Sarko, U. Haberkorn, W. Mier, *Curr Pharm Biotechnol* **2014**, *15*, 200-209.
[192] F. Madani, S. Lindberg, U. Langel, S. Futaki, A. Graslund, *J Biophys* **2011**, *2011*, 414729.
[193] W. B. Kauffman, T. Fuselier, J. He, W. C. Wimley, *Trends in biochemical sciences* **2015**, *40*, 749-764.
[194] M. C. Shin, J. Zhang, K. A. Min, K. Lee, Y. Byun, A. E. David, H. N. He, V. C. Yang, *J Biomed Mater Res A* **2014**, *102*, 575-587.
[195] M. A. Sani, F. Separovic, *Accounts Chem Res* **2016**, *49*, 1130-1138.
[196] C. Bechara, S. Sagan, *FEBS letters* **2013**, *587*, 1693-1702.
[197] D. Raucher, J. S. Ryu, *Trends in molecular medicine* **2015**, *21*, 560-570.
[198] S. Reissmann, *Journal of peptide science : an official publication of the European Peptide Society* **2014**, *20*, 760-784.
[199] I. Martin, M. Teixido, E. Giralt, *Pharmaceuticals (Basel)* **2010**, *3*, 1456-1490.
[200] K. Kurrikoff, M. Gestin, U. Langel, *Expert opinion on drug delivery* **2016**, *13*, 373-387.
[201] M. Mae, H. Myrberg, S. El-Andaloussi, U. Langel, *Int J Pept Res Ther* **2009**, *15*, 11-15.
[202] J. L. Crisp, E. N. Savariar, H. L. Glasgow, L. G. Ellies, M. A. Whitney, R. Y. Tsien, *Mol Cancer Ther* **2014**, *13*, 1514-1525.
[203] M. C. Shin, J. Zhang, K. Ah Min, K. Lee, C. Moon, J. P. Balthasar, V. C. Yang, *Journal of controlled release : official journal of the Controlled Release Society* **2014**, *194*, 197-210.
[204] M. Rizzuti, M. Nizzardo, C. Zanetta, A. Ramirez, S. Corti, *Drug discovery today* **2015**, *20*, 76-85.
[205] P. Jarver, I. Mager, U. Langel, *Trends Pharmacol Sci* **2010**, *31*, 528-535.
[206] F. Reichart, M. Horn, I. Neundorf, *Journal of peptide science : an official publication of the European Peptide Society* **2016**, *22*, 421-426.
[207] A. N. Shirazi, R. Tiwari, B. S. Chhikara, D. Mandal, K. Parang, *Mol Pharm* **2013**, *10*, 488-499.
[208] G. F. Gause, *Lancet* **1946**, *2*, 46.
[209] S. H. Joo, *Biomolecules & therapeutics* **2012**, *20*, 19-26.
[210] W. A. Toscano, Jr., D. R. Storm, *Pharmacology & therapeutics* **1982**, *16*, 199-210.
[211] T. Velkov, K. D. Roberts, R. L. Nation, P. E. Thompson, J. Li, *Future microbiology* **2013**, *8*, 711-724.
[212] A. Laupacis, P. A. Keown, R. A. Ulan, N. McKenzie, C. R. Stiller, *Canadian Medical Association journal* **1982**, *126*, 1041-1046.
[213] G. Moldenhauer, A. V. Salnikov, S. Luttgau, I. Herr, J. Anderl, H. Faulstich, *Journal of the National Cancer Institute* **2012**, *104*, 622-634.
[214] C. Ngambenjawong, J. M. Pineda, S. H. Pun, *Bioconjugate chemistry* **2016**, *27*, 2854-2862.
[215] R. J. Clark, H. Fischer, L. Dempster, N. L. Daly, K. J. Rosengren, S. T. Nevin, F. A. Meunier, D. J. Adams, D. J. Craik, *Proceedings of the National Academy of Sciences of the United States of America* **2005**, *102*, 13767-13772.
[216] A. Rozek, J. P. Powers, C. L. Friedrich, R. E. Hancock, *Biochemistry* **2003**, *42*, 14130-14138.
[217] M. L. Colgrave, D. J. Craik, *Biochemistry* **2004**, *43*, 5965-5975.
[218] E. M. Molhoek, A. van Dijk, E. J. Veldhuizen, H. P. Haagsman, F. J. Bikker, *Peptides* **2011**, *32*, 875-880.
[219] B. Liu, W. Zhang, S. Gou, H. Huang, J. Yao, Z. Yang, H. Liu, C. Zhong, J. Ni, R. Wang, *Journal of peptide science : an official publication of the European Peptide Society* **2017**, *23*, 824-832.
[220] A. F. B. Rader, M. Weinmuller, F. Reichart, A. Schumacher-Klinger, S. Merzbach, C. Gilon, A. Hoffman, H. Kessler, *Angew Chem Int Ed Engl* **2018**, *57*, 14414-14438.
[221] L. Gentilucci, R. De Marco, L. Cerisoli, *Curr Pharm Des* **2010**, *16*, 3185-3203.
[222] A. F. B. Rader, F. Reichart, M. Weinmuller, H. Kessler, *Bioorganic & medicinal chemistry* **2018**, *26*, 2766-2773.
[223] D. Mandal, A. Nasrolahi Shirazi, K. Parang, *Angew Chem Int Ed Engl* **2011**, *50*, 9633-9637.
[224] R. Wallbrecher, L. Depre, W. P. Verdurmen, P. H. Bovee-Geurts, R. H. van Duinkerken, M. J. Zekveld, P. Timmerman, R. Brock, *Bioconjugate chemistry* **2014**, *25*, 955-964.
[225] G. Lattig-Tunnemann, M. Prinz, D. Hoffmann, J. Behlke, C. Palm-Apergi, I. Morano, H. D. Herce, M. C. Cardoso, *Nature communications* **2011**, *2*, 453.
[226] P. Li, P. P. Roller, *Current topics in medicinal chemistry* **2002**, *2*, 325-341.
[227] C. J. White, A. K. Yudin, *Nature chemistry* **2011**, *3*, 509-524.
[228] I. Szabo, M. Manea, E. Orban, A. Csampai, S. Bosze, R. Szabo, M. Tejeda, D. Gaal, B. Kapuvari, M. Przybylski, F. Hudecz, G. Mezo, *Bioconjugate chemistry* **2009**, *20*, 656-665.
[229] M. Kovacs, B. Vincze, J. E. Horvath, J. Seprodi, *Peptides* **2007**, *28*, 821-829.

[230] F. Yang, S. S. Teves, C. J. Kemp, S. Henikoff, *Biochimica et biophysica acta* **2014**, *1845*, 84-89.
[231] C. Thomssen, M. Schmitt, L. Goretzki, P. Oppelt, L. Pache, P. Dettmar, F. Janicke, H. Graeff, *Clinical cancer research : an official journal of the American Association for Cancer Research* **1995**, *1*, 741-746.
[232] J. Mai, D. M. Waisman, B. F. Sloane, *Biochimica et biophysica acta* **2000**, *1477*, 215-230.
[233] G. Mezo, I. Szabo, I. Kertesz, R. Hegedus, E. Orban, U. Leurs, S. Bosze, G. Halmos, M. Manea, *Journal of Peptide Science* **2011**, *17*, 39-46.
[234] D. Rosik, A. Thibblin, G. Antoni, H. Honarvar, J. Strand, R. K. Selvaraju, M. Altai, A. Orlova, A. Eriksson Karlstrom, V. Tolmachev, *Bioconjugate chemistry* **2014**, *25*, 82-92.
[235] A. Raposo Moreira Dias, A. Pina, A. Dal Corso, D. Arosio, L. Belvisi, L. Pignataro, M. Caruso, C. Gennari, *Chemistry* **2017**, *23*, 14410-14415.
[236] P. Limonta, M. Montagnani Marelli, S. Mai, M. Motta, L. Martini, R. M. Moretti, *Endocr Rev* **2012**, *33*, 784-811.
[237] R. P. Millar, Z. L. Lu, A. J. Pawson, C. A. Flanagan, K. Morgan, S. R. Maudsley, *Endocr Rev* **2004**, *25*, 235-275.
[238] R. P. Millar, A. J. Pawson, K. Morgan, E. F. Rissman, Z. L. Lu, *Front Neuroendocrinol* **2008**, *29*, 17-35.
[239] P. Limonta, M. Manea, *Cancer Treat Rev* **2013**, *39*, 647-663.
[240] S. Stalmans, N. Bracke, E. Wynendaele, B. Gevaert, K. Peremans, C. Burvenich, I. Polis, B. De Spiegeleer, *PloS one* **2015**, *10*, e0139652.
[241] R. Bergmann, K. Splith, J. Pietzsch, M. Bachmann, I. Neundorf, *Journal of peptide science : an official publication of the European Peptide Society* **2017**, *23*, 597-609.
[242] H. Nguyen, S. Zhang, M. E. Morris, *Journal of pharmaceutical sciences* **2003**, *92*, 250-257.
[243] L. Jennes, D. Coy, P. M. Conn, *Peptides* **1986**, *7*, 459-463.
[244] K. R. Sedgley, A. R. Finch, C. J. Caunt, C. A. McArdle, *The Journal of endocrinology* **2006**, *191*, 625-636.
[245] Z. Zheng, H. Aojula, D. Clarke, *J Drug Target* **2010**, *18*, 477-487.
[246] M. Lelle, C. Freidel, S. Kaloyanova, I. Tabujew, A. Schramm, M. Musheev, C. Niehrs, K. Mullen, K. Peneva, *European journal of medicinal chemistry* **2017**, *130*, 336-345.
[247] L. Bodero, P. Lopez Rivas, B. Korsak, T. Hechler, A. Pahl, C. Muller, D. Arosio, L. Pignataro, C. Gennari, U. Piarulli, *Beilstein journal of organic chemistry* **2018**, *14*, 407-415.
[248] N. Papo, A. P. Silverman, J. L. Lahti, J. R. Cochran, *Proceedings of the National Academy of Sciences of the United States of America* **2011**, *108*, 14067-14072.
[249] A. Dal Pozzo, E. Esposito, M. Ni, L. Muzi, C. Pisano, F. Bucci, L. Vesci, M. Castorina, S. Penco, *Bioconjugate chemistry* **2010**, *21*, 1956-1967.
[250] K. Braun, M. Wiessler, R. Pipkorn, V. Ehemann, T. Bauerle, H. Fleischhacker, G. Muller, P. Lorenz, W. Waldeck, *Int J Med Sci* **2010**, *7*, 326-339.
[251] S. L. Goodman, H. J. Grote, C. Wilm, *Biol Open* **2012**, *1*, 329-340.
[252] T. Taga, A. Suzuki, I. Gonzalez-Gomez, F. H. Gilles, M. Stins, H. Shimada, L. Barsky, K. I. Weinberg, W. E. Laug, *Int J Cancer* **2002**, *98*, 690-697.
[253] S. Rissanen, M. Kumorek, H. Martinez-Seara, Y. C. Li, D. Jamroz, A. Bunker, M. Nowakowska, I. Vattulainen, M. Kepczynski, T. Rog, *J Phys Chem B* **2014**, *118*, 144-151.
[254] F. Heitz, M. C. Morris, G. Divita, *Br J Pharmacol* **2009**, *157*, 195-206.
[255] M. A. Russo, M. Paolillo, Y. Sanchez-Hernandez, D. Curti, E. Ciusani, M. Serra, L. Colombo, S. Schinelli, *International journal of oncology* **2013**, *42*, 83-92.
[256] B. A. Kellogg, L. Garrett, Y. Kovtun, K. C. Lai, B. Leece, M. Miller, G. Payne, R. Steeves, K. R. Whiteman, W. Widdison, H. Xie, R. Singh, R. V. Chari, J. M. Lambert, R. J. Lutz, *Bioconjugate chemistry* **2011**, *22*, 717-727.
[257] Y. A. Lin, A. G. Cheetham, P. Zhang, Y. C. Ou, Y. Li, G. Liu, D. Hermida-Merino, I. W. Hamley, H. Cui, *ACS Nano* **2014**, *8*, 12690-12700.
[258] E. A. Dubikovskaya, S. H. Thorne, T. H. Pillow, C. H. Contag, P. A. Wender, *Proceedings of the National Academy of Sciences of the United States of America* **2008**, *105*, 12128-12133.
[259] M. Nahrwold, C. Weiss, T. Bogner, F. Mertink, J. Conradi, B. Sammet, R. Palmisano, S. Royo Gracia, T. Preusse, N. Sewald, *Journal of medicinal chemistry* **2013**, *56*, 1853-1864.
[260] W. R. Owen, P. J. Stewart, *Journal of pharmaceutical sciences* **1979**, *68*, 992-996.
[261] G. Drin, B. Antonny, *FEBS letters* **2010**, *584*, 1840-1847.
[262] M. C. Manning, R. W. Woody, *Biopolymers* **1991**, *31*, 569-586.
[263] R. Lakshminarayanan, D. Fan, C. Du, J. Moradian-Oldak, *Biophysical journal* **2007**, *93*, 3664-3674.
[264] E. Meinjohanns, M. Meldal, T. Jensen, O. Werdelin, L. GalliStampino, S. Mouritsen, K. Bock, *J Chem Soc Perk T 1* **1997**, 871-884.

[265] A. S. Ressurreicao, A. Bordessa, M. Civera, L. Belvisi, C. Gennari, U. Piarulli, *J Org Chem* **2008**, *73*, 652-660.
[266] L. Vahdati, R. Fanelli, G. Bernadat, I. Correia, O. Lequin, S. Ongeri, U. Piarulli, *New J Chem* **2015**, *39*, 3250-3258.
[267] R. Delatouche, M. Durini, M. Civera, L. Belvisi, U. Piarulli, *Tetrahedron Lett* **2010**, *51*, 4278-4280.
[268] J. Chen, Zhang, B., Xie, C., Lu, Y., Wu, W., *Chinese Chemical Letters* **2010**, *21*, 391-394.
[269] A. Gronewold, M. Horn, I. Neundorf, *Beilstein journal of organic chemistry* **2018**, *14*, 1378-1388.
[270] K. Wüthrich, *NMR of proteins and nucleic acids*, John Wiley and Sons Inc, New York, **1986**.
[271] I. Guzzetti, M. Civera, F. Vasile, D. Arosio, C. Tringali, U. Piarulli, C. Gennari, L. Pignataro, L. Belvisi, D. Potenza, *Chemistryopen* **2017**, *6*, 128-136.
[272] J. M. Siegfried, T. G. Burke, T. R. Tritton, *Biochemical pharmacology* **1985**, *34*, 593-598.
[273] J. R. Vargas, E. G. Stanzl, N. N. Teng, P. A. Wender, *Mol Pharm* **2014**, *11*, 2553-2565.
[274] J. Regberg, A. Srimanee, U. Langel, *Pharmaceuticals (Basel)* **2012**, *5*, 991-1007.
[275] D. Calebiro, F. Rieken, J. Wagner, T. Sungkaworn, U. Zabel, A. Borzi, E. Cocucci, A. Zurn, M. J. Lohse, *Proceedings of the National Academy of Sciences of the United States of America* **2013**, *110*, 743-748.
[276] W. Zhang, J. Song, B. Zhang, L. Liu, K. Wang, R. Wang, *Bioconjugate chemistry* **2011**, *22*, 1410-1415.
[277] K. Shi, J. Li, Z. Cao, P. Yang, Y. Qiu, B. Yang, Y. Wang, Y. Long, Y. Liu, Q. Zhang, J. Qian, Z. Zhang, H. Gao, Q. He, *Journal of controlled release : official journal of the Controlled Release Society* **2015**, *217*, 138-150.

8. Attachment

8.1. List of abbreviations

ACN	acetonitrile
AcOH	acetic acid
ADC	antibody-drug conjugate
Aoa	aminooxyacetic acid
Aoa=X	aminooxyacetic acid conjugated via oxyme bond to X
AUC	area under the curve
BBB	blood-brain barrier
Boc	*tert*-butyloxycarbonyl
Boc_2O	di-*tert*-butyl dicarbonate
BOP	(Benzotriazol-1-yloxy)tris(dimethylamino)phosphonium hexafluorophosphate
BSA	bovine serum albumin
Bu	butyryl
Cbl	chlorambucil
CD	circular dichroism
CF	5(6)-carboxyfluorescein
CLSM	confocal laser scanning microscopy
CPP	cell-penetrating peptide
Cry	cryptophycin
CuAAC	copper-catalyzed azide-alkyne cycloaddition
Dau	daunorubicin
ddH_2O	double distilled water
DCM	dichloromethane
Dde	1-(4,4-dimethyl-2,6-dioxocyclohex-1-ylidene)ethyl

DIC	N,N-diisopropylcarbodiimide
DIPEA	N,N-diisopropylethylamine
DKP	diketopiperazine
DMEM	Dulbecco´s modified Eagle Medium
DMF	N,N-dimethylformamide
DMSO	dimethyl sulfoxide
DPBS	Dulbecco's Phosphate-Buffered Saline
DTT	dithiothreitol
EC_{50}	half maximal effective concentration
ECM	extracellular matrix
EDT	1,2-ethanedithiol
EDTA	ethylenediaminetetraacetic acid
ELTE	Eötvös Loránd University (Budapest)
eq.	equivalent
ESI-MS	electrospray ionization mass spectrometry
Et_2O	diethyl ether
EtOAc	ethyl acetate
EtOH	ethanol
FA	formic acid
FACS	Fluorescence Activated Cell Sorting
FDA	Food and Drug Administration
FBS	Fetal Bovine Serum
FITC	fluorescein isothiocyanate
Fmoc	9-fluorenylmethyloxycarbonyl
GnRH	Gonadotropin Releasing Hormone

GnRH-R	Gonadotropin Releasing Hormone receptor
HATU	*O*-(7-azabenzotriazol-1-yl)-*N,N,N',N'*-tetramethyluronium hexafluorophosphate
HeLa	human cervical carcinoma cell line
HOBt	hydroxybenzotriazole
Hoechst	bisBenzimide H 33342 trihydrochloride
HPLC	high performance liquid chromatography
HT-29	human colon cancer cell line
IC_{50}	half maximal inhibitory concentration
KCN	potassium cyanide
KO	Knock-Out
LC-MS	liquid chromatography–mass spectrometry
m/z	mass-to-charge ratio
mβ-cd	methyl-β-cyclodextrin
mAb	monoclonal antibody
MCF-7	human breast adenocarcinoma cell line
MDR	multi-drug resistant
MeOH	methanol
MIDAS	metal ion-dependent adhesion site
MMP-2	metalloproteinase 2
MTT	3-(4,5-dimethylthiazol-2-yl)-2,5-diphenyltetrazolium bromide
MW	molecular weight
NMP	*N*-Methyl-2-pyrrolidone
NMR	nuclear magnetic resonance
OOI	National Institute of Oncology (Budapest)

PANC-1	human pancreatic cancer cell line
PBS	Phosphate-Buffered Saline
PEG	polyethylene glycol
PFA	paraformaldehyde
PLL	Poly-L-Lysine
PyBOP	benzotriazol-1-yl-oxytripyrrolidinophosphonium hexafluorophosphate
RP	reversed phase
RPMI 1640	Roswell Park Memorial Institute, cell culture medium
rt	room temperature
SAR	structure activity relationship
SD	standard deviation
SMDC	small molecule-drug conjugate
SPPS	solid phase peptide synthesis
t-Bu	*tert*-butyl
t-BuOH	*tert*-butyl alcohol
TFA	trifluoroacetic acid
TFE	trifluoroethanol
TIS	triisopropylsilane
U87	human primary glioblastoma cell line
v/v	volume per volume
VEGFR	vascular endothelial growth factor receptor

amino acids

<E	Glp	pyroglutamic acid
βAla		β-alanine

A	Ala	alanine
B	Pra	propargylglycine
D	Asp	aspartic acid
E	Glu	glutamic acid
F	Phe	phenylalanine
f	D-Phe	D-phenylalanine
G	Gly	glycine
H	His	histidine
I	Ile	isoleucine
K	Lys	lysine
K(Bu)	Lys(Bu)	butyrilated lysine
L	Leu	leucine
N	Asn	asparagine
P	Pro	proline
Pen		penicillamine
Q	Gln	glutamine
R	Arg	arginine
S	Ser	serine
V	Val	valine
Y	Tyr	tyrosine
W	Trp	tryptophan

8.2. Attachment of supplementary data: spectra, chromatograms and figures

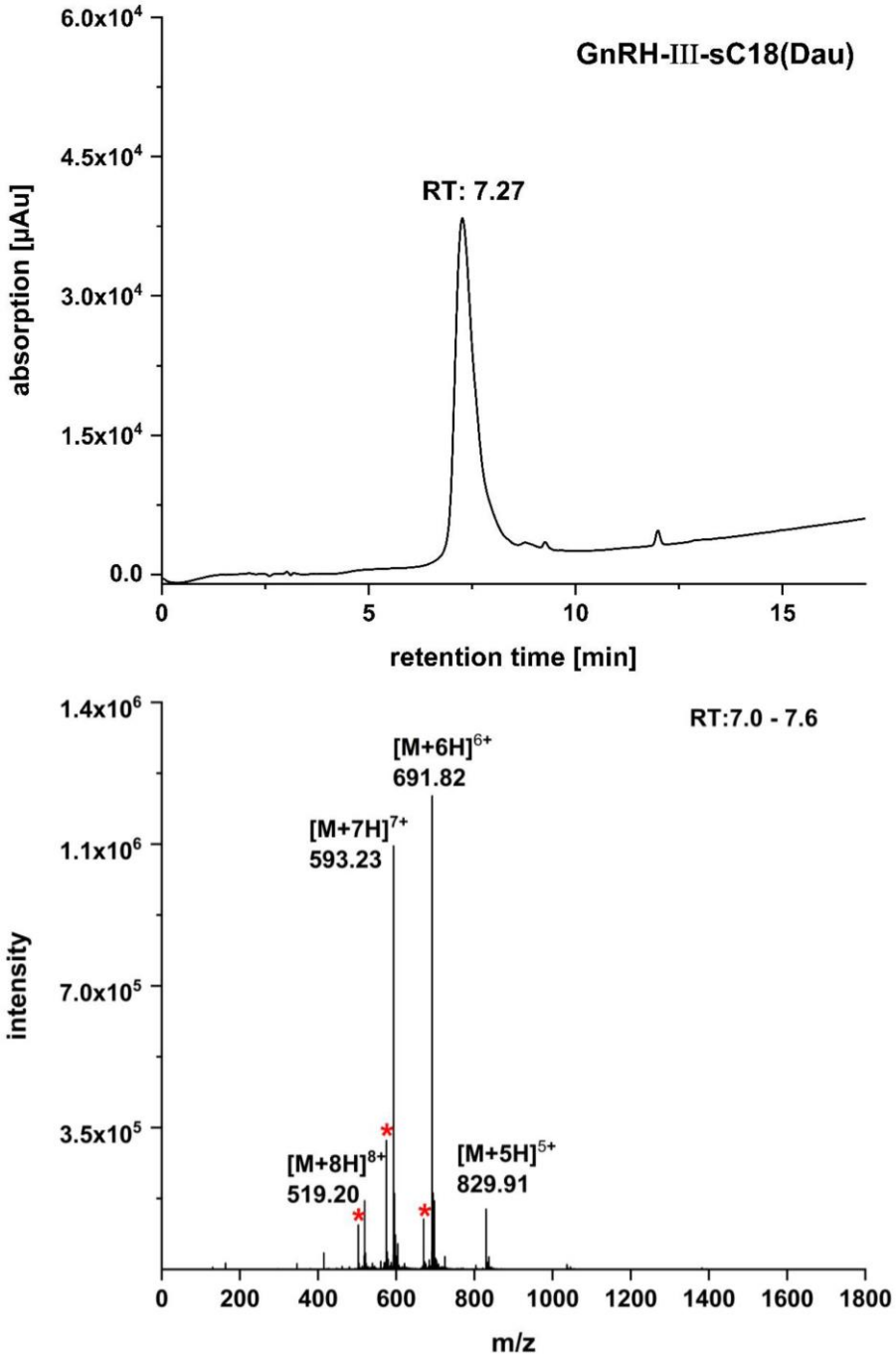

Figure 57. LC-MS analysis of peptide GnRH-III-sC18(Dau); MW calculated: 4143.8 g/mol. Purity: 93%. UV chromatogram (194 nm) and ESI-MS mass spectrum. Gradient: 10-60% B in A in 15 min, 0.6 ml/min. A: 0.1% FA in H_2O; B: 0.1% FA in ACN. Red asterisks: peaks corresponding to the product without daunosamine after mass fragmentation.

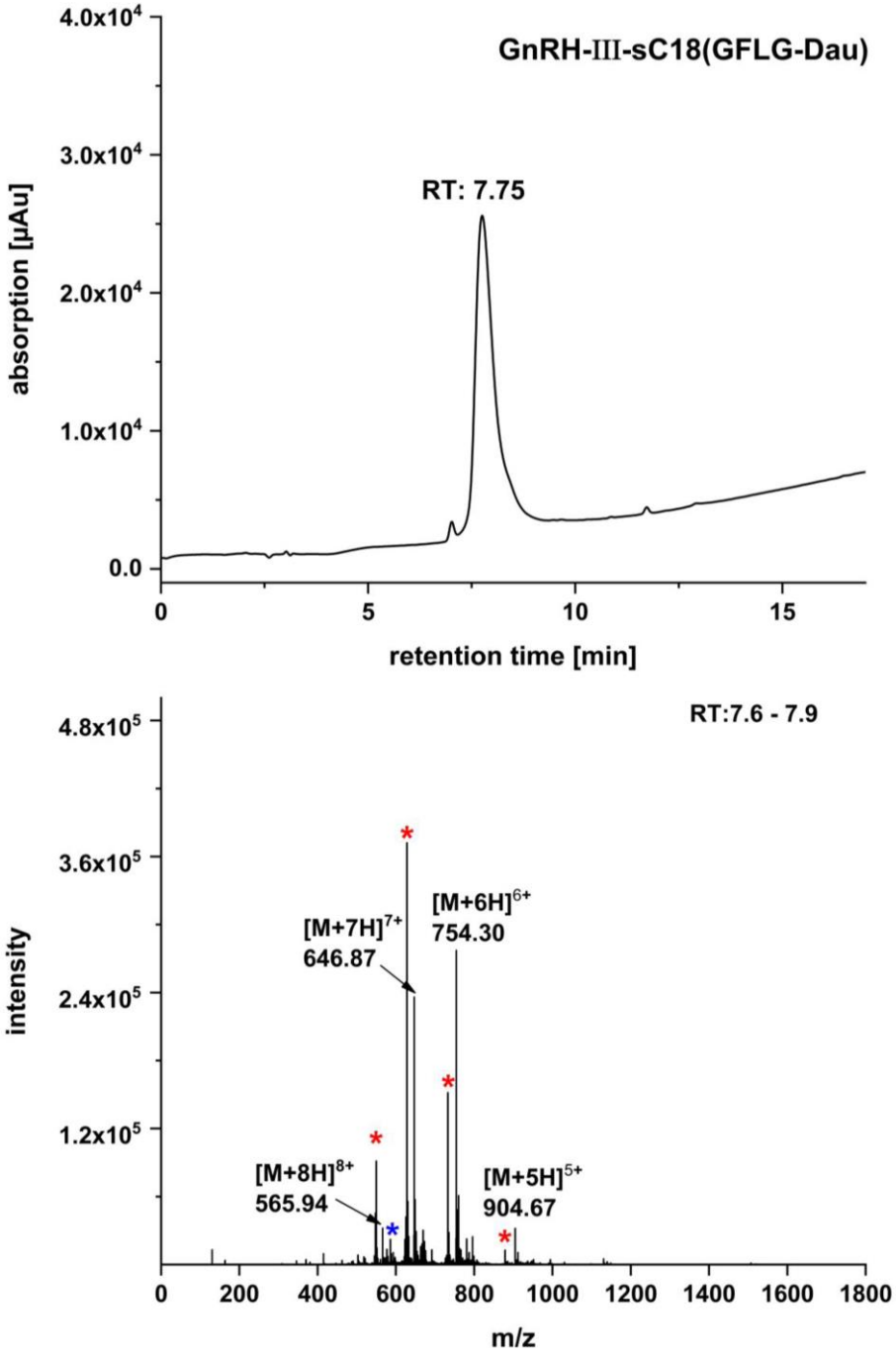

Figure 58. LC-MS analysis of peptide GnRH-III-sC18(GFLG-Dau); MW calculated: 4518.2 g/mol. Purity: 95%. UV chromatogram (194 nm) and ESI-MS mass spectrum. Gradient: 10-60% B in A in 15 min, 0.6 ml/min. A: 0.1% FA in H_2O; B: 0.1% FA in ACN. Blue asterisks: peaks corresponding to the TFA adducts (delta mass +114); red asterisks: peaks corresponding to the product without daunosamine after mass fragmentation.

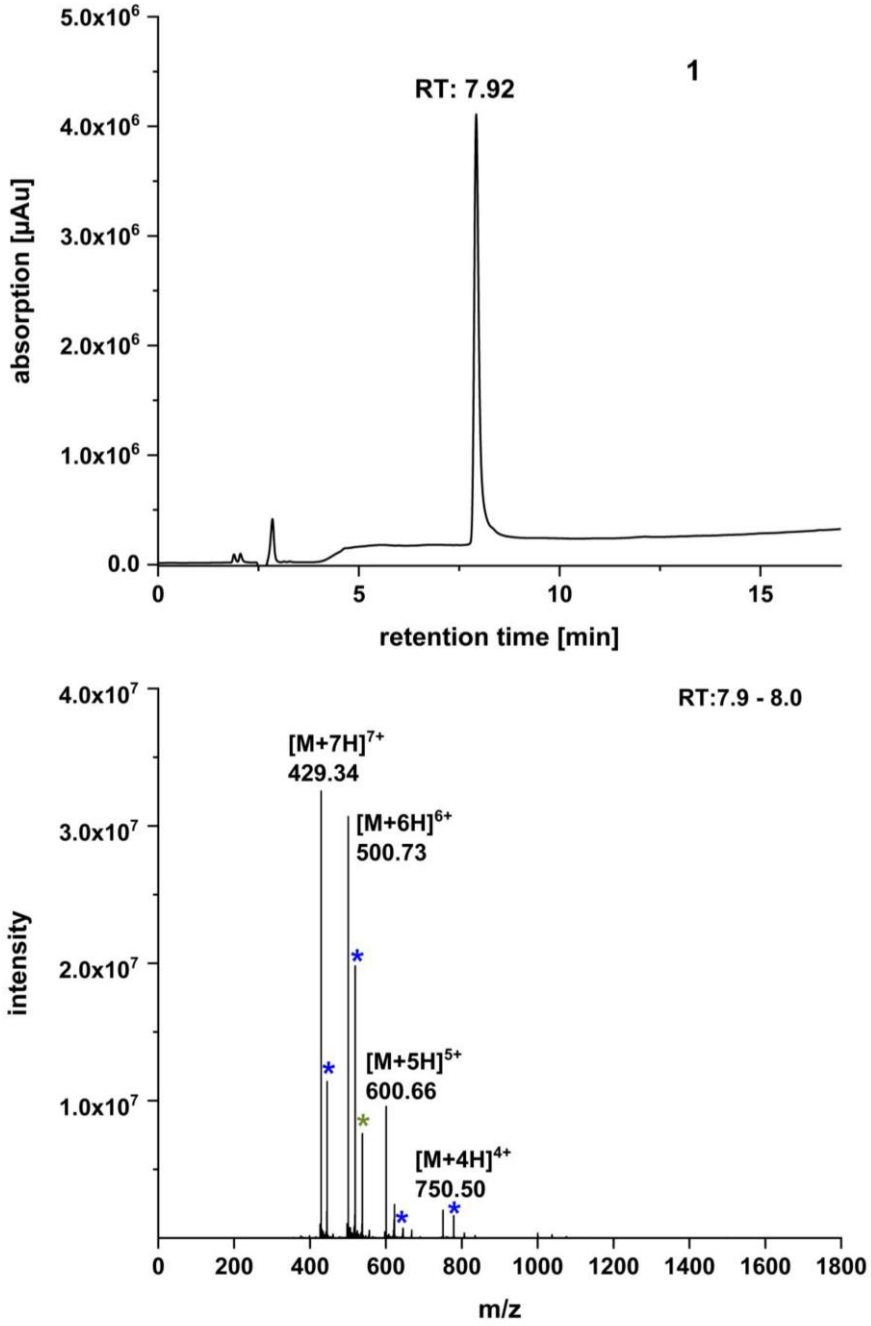

Figure 59. LC-MS analysis of peptide 1; MW calculated: 2998.2 g/mol. Purity: >99%. UV chromatogram (220 nm) and ESI-MS mass spectrum. Gradient: 10-60% B in A in 15 min, 0.6 ml/min. A: 0.1% TFA in H_2O; B: 0.1% TFA in ACN. Blue asterisks: peaks corresponding to the TFA adducts (delta mass +114); green asterisk: peaks corresponding to the TFA adducts (delta mass +228).

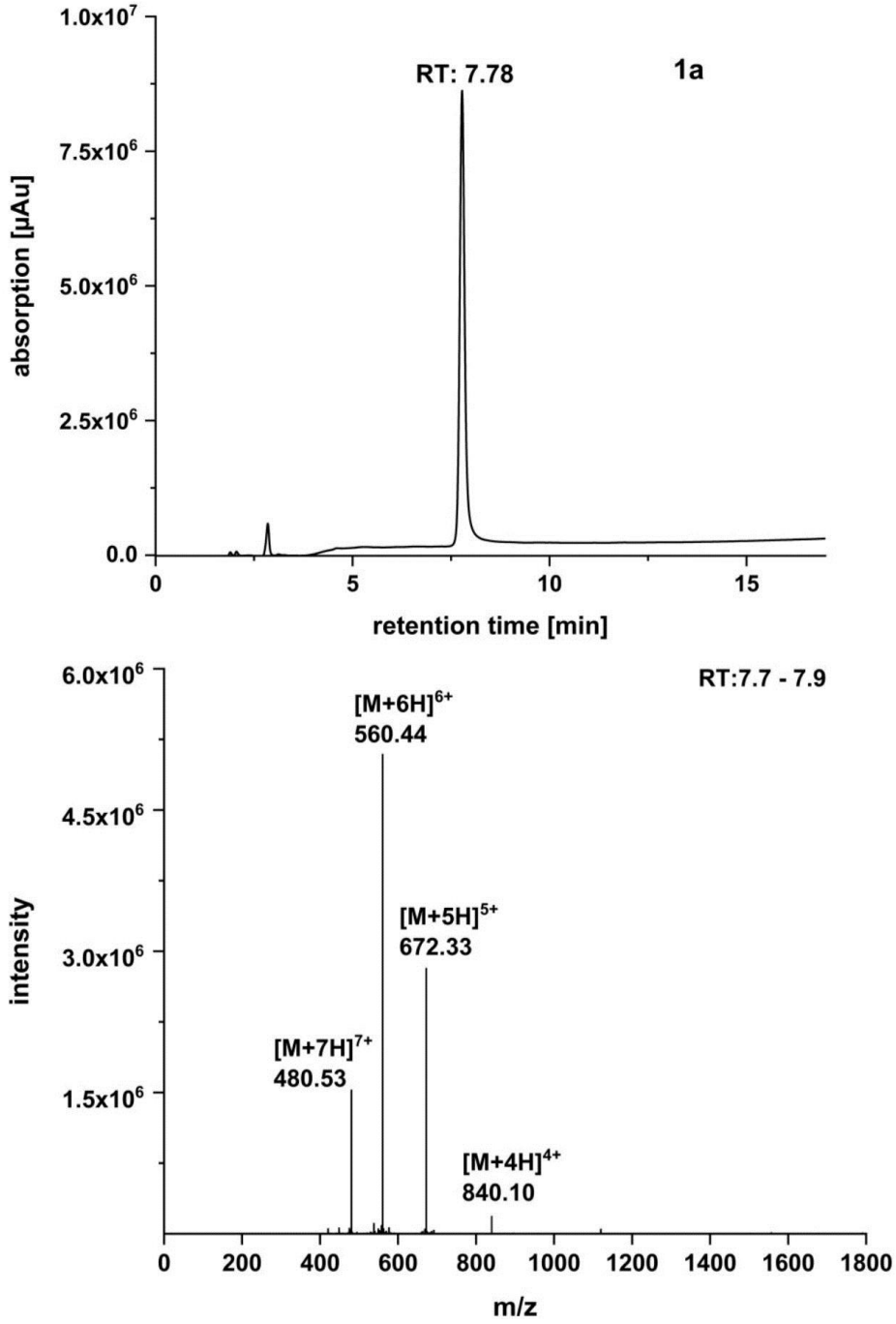

Figure 60. LC-MS analysis of peptide 1a; MW calculated: 3355.9 g/mol. Purity: >99%. UV chromatogram (220 nm) and ESI-MS mass spectrum. Gradient: 10-60% B in A in 15 min, 0.6 ml/min. A: 0.1% TFA in H_2O; B: 0.1% TFA in ACN.

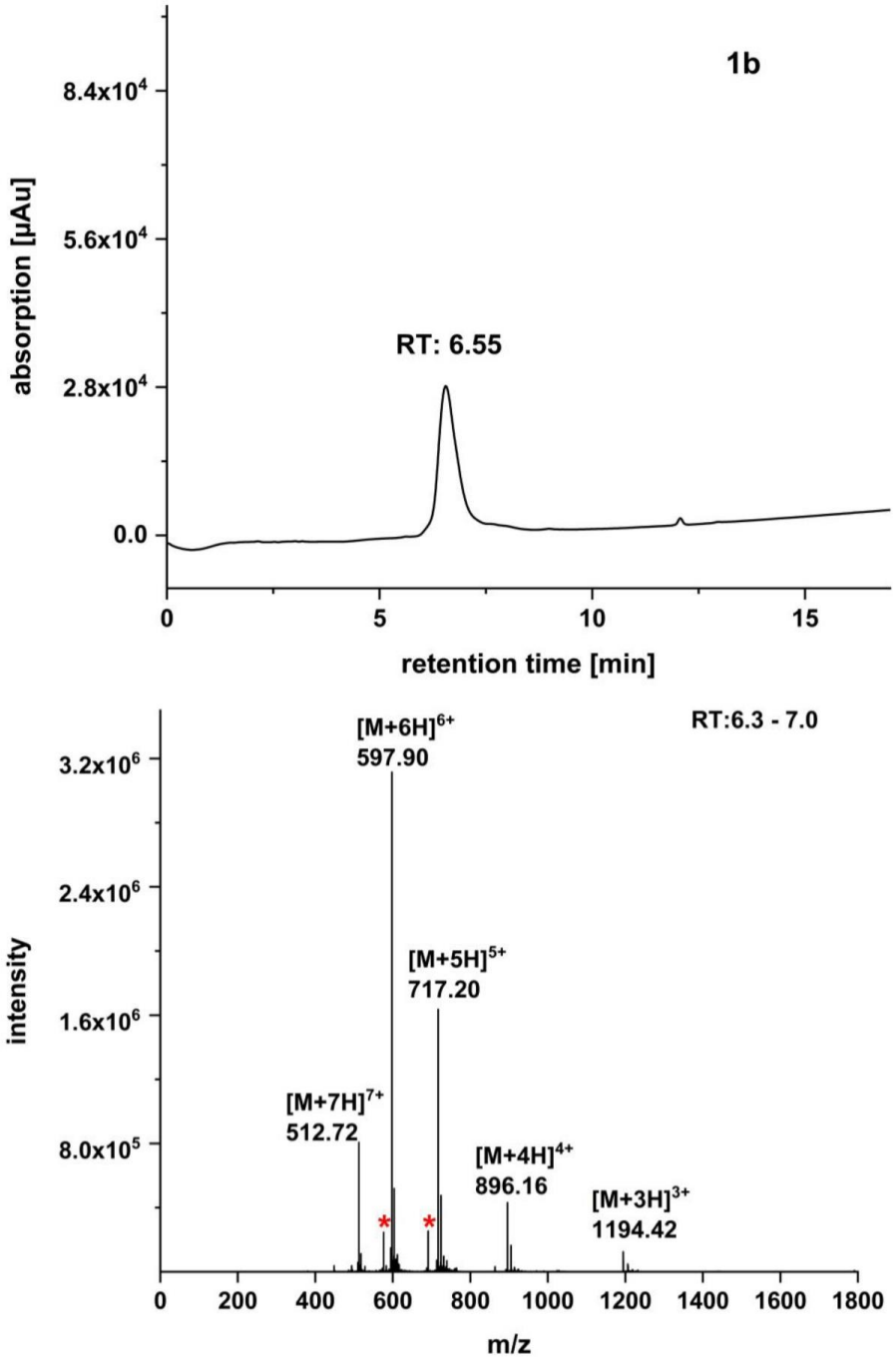

Figure 61. LC-MS analysis of peptide 1b; MW calculated: 3580.1 g/mol. Purity: 95%. UV chromatogram (194 nm) and ESI-MS mass spectrum. Gradient: 10-60% B in A in 15 min, 0.6 ml/min. A: 0.1% FA in H_2O; B: 0.1% FA in ACN. Red asterisks: peaks corresponding to the product without daunosamine after mass fragmentation.

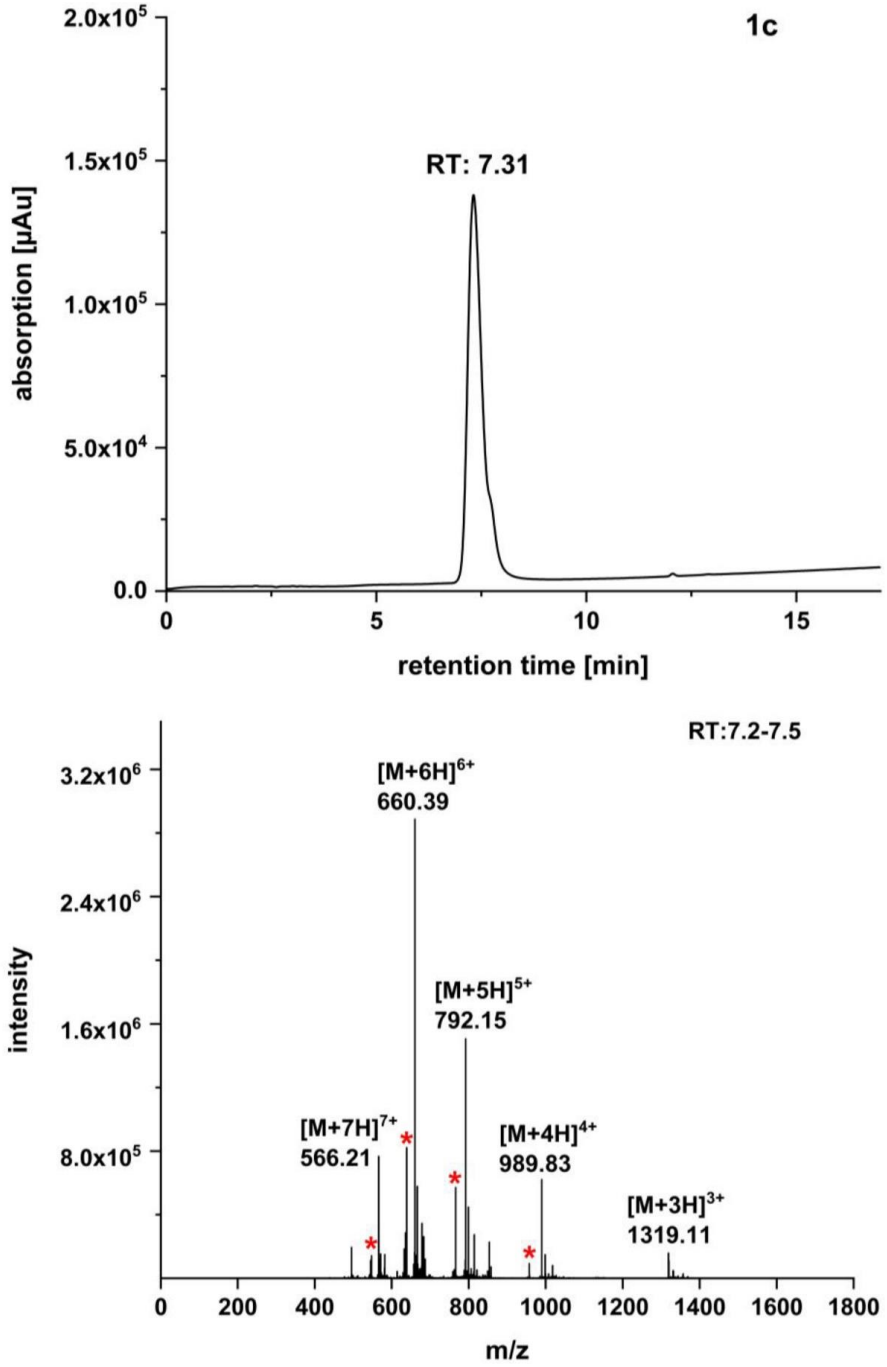

Figure 62. LC-MS analysis of peptide 1c; MW calculated: 3954.6 g/mol. Purity: >99%. UV chromatogram (194 nm) and ESI-MS mass spectrum. Gradient: 10-60% B in A in 15 min, 0.6 ml/min. A: 0.1% FA in H_2O; B: 0.1% FA in ACN. Red asterisks: peaks corresponding to the product without daunosamine after mass fragmentation.

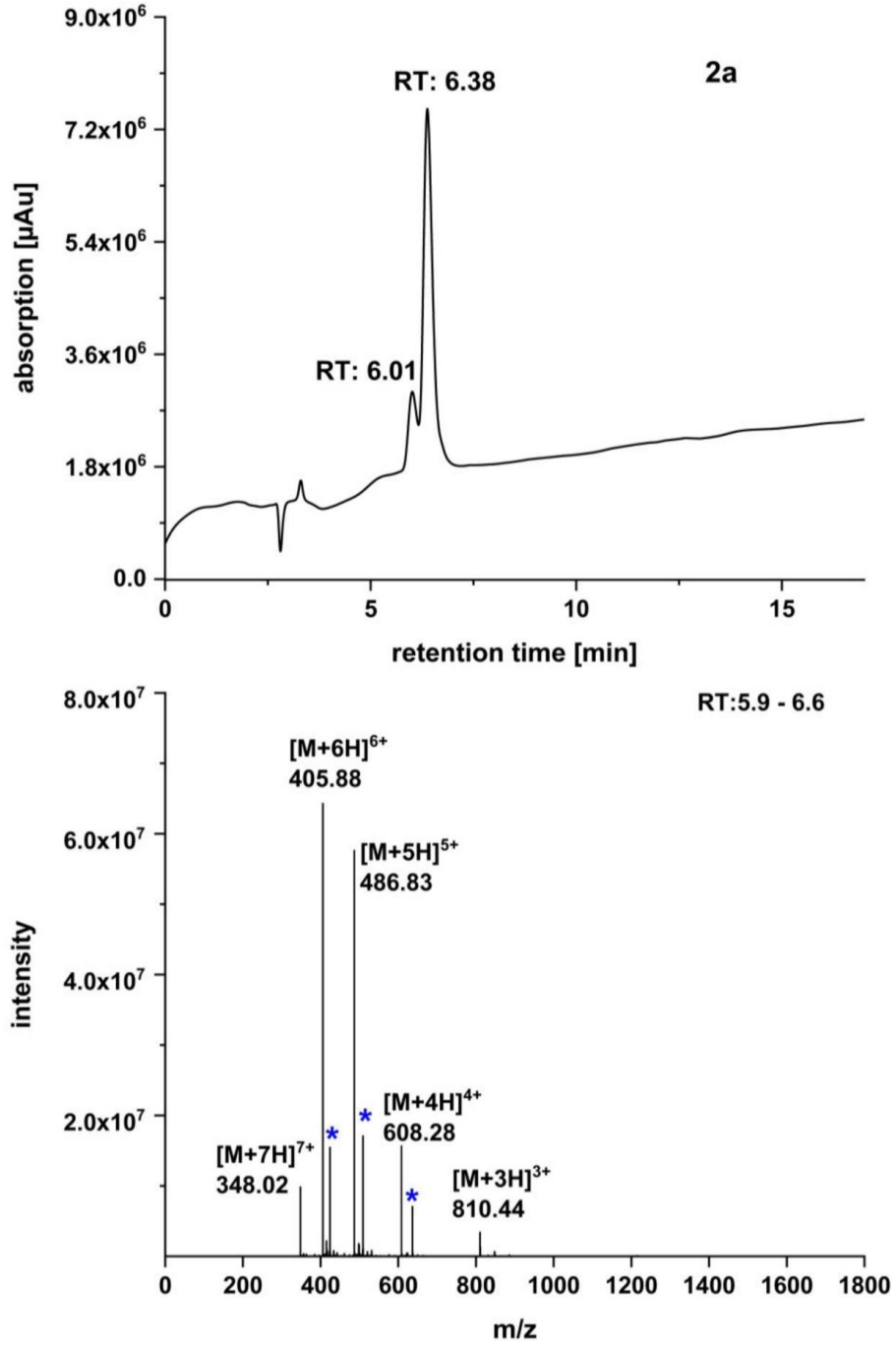

Figure 63. LC-MS analysis of peptide 2a; MW calculated: 2427.9 g/mol. Purity: >99%. UV chromatogram (254 nm) and ESI-MS mass spectrum. Gradient: 10-60% B in A in 15 min, 0.6 ml/min. A: 0.1% FA in H_2O; B: 0.1% FA in ACN. Blue asterisks: peaks corresponding to the TFA adducts (delta mass +114).

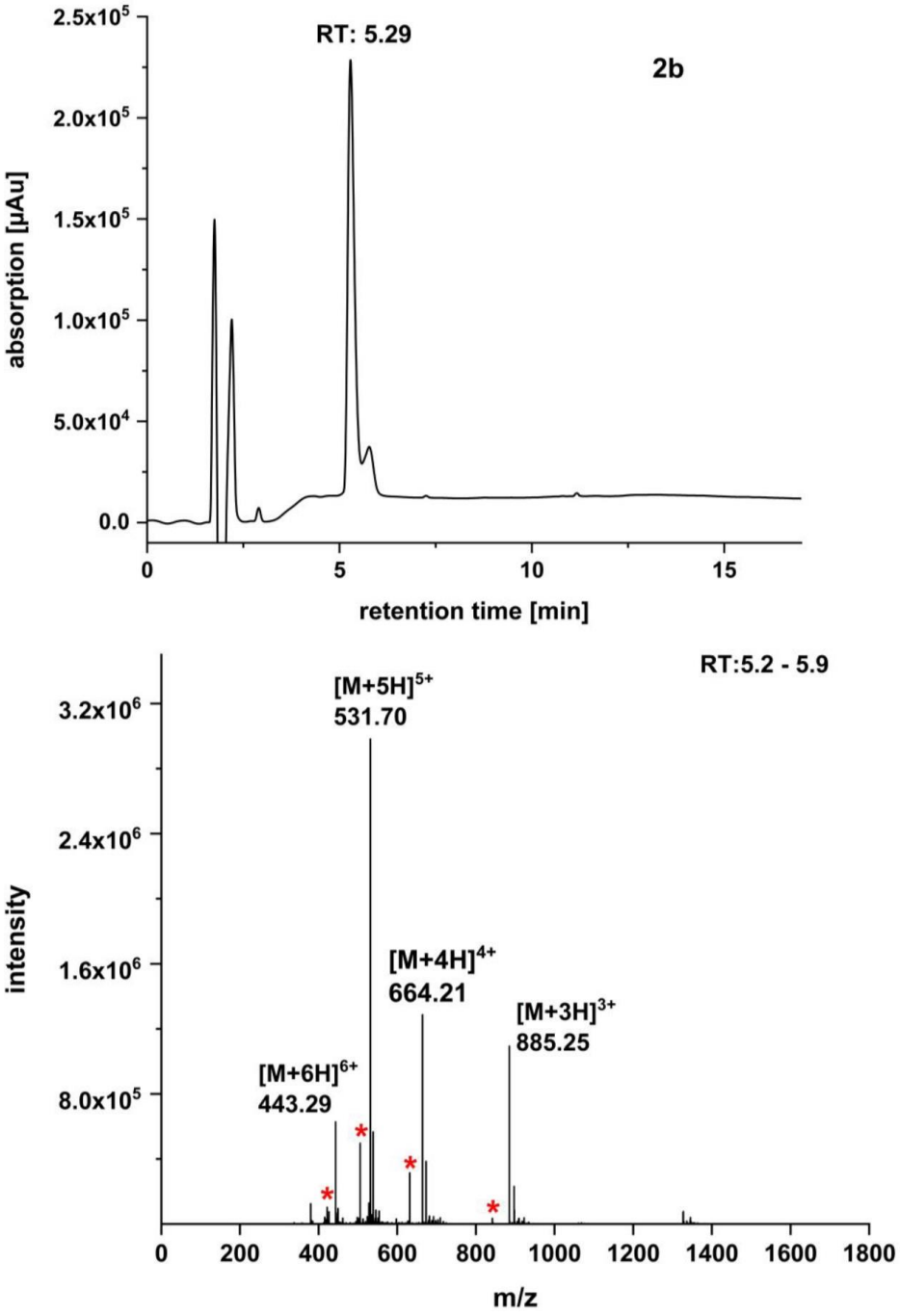

Figure 64. LC-MS analysis of peptide 2b; MW calculated: 2652.2 g/mol. Purity: 97%. UV chromatogram (254 nm) and ESI-MS mass spectrum. Gradient: 10-60% B in A in 15 min, 0.6 ml/min. A: 0.1% FA in H_2O; B: 0.1% FA in ACN. Red asterisks: peaks corresponding to the product without daunosamine after mass fragmentation.

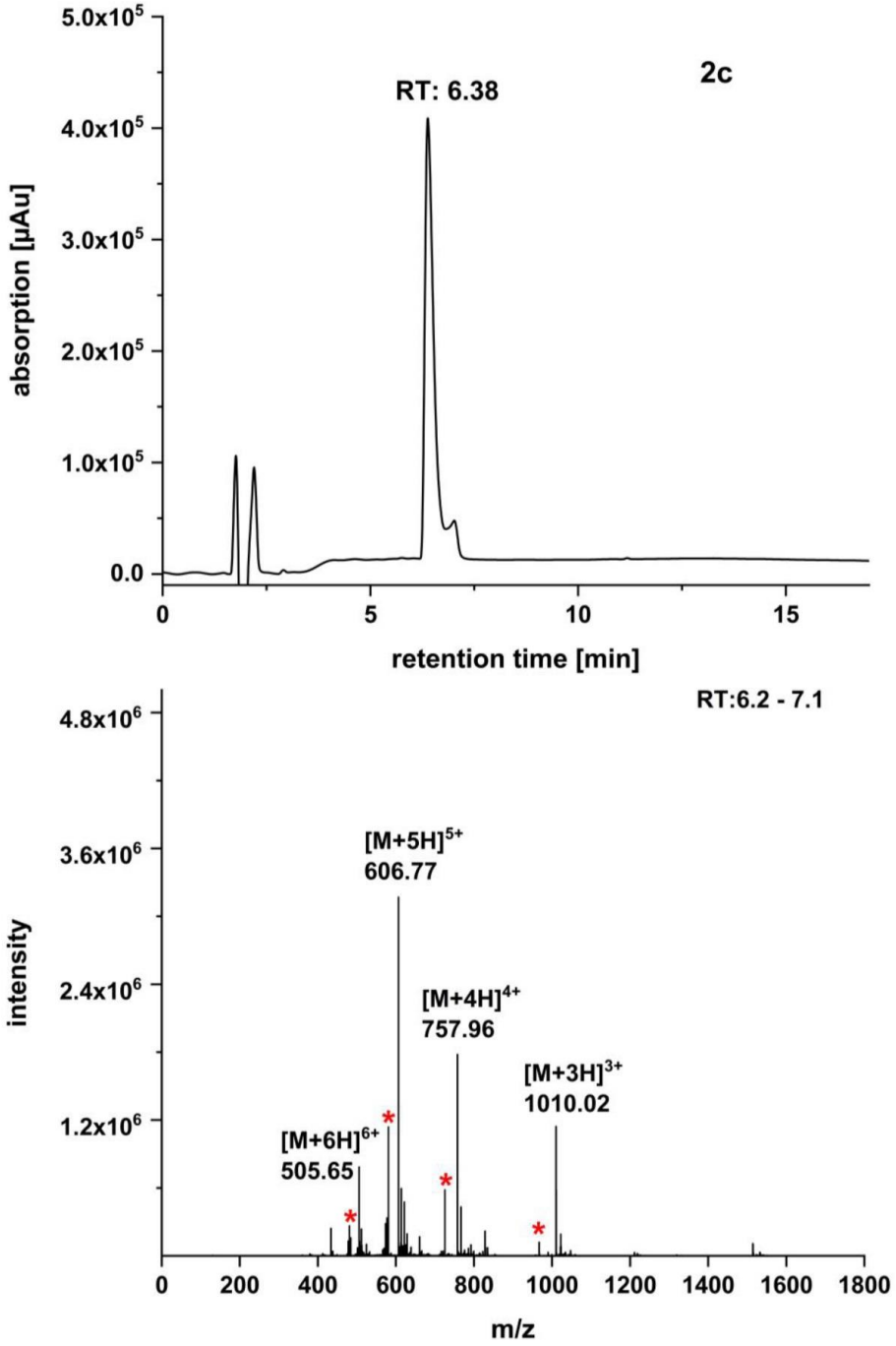

Figure 65. LC-MS analysis of peptide 2c; MW calculated: 3026.7 g/mol. Purity: >99%. UV chromatogram (254 nm) and ESI-MS mass spectrum. Gradient: 10-60% B in A in 15 min, 0.6 ml/min. A: 0.1% FA in H_2O; B: 0.1% FA in ACN. Red asterisks: peaks corresponding to the product without daunosamine after mass fragmentation.

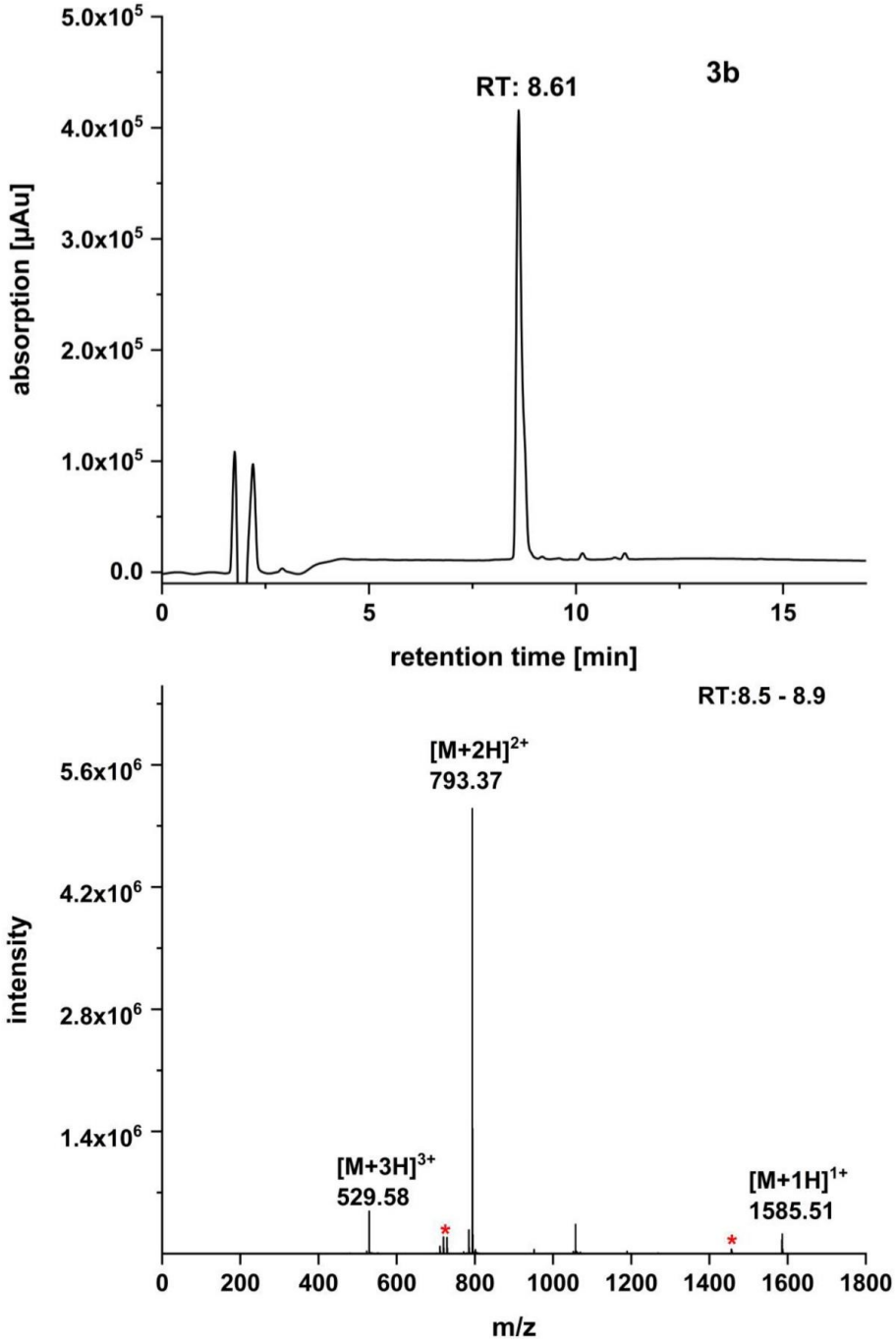

Figure 66. LC-MS analysis of peptide 3b; MW calculated: 1584.2 g/mol. Purity: 95%. UV chromatogram (254 nm) and ESI-MS mass spectrum. Gradient: 10-60% B in A in 15 min, 0.6 ml/min. A: 0.1% FA in H_2O; B: 0.1% FA in ACN. Red asterisks: peaks corresponding to the product without daunosamine after mass fragmentation.

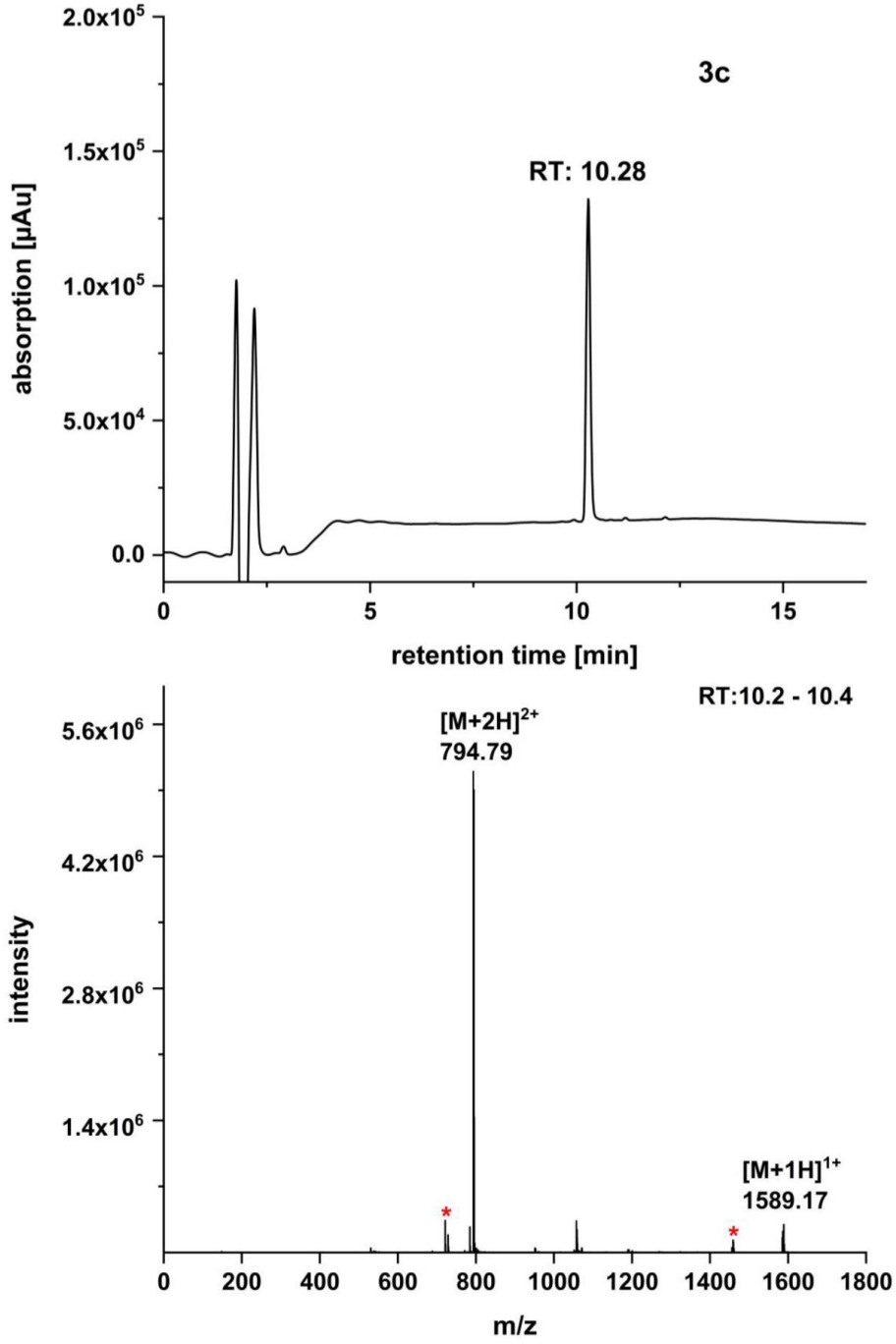

Figure 67. LC-MS analysis of peptide 3c; MW calculated: 1587.4 g/mol. Purity: 98%. UV chromatogram (254 nm) and ESI-MS mass spectrum. Gradient: 10-60% B in A in 15 min, 0.6 ml/min. A: 0.1% FA in H_2O; B: 0.1% FA in ACN. Red asterisks: peaks corresponding to the product without daunosamine after mass fragmentation.

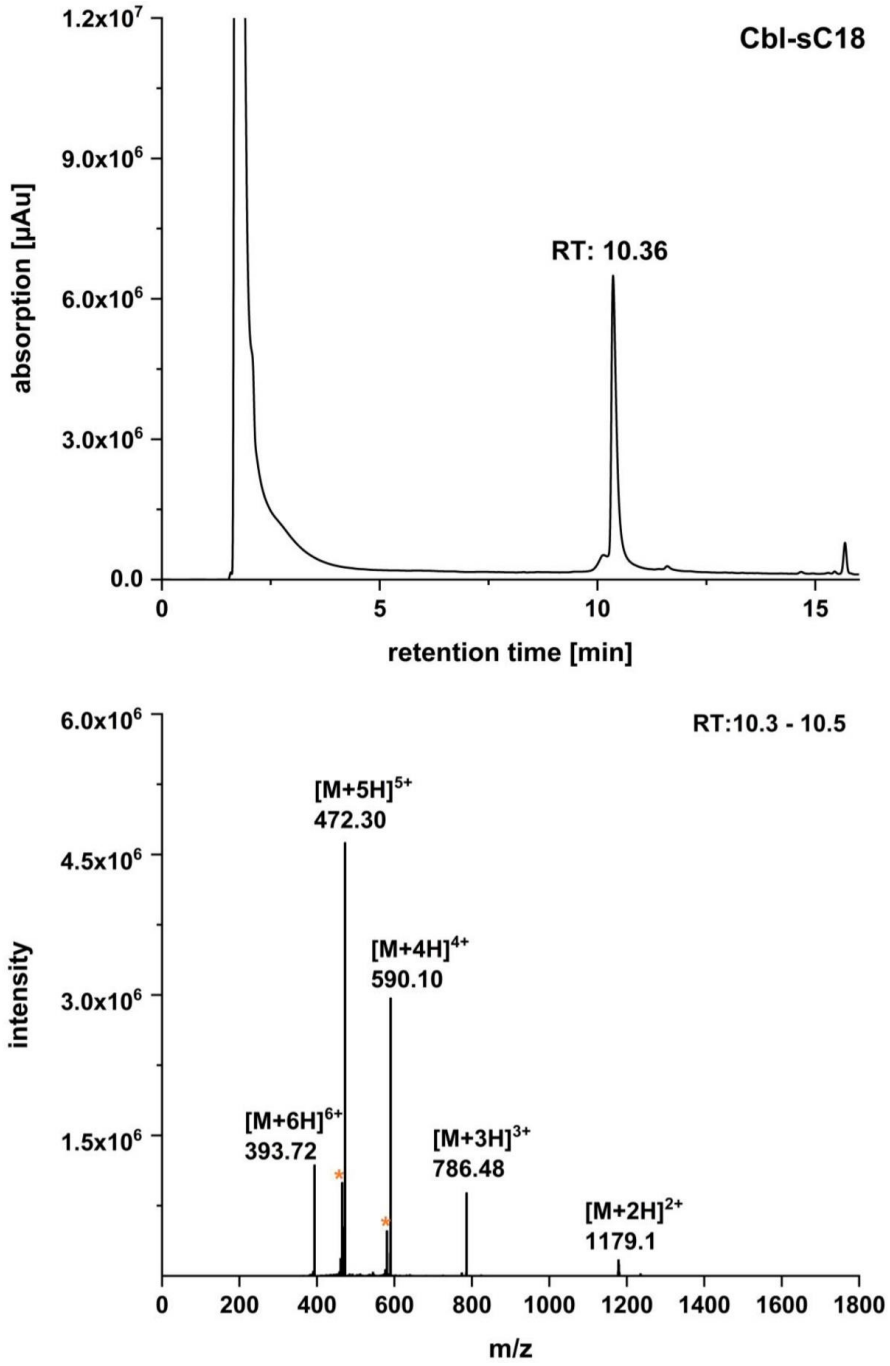

Figure 68. LC-MS analysis of peptide Cbl-sC18; MW calculated: 2356.8 g/mol. Purity: 91%. UV chromatogram (220 nm) and ESI-MS mass spectrum. Gradient: 10-60% B in A in 15 min, 0.6 ml/min. A: 0.1% TFA in H_2O; B: 0.1% TFA in ACN. Yellow asterisks: peaks corresponding to the hydrolysed product. The first peak is DMSO since the compound was dissolved in DMSO to avoid hydrolysis.

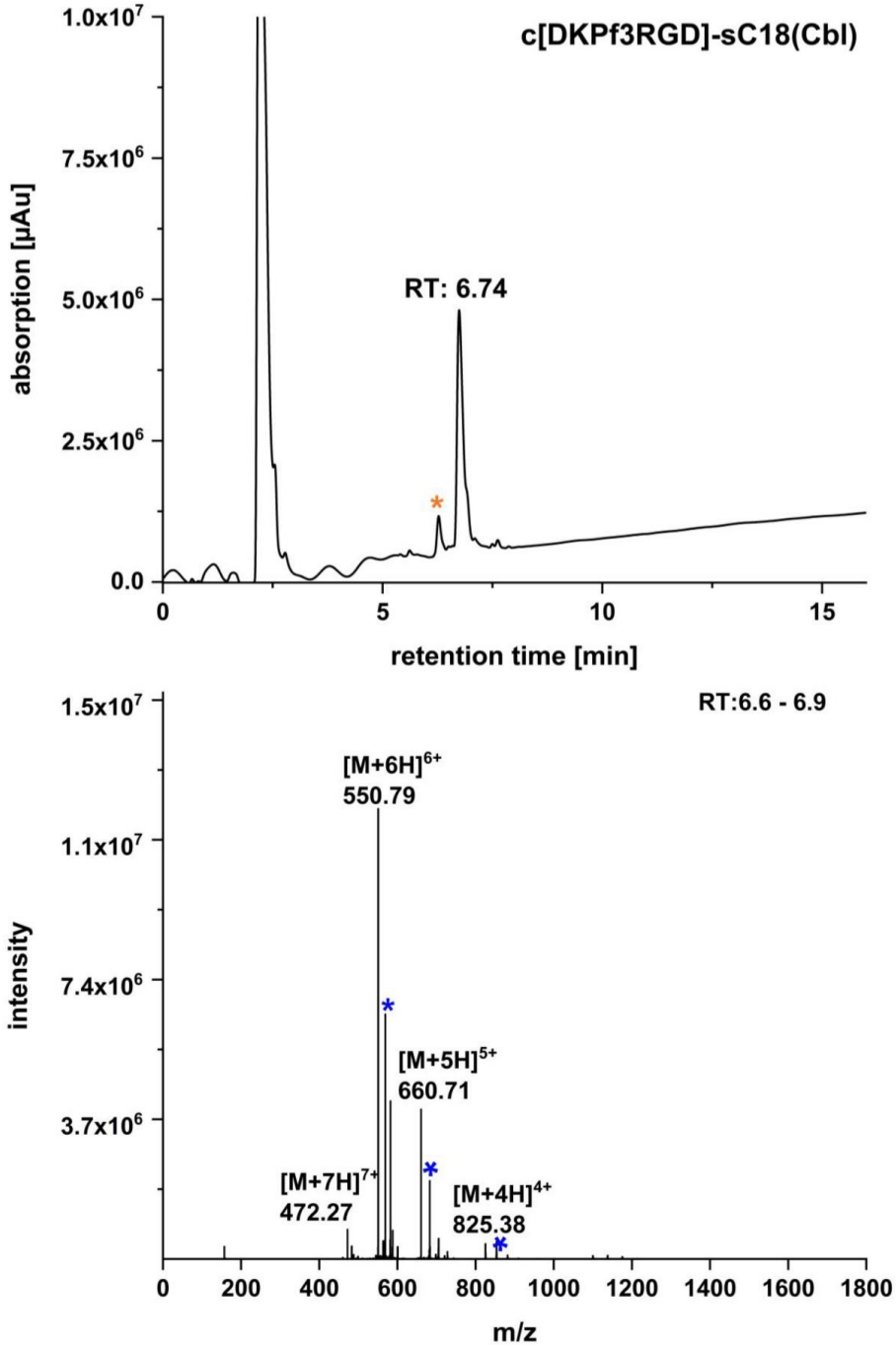

Figure 69. LC-MS analysis of peptide c[DKP*f3*RGD]-sC18(Cbl); MW calculated: 3296.5 g/mol. Purity: 86%. UV chromatogram (220 nm) and ESI-MS mass spectrum. Gradient: 10-60% B in A in 15 min, 0.6 ml/min. A: 0.1% FA in H_2O; B: 0.1% FA in ACN. Yellow asterisk: peaks corresponding to the hydrolysed product; blue asterisks: peaks corresponding to the TFA adducts (delta mass +114). The first peak is DMSO since the compound was dissolved in DMSO to avoid hydrolysis.

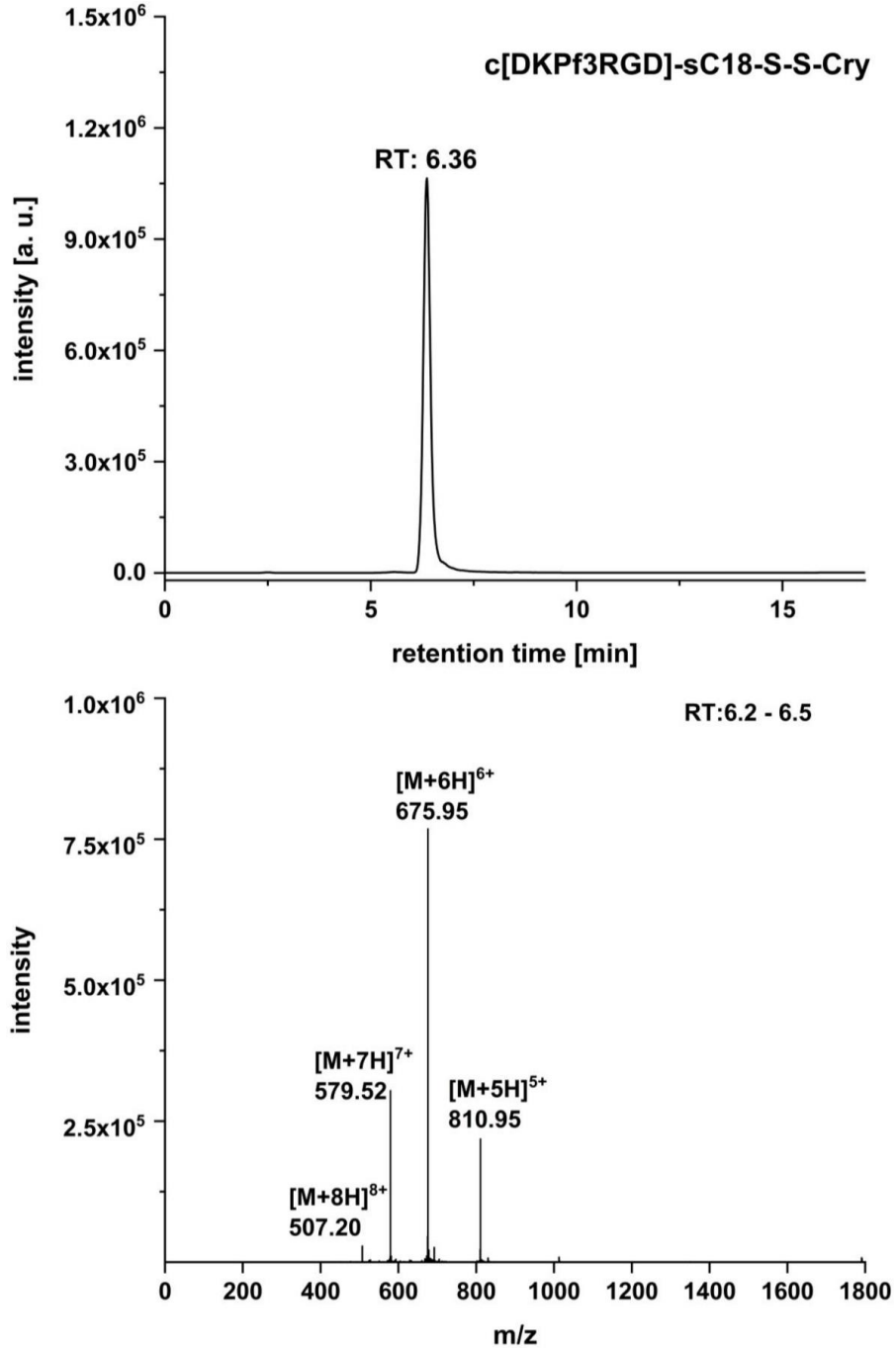

Figure 70. LC-MS analysis of peptide c[DKP*f3*RGD]-sC18-S-S-Cry; MW calculated: 4048.3 g/mol. Purity: 95%. Ion current and ESI-MS mass spectrum. Gradient: 10-60% B in A in 15 min, 0.6 ml/min. A: 0.1% FA in H_2O; B: 0.1% FA in ACN.

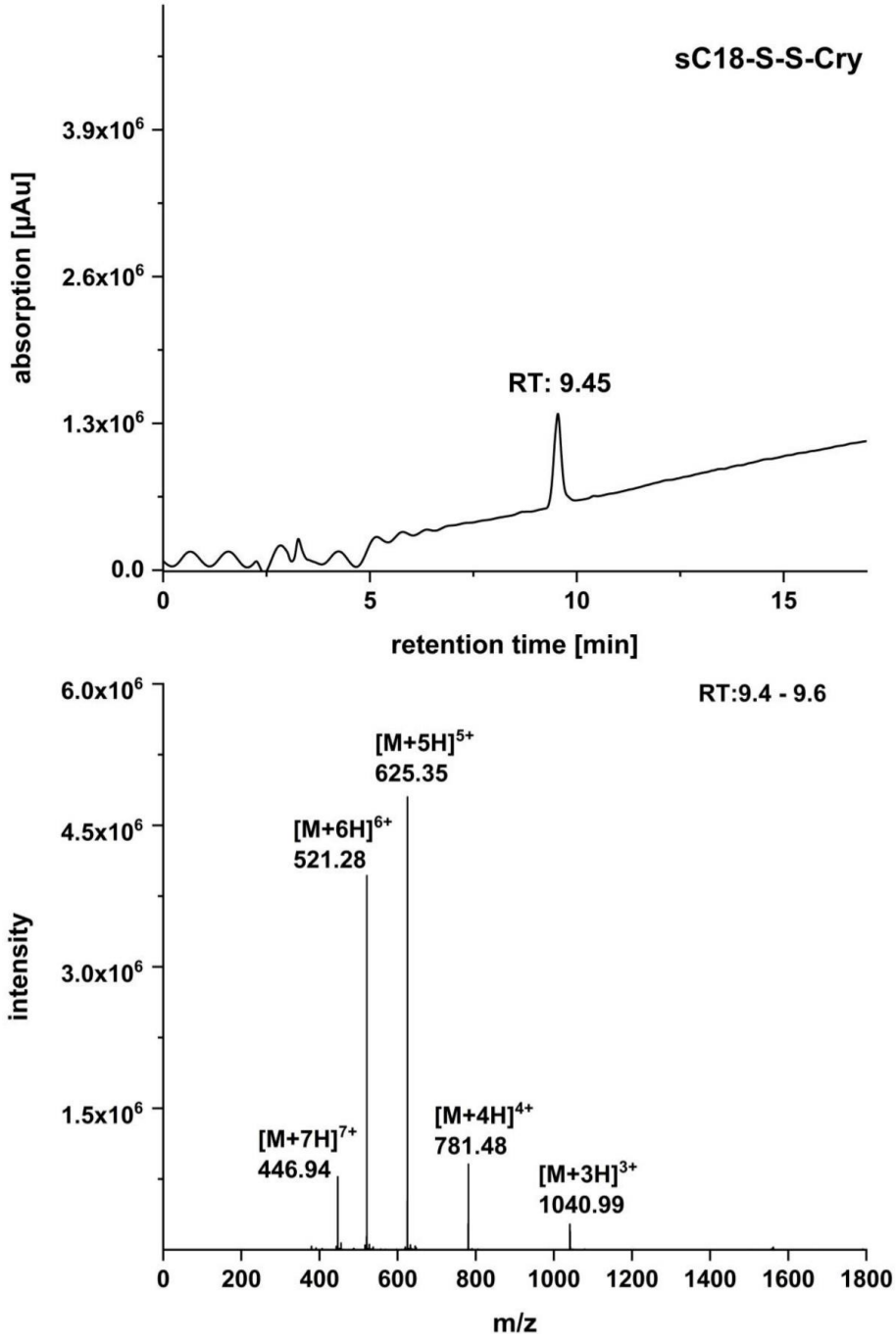

Figure 71. LC-MS analysis of peptide sC18-S-S-Cry; MW calculated: 3121.7 g/mol. Purity: 97%. UV chromatogram (220 nm) and ESI-MS mass spectrum. Gradient: 10-60% B in A in 15 min, 0.6 ml/min. A: 0.1% FA in H_2O; B: 0.1% FA in ACN.

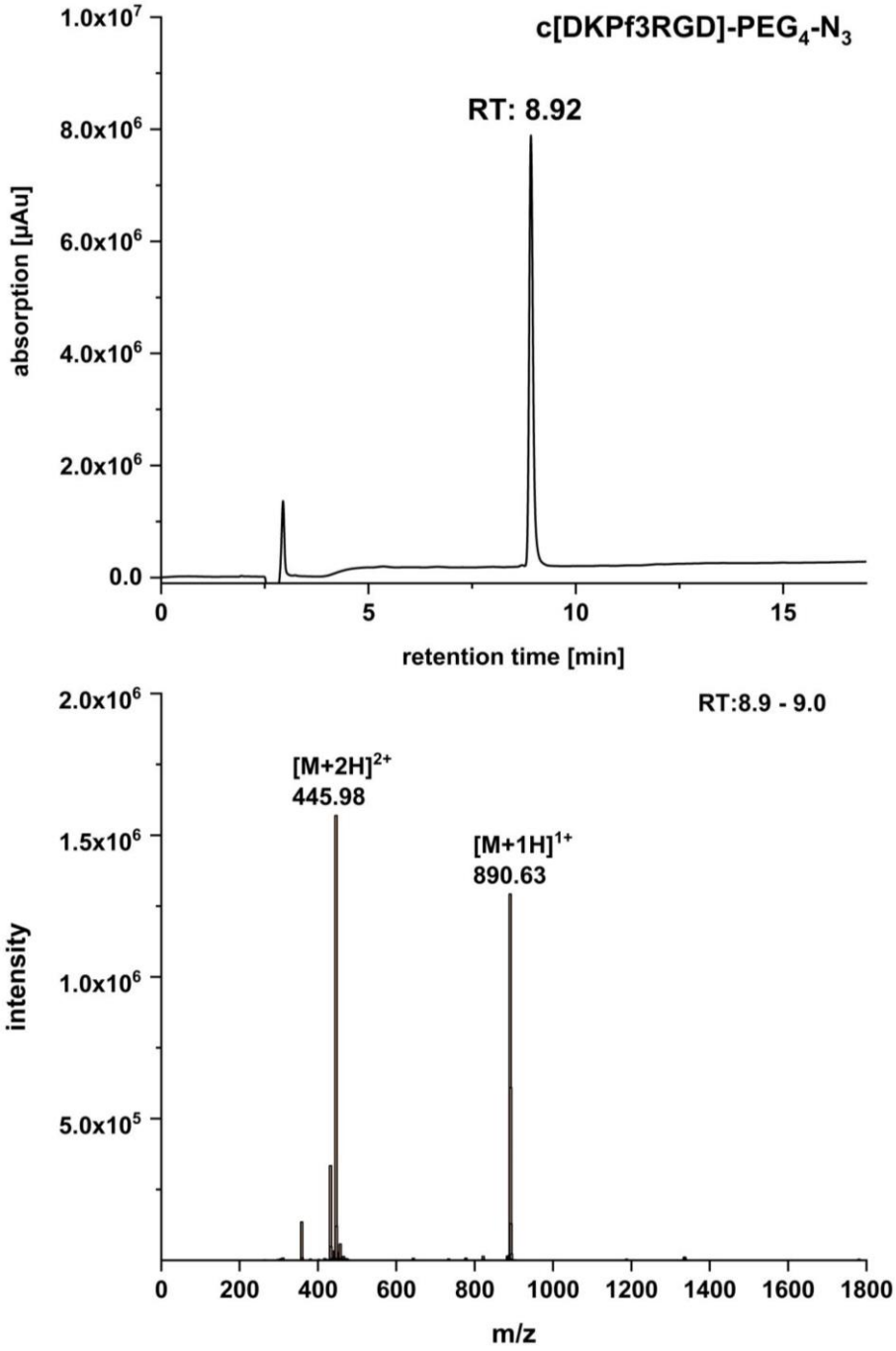

Figure 72. LC-MS analysis of peptide c[DKP*f3*RGD]-PEG_4-N_3; MW calculated: 889.6 g/mol. Purity: >99%. UV chromatogram (220 nm) and ESI-MS mass spectrum. Gradient: 10-60% B in A in 15 min, 0.6 ml/min. A: 0.1% TFA in H_2O; B: 0.1% TFA in ACN.

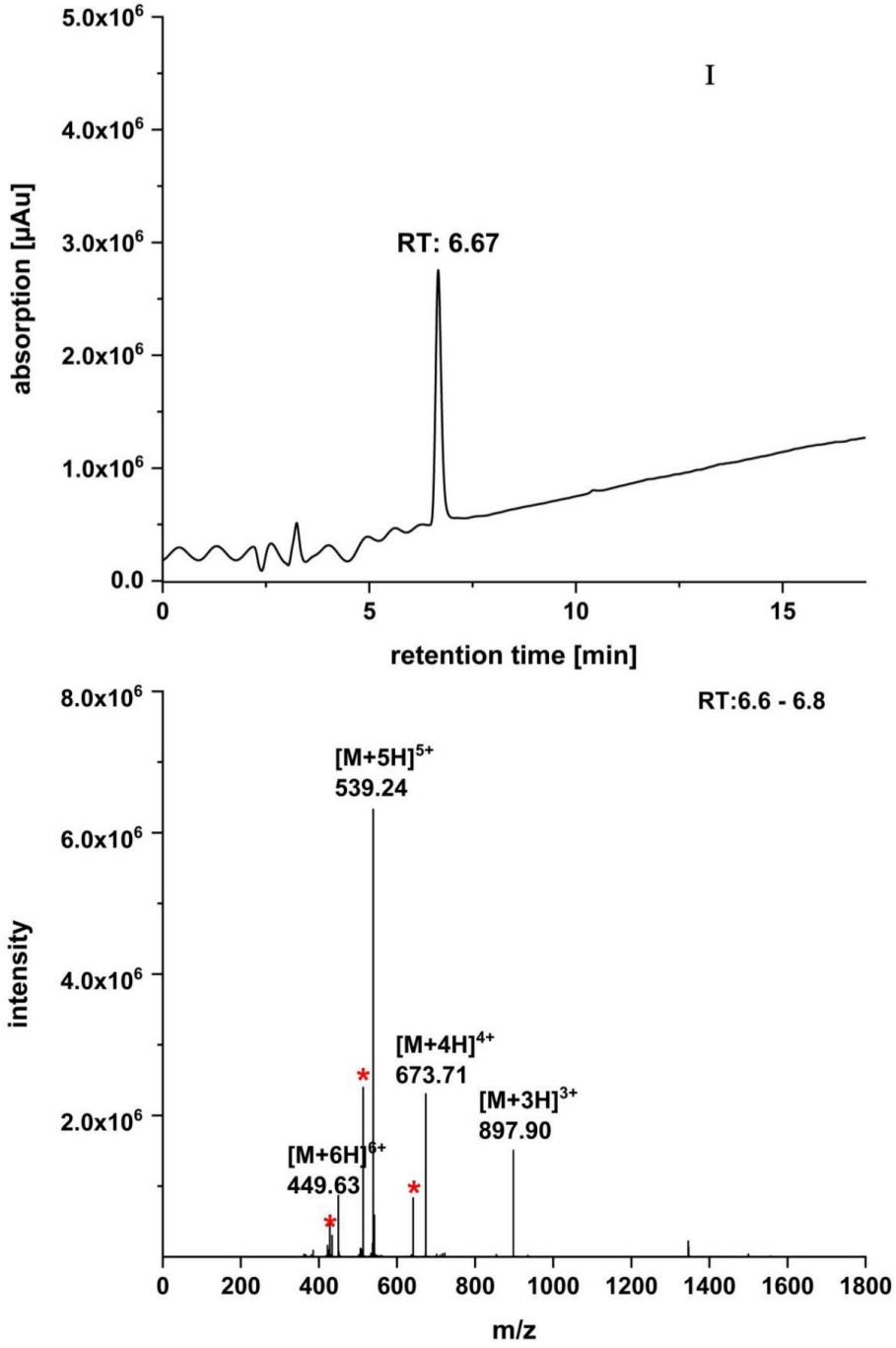

Figure 73. LC-MS analysis of peptide I; MW calculated: 2690.2 g/mol. Purity: 98%. UV chromatogram (220 nm) and ESI-MS mass spectrum. Gradient: 10-60% B in A in 15 min, 0.6 ml/min. A: 0.1% FA in H_2O; B: 0.1% FA in ACN. Red asterisks: peaks corresponding to the product without daunosamine after mass fragmentation.

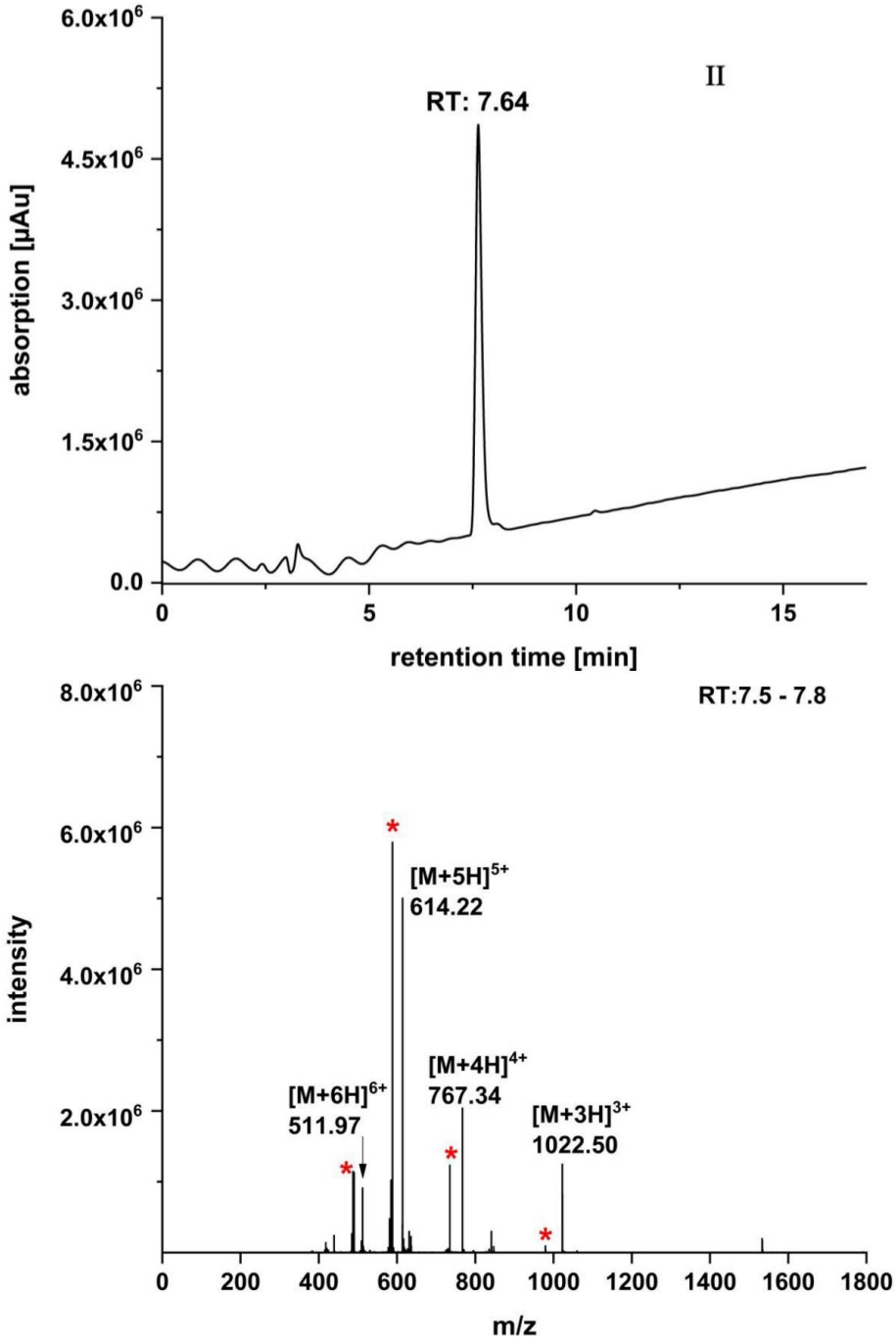

Figure 74. LC-MS analysis of peptide II; MW calculated: 3064.7 g/mol. Purity: 95%. UV chromatogram (220 nm) and ESI-MS mass spectrum. Gradient: 10-60% B in A in 15 min, 0.6 ml/min. A: 0.1% FA in H_2O; B: 0.1% FA in ACN. Red asterisks: peaks corresponding to the product without daunosamine after mass fragmentation.

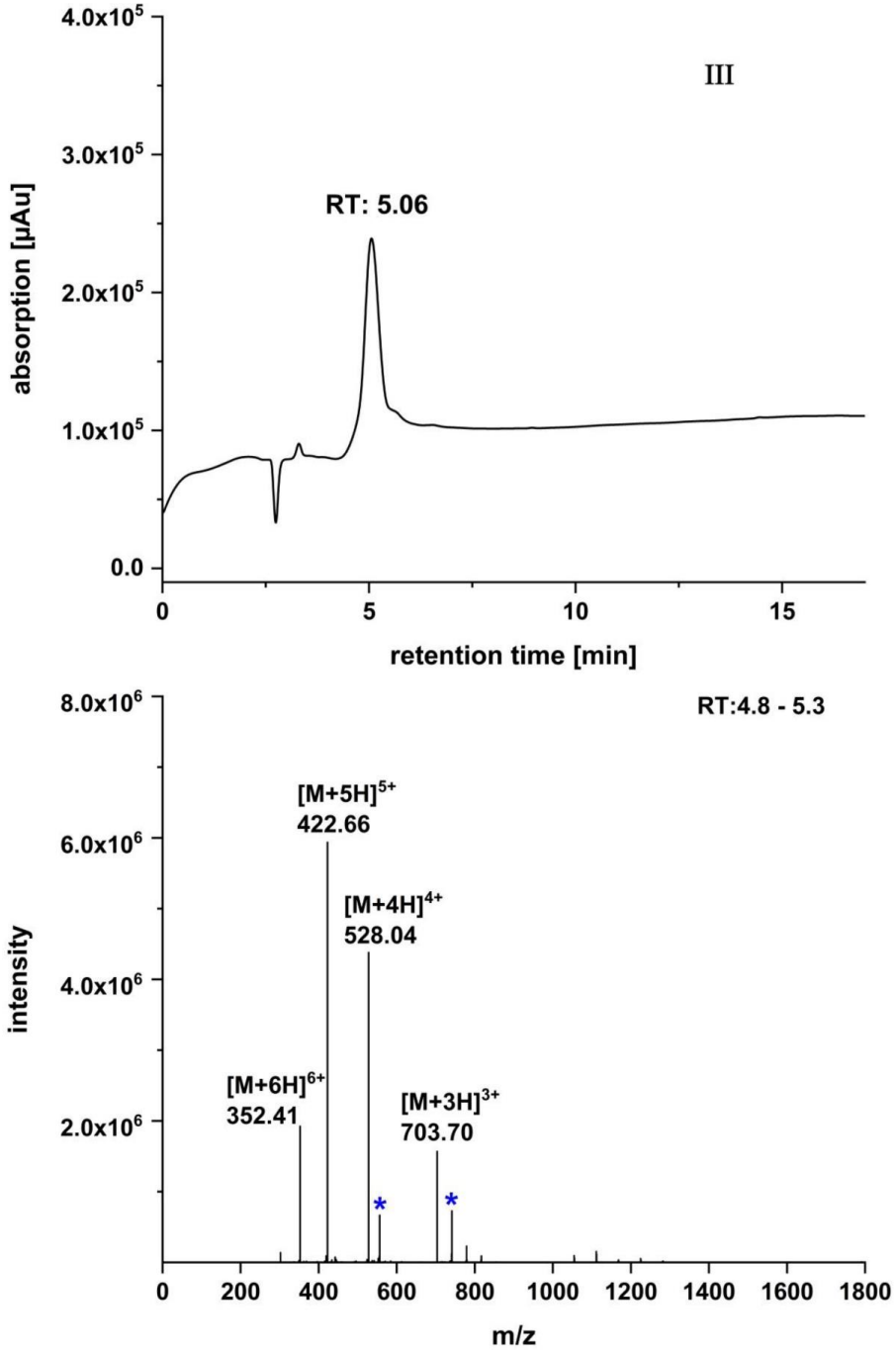

Figure 75. LC-MS analysis of peptide III (R=H); MW calculated: 2107.6 g/mol. Purity: >99%. UV chromatogram (254 nm) and ESI-MS mass spectrum. Gradient: 5-55% B in A in 15 min, 0.6 ml/min. A: 0.1% FA in H_2O; B: 0.1% FA in ACN. Blue asterisks: peaks corresponding to the TFA adducts (delta mass +114).

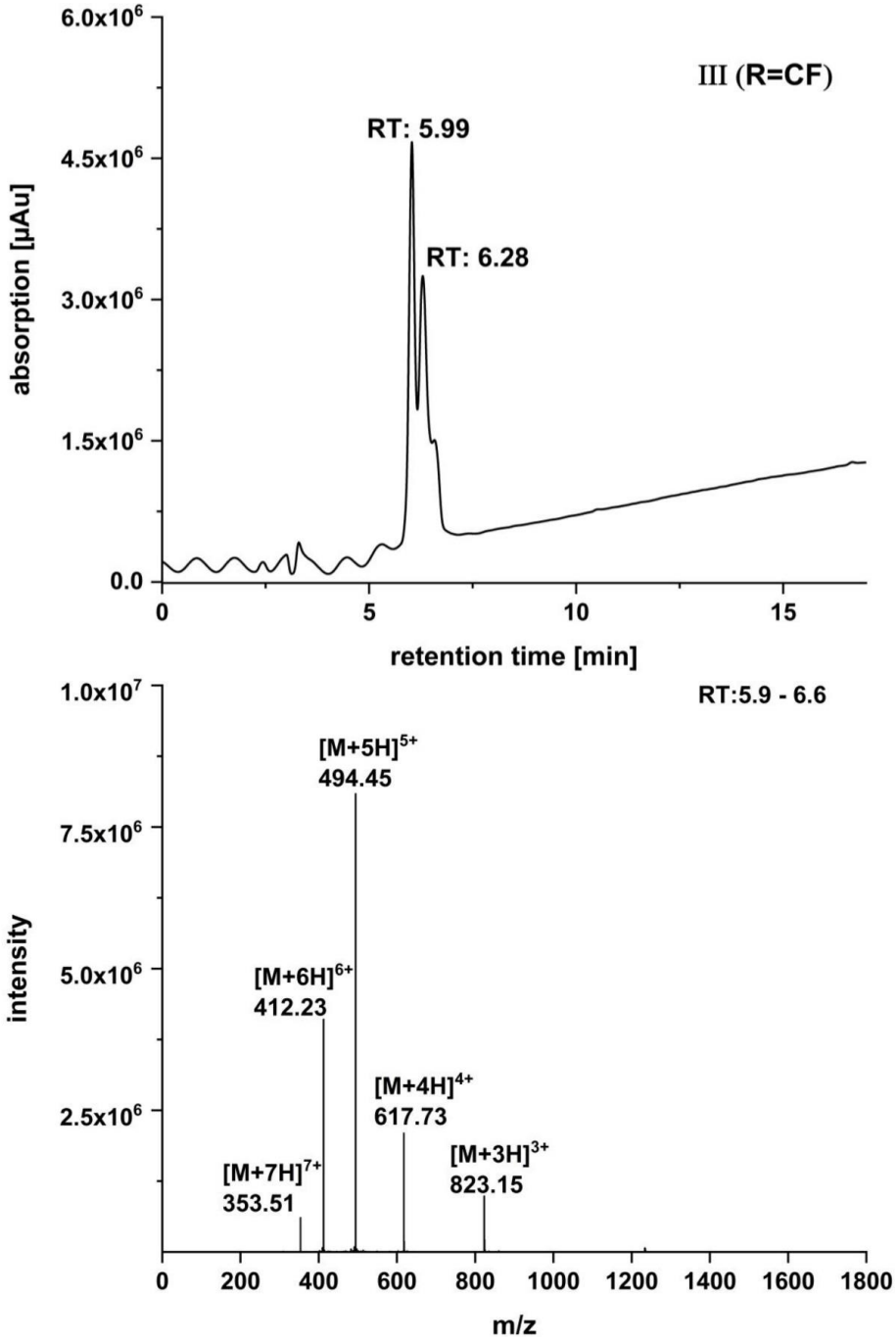

Figure 76. LC-MS analysis of peptide III (R=CF); MW calculated: 2466.0 g/mol. Purity: >99%. UV chromatogram (220 nm) and ESI-MS mass spectrum. Gradient: 10-60% B in A in 15 min, 0.6 ml/min. A: 0.1% FA in H_2O; B: 0.1% FA in ACN.

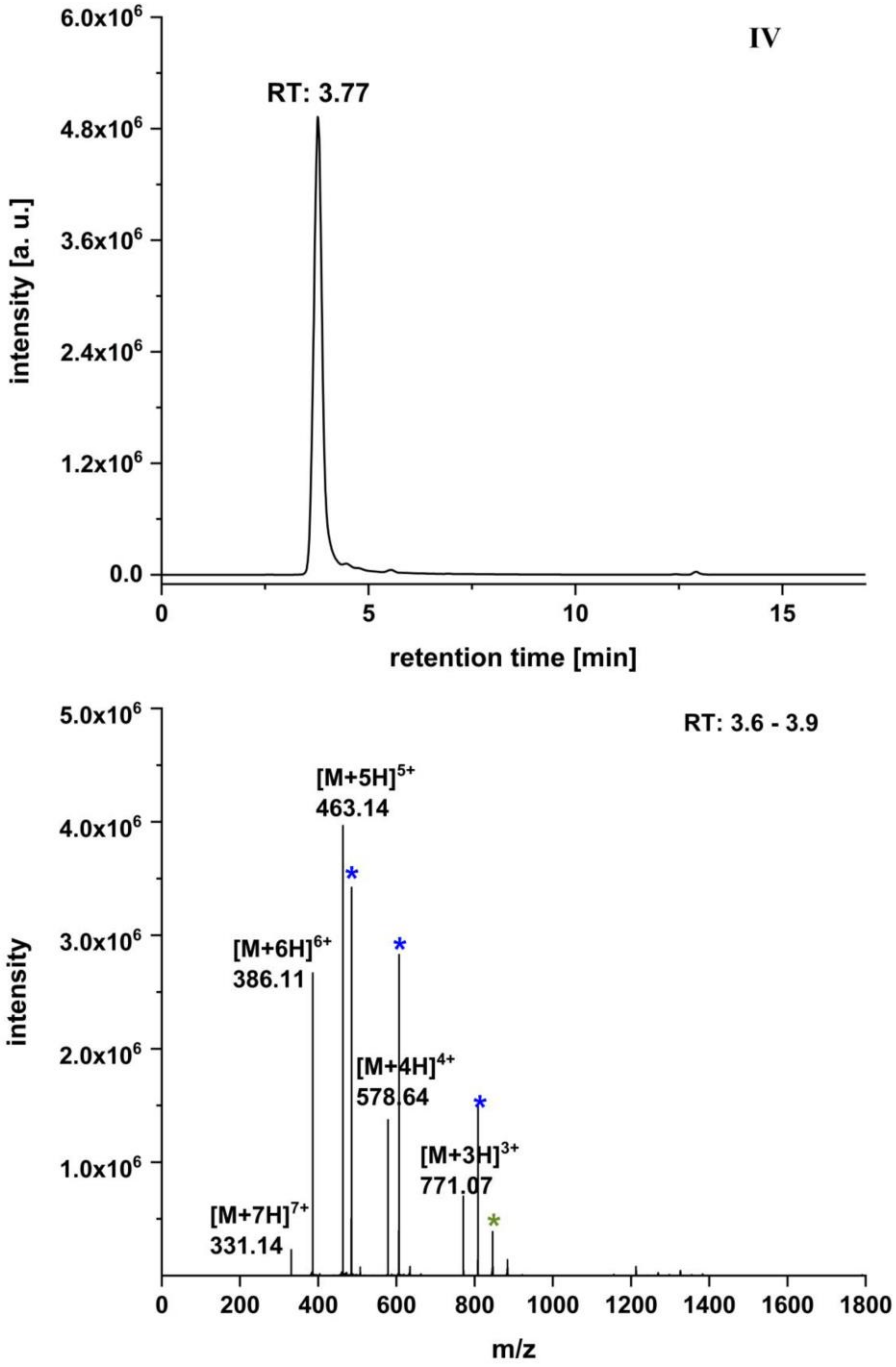

Figure 77. LC-MS analysis of peptide IV; MW calculated: 2309.92 g/mol. Purity: 95%. Ion current and ESI-MS mass spectrum. Gradient: 10-60% B in A in 15 min, 0.6 ml/min. A: 0.1% FA in H_2O; B: 0.1% FA in ACN. Blue asterisks: peaks corresponding to the TFA adducts (delta mass +114); green asterisk: peak corresponding to the TFA adducts (delta mass +228).

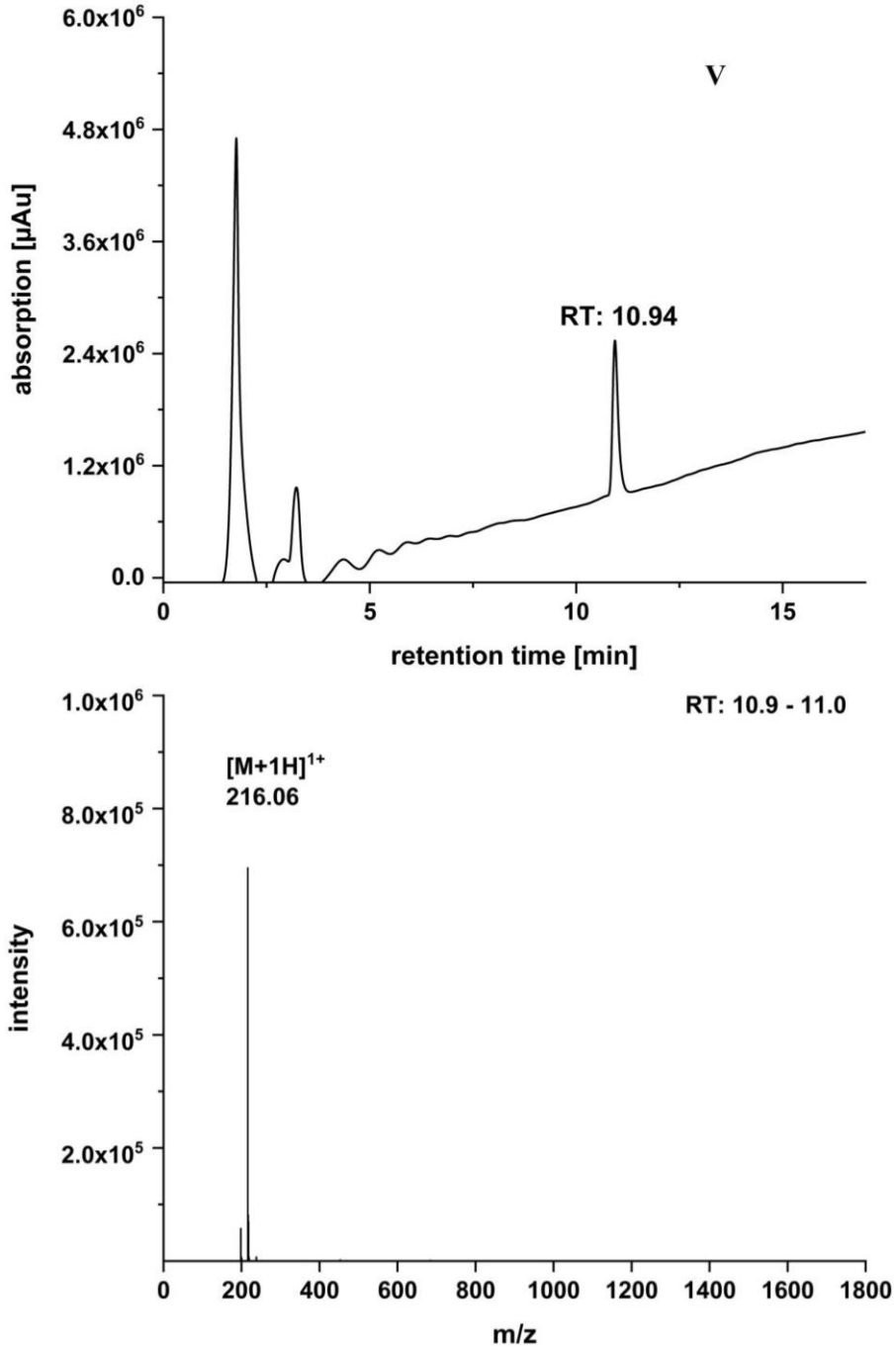

Figure 78. LC-MS analysis of peptide V; MW calculated: 215.29 g/mol. Purity: >99%. UV chromatogram (220 nm) and ESI-MS mass spectrum. Gradient: 10-60% B in A in 15 min, 0.6 ml/min. A: 0.1% FA in H_2O; B: 0.1% FA in ACN.

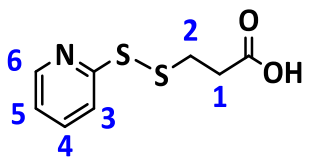

^{1}H NMR (300 MHz, DMSO) δ 8.49 – 8.43 (m, 1H, H_6), 7.86 – 7.79 (m, 1H, H_4), 7.76 (d, J = 8.1 Hz, 1H, H_3), 7.25 (ddd, J = 7.1, 4.8, 1.2 Hz, 1H, H_5), 3.00 (t, J = 6.9 Hz, 2H, H_2), 2.63 (t, J = 6.9 Hz, 2H, H_1)

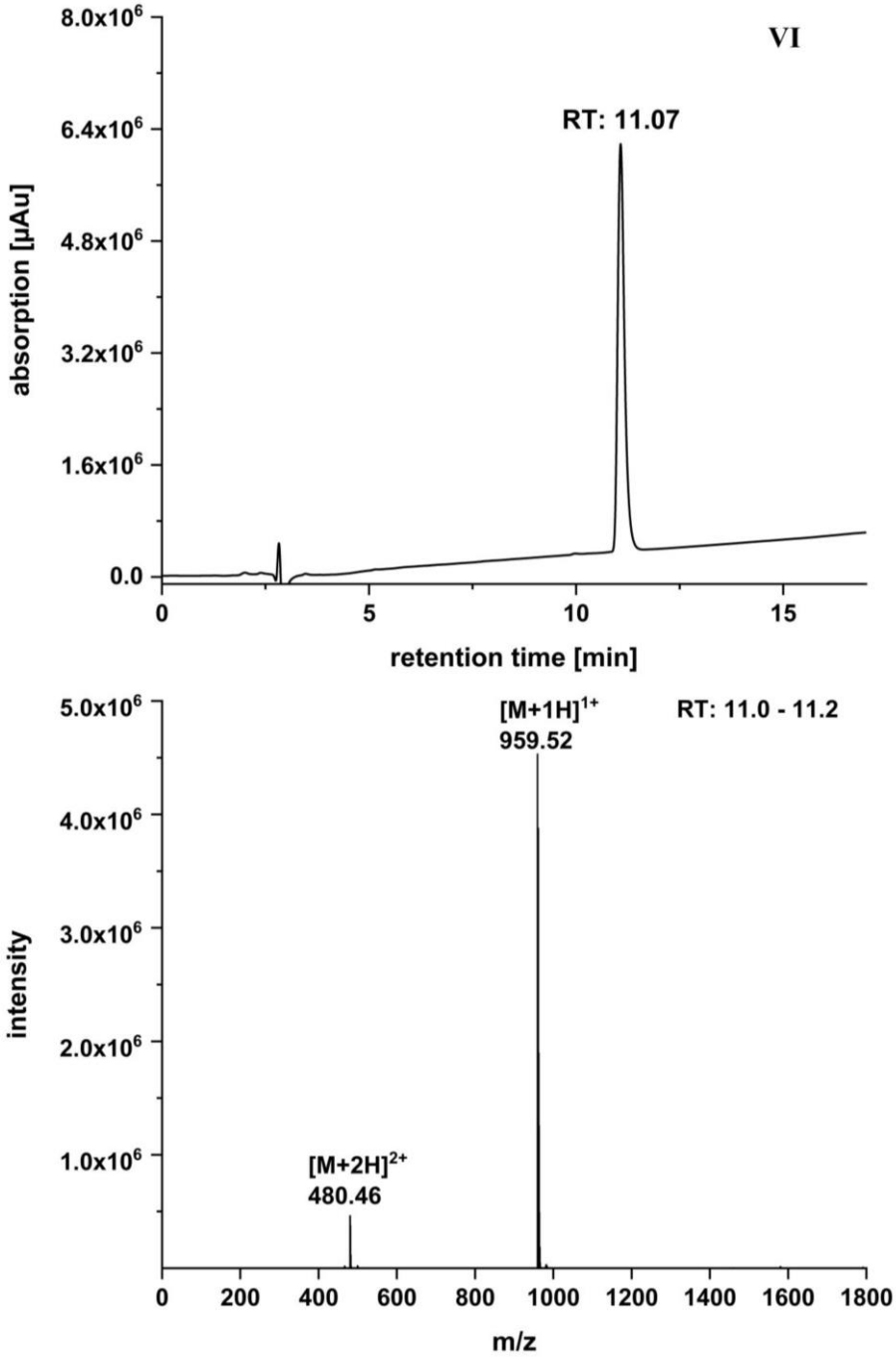

Figure 79. LC-MS analysis of peptide VI; MW calculated: 959.0 g/mol. Purity: >99%. UV chromatogram (220 nm) and ESI-MS mass spectrum. Gradient: 50-90% B in A in 15 min, 0.6 ml/min. A: 0.1% FA in H_2O; B: 0.1% FA in ACN.

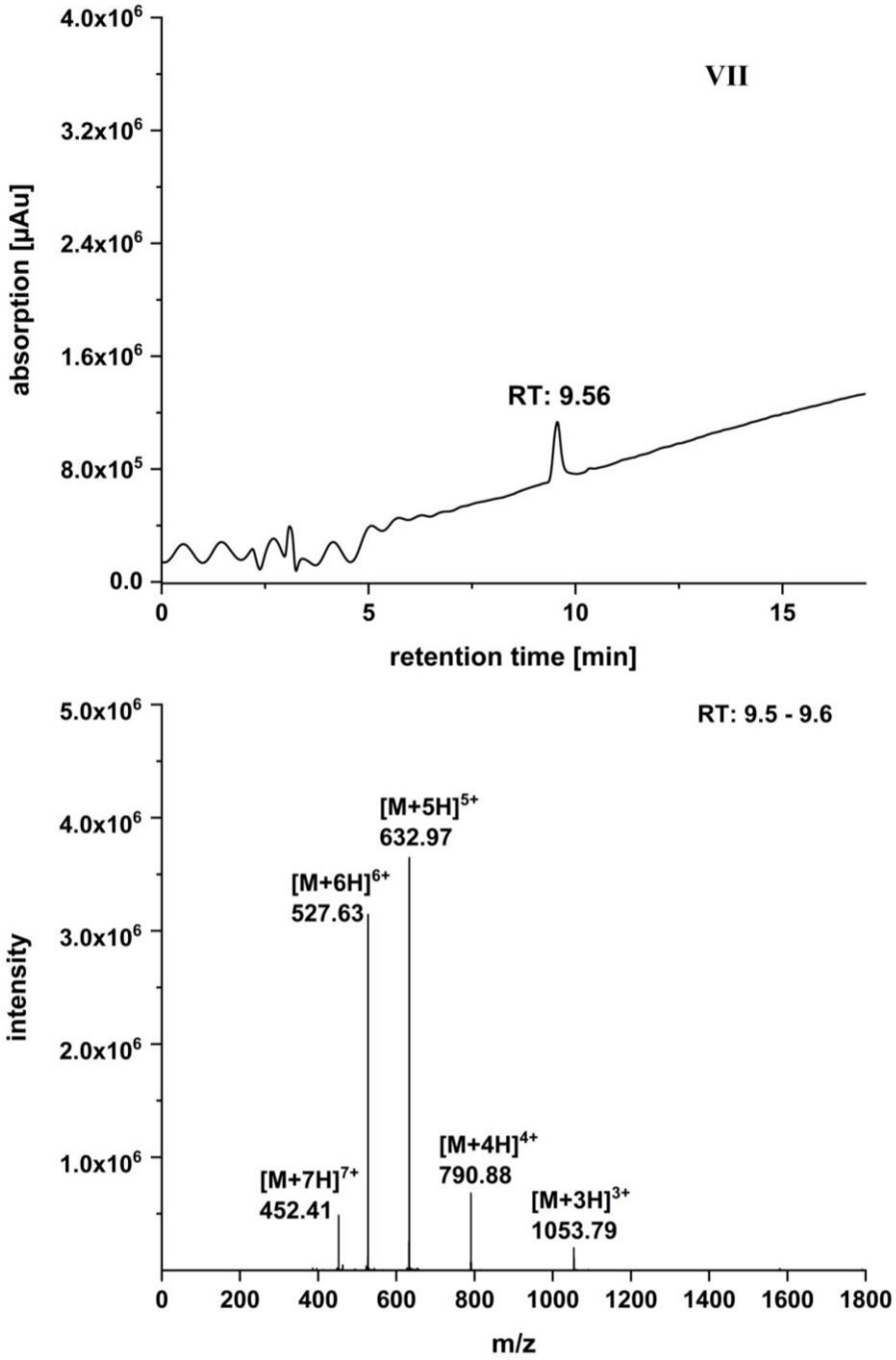

Figure 80. LC-MS analysis of peptide VII; MW calculated: 3158.8 g/mol. Purity: 95%. UV chromatogram (220 nm) and ESI-MS mass spectrum. Gradient: 10-60% B in A in 15 min, 0.6 ml/min. A: 0.1% FA in H_2O; B: 0.1% FA in ACN.

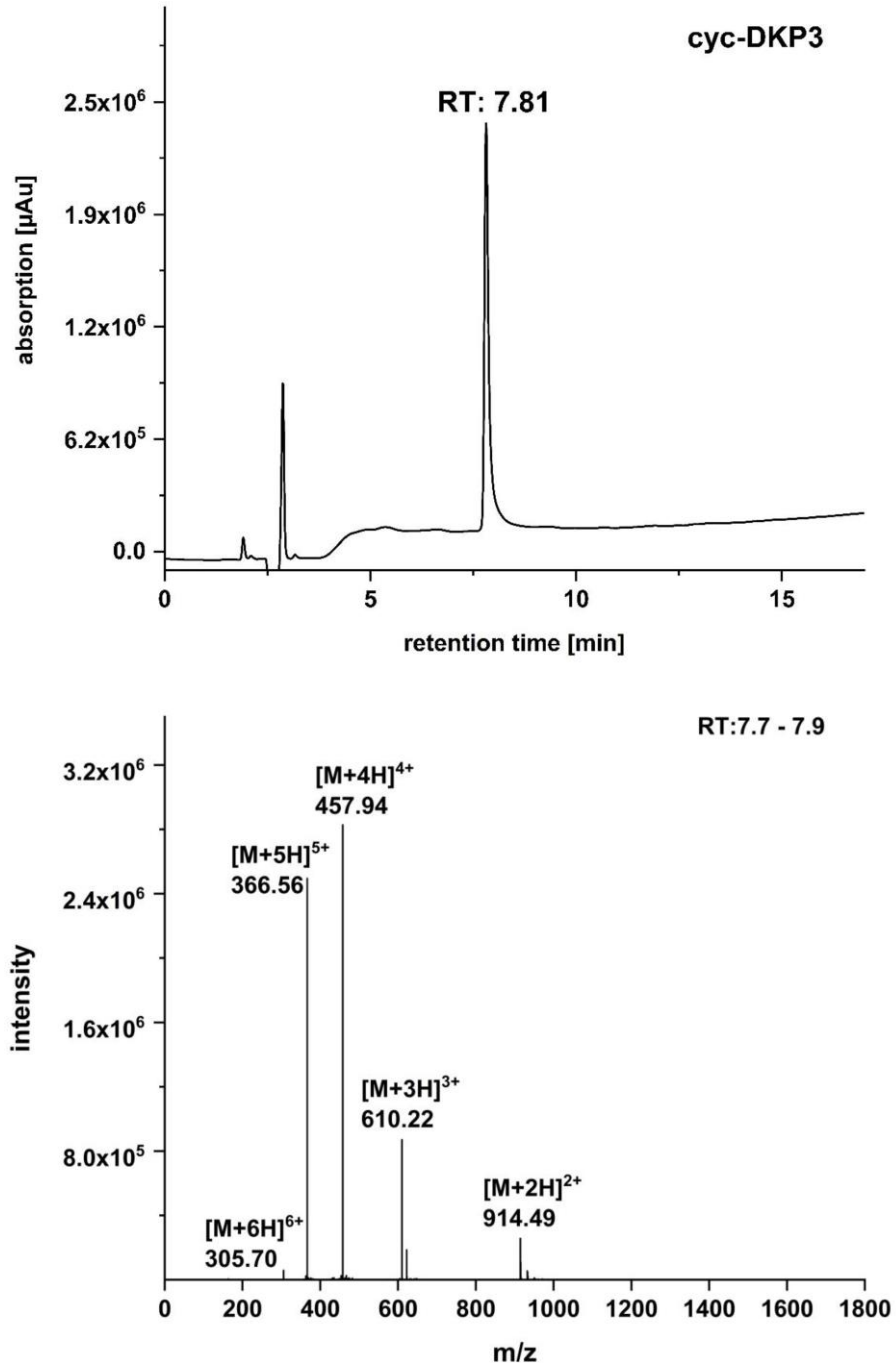

Figure 81. LC-MS analysis of peptide cyc-DKP3; MW calculated: 1827.3 g/mol. Purity: >99%. UV chromatogram (220 nm) and ESI-MS mass spectrum. Gradient: 10-60% B in A in 15 min, 0.6 ml/min. A: 0.1% TFA in H_2O; B: 0.1% TFA in ACN.

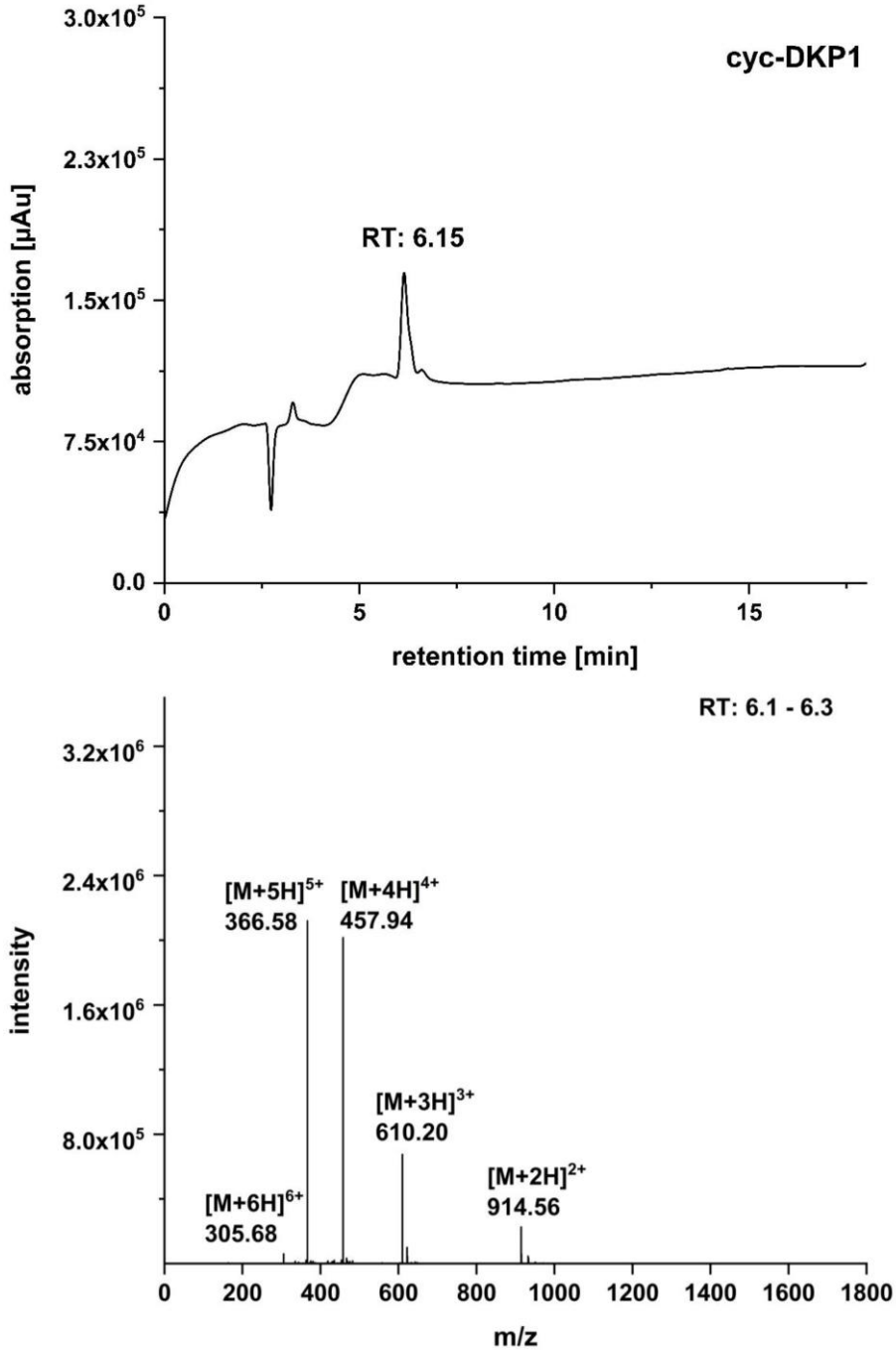

Figure 82. LC-MS analysis of peptide cyc-DKP1; MW calculated: 1827.3 g/mol. Purity: 99%. UV chromatogram (194 nm) and ESI-MS mass spectrum. Gradient: 5-55% B in A in 15 min, 0.6 ml/min. A: 0.1% FA in H_2O; B: 0.1% FA in ACN.

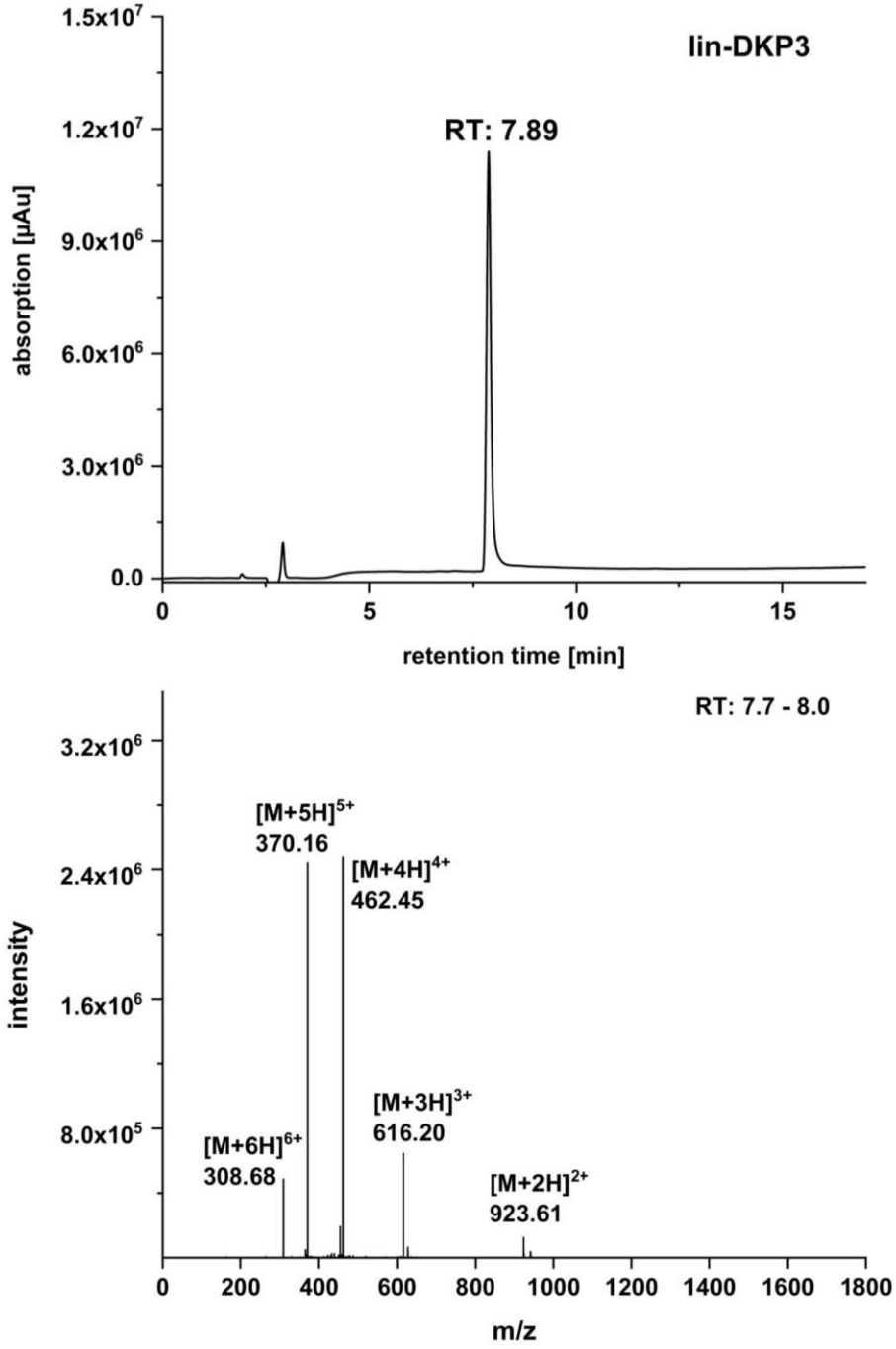

Figure 83. LC-MS analysis of peptide lin-DKP3; MW calculated: 1845.3 g/mol. Purity: 99%. UV chromatogram (220 nm) and ESI-MS mass spectrum. Gradient: 10-60% B in A in 15 min, 0.6 ml/min. A: 0.1% TFA in H_2O; B: 0.1% TFA in ACN.

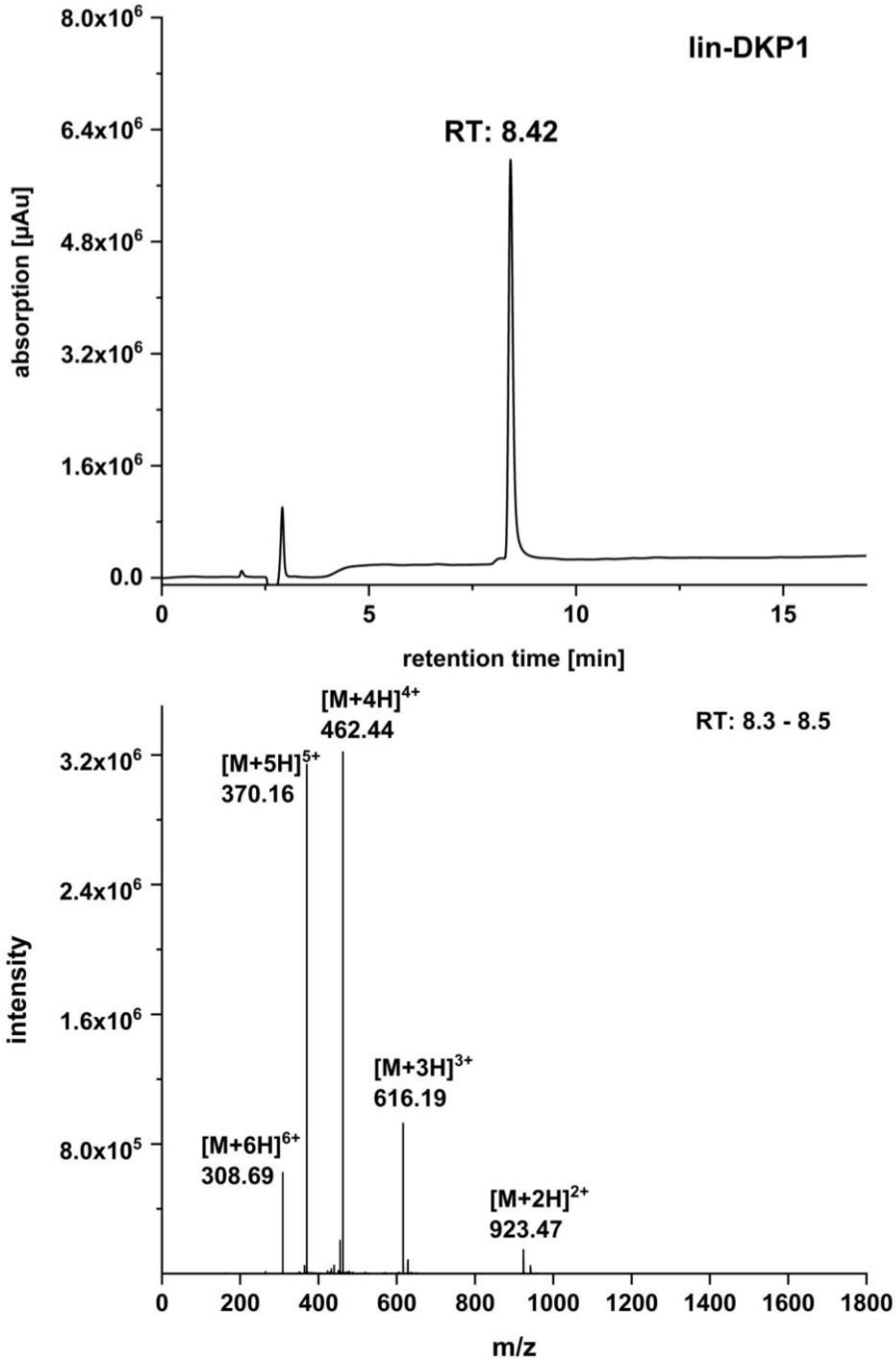

Figure 84. LC-MS analysis of peptide lin-DKP1; MW calculated: 1845.3 g/mol. Purity: 97%. UV chromatogram (220 nm) and ESI-MS mass spectrum. Gradient: 10-60% B in A in 15 min, 0.6 ml/min. A: 0.1% TFA in H_2O; B: 0.1% TFA in ACN.

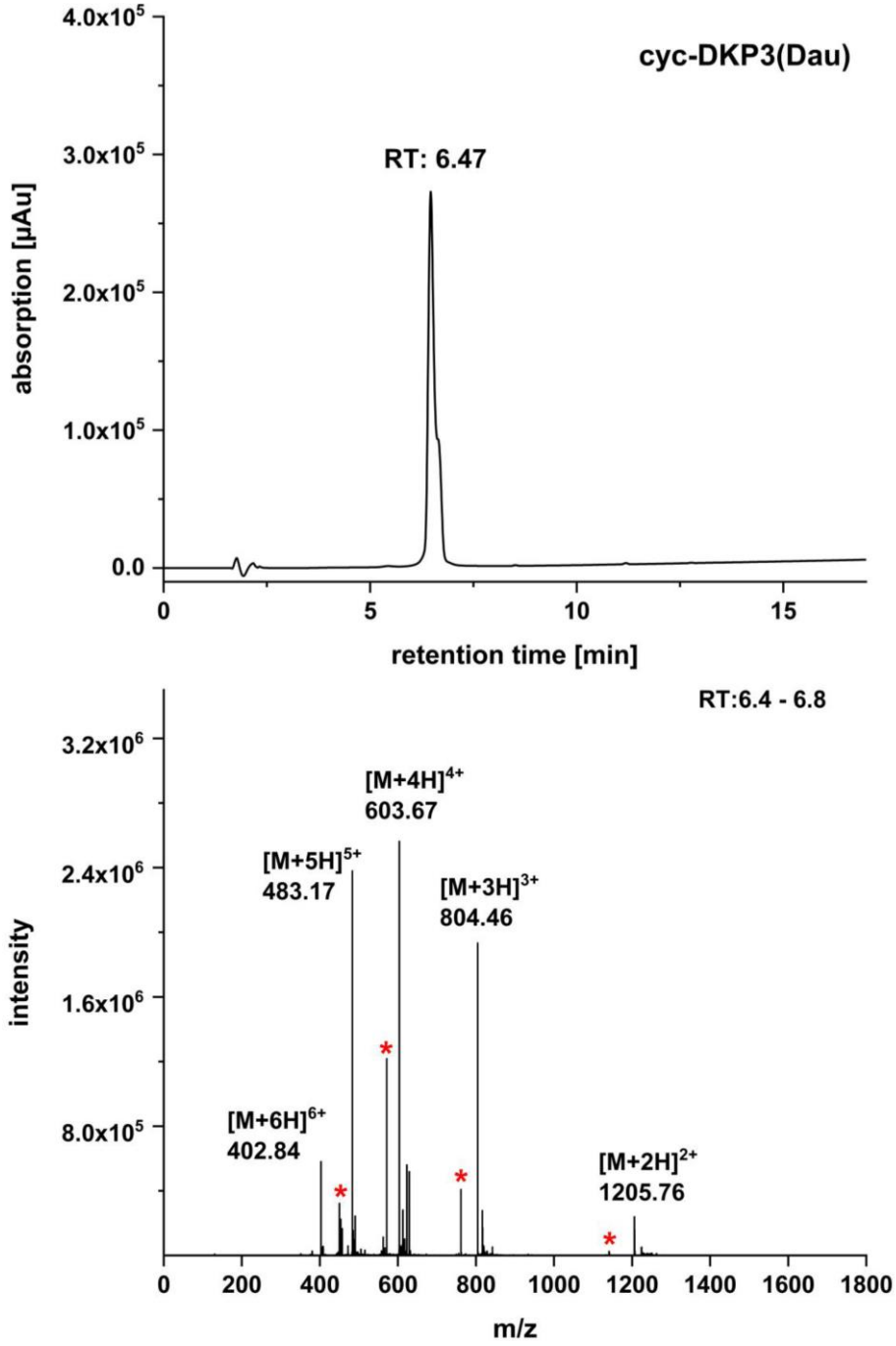

Figure 85. LC-MS analysis of peptide cyc-DKP3(Dau); MW calculated: 2409.8 g/mol. Purity: >99%. UV chromatogram (254 nm) and ESI-MS mass spectrum. Gradient: 10-60% B in A in 15 min, 0.6 ml/min. A: 0.1% FA in H_2O; B: 0.1% FA in ACN. Red asterisks: peaks corresponding to the product without daunosamine after mass fragmentation.

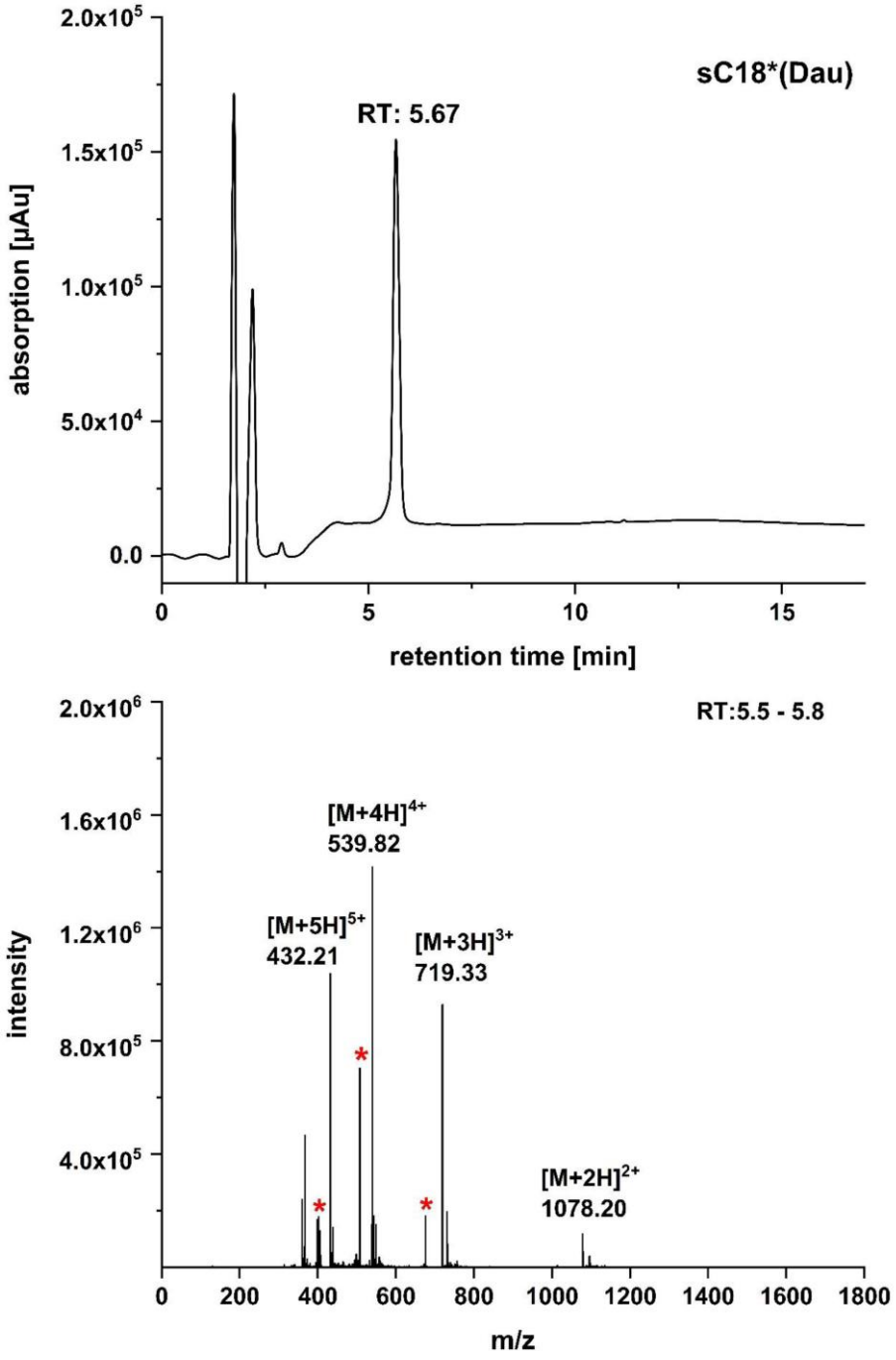

Figure 86. LC-MS analysis of peptide sC18*(Dau); MW calculated: 2154.5 g/mol. Purity: >99%. UV chromatogram (254 nm) and ESI-MS mass spectrum. Gradient: 10-60% B in A in 15 min, 0.6 ml/min. A: 0.1% FA in H_2O; B: 0.1% FA in ACN. Red asterisks: peaks corresponding to the product without daunosamine after mass fragmentation.

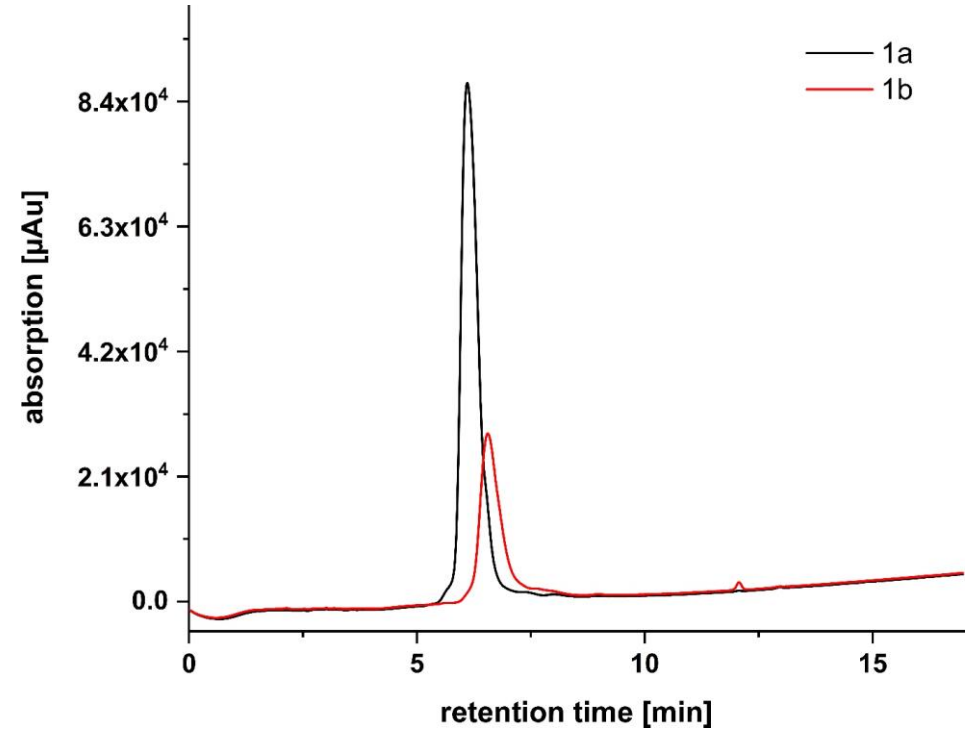

Figure 87. UV-chromatogram (194 nm) of 1a and 1b to compare the respective retention time. Gradient: 10-60% B in A in 15 min, 0.6 ml/min. A: 0.1% FA in H_2O; B: 0.1% FA in ACN.

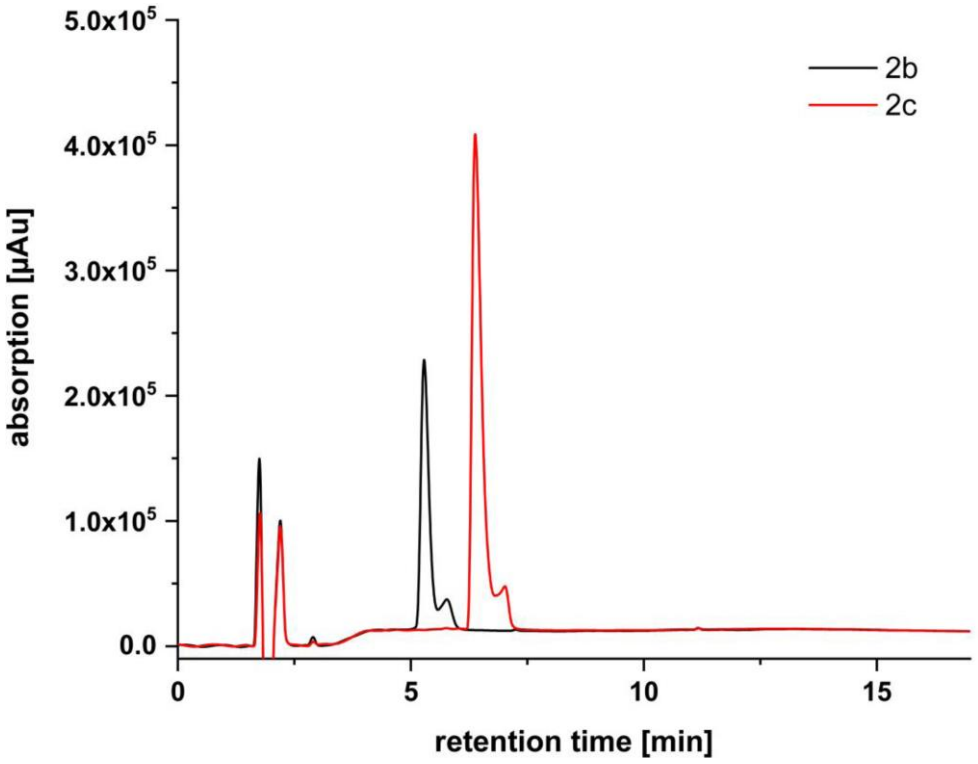

Figure 88. UV-chromatogram (254 nm) of sC18(Dau), namely 2b, and sC18(GFLG-Dau), namely 2c, to compare the respective retention time. Gradient: 10-60% B in A in 15 min, 0.6 ml/min. A: 0.1% FA in H_2O; B: 0.1% FA in ACN.

Table 20. Yields obtained after the CuAAC reaction between the differently labeled CPP sequence and the ligands GnRH-III-N_3 and c[DKP*f3*RGD]-PEG_4-N_3.

Compound	Yield of "click" reaction (%)
GnRH-III-sC18	41
GnRH-III-sC18(Dau)	79
GnRH-III-sC18(GFLG-Dau)	91
c[DKP*f3*RGD]-sC18-S-S-Cry	4
1	30
1a	90
1b	85
1c	75

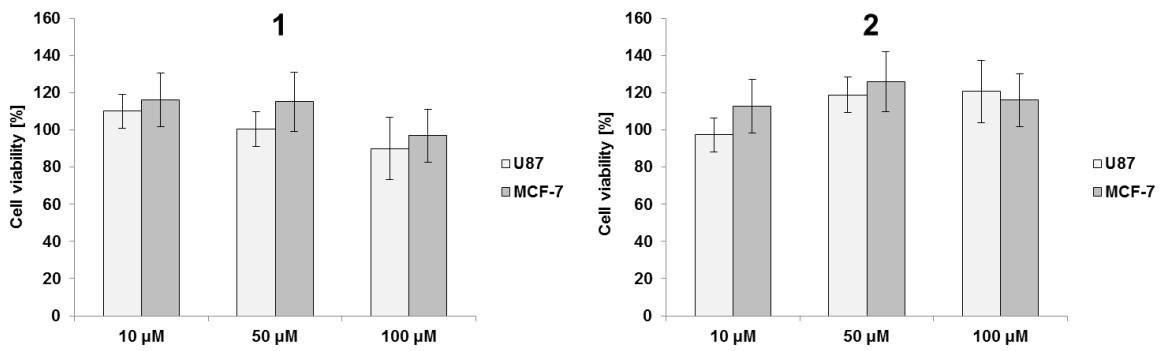

Figure 89. Effect of 1 and 2 on the cell viability measured by resazurin-based assay on U87 and MCF-7 cells. Evaluation of the resorufin fluorescence generated from resazurin by viable cells after 24h incubation with the peptide solution. Untreated cells were used as negative control and set to 100%; positive control was represented by cells treated for 10 minutes with 70% EtOH and it was subtracted from the other values. The experiment was performed in triplicate with *n=2.*

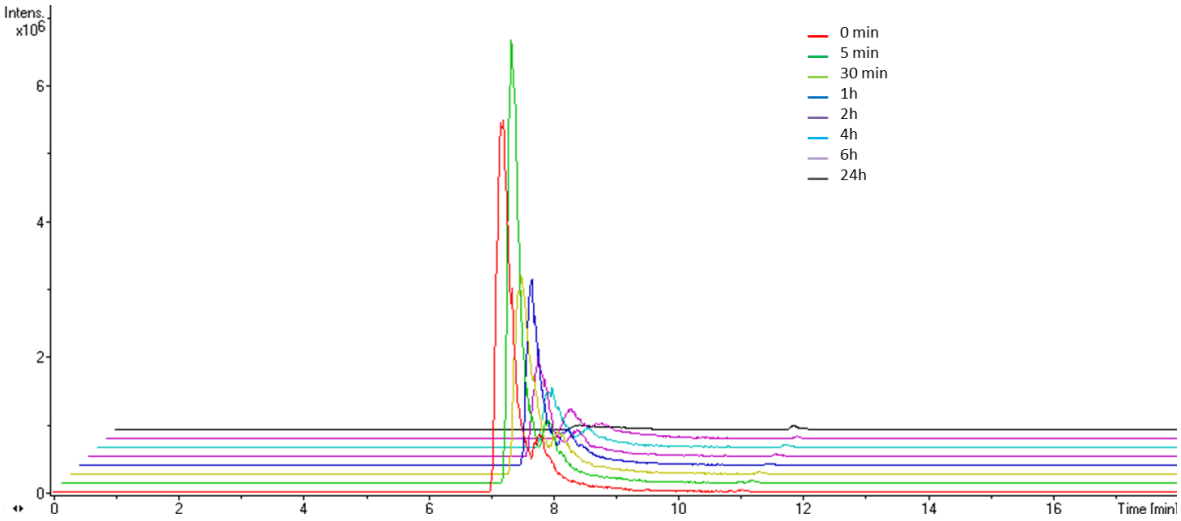

Figure 90. Plasma stability investigation. Compound **2** was dissolved in water to a concentration of 300 pmol/µl and then diluted with plasma (final conjugate concentration: 30 pmol/µl). The mixture was incubated at 37 °C for 24 h. Samples of 100 µl were taken at time points of 0 min, 5 min, 30 min, 1 h, 2 h, 4 h, 6 h, 24 h. After addition of ACN, the solutions were centrifuged using a membrane with a nominal molecular weight limit of 10 kDa and afterwards monitored by RP-HPLC.

8.3. List of figures

8.4. List of tables

8.5. Acknowledgment

I would like to express my gratitude to all those people who made it possible to achieve this goal.

First, I would like to thank my supervisor, Prof. Dr. Ines Neundorf, for choosing me almost four years ago as Ph.D. candidate. Thanks to her I undertook this path, probably the most important of my life. During this time I always felt her strong support in every occasion. She made me understand that making mistakes is not the end of the world but the important thing is to notice them in time, take the chance to learn from them and not lose hope. I take this opportunity also to apologize for my small and big crises which she always knew how to handle, making me see the bright side.

I would also like to thank Prof. Dr. Norbert Sewald for accepting the role of co-supervisor and for the outstanding organization of the Magicbullet project. At the end of the three years I feel that we have become a small “scientific family” and I am grateful to all the members because they have been a great source of inspiration.

In particular, I would like to thank Prof. Dr. Umberto Piarulli for the very formative discussions, the Skype calls and for welcoming me in Como during the three months of my secondment. I am very grateful to Prof. Dr. Gabor Mező for providing me with the best working conditions I could have wished for during my secondment in Budapest and for always being so helpful and kind. A special thanks goes to Dr. József Tóvári for bringing me to the hill of flowers but above all for introducing me to the world of *palinka* and local beer.

Thank you Prof. Dr. Kay Hofmann for your willingness to make the day of my graduation become happen.

I am especially grateful to Dr. Dolores Díaz and Linda Jütten, for the countless help with my thesis and above all for our intense collaboration which made it possible to perform all the measurements with very small amount of product.

I would also like to thank Dr. Daniela Arosio for being always so efficient in testing my conjugates.

I want to thank all my colleagues from the Magicbullet network because among them I found real friends. What kind of world would be without you? I will always remember the exhausting conferences: the day program was sometimes tough but the thought that in the evening I would meet them and live some unforgettable moments, made me go through it with a smile. One page would not be enough to thank my Sabi, the star of my Ph.D., my pink panther, my best balkan music compilation but also the companion of the most silly thing we could do while leaving the backpacks on the beach. Thank you for doing it too, because of that I feel less

stupid. Andrea, I do NOT thank you for introducing me to the world of fitness but for the kókuszgolyó, for the isler, and for the Friday night when we were locked inside the hospital. Eduard, I send you a special thanks because if you had not accepted the place in Bielefeld I would not be writing these acknowledgments right now. Besides that, thank you for the thousand adventures starting from the carnival to Hamburg to the donuts at the railway station. Thank you Ivan, for introducing me to cell culture and for cheering me up with sweet words when bad feelings prevailed. Thank you André for helping me when I was struggling, Clém for the amazing weekend in Montauroux, Adina for helping me the last day before printing the thesis and thank you Franci, Barbie, Lizeth, Paula, Ana, JK and Abi, for these wonderful years toghether!

I am very grateful to Sara for sharing my own madness. I will always remember your reaction when I told you that you had taken the wrong amino acid. I also remember how it was good to work with you in Como and Cologne. And thank you Silvia because you saved me with your "dirty" RGD.

I also want to thank Anja, Claudia and Gabi for their big support in the everyday lab life.

And now I would like to move on to express my thankfulness to my colleagues. Thank you so much for welcoming me in "AG Novevillaggio". Thank you André, not for the jokes about football nor for the music in the office, but for introducing me to the world of carnival, for the parties at home and for waiting for me when I could not come in time for lunch, I know that it was a great sacrifice! Thanks to Anja for the first Skype interview and for being always very supportive. Mareike, thank you for always being so sweet and kind, thanks for the help in the laboratory, for replying to my messages at 6 in the morning and for correcting my work so fast. Thanks to Florian, my little *Gürckchen* because I could understand less than half of the things he said, and though he knew it, he persisted while I kept smiling pretending to follow. My little Tammy deserves a special thanks for the super corrections of my thesis during Christmas holidays. Thank you for cheering me up in difficult times and for the unleashing dances in the office (we should definitely repeat it). And Anni, thanking you is the hardest of all jobs. I do not even know from where to start. Perhaps from all the times you offered me your shoulder to cry? For helping me anytime I needed? For staying with me in the lab till 11 p.m.? For the entertaining trips to Anröchte? For the pasta with peas and yoghurt? Two simple words do not express my infinite gratitude.

I would like to thank all the students who I have had the pleasure to meet during these years: Kathi, always full of positive energy and Ben, for not calling the mental hospital when I threw thousands of pipette tips on the floor screaming and crying. Thank you Marco for the *"Wo ist der Baum?"* and Benedikt for replying that *"der Baum"* was there.

Last but not least, I want to thank Cologne, because everything would have been different if it wouldn't have happened there, because every time I pass over the Rhein my heart is swelling with joy: you are simply *"meine Stadt".*

Passo ora ai ringraziamenti in italiano cominciando da Marghe e Simo. Fratelli con genitori diversi, mi avete accolto nel migliore dei modi e devo ringraziare soprattutto voi se sono riuscita a superare tutti questi anni. Grazie per non avermi abbandonato al mio stress, grazie per gli innumerevoli pomeriggi a casa di Marghe a bere thé, grazie per le corsette, per le spade con Babette, per le gite fuori porta, per le frittate di pasta, per le cenette dietetiche, per essere stati quasi cacciati dal corso di yoga e per tutto l'amore che mi avete dato.

Grazie a Bru, il secondo popino, o sei tu che devi ringraziare me? Condizione di parassitismo o simbiosi? Dai, a volte, ma solo a volte mi hai tenuto anche tanta, tanta compagnia. Grazie per lasciarti tirare addosso scarpe e per condividere le stesse passioni, come alberi di natale argentati e simpatici cagnoloni.

Grazie a Emma perché anche se lontana è sempre e comunque vicina e le vacanzine a Colonia ne sono sempre stata la prova lampante. Forse dovrei ringraziare anche La Latina? Grazie per farmi credere in me stessa, grazie perché dopo che ti sei chiusa fuori dall'appartamento ho capito che c'è gente messa peggio di me ma NON ti ringrazio per non aver iniziato la tua storia d'amore con Fabio!

Grazie Chiara per condividere le mie paturnie, per impiegare un mese a decidere che vestito mettersi e poi cambiare il giorno prima e per avere sempre mille impegni ma essere pronta a spostarli senza indugio quando ne ho bisogno.

Grazie a tutte le mie amiche: Betty per le profonde discussioni su Grey's anatomy, Elena per farmi sognare l'Argentina che è sempre più vicina, Moni per i preziosi weekend ad Alba, Laura per indossare le scarpe appena comprate prima di fare mille chilometri, Gemma per le colazioni costosissime, Ile per la sua passione per i toy boys e la Fra per i suoi racconti surreali (sempre sui toy boys). Grazie perché è bello sapere che quando torno vi trovo sempre ad aspettarmi!

Grazie ad Ale e Chico per essere stati i migliori coinquilini che mai potessi desiderare soprattutto in un periodo estremamente buio del dottorato.

Grazie ad Iri ed Andrea, California here we come! Questo viaggio mi ha dato la forza di mettercela tutta nel minor tempo possibile quindi grazie. Ora che non ho più questo stress farò di tutto per migliorare la mia posizione di testimone di nozze! E grazie a Simo per essermi venuta a trovare in ogni luogo.

Grazie ad Ale e Esmi perché con le foto dell'aurora boreale non mi hanno di certo aiutato ad affrontare le ultime settimane di correzioni ma mi hanno fatto un po' sognare. E grazie alla mia nonna che tutte le sere si ricorda di me.

Grazie ad Antonio, il primo popino, perché ha dovuto subire il lato peggiore di me e perché mi ha sempre dato la forza di iniziare, continuare e terminare questo bellissimo ma impervio percorso. Grazie per accettare regali non impacchettati, pere lanciate fuori dalla finestra, minacce con tanto di coltello, vacanze rovinate per colpa dello studio e per avermi dato la libertà di fare le mie scelte.

E per ultimi, sperando di non fare un errore di calligrafia come nella tesi di laurea, ringrazio i miei genitori perché anche se non lo dico mai, li amo tanto. Grazie.

8.6. Statement about collaborations

I hereby declare that the work presented in this thesis has been done by me without the use of any means other than that stated. Here, the experiments performed and the molecules synthesized by other people are listed for a clearer overview:

Chapter 3.1

- **GnRH-III-Dau** and **GnRH-III** synthesized by the PhD student Sabine Schuster (research group of Prof. Mező, ELTE university) ;
- triptorelin binding assay (Department of Biopharmacy, University of Debrecen);
- western blot performed by Sabine Schuster.

Chapter 3.2

- c[DKP*f3*RGD] synthesized by the PhD student Sara Parente and Dr. Silvia Panzeri (group of Prof. Piarulli, Università dell'Insubria, Como);
- unfunctionalized ligand c[DKP*3*RGD] and Cbl-conjugates synthesized by Clémence Robert (group of Prof. Piarulli, Università dell'Insubria, Como);
- inhibition of biotinylated vitronectin binding to $\alpha_v\beta_3$ and $\alpha_v\beta_5$ receptors performed by Dr. Daniela Arosio (Istituto di Scienze e Tecnologie Molecolari, Milan);
- Cry-55-glycinate synthesized by the PhD student Eduard Figueras Agustì (research group of Prof. Norbert Sewald, University of Bielefeld);
- **3b** and **3c** synthesized by Sara Parente.

Chapter 4.1

- DKP1 and DKP3 synthesized by Sara Parente;
- **cyc-DKP1**: preliminary trials performed by Sara Parente;
- NMR investigation performed by Dr. Diaz and the PhD student Linda Jütten (Department of Chemistry, University Cologne).

8.7. Declaration

Ich versichere, dass ich die von mir vorgelegte Dissertation selbstständig angefertigt, die benutzten Quellen und Hilfsmittel vollständig angegeben und die Stellen der Arbeit – einschließlich Tabellen, Karten und Abbildungen –, die anderen Werken im Wortlaut oder dem Sinn nach entnommen sind, in jedem Einzelfall als Entlehnung kenntlich gemacht habe; dass diese Dissertation noch keiner anderen Fakultät oder Universität zur Prüfung vorgelegen hat; dass sie – abgesehen von unten angegebenen Teilpublikationen – noch nicht veröffentlicht worden ist, sowie, dass ich eine solche Veröffentlichung vor Abschluss des Promotionsverfahrens nicht vornehmen werde. Die Bestimmungen der Promotionsordnung sind mir bekannt. Die von mir vorgelegte Dissertation ist von Frau Prof. Dr. Ines Neundorf betreut worden.

Teilpuplikationen:

- **Feni, L.; Omrane, M.A.; Fischer, M.; Zlatopolskiy, B.D.; Neumaier, B.; Neundorf, I. (2017)** Convenient Preparation of ^{18}F-Labeled Peptide Probes for Potential Claudin-4 PET Imaging. *Pharmaceuticals*, *10*, 99.
- **Feni, L.; Neundorf, I. (2017)** The Current Role of Cell-Penetrating Peptides in Cancer Therapy. In: Sunna A., Care A., Bergquist P. (eds) Peptides and Peptide-based Biomaterials and their Biomedical Applications. Advances in Experimental Medicine and Biology, vol 1030. Springer, Cham
- **Feni, L.; Parente, S.; Robert, C.; Gazzola, S.; Arosio, D.; Piarulli U; Neundorf I. (2019)** Kiss and Run: Promoting Effective and Targeted Cellular Uptake of a Drug Delivery Vehicle Composed of an Integrin-Targeting Diketopiperazine Peptidomimetic and a Cell-Penetrating Peptide. *Bioconjugate Chemistry* (just accepted manuscript)

Posterpräsentationen:

- **Feni L., Robert C., Piarulli U., Neundorf, I. (2016)** Synthesis of novel CPP-integrin ligand conjugates for targeted cancer therapy. 34th European Peptide Symposium, Leipzig, Deutschland
- **Feni L.; Robert C.; Piarulli U.; Neundorf, I. (2017)** Synthesis of novel CPP-integrin ligand conjugates for targeted cancer therapy. 13th German Peptide Symposium, Erlangen, Deutschland

- **Feni, L.; Parente, S.; Robert, C.; Piarulli, U.; Neundorf, I. (2018)** Synthesis of novel CPP-integrin ligand conjugates for targeted cancer therapy. Meeting: “Peptides and conjugates for tumor targeting, therapy and diagnosis”, Rimini, Italien
- **Feni, L.; Jütten, L., Parente, S.; Piarulli, U.; Díaz, D.; Neundorf, I (2019)** Head-to-tail cyclization of a cell-penetrating peptide through DKP scaffolds for cargo delivery. Investigation of structural and biological properties. 14th German Peptide Symposium, Köln, Deutschland

Ort, Datum

Lucia Feni